SAND2020-10498R

Surrogate Assembly 30 cm Drop Test

Spent Fuel and Waste Disposition

Prepared for
US Department of Energy
Spent Fuel and Waste Science and Technologies

Elena Kalinina, Doug Ammerman, Carissa Grey, Gregg Flores, Lucas Lujan, Sylvia Saltzstein, and Danielle Michel
Sandia National Laboratories

September 28, 2020

M2SF-20SN010202022
SAND2020-XXXX

APPENDIX E

NTRD DOCUMENT COVER SHEET[1]

Name/Title of Deliverable/Milestone/Revision No. 30 cm Drop Test, M3SF-20SN010202022

Work Package Title and Number Transportation, SF-20SN01020202

Work Package WBS Number 1.08.01.02.02

Responsible Work Package Manager Elena Kalinina (Name/Signature)

Date Submitted

Quality Rigor Level for Deliverable/Milestone[2]	☐ QRL-1 ☐ Nuclear Data	☐ QRL-2	☐ QRL-3	☒ QRL-4 Lab- Specific

This deliverable was prepared in accordance with Sandia National Laboratories
(Participant/National Laboratory Name)

QA program which meets the requirements of

☐ DOE Order 414.1 ☐ NQA-1 ☐ Other

This Deliverable was subjected to:

☒ Technical Review ☐ Peer Review

Technical Review (TR)
Review Documentation Provided

☐ Signed TR Report or,
☐ Signed TR Concurrence Sheet or,
☒ Signature of TR Reviewer(s) below

Name and Signature of Reviewers

Robert Kalan Robert Kalan

Peer Review (PR)
Review Documentation Provided

☐ Signed PR Report or,
☐ Signed PR Concurrence Sheet or,
☐ Signature of PR Reviewer(s) below

NOTE 1: *Appendix E should be filled out and submitted with the deliverable. Or, if the PICS:NE system permits, completely enter all applicable information in the PICS:NE Deliverable Form. The requirement is to ensure that all applicable information is entered either in the PICS:NE system or by using the NTRD Document Cover Sheet.*

- *In some cases there may be a milestone where an item is being fabricated, maintenance is being performed on a facility, or a document is being issued through a formal document control process where it specifically calls out a formal review of the document. In these cases, documentation (e.g., inspection report, maintenance request, work planning package documentation or the documented review of the issued document through the document control process) of the completion of the activity, along with the Document Cover Sheet, is sufficient to demonstrate achieving the milestone.*

NOTE 2: *If QRL 1, 2, or 3 is not assigned, then the QRL 4 box must be checked, and the work is understood to be performed using laboratory specific QA requirements. This includes any deliverable developed in conformance with the respective National Laboratory / Participant, DOE or NNSA-approved QA Program.*

Disclaimer

This information was prepared as an account of work sponsored by an agency of the U.S. Government. Neither the u.s. government nor any agency thereof, nor any of their employees, makes any warranty, expressed or implied, or assumes any legal liability or responsibility for the accuracy, completeness, or usefulness, of any information, apparatus, product, or process disclosed, or represents that its use would not infringe privately owned rights. References herein to any specific commercial product, process, or service by trade name, trade mark, manufacturer, or otherwise, does not necessarily constitute or imply its endorsement, recommendation, or favoring by the U.S. Government or any agency thereof. The views and opinions of authors expressed herein do not necessarily state or reflect those of the U.S. government or any agency thereof.

Sandia National Laboratories is a multi-mission laboratory managed and operated by National Technology and Engineering Solutions of Sandia LLC, a wholly owned subsidiary of Honeywell International Inc. for the U.S. Department of Energy's National Nuclear Security Administration under contract DE-NA0003525.

SUMMARY

The 30 cm drop is the remaining NRC normal conditions of transport (NCT) regulatory requirement (10 CFR 71.71) for which there are no data on the actual surrogate fuel. While obtaining data on the actual fuel is not a direct requirement, it provides definitive information which aids in quantifying the risk of fuel breakage resulting from a cask drop from a height of 30 cm or less. The 30 cm drop test with the full-scale surrogate assembly conducted in May 2020 was the last step needed for quantifying the strains on the surrogate assembly rods under NCT.

The full-scale surrogate assembly used in the 2020 30 cm drop test was built using a new 17x17 Pressurized Water Reactor (PWR) Westinghouse skeleton filled with the copper rods and 3 zircaloy rods from the full-scale surrogate assembly used in the Multi-Modal Transportation Test (MMTT) [1]. Felt pads were attached to the surrogate assembly bottom prior to the 30 cm drop to adequately represent the effects of the impact limiters and the cask. Note that felt “programming material” has been used extensively in past drop tests and is known to be a good material for programming a desired shock pulse. The felt pad configuration was determined during a previous series of tests reported in [10]. The acceleration pulses observed on the surrogate assembly during the test were in good agreement with the expected pulses. This confirmed that during the 30 cm drop the surrogate assembly experienced the same conditions as it would if it was dropped in the cask with the impact limiters.

A 30 cm drop test was also conducted in June 2019 with the old full-scale surrogate assembly. The old assembly was damaged when accidently dropped prior to the test from a height of about 7 incches without felt pads attached. The comparison of 2020 and 2019 test data provided useful information regarding the strain due to the pre-existing damage. This information can be also applied to successive damage due to multiple drops. In both the 2019 and 2020 tests the impact side of some of the spacer grids experienced buckling and permanent deformation.

In the 2020 test the maximum negative peak strain (corrected for bias) was recorded by strain gauge SG10-0 (1,723 microstrain). The next two highest negative values were recorded by SG11-0 (1,169) and SG-12 (1,067). These three strain gauges were located at the bottom (slap down) end of the assembly that hit the target a few milliseconds later than the top end. In the 2019 test the maximum negative peak strain (corrected for bias) was recorded by strain gauge SG8-0 (1,736 microstrain) located on the top end of the assembly.

Pressure paper was inserted between the rods within the two long spacer grid spans (top and bottom end of the assembly) and within two shorter spacer grid spans (mid-part of the assembly) prior to the 2020 test. The pressure paper sheets from the two short spans were blank, indicating no rod-to-rod contact in these spans. All, except a few, pressure paper sheets from the two long spans between spacer grids showed marks indicating rod-to-rod or rod-to-guide tube contact. A contact pressure of 4.1 ksi is a reasonable estimate of the maximum rod-to-rod contact pressure in the 2020 test. The points of the maximum pressure are located at the middle of the span where the bending is maximum.

The longitudinal bending stress corresponding to the maximum observed strain value (calculated from the strain-stress curve in [19]) was 22.3 ksi. The maximum calculated rod-to-rod contact pressure was 4.1 ksi. Both values are significantly below the yield strength of the cladding. The stress corresponding to the maximum strain value observed in the 2019 test with the damaged assembly (calculated from the strain-stress curve in [19]) was only slightly higher - 22.9 ksi.

The major conclusion that can be drawn from the 30 cm drop test is that the fuel rods will maintain their integrity during the 30 cm drop.

This page is intentionally left blank.

ACKNOWLEDGEMENTS

The authors would like to thank Ned Larson from DOE NE for his programmatic leadership. The authors are grateful to the technical reviewers for the excellent comments. The authors appreciate the opportunity to use the Westinghouse 17x17 PWR assembly skeleton in the 30 cm drop test and thank Westinghouse staff for their review of the report. The authors would like to acknowledge the SNL drop tower staff that supported the activities under the COVID-19 conditions.

This page is intentionally left blank.

CONTENTS

LIST OF FIGURES

LIST OF TABLES

REVISION HISTORY

Revision	Date	Description of Revision
0	09/28/20	Initial Issue

ACRONYMS

BAM	Bundesanstalt for Materialforschung und -prufung
CFR	Code of Federal Regulations
DAQ	Data Acquisition
DOE	US Department of Energy
ENSA	Equipos Nucleares, S.A., S.M.E.
ENUN	ENSA Universal [cask]
FFT	Fast Fourier Transform
IAEA	International Atomic Energy Agency
MMC	Metal Matrix Composite
MMTT	Multi-Modal Transportation Test
NCT	Normal Conditions of Transport
NRC	Nuclear Regulatory Commission
PNNL	Pacific Northwest National Laboratory
PSD	Power Spectra Density
PWR	Pressurized Water Reactor
SFWST	spent fuel and waste science and technology
SNL	Sandia National Laboratories
SRS	Shock Response Spectra
TTCI	Transportation Technology Center, Inc.

This page is intentionally left blank.

SPENT FUEL AND WASTE DISPOSITION

SURROGATE ASSEMBLY 30 CM DROP TEST

1. INTRODUCTION

The 30 cm drop tests were a follow-on to the 2017 Spanish/US/Korean Multi-Modal Transportation Test (MMTT) that obtained strain and acceleration data during Normal Conditions of Transport (NCT) on surrogate fuel within the ENUN 32P dual purpose rail cask. The goal of the MMTT was to validate the hypothesis that spent nuclear fuel can withstand the shocks and vibrations from NCT. Data were collected during actual heavy-haul truck transport through Spain, small ship transport from Spain to Belgium, large ship transport from Belgium to the USA (port of Baltimore), and rail transport from Baltimore to Transportation Technology Center, Inc. (TTCI) in Pueblo (Colorado). The detailed report is available at [1]. The summary of the results can be found in [2-8]. A short video documenting the major test events is available on YouTube [9].

Note that the common assumption is that during transport the cask content experiences the same accelerations as the cask itself. The data from the MMTT demonstrated that the inputs from the shock events were amplified from the cask to the surrogate assemblies at frequencies above 60 Hz. The maximum strain on the surrogate assembly fuel rods observed in MMTT (99 microstrain in 8 mph coupling rail test at TTCI) was significantly below the yield strength of the cladding. The amplification from the cask-to-surrogate assemblies observed in the MMTT was one of the motivations for conducting the 30 cm drop test. The purpose of the test was to measure accelerations and strains on the surrogate fuel assembly and to determine whether the fuel rods can maintain their integrity inside a cask when dropped from a height of 30 cm.

The 30 cm drop is the remaining NRC NCT regulatory requirement (10 CFR 71.71) for which there are no data on the actual surrogate fuel. While obtaining data on the actual fuel is not a direct requirement, it provides definitive information which aids in quantifying the risk of fuel breakage resulting from a cask drop from a height of 30 cm or less. Obtaining these data allows for the following.:

- Completing the NCT mechanical testing environment,
- Better understanding the potential implications of handling incidents,
- Quantifying the risk of fuel breakage under the 30 cm drop conditions, and
- Defining the transfer function from the cask to the fuel for more severe impacts than the shocks observed during the MMTT.

Ideally, the 30 cm drop test would be conducted with the full-scale cask containing surrogate assemblies. However, the cost of a full-scale cask and impact limiters make this test impractical. At the same time, the 1/3 scale cask with impact limiters and dummy assemblies was available for the program at nominal cost. The decision was made to perform the 30 cm drop tests with the 1/3 scale cask first and then follow with the 30 cm drop tests with the full-scale dummy and surrogate assemblies. This allows for obtaining the accelerations and strains on the full-scale surrogate fuel assembly in the 3 consecutive steps shown in Figure 1-1. The term “dummy assembly” refers to a hollow steel representation of a 17x17 Pressurized Water Reactor (PWR) assembly with the same mass and center of gravity. The term “surrogate assembly” refers to an assembly made of unirradiated 17x17 PWR hardware fully populated with copper rods filled with lead rope and 3 zircoloy rods, one filled with lead rope, one filled with lead pellets, and one filled with molybdenum pellets.

Step 1 was a 30 cm drop test of the 1/3 scale cask. The goal of this test was to obtain acceleration data on the cask and on the 1/3 scale dummy assemblies. The acceleration pulse on the 1/3 scale dummy

assemblies was converted to the expected acceleration pulse on the full-scale dummy assembly. This test took place in December 2018 at the Bundesanstalt for Materialforschung und -prufung (BAM) indoor facility in Berlin, Germany.

Step 2 was a 30 cm drop of the full-scale dummy assembly. The goal of this test was to find the condition under which the observed acceleration pulse would be in good agreement with the expected acceleration pulse derived from Step 1. Achieving this condition means that the effect of the cask and the impact limiters are adequately represented. This step was required because the accelerations on the 1/3 scale dummy assembly were only applicable to the full-scale dummy assembly which was structurally very different from the full-scale surrogate assembly. This involved a series of 30 cm drop tests using different shock absorbing conditions in order to select the shock absorbing material that best mimics the cask and impact limiters. These tests took place in June 2019 at the SNL drop tower facility in Albuquerque (NM).

Step 3 was a 30 cm drop of the surrogate assembly. The goal of this test was to obtain the accelerations and strains at multiple locations on the full-scale surrogate fuel assembly. The test took place on May 7, 2020 at the SNL drop tower facility in Albuquerque (NM). The test was conducted using the shock conditions derived in Step 2.

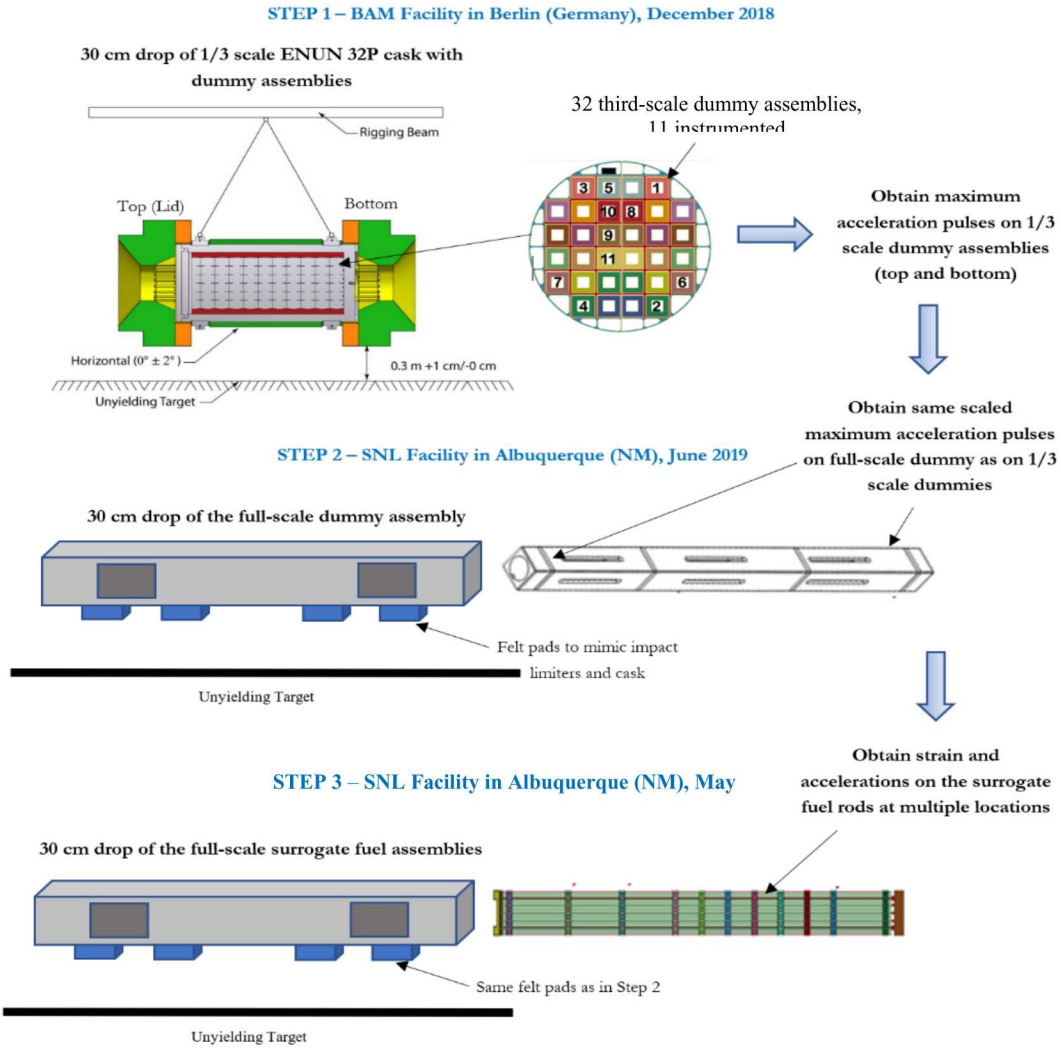

Figure 1-1. Three Steps to Obtain Accelerations and Strains on the Full-Scale Surrogate Assembly.

Step 1 and Step 2 are documented in [10] and summarized in [11] and [12]. This report describes step 3 - the 30 cm drop test of the full-scale surrogate assembly.

A summary of the results obtained during Step 1 and Step 2 is provided below.

30 cm Drop Test of the 1/3 Scale Cask

The hardware for this test was provided by Equipos Nucleares, S.A., S.M.E. (ENSA). The 1/3-scale cask included scaled impact limiters, basket, modified (to allow for internal instrumentation) lid, and 32 dummy assemblies. The dummy assemblies were hollow steel blocks with the same mass as the fuel assemblies, but very different from the fuel assemblies structurally. The test was conducted at the BAM facility in Berlin (Germany) in December 2018. The sampling rate for the accelerometer data was 200,000 Hz.

Four locations (top and bottom on the lid end and top and bottom on the back end) on the exterior of the cask were instrumented. Eleven dummy assemblies were instrumented on the lid end (side A) and 7 on the back end (side D). One location on the lid end of the basket was instrumented as well.

Comparison of the accelerations at the different locations demonstrated that the horizontal drop was not exactly horizontal (Figure 1-2). The lid (front) end of the cask hit approximately 2 milliseconds before the back end of the cask. This resulted in two acceleration peaks with the higher accelerations on the cask and the dummy assemblies associated with the second (later) peak.

The maximum accelerations on the dummy assemblies varied significantly depending on the location within the cask (Figure 1-3) with the maximum observed accelerations being ~2.4 times higher than the minimum. The locations closer to the top (location 10 on side A and location 5 on side D) were the ones with the highest accelerations. The accelerations in these locations during the first impact are shown in Figure 1-4. These accelerations were converted (scaled) to the accelerations expected in the 30 cm drop of the full-scale dummy assembly (Figure 1-4).

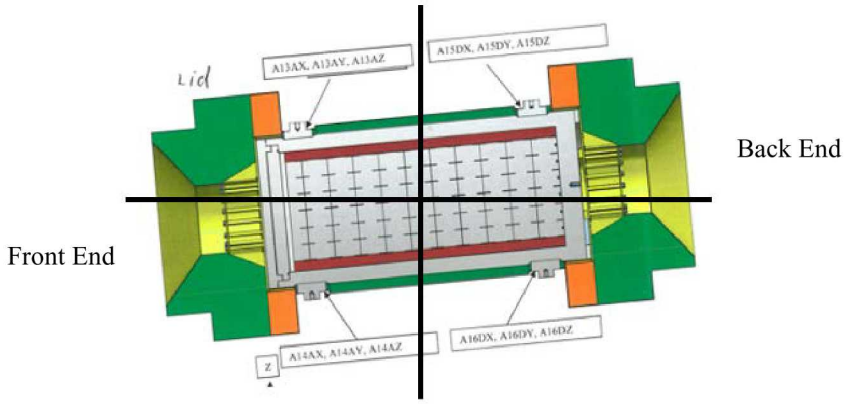

Note: the angle between the lateral cask orientation and horizontal surface shown in diagram is not to scale.

Figure 1-2. Lateral Orientation During First Impact.

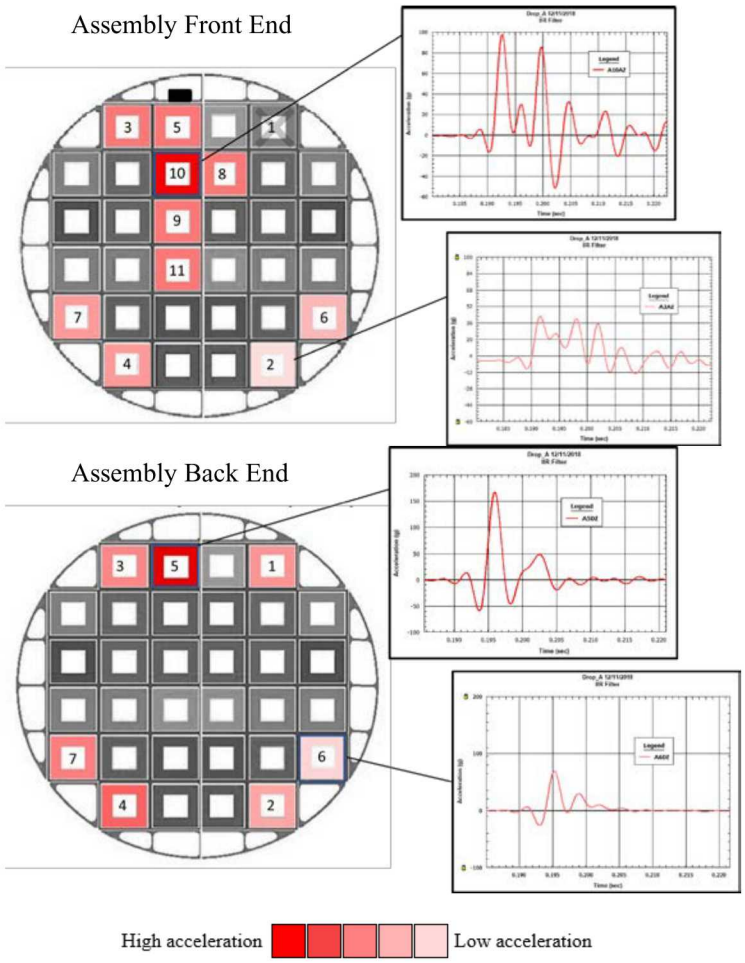

Figure 1-3. Maximum Accelerations on Assembly Front End (Side A) and Back End (Side D).

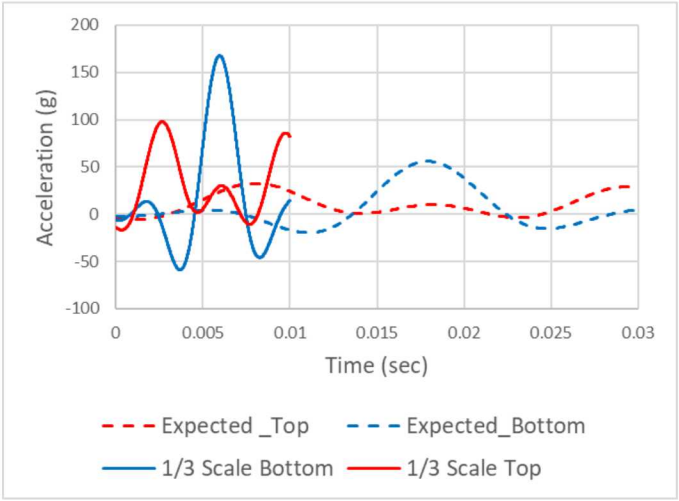

Figure 1-4. Observed 1/3 Scaled and Projected Full-Scale Dummy Assembly Accelerations in 30 cm Drop.

30 cm Drop Test of the Full-Scale Dummy Assembly

The full-scale dummy assembly is the enlarged by 3 times equivalent of the 1/3 scale dummy assembly (Figure 1-5) . It was manufactured by ENSA using the same materials, scaled dimensions, and manufacturing processes as the 1/3 scale dummy assemblies.

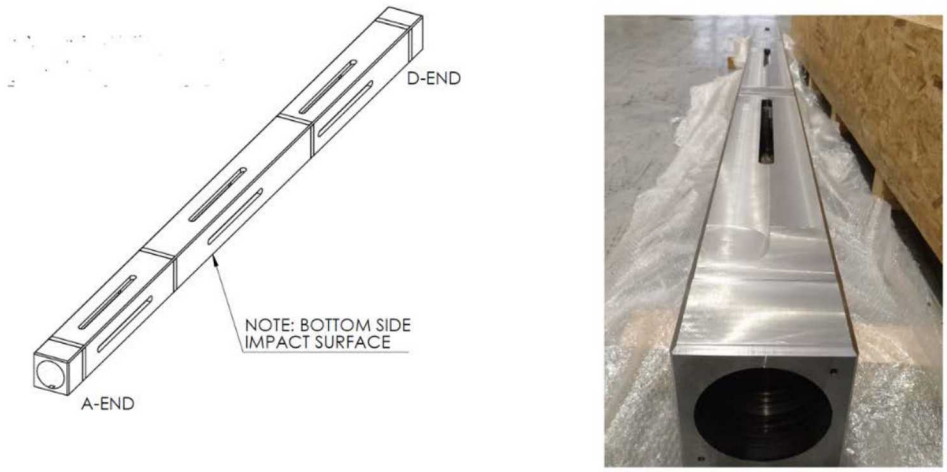

Figure 1-5. Drawing (left) and Photo (right) of the Full-Scale Dummy Assembly.

The full-scale dummy assembly was dropped in the full-scale 17x17 PWR Metal Matrix Composite (MMC) basket tube. A basket tube was purchased from ENSA to mimic the boundary conditions the dummy assemblies experienced during the 30 cm drop of 1/3 scale cask.

The full-scale dummy assembly was instrumented with tri-axial accelerometers on the top and bottom ends to obtain the acceleration data comparable with the 1/3 scale drop test.

Felt pads were used as a shock absorbing material to mimic the behavior of the impact limiters and the cask in the 1/3 scale cask drop test. Four pads were attached to the bottom face of the basket tube (Figure 1-6). The drop test was conducted in June 2019 at the SNL drop tower (Albuquerque, NM). The data collection frequency was 51,200 Hz.

Four drop tests were performed to get the desired acceleration pulses. The felt pad configuration in Test 4 is shown in Figure 1-6. In the fourth drop test the full-scale acceleration pulses were in good agreement with the expected ones (Figure 1-7). Note that the full-scale dummy assembly drop was virtually horizontal and the accelerations on the top and bottom ends of the dummy assembly were very similar and occurred practically at the same time. In the 1/3 scale cask drop, the cask lid (top) end hit the target first. This resulted in the different timing of the peak accelerations on the top and bottom ends of the assemblies that was impossible to reproduce with a strictly horizontal drop.

The felt configuration used in Test 4 represented the major input into the third step (Figure 1-1), a 30 cm drop of the full-scale surrogate assembly.

In the following sections two 30 cm drop test are discussed, one conducted in June 2019 with an old surrogate assembly and one conducted in May 2020 with a new surrogate assembly. The old assembly was damaged in the handling accident prior to the test. All the references to the 2019 test are to this old assembly. All the references to the 2020 test are to the new surrogate assembly. The analysis focused on the 2020 test with the new surrogate assembly. The results of the 2019 test were mostly used in the comparisons with the results of the 2020 test.

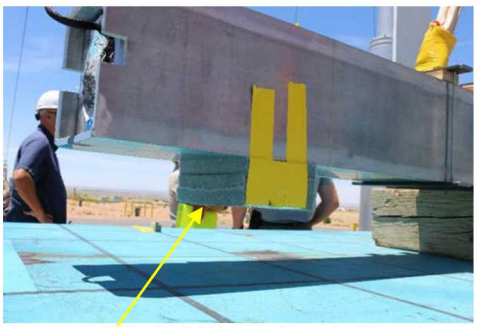

Felt Pad Dimensions in Test 4
6 inches (L)x10 inches (W)x3 inches (H)

Figure 1-6. Felt Pad Locations (left) and Configuration in Test 4 (right).

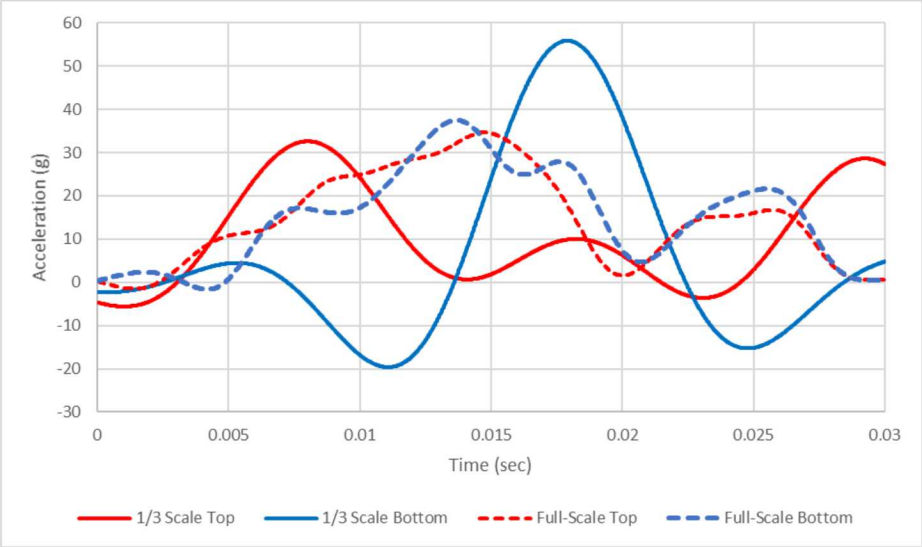

Figure 1-7. Scaled Acceleration Pulses on 1/3 Scale Dummy Assembly Compared to Test 4 Acceleration Pulses.

2. 30 CM DROP OF OLD DAMAGED SURROGATE ASSEMBLY (2019 TEST)

An old surrogate assembly, the one that was used in MMTT, was instrumented, inserted in the basket tube and ready for the 30 cm drop test on June 12, 2019. The test hardware was the same as described in Section 3.1. The handling and test set up were the same as described in Sections 3.1.3 and 3.1.7. The instrumentation was the same as described in Section 3.1.8. The surrogate assembly was transported from the SNL test facility to the drop tower in the morning of June 13, 2019. A forklift was used to unload the surrogate assembly from the transportation vehicle. When the forklift approached the target as shown in Figure 2-1, the left sling slid off the fork tine. The left end of the unit fell onto the target with no felt on it. Figure 2-2 shows how the approximate drop height was estimated from the photo taken just before the accident. It was estimated that the accidental drop height was 6.9-7.8 inches (17.5-19.8 cm).

Figure 2-1. Forklift with the Surrogate Assembly Shortly Before the Accidental Drop.

Figure 2-2. Pre-Accident Photo Used in Estimating Accidental Drop Height.

Buckling of the surrogate assembly spacer grids after the accidental drop was observed in the two windows cut in the basket tube. Only two spacer grids were visible to check. The bottom of the basket tube experienced slight plastic deformation. This is illustrated in Figure 2-3. Rod-to-rod contact was also observed on the visible parts of the pressure paper sheets.

The decision was made to conduct the 30 cm drop after the accidental drop and then to repeat the 30 cm drop with a new surrogate assembly. It was inferred that a valuable insight can be obtained by comparing the 30 cm drop tests with a damaged and an undamaged assembly. The comparisons are provided throughout Section 4.

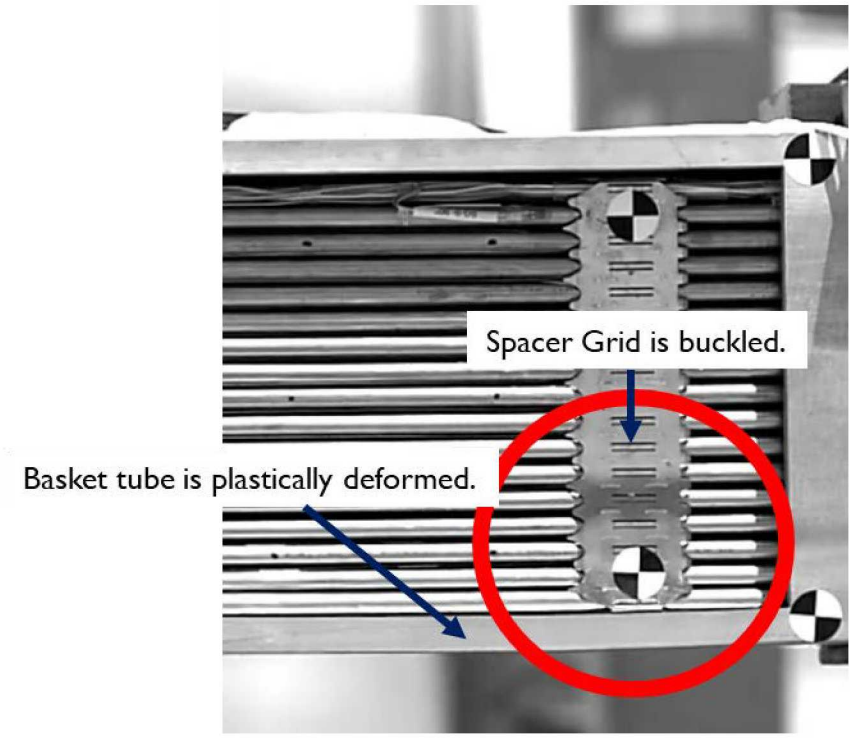

Figure 2-3. Damage Observed After the Accidental Drop Shortly before the 2019 Test.

Three additional pressure paper sheets were placed between the bottom rods through the window in the basket before the test (Figure 2-4).

The test took place on June 13, 2019. Figure 2-5 shows the test setup. Figure 2-6 shows the positions of the high-speed cameras looking at the two windows in the basket tube. The high-speed camera videos showed the upward and downward bending of the rods after the impact. Figure 2-7 shows a snapshot of the window view shortly after the impact and illustrates the rod-to-rod contact.

Figure 2-4. Additional Pressure Paper Installed before the 2019 Test.

Figure 2-5. 30 cm Drop Test Setup, June 13, 2019.

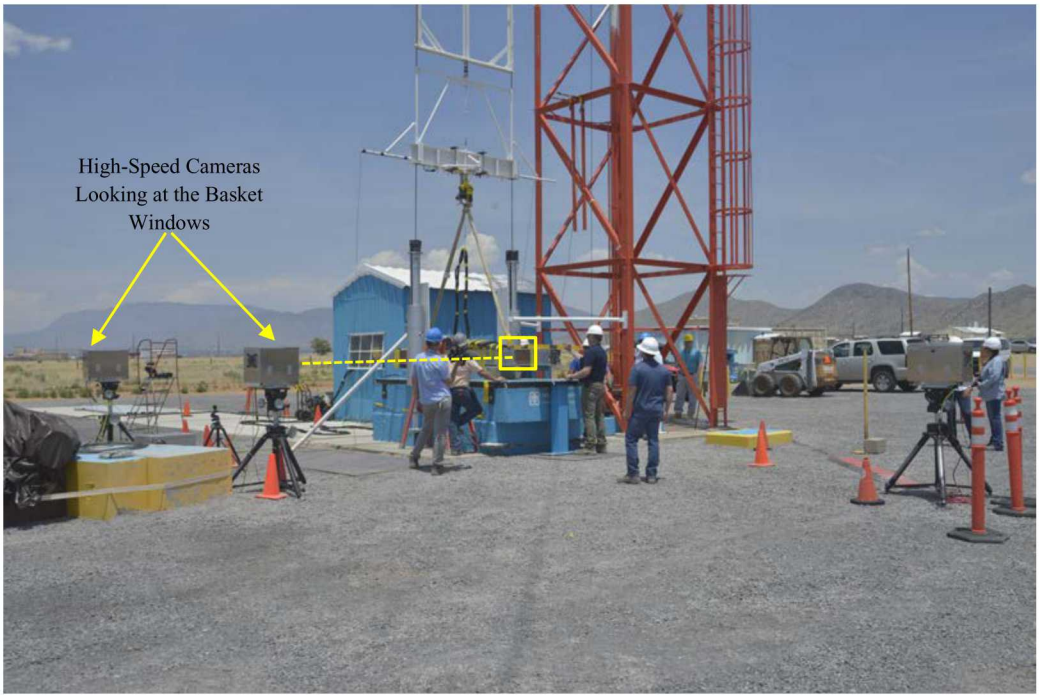

Figure 2-6. Positions of High-Speed Cameras Looking at the Basket Tube Windows (2019 Test).

Figure 2-7. Snapshot from the High-Speed Camera Looking at the Basket Tube Window Shortly after the Impact (2019 Test).

After the test the surrogate assembly was transported back to the test facility and pulled out from the basket tube. The pressure paper sheets were extracted and scanned, and the assembly was examined. The pressure papers in the middle of the assembly showed no rod-to-rod contact. The pressure paper at the top of the assembly showed the guide tube contact. The pressure paper at the bottom of the assembly showed the contact at all rods. This is illustrated in Figure 2-8 that shows the pressure paper sheets from the long span next to the assembly top. The additional pressure paper sheets inserted after the accident and before

the test showed rod-to rod contact. The pressure paper sheet from the long span next to the assembly top inserted between the 15th and 16th rods (rods were counted from the assembly top) is shown in Figure 2-9.

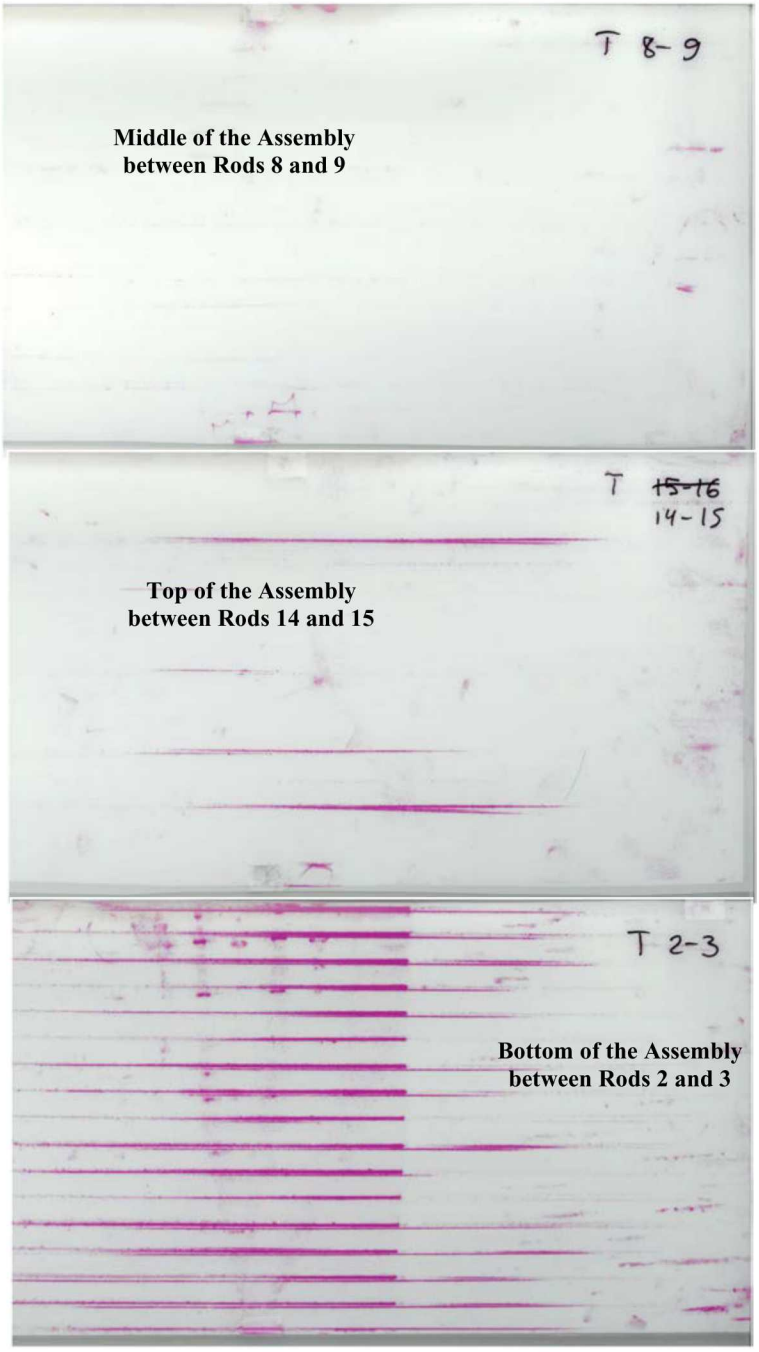

Figure 2-8. Pressure Paper Sheets from the Long Span Next to the Assembly Top (2019 Test).

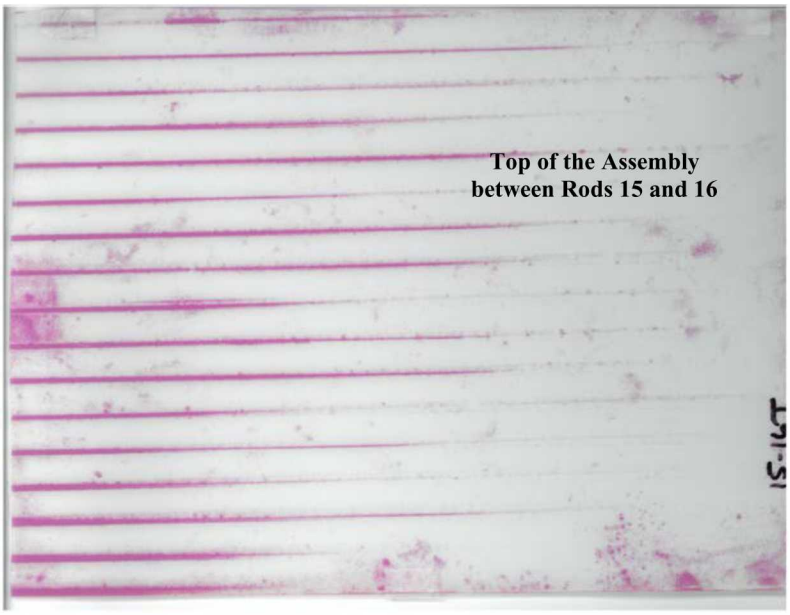

Figure 2-9. Additional Pressure Paper Sheet from the Long Span Next to the Assembly Top (2019 Test).

The assembly examination showed that the spacer grids with long spans on either side were significantly buckled (Figure 2-10). The spacer grids with short spans were barely damaged (Figure 2-11).

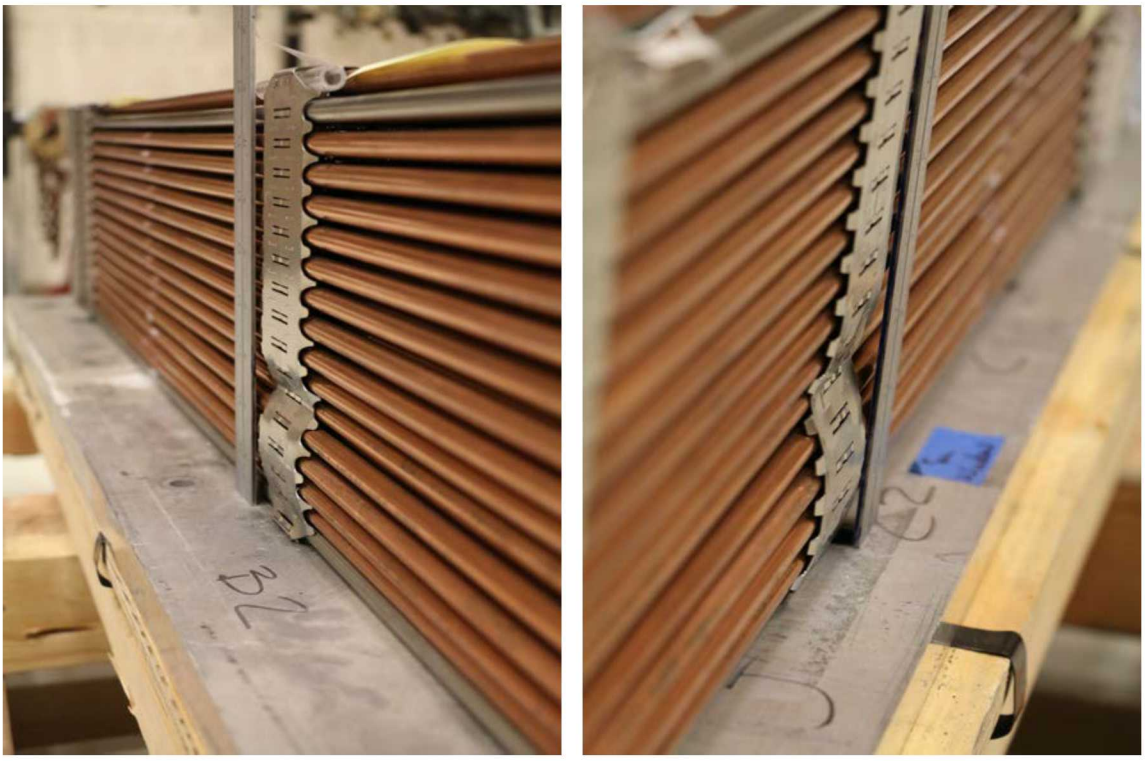

Figure 2-10. Long Span Spacer Grid After 2019 Test.

Figure 2-11. Short Span Spacer Grid After 2019 Test.

After the results of the examination were documented, the nozzles were removed and the rods were pulled out of the assembly. Neither nozzles nor rods were damaged.

3. 30 CM DROP OF NEW FULL-SCALE SURROGATE ASSEMBLY (2020 TEST)

The following sections describe test hardware, handling, test setup, instrumentation, and 30 cm drop of the new surrogate assembly. The test was conducted in accordance with the 30 cm Drop Test Plan [13] and the Quality Assurance Implementation Procedure [14]. All the sensors were calibrated and the calibration certification documents are in the test records. The test records also contain a library of photos, videos (including high-speed camera videos), and other documents.

3.1 Test Hardware

3.1.1 New Full-Scale Surrogate Assembly

A new 17x17 PWR assembly skeleton was purchased from Westinghouse in the fall of 2019. The skeleton was populated with the rods from the old assembly in December 2019 by SNL technologists. The old assembly nozzles were re-used.

All rods, except 3, were copper tubes with lead rope inside (Figure 3-1). Three rods were zircaloy tubes, one with the lead rope, one with the lead pellets, and one with molybdenum pellets (Figure 3-1). These three rods were instrumented (Section 3.1.8).

The weight of the surrogate assembly was 785 kg. A few photos of the new full-scale surrogate assembly with different level of details are shown in Figure 3-1. The locations of zircaloy tubes are identified on the bottom right photo and the copper tube and its specifications are shown in the top right photo. A full-scale surrogate assembly drawing is shown in Figure 3-2.

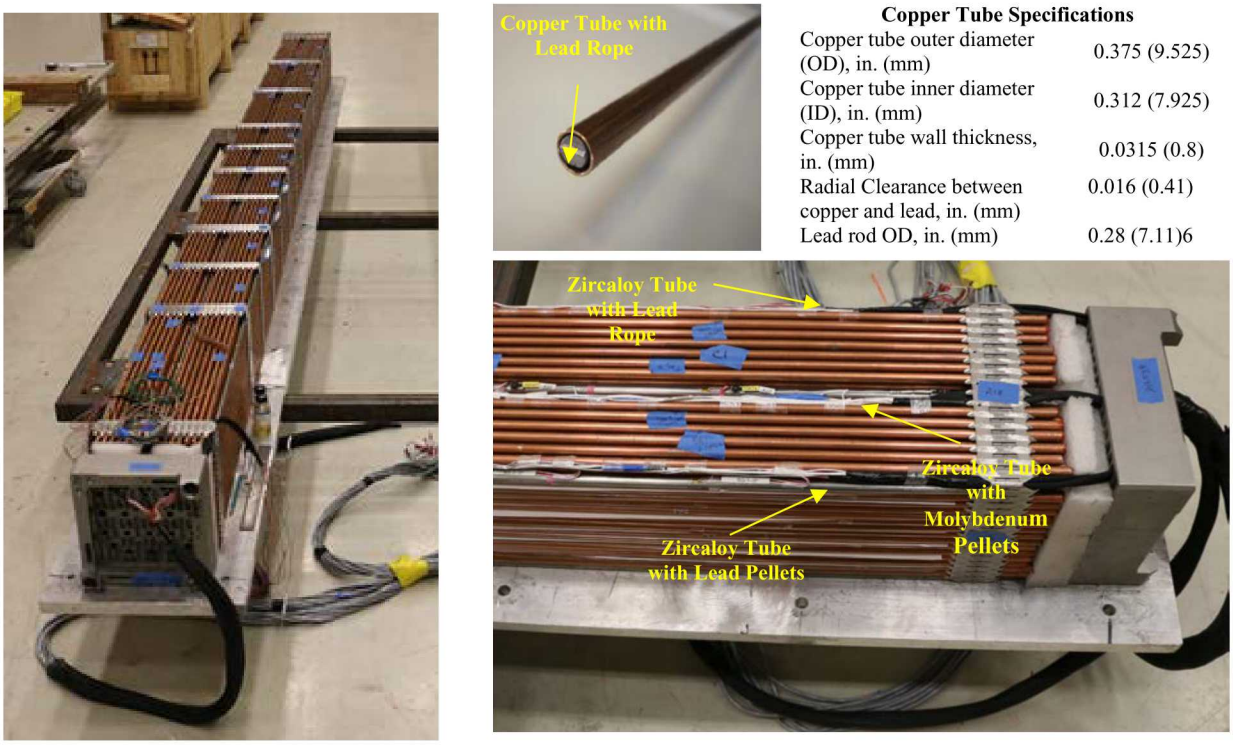

Figure 3-1. New Full-Scale Surrogate Assembly Photo.

Figure 3-2. New Full-Scale Surrogate Assembly Drawing.

3.1.2 Basket Tube

A full-scale 17x17 PWR MMC basket tube was purchased from ENSA to mimic the boundary conditions the assembly experienced during the 30 cm drop of the 1/3 scale cask. The basket tube weight was 145 kg. The basket tubes in the 1/3 scale cask test were the scaled equivalent of this basket tube. The same basket tubes were in the full-scale ENUN 32P cask used during the MMTT.

As was described in Section 2, the old full-scale surrogate assembly was first accidently dropped and then dropped 30 cm (2019 test) in this tube. Slight plastic deformation was observed at the bottom of the tube beneath the windows cut in the tube. Two windows were cut on one side of the basket tube (Figure 3-3) to record the behavior of the surrogate assembly rods during the 30 cm drop test with high-speed video cameras. The windows weakened the basket and were the cause of the plastic deformation.

The basket tube was rotated such that the damage was on the upper surface and the surrogate fuel assembly was dropped on the undamaged surface. The surrogate fuel assembly is much less stiff than the basket tube, and any small deviations of the basket tube from its original geometry does not change the cladding strains or the accelerations of the surrogate fuel assembly.

Photos of the basket tube are shown in Figure 3-3 and a drawing with associated dimensions is shown in Figure 3-4.

Figure 3-3. 17x17 PWR Assembly Basket Tube Photos.

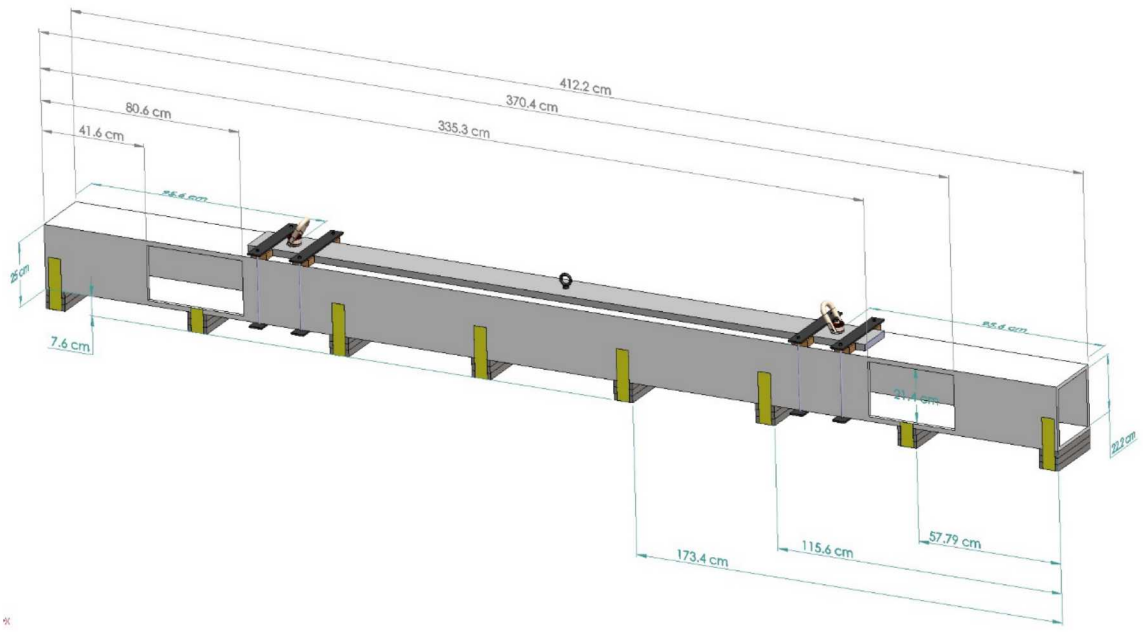

Figure 3-4. 17x17 PWR Assembly Basket Tube Drawing.

3.1.3 Handling Hardware

Lifting the basket tube with the dummy assembly inside required a special approach. The basket tube is made of MMC, which consists of a matrix of 'pure' aluminum material (very soft) with boron carbide insertions in it (extremely hard). This made it very difficult to machine or grind the basket tube - neither drilling holes or welding was possible. To handle the basket tube, a unique lifting method was developed. Figure 3-5 shows the hardware on one side of the basket tube. Similar hardware was installed on the other side (Figure 3-6).

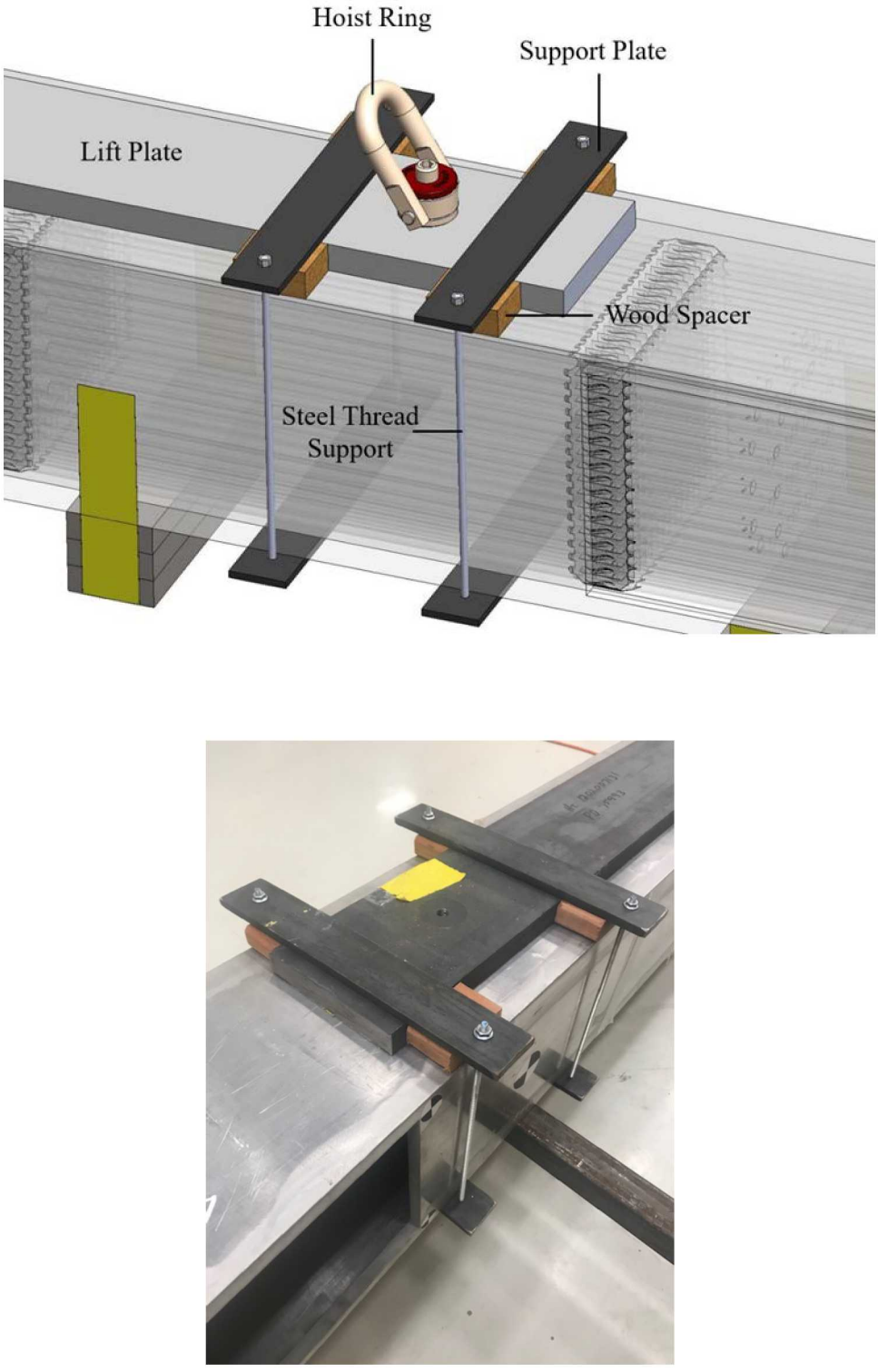

Figure 3-5. Drawing (top) and Photo (bottom) of the Handling Hardware Components.

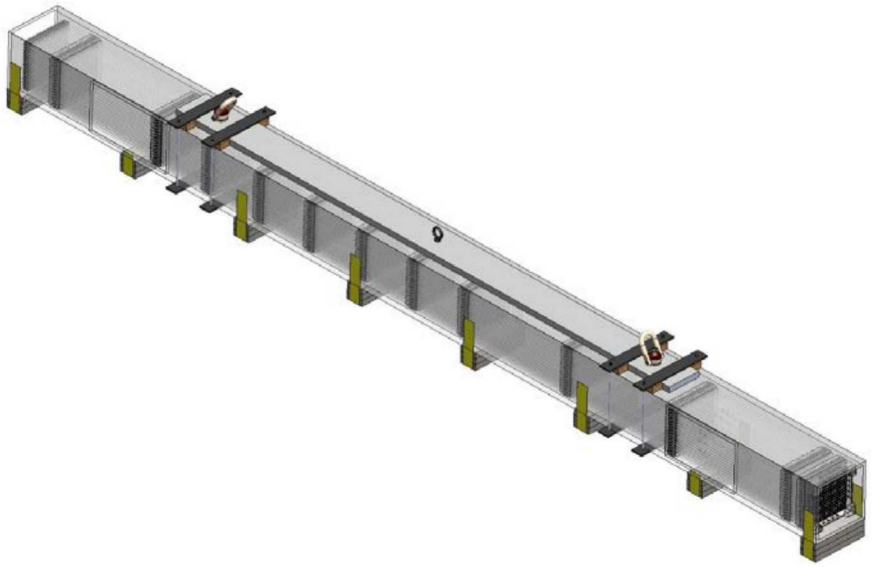

Figure 3-6. Basket Tube with Handling Hardware.

A single steel plate (lift plate in Figure 3-5) was mounted to the top of the basket tube using a custom bracket assembly. The bracket assembly consists of support plates, wood spacers, and steel thread supports. Two support plates were placed atop the lift plate and two were placed beneath basket tube. Wood spacers were placed on either side of the lift plate between the support plates and basket tube. This decreases bending in the support plates while the surrogate assembly is being lifted. The steel thread supports were used to keep the support plates in contact with the lift plate and basket tube. Finally, the hoist rings were threaded into the threaded hole insert of the lift plate. All lifting hardware was manufactured at SNL. Figure 3-6 shows the surrogate assembly lifting hardware. Analysis of the capacity of the lifting hardware is documented in [15].

3.1.4 Felt Pads

Four felt pads 6 inches (L)x10 inches (W)x3 inches(H) were used in the 30 cm drop test with the damaged surrogate assembly in June 2019. Figure 3-7 shows the configuration and locations of these felt pads. These are the same locations and the same configuration as in the Test 4 with the full-scale dummy assembly (Figure 1-6). Note that felt “programming material” has been used extensively in past drop tests and is known to be a good material for programming a desired shock pulse.

Figure 3-7. Configuration of Felt Pads in 30 cm Drop Test with Damaged Surrogate Assembly (June 2019)

Because the basket tube experienced slight deformation at the bottom in the 30 cm drop test with the damaged assembly (2019 test), the decision was made to install felt pads in 8 locations to reduce the loads on the basket tube in the 30 cm drop with the new assembly (2020 test). The total length of the 8 pads (8x3=24") was the same as the total length of 4 pads (4x6=24 inches). The width and the thickness of 8 pads were the same as the width and the thickness of 4 pads. Figure 3-8 shows the surrogate assembly with 8 pads attached to its bottom (left) and the felt pad configuration (right). Figure 3-9 shows the felt spacing. The felt pads were attached to the basket tube at the SNL test facility before its transport to the drop tower.

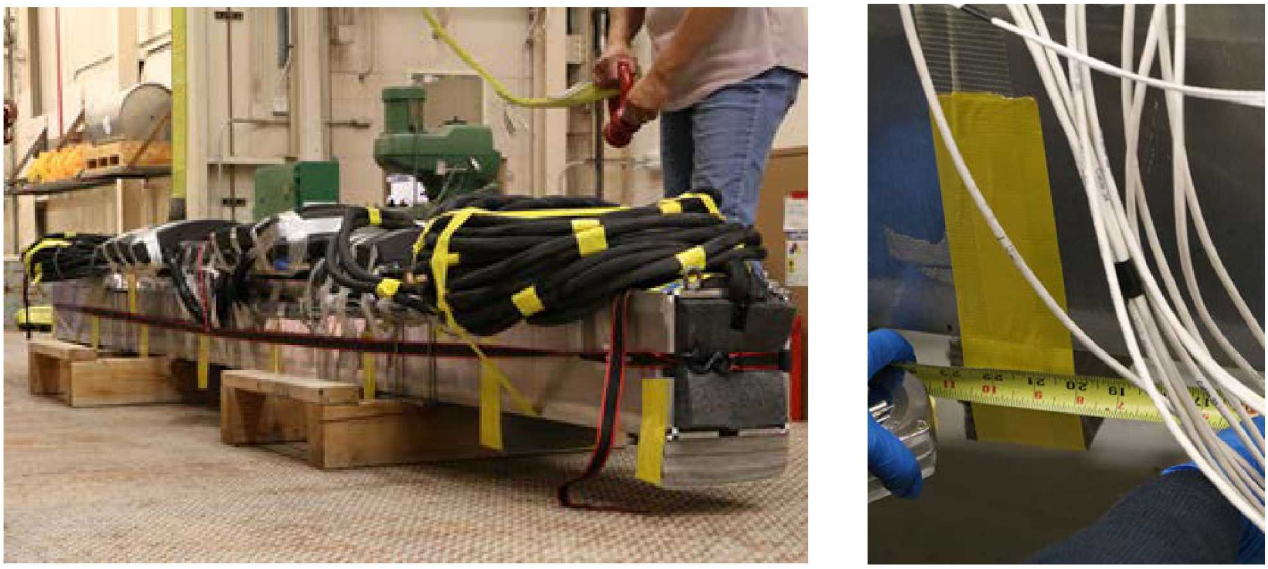

Figure 3-8. New Surrogate Assembly with 8 Felt Pads (left) and Close View of Felt Pad (right).

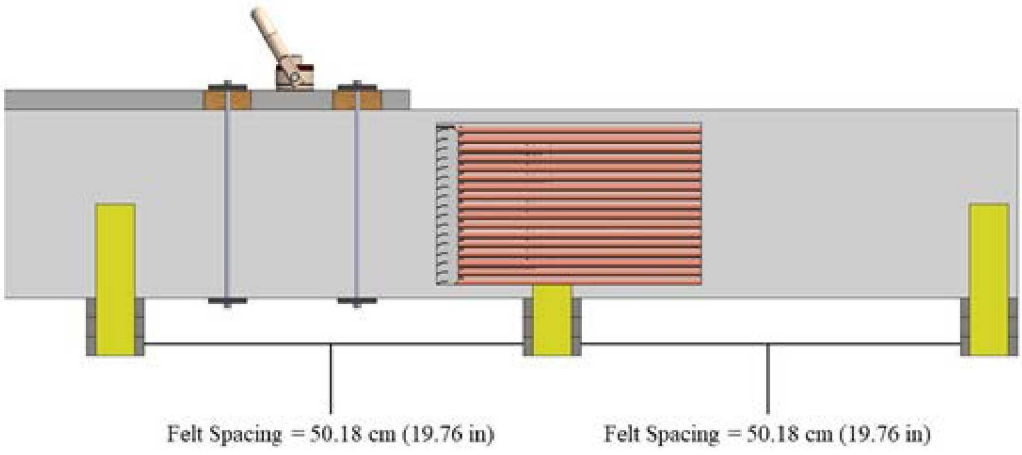

Figure 3-9. Felt Pad Spacing (2020 Test).

3.1.5 Pressure Paper

Pressure paper (Fujifilm) was used in both 30 cm drop tests (2019 and 2020) to record any contact between the rods and associated pressures. Table 3-1 shows the available types of the pressure paper. The types acquired were: Extreme Low (A), Super Low (B), Low (C), and Medium (D).

The pressure paper sheets were installed between 15 rods of the new surrogate assembly in 2 long spans and 2 short spans as shown in Figure 3-10 (top). The first pressure paper sheet was between rods 16 and 15 (counting from the assembly bottom) and the last one between the rods 1 and 2. The instrumentation precluded installation of the pressure paper between the rods 16 and 17. The details are provided in Section 4.4 (Figures 4-45 and 4-47).

The sequences in which the pressure sheets were installed are shown in Figure 3-10. The sequence started on the assembly top and was repeated until the assembly bottom. The covered pressure range was from 7.2 psi to 7,100 psi in the long spans and 7.2 psi to 350 psi in the short spans.

Originally, only the Extreme Low (A) and Super Low (B) paper was proposed for the 30 cm drop test because rod-to-rod contact was not anticipated. The 30 cm drop test with the damaged surrogate assembly (2019 test) suggested that such contact was possible. As a result, the Low (C) and Medium (D) pressure paper was added to the 2020 test and the pressure paper was also installed in two additional (short) spans. Figure 3-10 (bottom) shows how the pressure paper was installed in the 30 cm drop test with the damaged surrogate assembly (2019 test).

Figure 3-11 shows the installation of the pressure paper in 2020. The pressure paper was installed at the SNL test facility prior to the surrogate assembly placement into the basket tube.

Table 3-1. Fujifilm Pressure paper Specifications.

Table 1: Fujifilm Prescale® Specifications		
Film Type	**Roll Dimensions**	**Pressure Range**
Extreme Low (LLLLW/4LW)	9.8 ft × 12.2in (3 m × 310mm)	7.2–28 psi (0.5–1.97 kg/cm^2)
Ultra Low (LLLW)	16.4 ft × 10.6in (5 m × 270mm)	28–85 psi (2–6 kg/cm^2)
Super Low (LLW)	19.7 ft × 10.6in (6 m × 270mm)	70–350 psi (5–25 kg/cm^2)
Low (LW)	39.4 ft × 10.6in (12 m × 270mm)	350–1,400 psi (25–100 kg/cm^2)
Medium (MS)	39.4 ft × 10.6in (12 m × 270mm)	1,400–7,100 psi (100–500 kg/cm^2)
High (HS)	39.4 ft × 10.6in (12 m × 270mm)	7,100–18,500 psi (500–1,300 kg/cm^2)
Super High (HHS)	39.4 ft × 10.6in (12 m × 270mm)	18,500–43,200 psi (1,300–3,000 kg/cm^2)

New Surrogate Assembly (2020 Test)

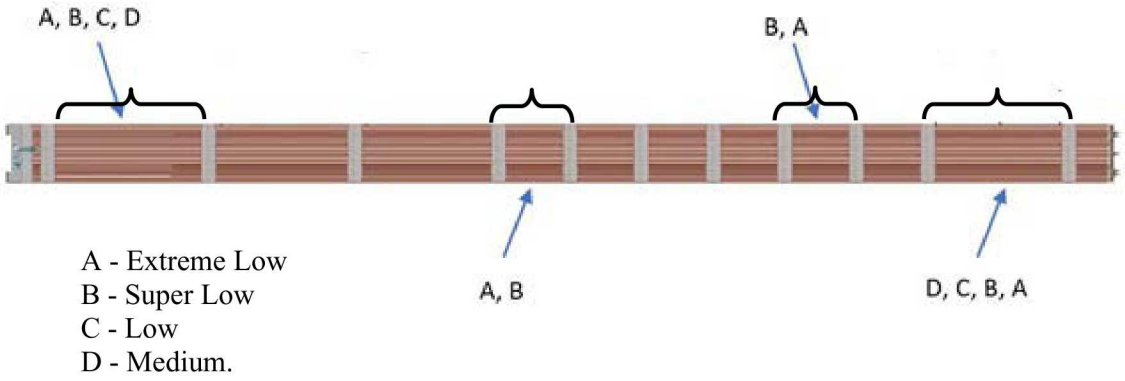

Old Damaged Surrogate Assembly (2019 Test)

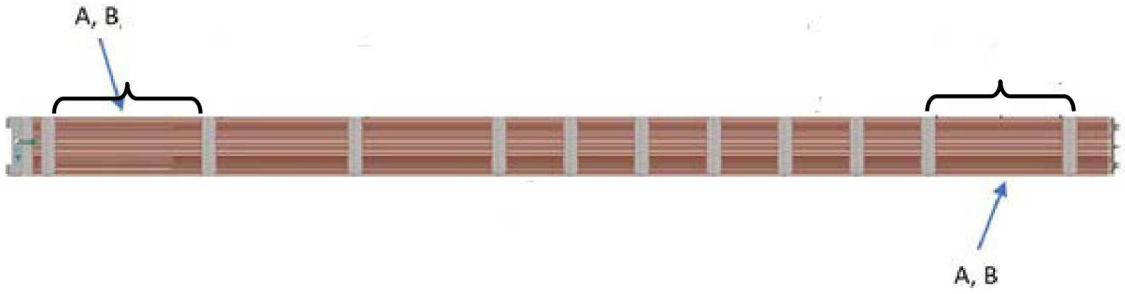

Figure 3-10. Pressure Paper Locations and Specifications.

Figure 3-11. Installation of Pressure Paper (2020 Test).

3.1.6 Handling

The instrumented surrogate assembly had to be inserted into the basket tube, transported to the SNL drop tower, and placed on the target for preparations for the tests. Figure 3-12 shows how the surrogate assembly was inserted into the basket tube.

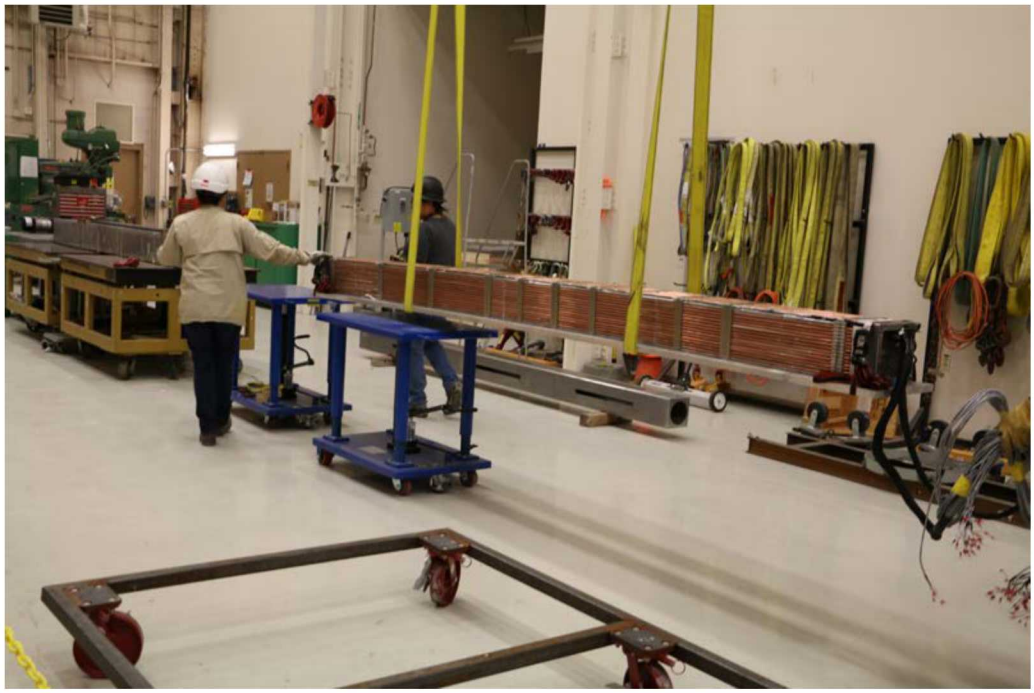

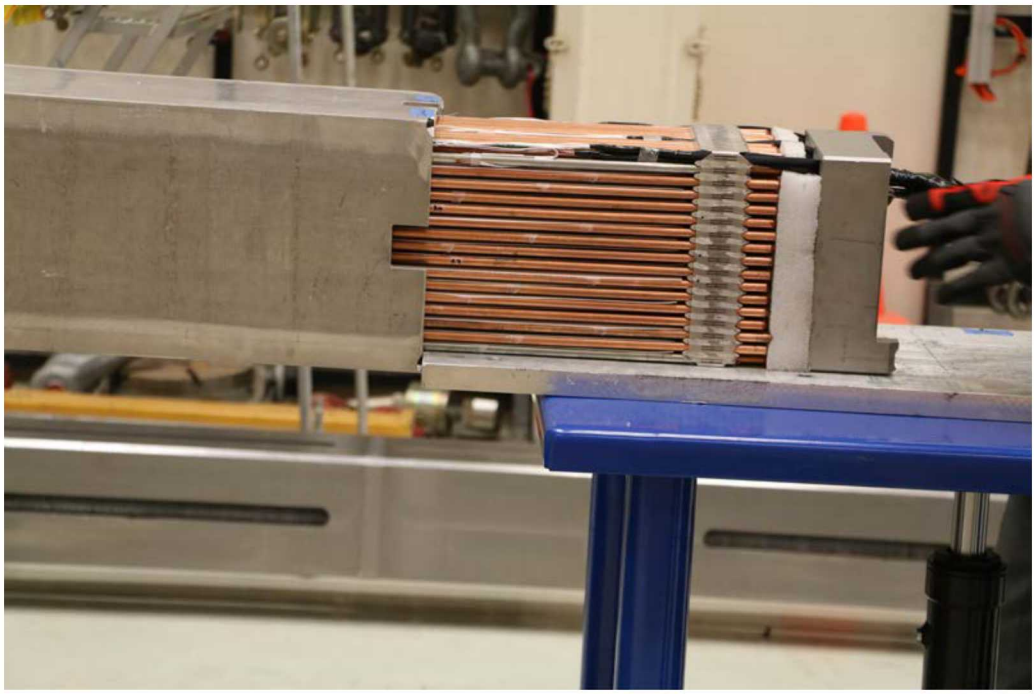

Figure 3-12. Surrogate Assembly Placement into the Basket Tube (2020 Test).

Prior to transport of the test unit, additional pressure paper sheets were placed between the rods through the basket window (Figure 3-13). This was done to provide evidence that vibration during the transport did not cause rod-to-rod contact.

The basket tube with the surrogate assembly was then loaded onto a flatbed trailer truck (Figure 3-14) and transported to the drop tower where it was unloaded (Figure 3-15) and placed on the target (Figure 3-16). Because of the handling accident in 2019 (Section 2), a critical lift plan was developed for the operations at the drop tower.

The additional pressure paper sheets were extracted and examined. They were blank meaning that no rod-to rod contact occurred during transport of the test unit.

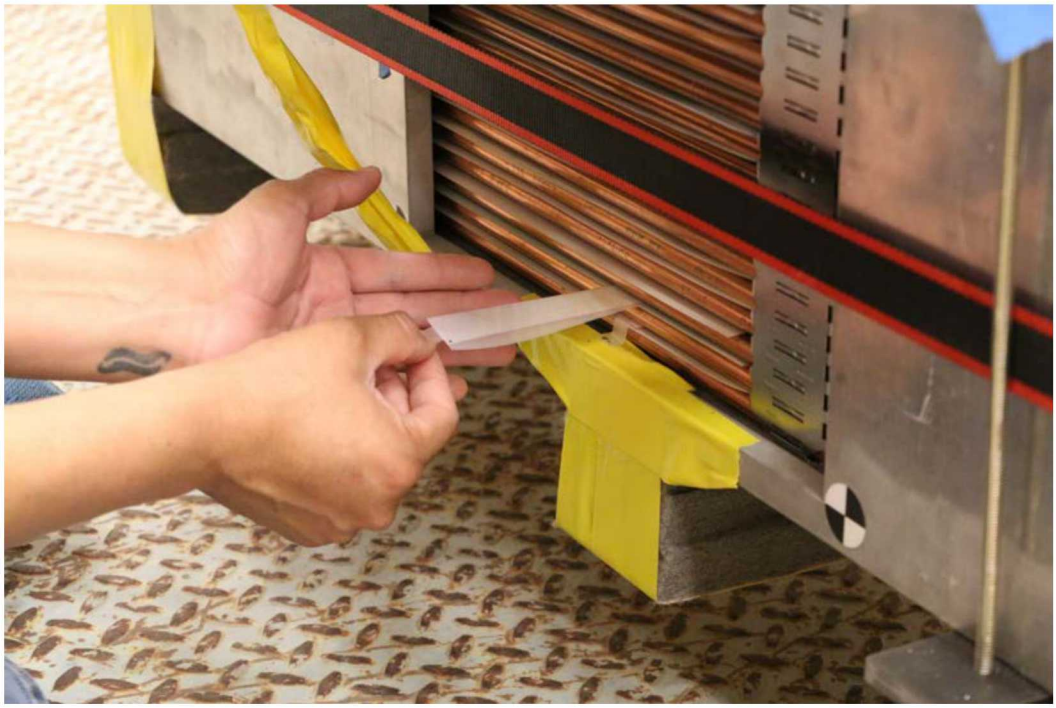

Figure 3-13. Placement of Pressure Paper Prior to Transport to the Drop Tower (2020 Test).

Figure 3-14. Test Unit Loaded on the Flatbed Trailer Truck (2020 Test).

Figure 3-15. Unloading Test Unit at the Drop Tower (2020 Test).

Figure 3-16. Placing the Test Unit on the Target (2020 Test).

3.1.7 Test Setup

The test setup is shown in Figure 3-17. A drawing of the unyielding target is shown in Figure 3-18. A photo of the SNL drop tower is shown in Figure 3-19.

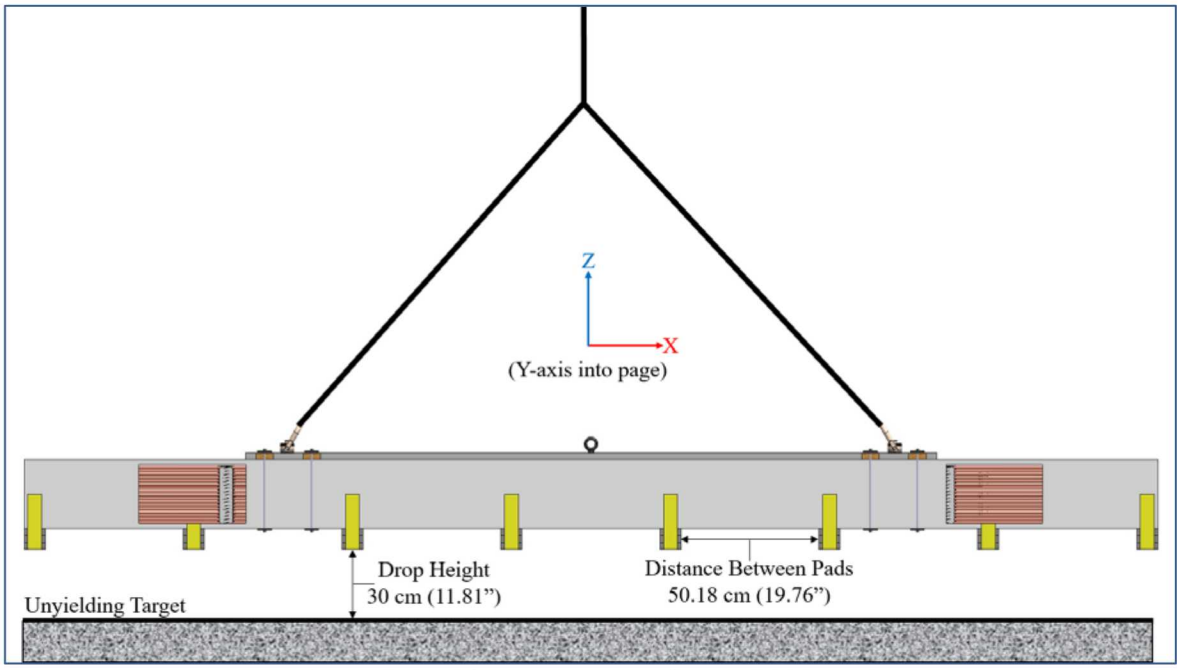

Figure 3-17. 30 cm Drop Test Setup (2020 Test).

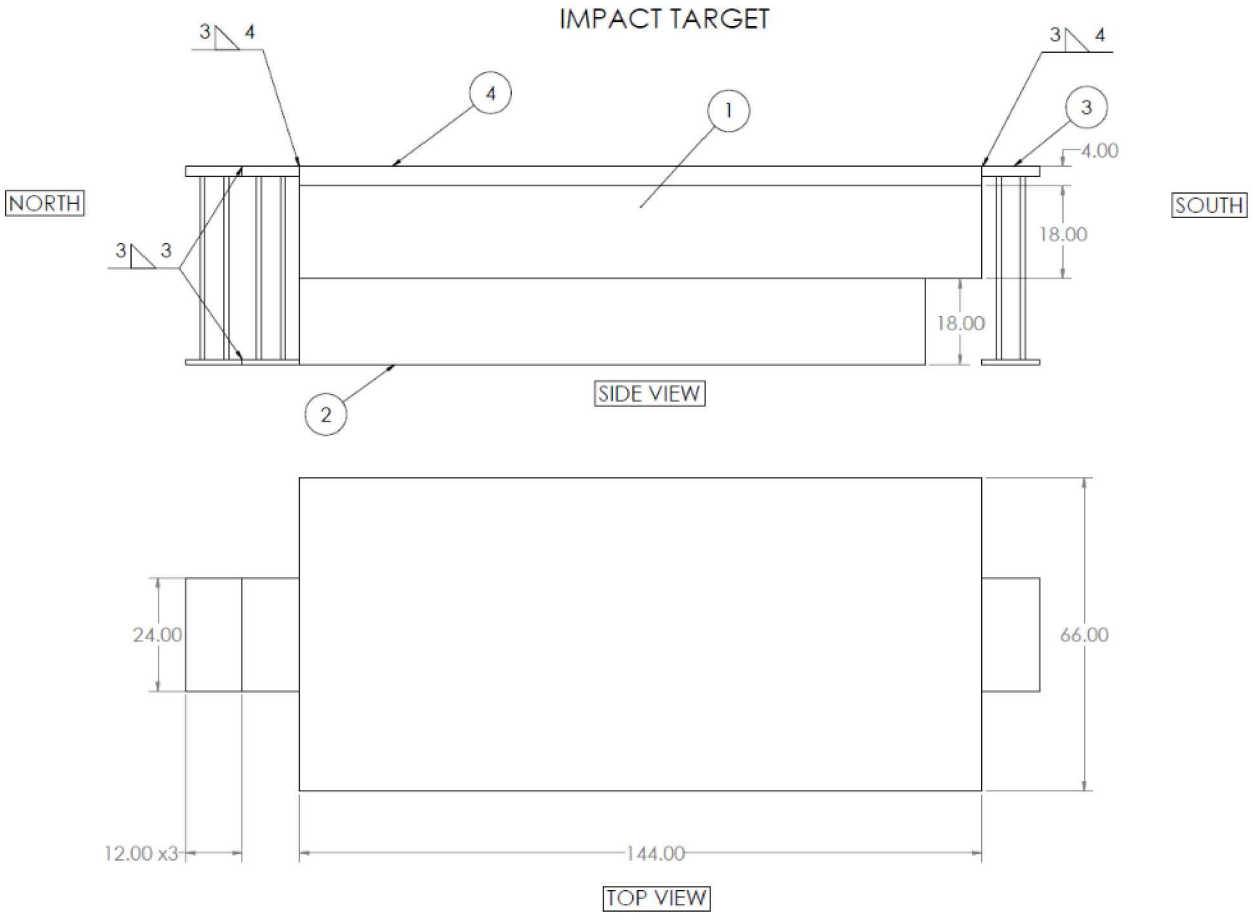

ITEM NO.	PART NUMBER	DESCRIPTION	QTY.
1	185' DT Concrete Target	Rienforced Concrete	1
2	185' DT Concrete Base	Rienforced Concrete	1
3	Steel Plate Extenders	A36 STEEL	3
4	185' DT Steel Plate	A36 STEEL	1

Figure 3-18. Unyielding Target Drawing.

Figure 3-19. SNL Outdoor Drop Tower.

3.1.8 Instrumentation

To provide consistency between the MMTT and 30 cm drop test, the full-scale surrogate assembly was instrumented in the same way as in the MMTT in both the 2019 and 2020 tests. The instrumentation of the surrogate assembly in the MMTT was guided by finite element modeling [16]. The locations of the sensors were selected to capture the peak strain values shown in Figure 3-20. Additional strain gauges were installed for the 30 cm drop test to provide the data required for validation of the modeling.

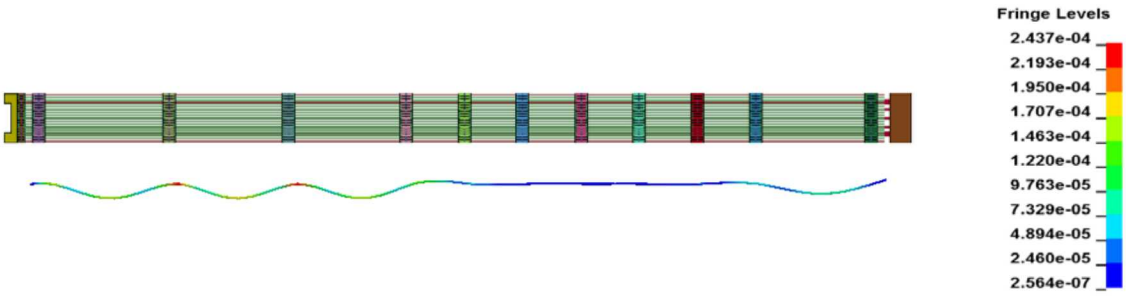

Figure 3-20. Peak Strain Locations for the 56.4 Hz Forced Vertical Excitation from [16].

The surrogate assembly instrumentation based on MMTT is shown in Figure 3-21 for the top nozzle end and in Figure 3-22 for the bottom nozzle end. The additional sensors on the surrogate assembly are shown in Figure 3-23. The instrumentation on the basket tube is shown in Figure 3-24. The instrumentation on the target surface is shown in Figure 3-25. The basket tube and target surface instrumentation was the same as in the 30 cm drop test of the dummy assembly [10].

The accelerometers were calibrated as documented in the instrumentation procedure.

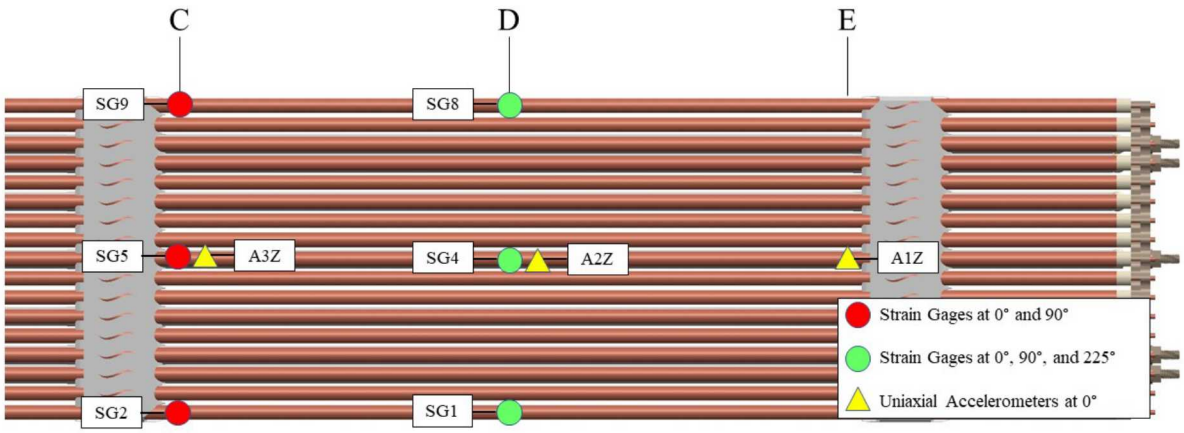

Figure 3-21. Top Nozzle End Instrumentation Based on MMTT (2019 and 2020 Tests).

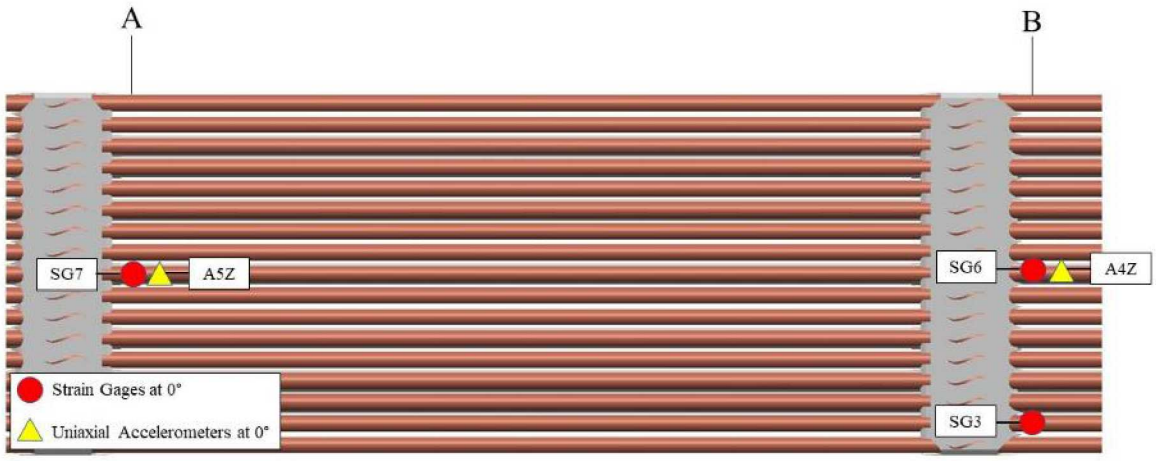

Figure 3-22. Bottom Nozzle End Instrumentation Based on MMTT (2019 and 2020 Tests).

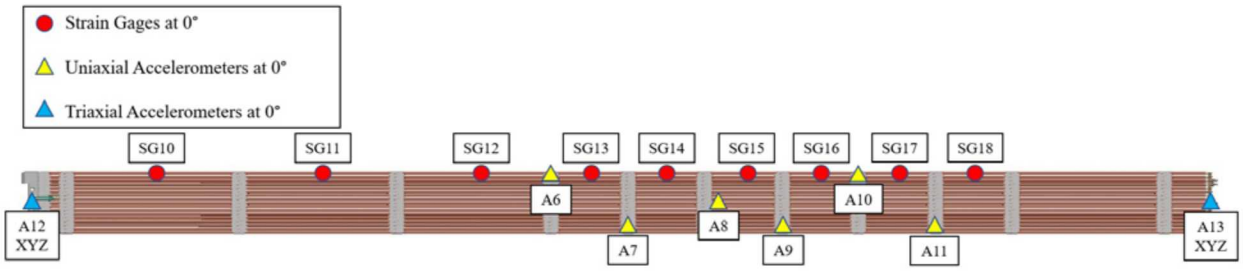

Figure 3-23. Additional Gauges Used in the 30 cm Drop Test (2019 and 2020 Tests).

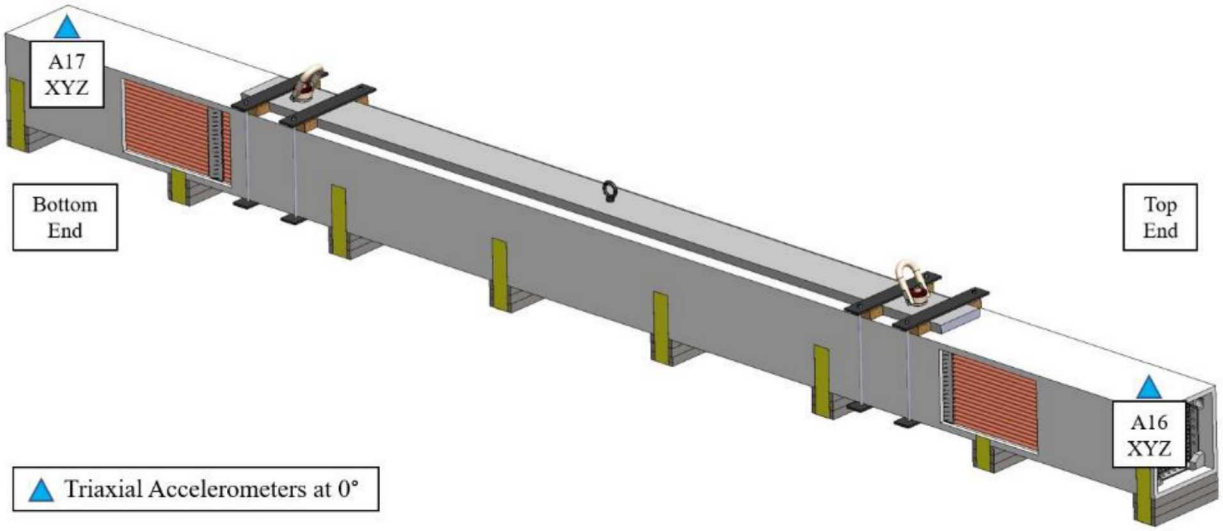

Figure 3-24. Basket Tube Instrumentation (2019 and 2020 Tests).

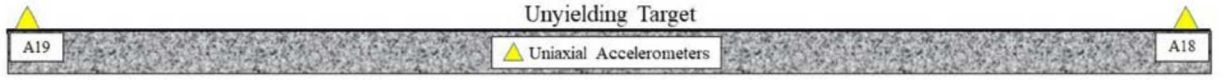

Figure 3-25. Target Surface Instrumentation (2019 and 2020 Tests).

Table 3-2 provides the nomenclature and locations for the accelerometers. Eleven uniaxial (vertical) accelerometers were installed on the surrogate assembly. Two triaxial accelerometers were installed – one on the top and one on the bottom nozzle. The sign convention for the accelerometer measurements was a right-hand rule with the longitudinal (x) along the assembly toward direction of the top nozzle, lateral (y) positive to the left when facing the bottom in a direction toward the top nozzle, and the vertical (z) positive upwards.

Three different Endevco Corporation accelerometer models (Table 3-2) were used:

- 7270A-20K (acceleration up to 20,000 g)
- 727-2K (acceleration up to 2,000 g)
- 7265A (acceleration up to 100 g)

The choice of the accelerometers was based on their availability, their use in the MMTT, and their size. The accelerometers are shown in Figure 3-26.

Figure 3-26. Accelerometer Models Used in 30 cm Drop Test (2019 and 2020).

Table 3-2. Accelerometer Locations and Nomenclature (2019 and 2020 Tests).

Channel	Gauge ID	Model Number	Location	Angular Location	Measurement Direction
31	A1Z	727-2K-10-120	Molly Pellets Rod	0°	Z
32	A2Z	727-2K-10-120	Molly Pellets Rod	0°	Z
33	A3Z	727-2K-10-120	Molly Pellets Rod	0°	Z
34	A4Z	727-2K-10-120	Molly Pellets Rod	0°	Z
35	A5Z	727-2K-10-120	Molly Pellets Rod	0°	Z
36	A6Z	727-2K-10-120	Lead Pellets Rod	0°	Z
37	A7Z	727-2K-10-120	Lead Rope	0°	Z
38	A8Z	727-2K-10-120	Molly Pellets Rod	0°	Z
39	A9Z	727-2K-10-120	Lead Rope	0°	Z
40	A10Z	727-2K-10-120	Lead Pellets Rod	0°	Z
41	A11Z	727-2K-10-120	Lead Rope	0°	Z
42	A12X	727-2K-10-120	Bottom Nozzle	0°	X
43	A12Y	727-2K-10-120	Bottom Nozzle	0°	Y
44	A12Z	727-2K-10-120	Bottom Nozzle	0°	Z
45	A13X	727-2K-10-120	Top Nozzle	0°	X
46	A13Y	727-2K-10-120	Top Nozzle	0°	Y
47	A13Z	727-2K-10-120	Top Nozzle	0°	Z
54	A16X	7270A-20K	Basket Tube	0°	X
55	A16Y	7270A-20K	Basket Tube	0°	Y
56	A16Z	7270A-20K	Basket Tube	0°	Z
57	A17X	7270A-20K	Basket Tube	0°	X
58	A17Y	7270A-20K	Basket Tube	0°	Y
59	A17Z	7270A-20K	Basket Tube	0°	Z
60	A18Z	7265A	Impact Surface	0°	Z
61	A19Z	7265A	Impact Surface	0°	Z

Note: The instrumented rods were zircaloy tubes, one with lead rope, one with molybdenum (molly) pellets, and one with lead pellets.

Table 3-3 provides the nomenclature and locations for the strain gauges. Twenty-seven strain gauges in 18 locations were installed. Three locations had 3 strain gauges at 0^0, 90^0, and 225^0. Three locations had 2 strain gauges at $0^0$and 90^0. Twelve locations had one strain gauge at 0^0.

Table 3-3. Strain Gauge Locations and Nomenclature (2019 and 2020 Tests).

Channel	Micro-Measurement Part-number	Strain Gauge Designation	Angular Location	Cask Assembly
1	CEA03-062UW-350	SG1-0	0°	Lead Rope
2	CEA03-062UW-350	SG1-90	90°	Lead Rope
3	CEA03-062UW-350	SG1-225	225°	Lead Rope
4	CEA03-062UW-350	SG2-0	0°	Lead Rope
5	CEA03-062UW-350	SG2-90	90°	Lead Rope
6	CEA03-062UW-350	SG3-0	0°	Lead Rope
7	CEA03-062UW-350	SG4-0	0°	Surrogate
8	CEA03-062UW-350	SG4-90	90°	Molly Pellets Rod
9	CEA03-062UW-350	SG4-225	225°	Molly Pellets Rod
10	CEA03-062UW-350	SG5-0	0°	Molly Pellets Rod
11	CEA03-062UW-350	SG5-90	90°	Molly Pellets Rod
12	CEA03-062UW-350	SG6-0	0°	Molly Pellets Rod
13	CEA03-062UW-350	SG7-0	0°	Molly Pellets Rod
14	CEA03-062UW-350	SG8-0	0°	Lead Pellets Rod
15	CEA03-062UW-350	SG8-90	90°	Lead Pellets Rod
16	CEA03-062UW-350	SG8-225	225°	Lead Pellets Rod
17	CEA03-062UW-350	SG9-0	0°	Lead Pellets Rod
18	CEA03-062UW-350	SG9-90	90°	Lead Pellets Rod
19	CEA03-062UW-350	SG10-0	0°	Lead Pellets Rod
20	CEA03-062UW-350	SG11-0	0°	Lead Pellets Rod
21	CEA03-062UW-350	SG12-0	0°	Lead Pellets Rod
22	CEA03-062UW-350	SG13-0	0°	Lead Pellets Rod
23	CEA03-062UW-350	SG14-0	0°	Lead Pellets Rod
24	CEA03-062UW-350	SG15-0	0°	Lead Pellets Rod
25	CEA03-062UW-350	SG16-0	0°	Lead Pellets Rod
26	CEA03-062UW-350	SG17-0	0°	Lead Pellets Rod
27	CEA03-062UW-350	SG18-0	0°	Lead Pellets Rod

Note: The instrumented rods were zircaloy tubes, one with lead rope, one with molybdenum (molly) pellets, and one with lead pellets.

The strain gauges were type CEA-03-062UW-350 (Figure 3-27). Strain gauges with resistances of 350 ohms are commonly used in experimental stress analysis testing. 350-ohm gauges allow for reducing heat generation (for the same applied voltage across the gauge), to decrease leadwire effects, and to improve signal-to-noise ratios in the gauge circuit (CEA-062UWA-350 DATASHEET).

Figure 3-28 shows the installation of sensors on the top nozzle end of the surrogate assembly.

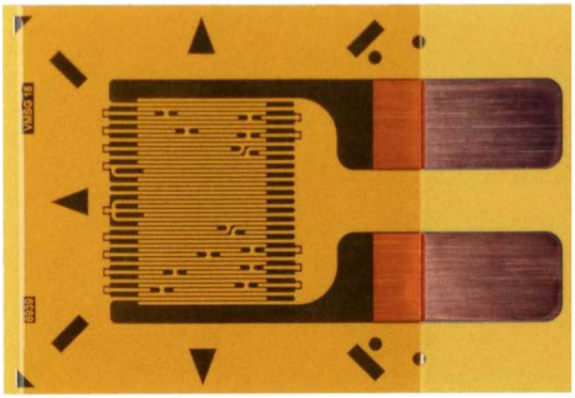

Figure 3-27. Strain Gauge CEA-03-062UW-350.

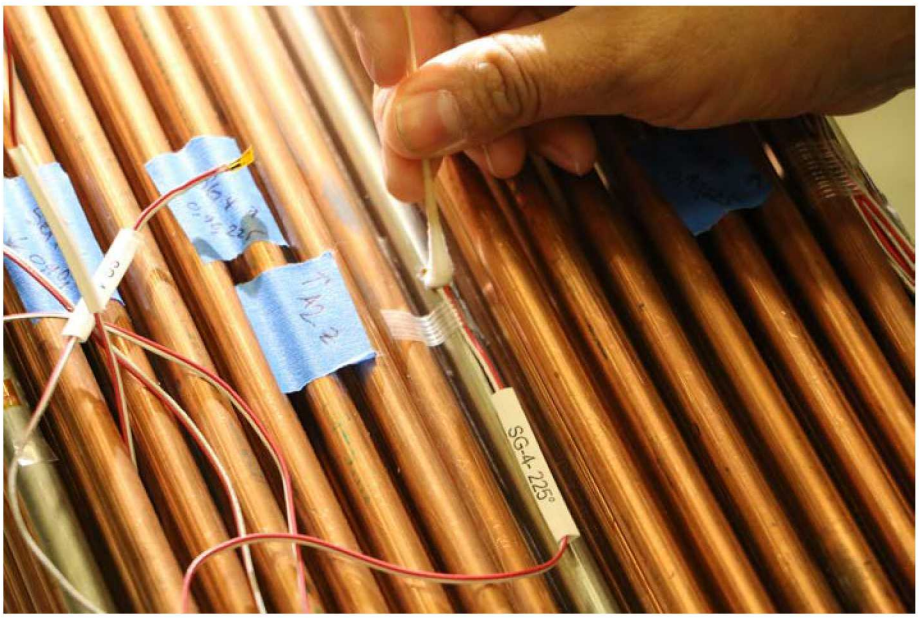

Figure 3-28. Installation of Sensors on the Top Nozzle End of the Surrogate Assembly (2020 Test).

3.1.9 Conducting Drop Tests

The test unit was transported to the drop tower in the morning of May 7, 2020. It was unloaded and placed on the target as described in Section 3.1.6. The test unit was then lifted up and situated in accordance with the test setup (Section 3.1.7). The measurements were taken to confirm that the lowest point of unit is 30 cm (+1 cm, -0 cm) above target and unit angle is horizontal 0° (± 0.5° axial and ±1.0° transverse). The following measurements were taken at the time of impact from the high-speed video cameras:

- Impact Velocity: 2.4 m/s
- Pitch: 0.1 +/- 0.1 deg
- Roll: 0.6 /- 0.3 deg
- Yaw: 1.8 +/- 0.1 deg

The test unit was connected to the same SNL portable data acquisition system that was used for the MMTT. The acceleration data were collected at a frequency of 204,800 Hz. The strain data were collected at a frequency of 102,400 Hz. Note that in 2019 the data collection frequency in the 30 cm drop test with

the dummy assembly and old damaged surrogate assembly was 51,200 Hz. This is because new data collection cards were purchased for the system in 2020 that allowed faster collection rates. Figure 3-29 shows the surrogate assembly seconds before it was dropped at 11:32 am on May 7, 2020. Figure 3-30 shows the surrogate assembly just before the impact.

Figure 3-29. Test Unit Seconds before the 30 cm Drop (May 7, 2020, 11:32 am).

Figure 3-30. Test Unit Just before the Impact (May 7, 2020).

After the test the surrogate assembly was loaded into the flatbed trailer truck and transported to the test facility.

On May 11, 2020 the surrogate assembly was removed from the basket tube (Figure 3-31). The pressure paper sheets were extracted and scanned. The original scans are provided in Appendix B. Appendix C provides the original scans from the 2019 30 cm drop test with an old damaged assembly.

The assembly was examined, and the examination results were documented.

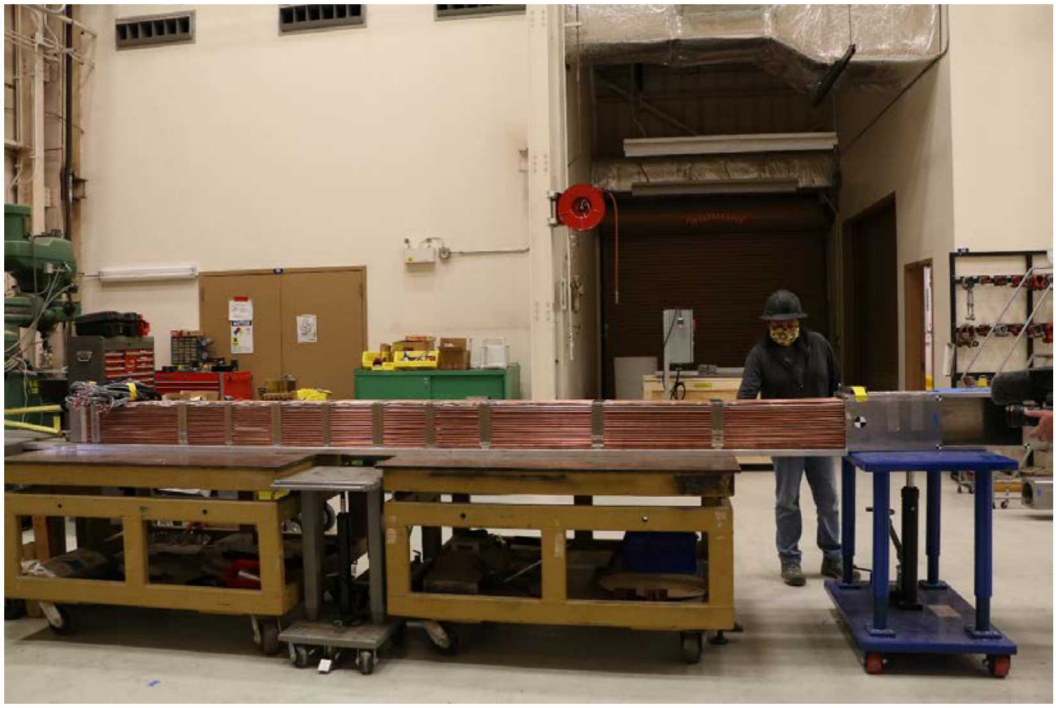

Figure 3-31. Removing Surrogate Assembly from the Basket Tube (May 11, 2020).

4. DATA ANALYSIS

4.1 Spacer Grid Examination

The surrogate assembly was pulled from the basket tube at the test facility on May 11, 2020. The visual examination of the assembly showed spacer grid deformation at the bottom of the grid. The height of the spacer grid was measured on the left and on the right sides of the surrogate assembly (as identified in Figure 4-1). The photos taken during the measurements are provided in Appendix A.

Figure 4-1 shows the spacer grid measurement nomenclature. Table 4-1 provides the post-test measurements. Figure 4-2 displays the post-test spacer grid height at each location on both sides of the assembly. The original spacer grid height was 214.2 mm. This height remained only in location 1. Some degree of deformation was observed at the other locations. The red rectangles in Figures 4-1 and 4-2 show two locations with the largest deformation. The maximum grid crushing of 6.1 mm was observed on the left side of the assembly at grid 10 (second spacer grid from the bottom nozzle end). The maximum difference between the spacer grid height on the left and right sides of the assembly (left and right sides are labeled in Figure 4-1) was 1.13 mm. The same height was measured on the left and right sides at location 5.

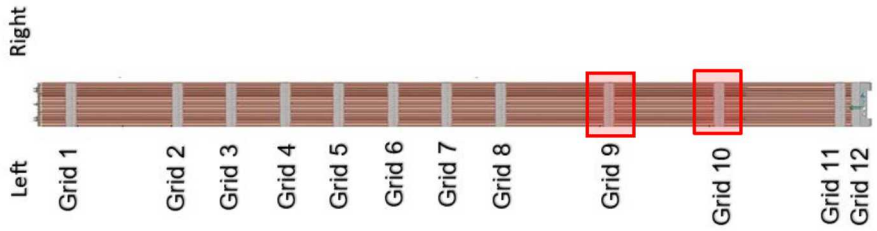

Figure 4-1. Spacer Grid Measurement Nomenclature.

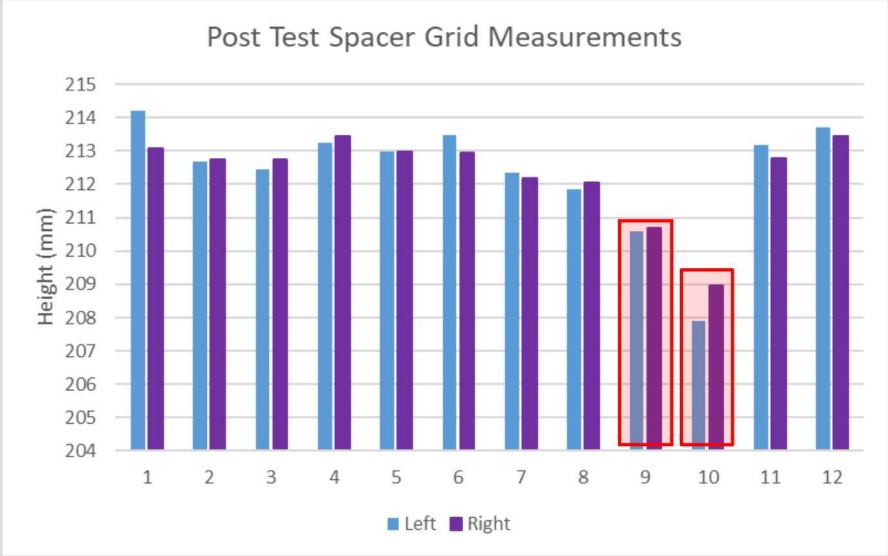

Note: Left and right sides are labeled in Figure 4-1.

Figure 4-2. Post Test Spacer Grid Height (2020 Test).

Table 4-1. Post-Test Spacer Grid Measurements* (2020 Test).

Grid # (Figure 4-1)	Left Side Measurement		Right Side Measurement	
	in.	mm	in.	mm
1	8.4340	214.22	8.3895	213.09
2	8.3730	212.67	8.3765	212.76
3	8.3635	212.43	8.3750	212.73
4	8.3955	213.25	8.4030	213.44
5	8.3850	212.98	8.3850	212.98
6	8.4045	213.47	8.3835	212.94
7	8.3600	212.34	8.3540	212.19
8	8.3405	211.85	8.3490	212.06
9	8.2915	210.60	8.2945	210.68
10	8.1850	207.90	8.2265	208.95
11	8.3925	213.17	8.3770	212.78
12	8.4140	213.72	8.4035	213.45

* The undeformed measurement for the spacer grid is 214.22 mm (8.434 in).

Figure 4-3 compares the spacer grid measurements performed on the old damaged surrogate assembly after the 2019 test and the new surrogate assembly after 2020 test. The damaged assembly has slightly larger spacer grid deformation, except a few locations. The spacer grid locations with the largest deformation were the same on the damaged and on the new surrogate assemblies. The maximum spacer grid crushing observed on the damaged surrogate assembly (2019 test) was 6.3 mm, which was 0.2 mm larger than the maximum spacer grid crushing on the new assembly (2020 test).

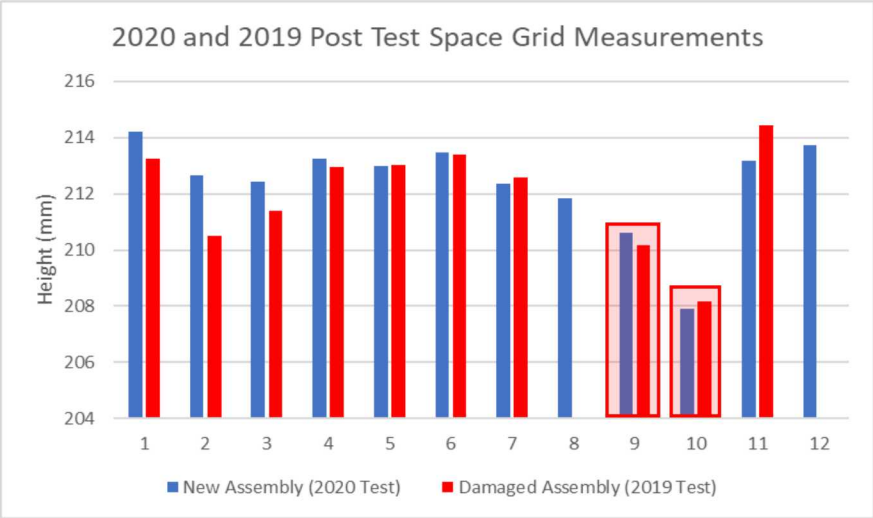

Figure 4-3. Post-Test Spacer Grid Height in the 2020 and 2019 Tests (assembly right side).

The photos of spacer grid 10 on the left and right sides of the assembly are shown in Figure 4-4 (2020 Test, new assembly) and Figure 4-5 (2019 Test, damaged assembly). In both cases, the deformation is at the bottom of the assembly.

The basket tube experienced deformation beneath the windows cut on the side of the tube during the 2019 drop test. Figure 4-6 shows the deformed portion of the basket tube. The maximum deformation was about 4 mm.

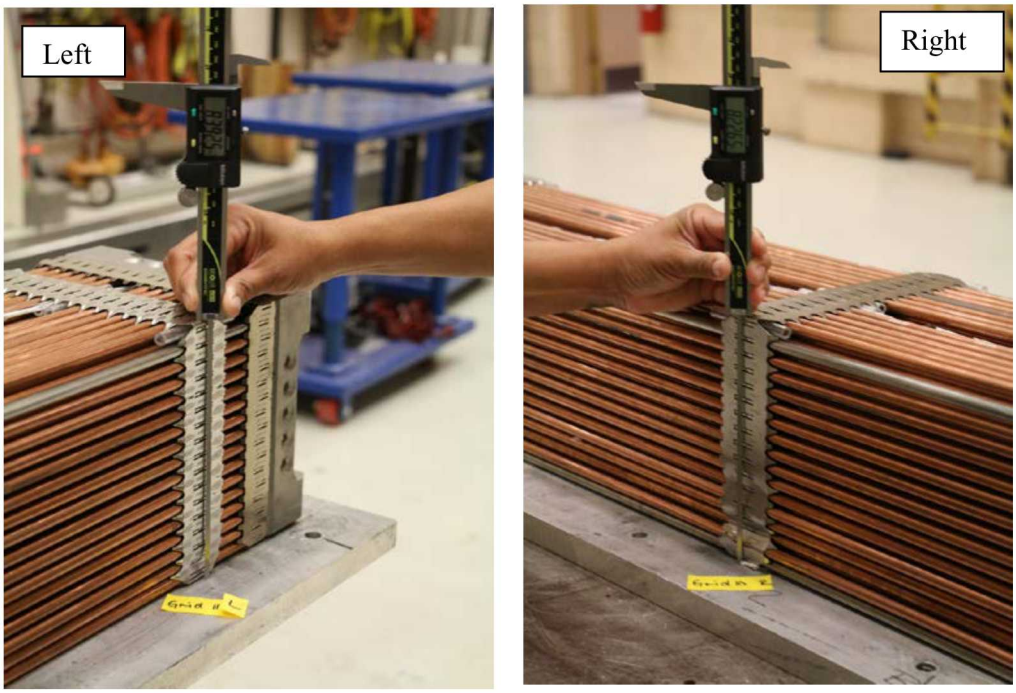

Figure 4-4. Spacer Grid 10 with Largest Deformation in the 2020 Test.

Figure 4-5. Spacer Grid 10 with Largest Deformation in the 2019 Test.

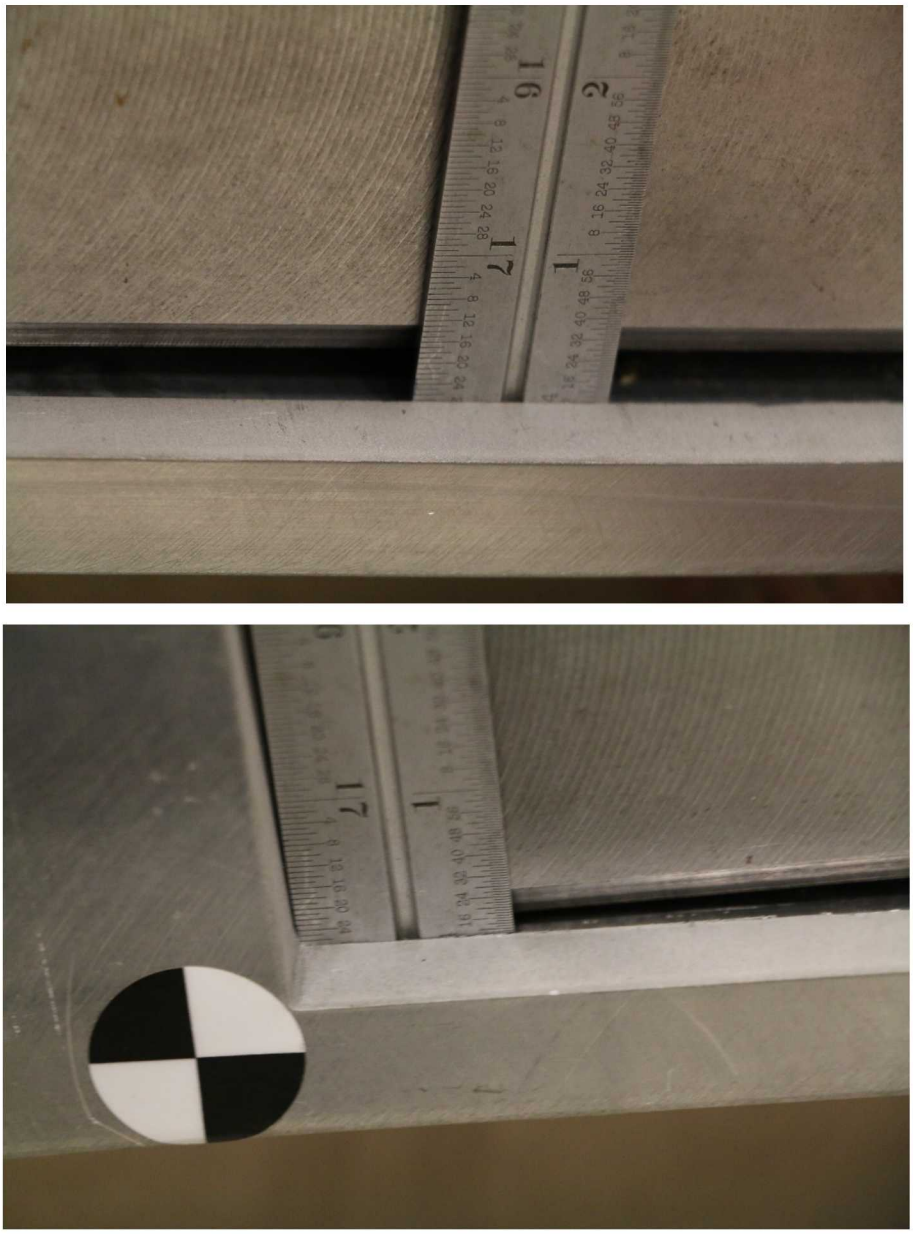

Figure 4-6. Basket Tube Deformation beneath the Observation Window (2020 Test).

4.2 Acceleration Data

The surrogate assembly instrumentation included 11 vertical accelerometers on the surrogate assembly rods and 2 triaxial accelerometers, one on the top and the other one on the bottom nozzle. The instrumentation details are provided in Section 3.1.8. The acceleration data were collected at a frequency of 204,800 Hz.

The data analysis used K2, an SNL software package that allows for processing very large data arrays using a variety of digital signal processing algorithms. Signal processing algorithms supported by this software include: Infinite Impulse Response (IIR) filters, Finite Impulse Response (FIR) filters, Fast Fourier Transform (FFTs), Integration, Differentiation, Force, Displacement, Power Spectra Density

(PSD), Shock Response Spectra (SRS), Convolution, Correlation, and many others. The algorithms implemented in K2 were taken from [17] and [18].

The expected acceleration pulses and the acceleration pulses observed on the full-scale dummy assembly are discussed in Section 1 and are shown in Figure 1-7. The expected peak acceleration on the top nozzle end was 33 g (this end hit the target first) and on the bottom nozzle end was 56 g. The observed peak acceleration on the dummy assembly was 37.5 g (both ends hit the target practically at the same time).

The acceleration pulses during the first impact on the top nozzle end (A1Z) and the bottom nozzle end (A5Z) of the new surrogate assembly during the 2020 test are shown in Figure 4-7. The accelerations were filtered to 300 Hz using a Butterworth low pass 6-pole filter. The peak accelerations were 38 g (top end) and 54 g (bottom end). The top end hit the target first, same as in the 1/3 scale cask 30 cm drop test. The averaged peak acceleration (Figure 4-7) was 36 g. The observed acceleration pulses are in good agreement with the expected ones. The averaged acceleration pulse is in good agreement with the observed acceleration pulse on the dummy assembly. Consequently, the effects of the impact limiters and cask were adequately represented in the 2020 test.

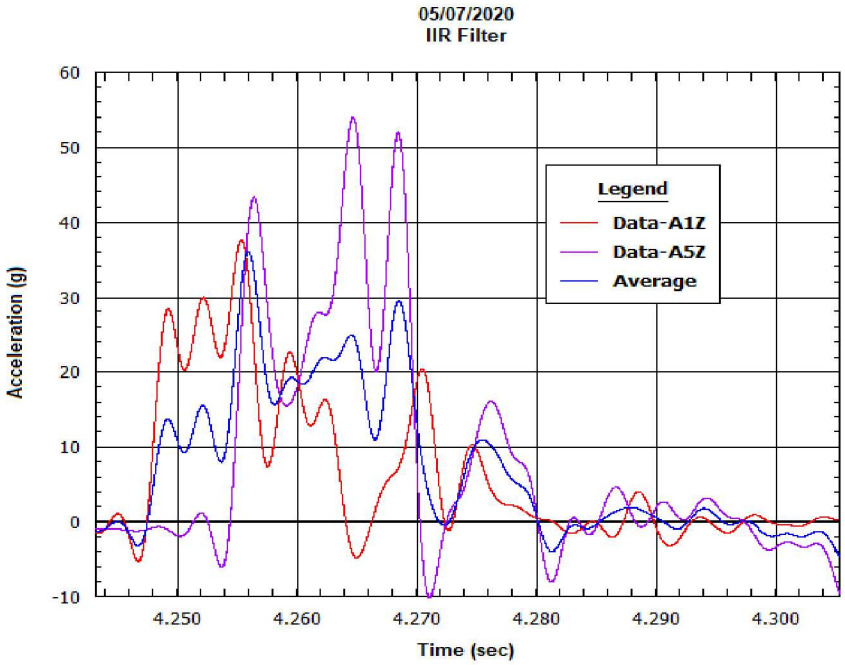

Note: A1Z is on the top end and A5Z is on the bottom end of the surrogate assembly.

Figure 4-7. Surrogate Assembly Acceleration Pulses During the First Impact (2020 Test).

Figure 4-8 compares the acceleration shock response spectra (SRS) of the dummy assembly, damaged surrogate assembly (2019 test), and new surrogate assembly (2020 test). The new assembly SRS is very similar to the dummy one up to 50 HZ. Some small differences are present in the higher frequency domain. The new surrogate assembly has a peak around 60 Hz related to the assembly natural frequency. Similar peaks were observed during the MMTT shock events [1]. The damaged surrogate assembly SRS envelops the responses of the dummy and new surrogate assemblies. It has 3 peaks in the lower frequency (up to 10 Hz). These peaks are not present in the dummy and new surrogate assembly SRS. They reflect the structural changes in the damaged assembly.

Figure 4-9 shows the acceleration power spectrum density (PSD) of the acceleration on the top end of the surrogate assembly (A1Z) during the first impact in the 2020 test. The greatest power spectra density is

within the frequency domain up to 150 Hz. Consequently, using the 300 Hz low pass filter is appropriate. The PSD, as well as SRS, has a peak associated with the assembly natural frequency.

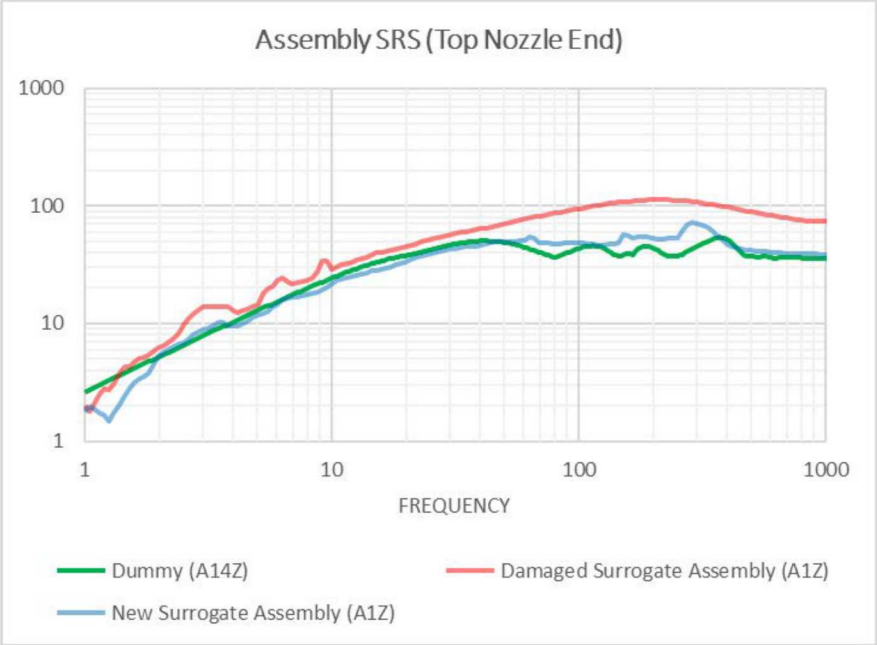

Figure 4-8. Acceleration SRS of Dummy and Damage Surrogate Assemblies (2019 Test) and New Surrogate Assembly (2020 Test).

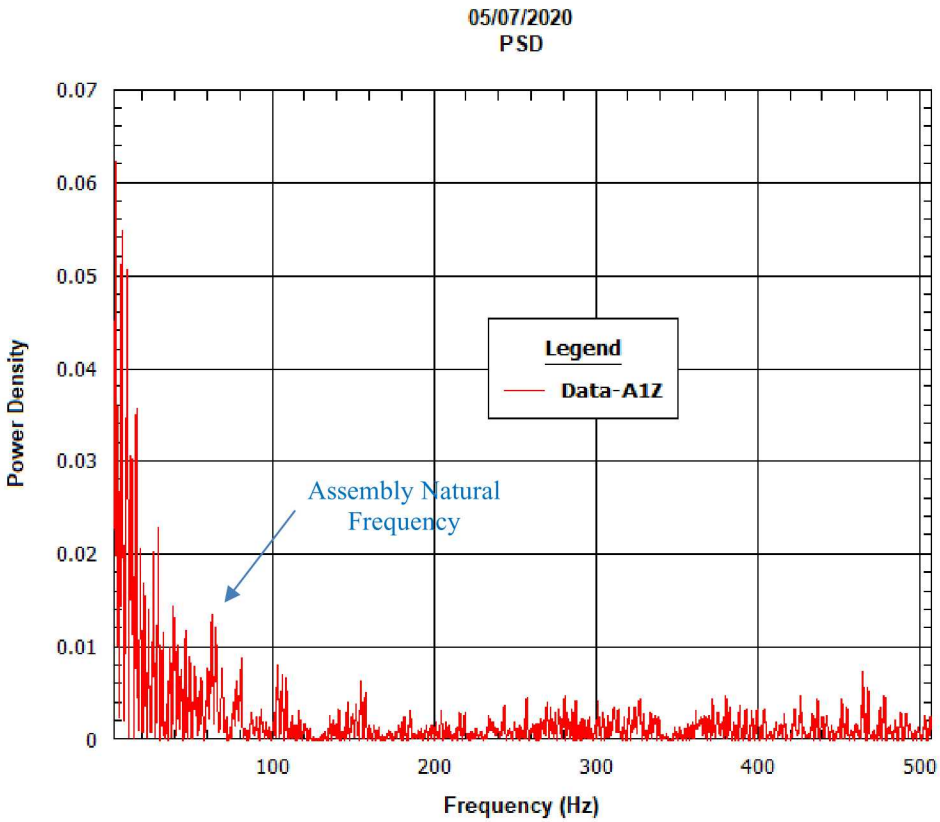

Figure 4-9. Acceleration PSD on the New Surrogate Assembly Top End (2020 Test).

Figure 4-10 shows the first impact velocity time histories (top end and bottom end) calculated by integrating the observed accelerations on the surrogate assembly. The velocity during the first impact is ~2.5 m/s. This is close to the video measurement (2.4 m/s).

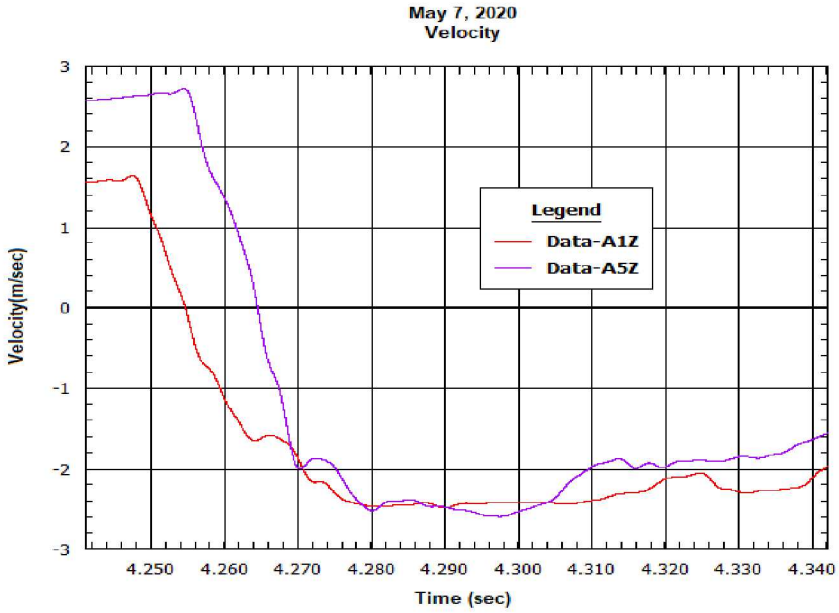

Figure 4-10. Surrogate Assembly Impact Velocity (2020 Test).

The acceleration pulses during the first impact on the other accelerometers on the top end of the surrogate assembly are shown in Figure 4-11. The pulse shapes and peak values are similar to the A1Z pulse shown in Figure 4-7.

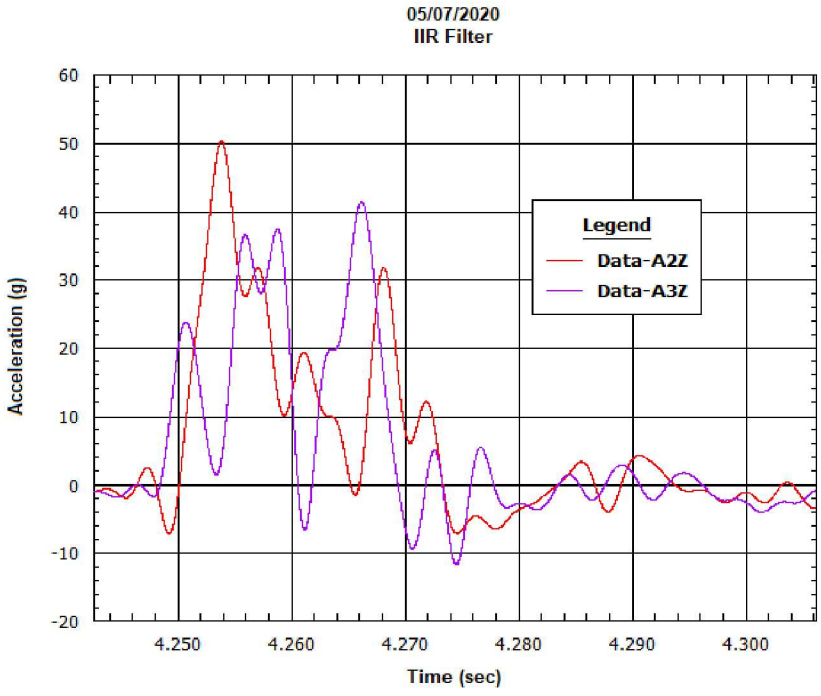

Figure 4-11. New Surrogate Assembly Acceleration Pulses During the First Impact (2020 Test).

The acceleration time histories in the 2020 and 2019 tests are compared in Figure 4-12 (top figure). They are similar in their shapes and peak values. The acceleration pulses during the first impact are compared in the bottom figure (Figure 4-12). The time in this figure is counted from the moment of the first impact to provide a better comparison.

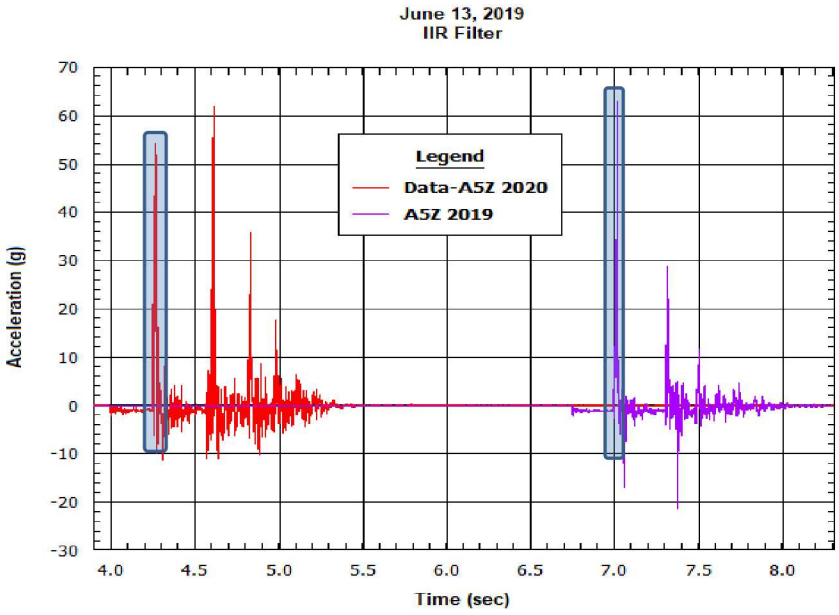

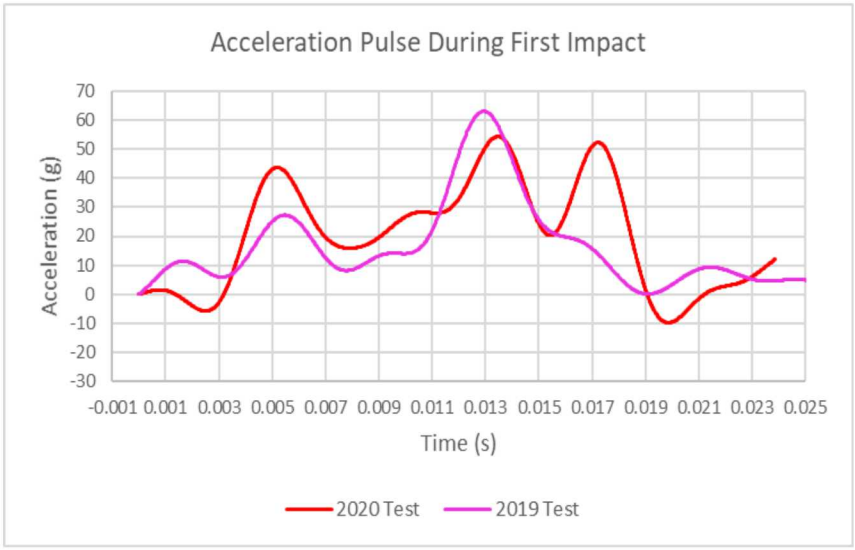

Note: Top figure shows the acceleration time histories for the duration of the test and the bottom figure shows the acceleration pulses during the first impact.

Figure 4-12. Surrogate Assembly Acceleration Time Histories in the 2020 and 2019 Tests.

The peak accelerations on the top and bottom ends of the new (2020 test) and damaged (2019 test) surrogate assemblies during the first impact are compared in Figure 4-13. In both cases, the impact occurred first on the top end. The peak accelerations on the top end are higher in the 2019 test compared to the 2020 test. The peak accelerations on the bottom end are lower in the 2019 test compared to the 2020 test. The bottom end was a slap down end in both the 2019 and 2020 tests. It appears that the assembly damage (crushed spacer grid) resulted in a smaller slap down effect or that the impact during

the 2019 test was closer to perfectly horizontal, perhaps due to the deformation of the basket tube from the 2019 test that was present at the start of the 2020 test.

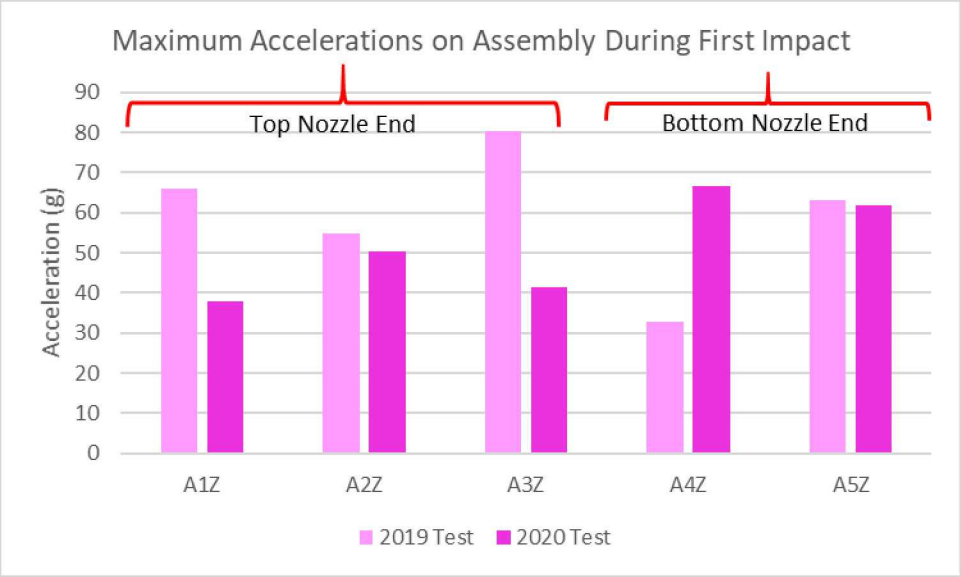

Figure 4-13. Peak Surrogate Assembly Accelerations During the First Impact in the 2020 and 2019 Tests.

The similar acceleration pulse shape and peak values suggest that comparable peak strains might be expected in 2019 and 2020 tests.

4.3 Strain Data

The axial strain was measured with 18 strain gauges (positioned at 0^0). The lateral strain was measured with 6 strain gauges (positioned at 90^0). The combination (axial and lateral) strain was measured with 3 strain gauges (positioned at 225^0). The instrumentation details are provided in Section 3.1.8. The strain data were collected at a frequency 102,400 Hz.

The minimum and maximum strain values were derived from the analysis of unfiltered time histories corrected for bias. The bias function available in K2 was used. The Bias function performs an offset on the Y (acceleration or strain) axis input data. This does not change the data; it corrects for any offset in the data by taking the average Y-value in the time period before the impact and subtracting this value from the entire data record. This allows for obtaining adequate (not affected by an offset) maximum and minimum values. Figure 4-14 shows an example of the original strain time history and the time history corrected for bias for the strain gauge SG2-0.

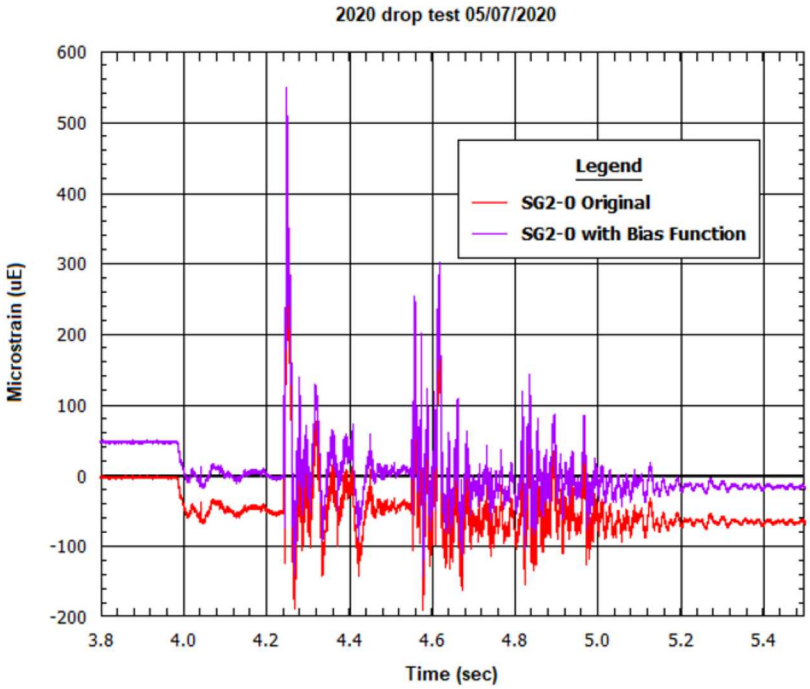

Figure 4-14. Example of Strain Data Correction for Bias (Strain Gauge SG2-0), 2020 Test.

The corrected for bias peak strain values are provided in Table 4-2 for the 2020 (new surrogate assembly) and 2019 tests (old damaged surrogate assembly). The peak values were derived from all the data, not just the first impact data. In a few occasions the peak values were higher during the second impact in response to the higher accelerations during the second impact (Figure 4-12).

Table 4-2. Corrected for Bias Peak Strain in the 2020 and 2019 Tests.

Strain Gauge	Corrected for Bias Peak Strain (microstrain)			
	2020 Test (New Assembly)		2019 Test (Old Damaged Assembly)	
	Min	Max	Min	Max
SG1-0	-940.3	257.2	-1639.6	906.7
SG1-225	-240.6	530.4	-742.8	1255.2
SG1-90	-233.4	298.3	-114.9	109.7
SG2-0	-150.7	539.3	-297.8	579.7
SG2-90	-146.0	121.8	-423.0	739.8
SG3-0	-372.2	815.4	-105.4	101.3
SG4-0	-465.8	441.7	-880.2	305.6
SG4-225	-440.1	326.4	-254.6	472.6
SG4-90	-156.0	268.5	-164.0	246.6
SG5-0	-213.6	395.0	-650.3	111.4
SG5-90	-86.9	221.0	-107.8	273.0
SG6-0	-213.2	609.2	-519.9	140.0
SG7-0	-324.9	689.0	-310.1	657.4
SG8-0	-1008.2	221.1	-1736.0	605.5
SG8-225	-175.4	639.9	-606.1	1412.3
SG8-90	-194.3	121.0	-164.6	173.0
SG9-0	-164.4	473.0	-588.9	248.4
SG9-90	-66.6	119.4	-95.0	150.8
SG10-0	-1723.5	467.0	-1209.8	416.1
SG11-0	-1169.2	637.5	-696.9	316.6
SG12-0	-1027.8	524.6	-777.0	287.5
SG13-0	-516.5	397.5	-360.8	185.7
SG14-0	-464.2	290.6	-351.0	195.5
SG15-0	-404.2	284.8	-305.6	188.9
SG16-0	-440.5	239.4	-531.7	276.9
SG17-0	-464.3	306.4	-256.1	340.3
SG18-0	-585.3	314.3	-571.5	269.0

Table 4-3. Raw (Not Corrected for Bias) Peak Strain in the 2020 and 2019 Tests.

Strain Gauge	Raw Peak Strain (microstrain)			
	2020 Test (New Assembly)		2019 Test (Old Damaged Assembly)	
	Min	Max	Min	Max
SG1-0	-941.621	255.833	-1639.34	906.94
SG1-225	-233.568	298.12	-742.664	1255.32
SG1-90	-240.77	530.274	-115.034	109.609
SG2-0	-190.733	499.261	327.835	549.741
SG2-90	-131.011	136.841	-463.041	699.796
SG3-0	-373.379	814.167	-106.734	100.044
SG4-0	-466.837	440.682	-840.189	345.582
SG4-225	-156.305	268.143	-284.565	442.556
SG4-90	-440.152	326.34	184.038	226.579
SG5-0	-283.574	325.022	-640.296	121.421
SG5-90	-87.1128	220.748	-117.84	263.029
SG6-0	-213.971	608.462	-499.863	160.032
SG7-0	-384.885	629.022	-330.117	637.386
SG8-0	-1011.74	217.553	-1656.01	685.468
SG8-225	-193.317	121.964	-676.097	1342.3
SG8-90	-174.946	640.393	-166.512	171.113
SG9-0	-254.39	382.954	-548.885	288.376
SG9-90	-66.0391	119.945	-105.039	140.777
SG10-0	-1725.1	465.324	-1169.76	456.069
SG11-0	-1169.88	636.83	-676.926	336.637
SG12-0	-1028.51	523.854	-776.825	287.759
SG13-0	-516.714	397.222	-361.031	185.53
SG14-0	-464.764	289.982	-316.493	272.592
SG15-0	-404.462	284.483	-325.573	168.946
SG16-0	-441.068	238.859	-561.738	246.925
SG17-0	-484.269	286.365	-296.056	300.305
SG18-0	-625.3	274.25	-551.531	289.018

To display the strain data statistics the box and whisker plots were used. The bottom end of the box represents the first quartile. The top end of the box represents the third quartile. The median and mean are shown as a line and a cross inside the box respectively . The whiskers indicate variability outside the upper and lower quartiles and any point outside those lines or whiskers is considered an outlier. The whisker ends show the minimum and maximum values if these values are within the variability range.

Figure 4-15 compares the statistics of the peak negative and peak positive strain data for all 27 strain gauges (0^0, 90^0, and 225^0). Figure 4-16 compares the statistics of the peak negative and peak positive axial (0^0) strain data (18 strain gauges). The absolute negative peak strain values are larger than the positive strain values in both figures. However, when only the axial peak strain data are compared, the

positive peak strain values become noticeably lower than the absolute negative peak strain values. This indicates that the upward bending is noticeably greater than the downward bending, which is an expected response to an upward impact force.

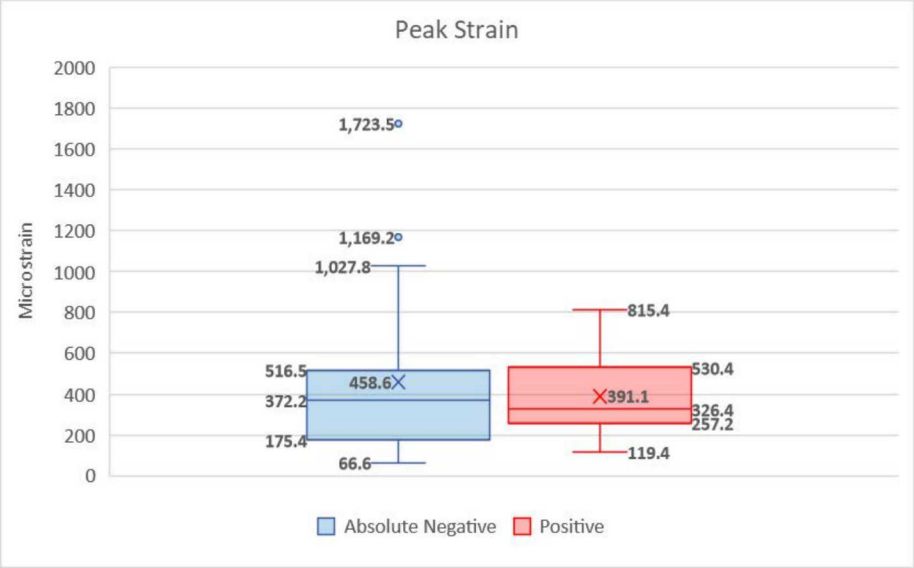

Figure 4-15. Statistics of Negative and Positive Peak Strain (2020 Test).

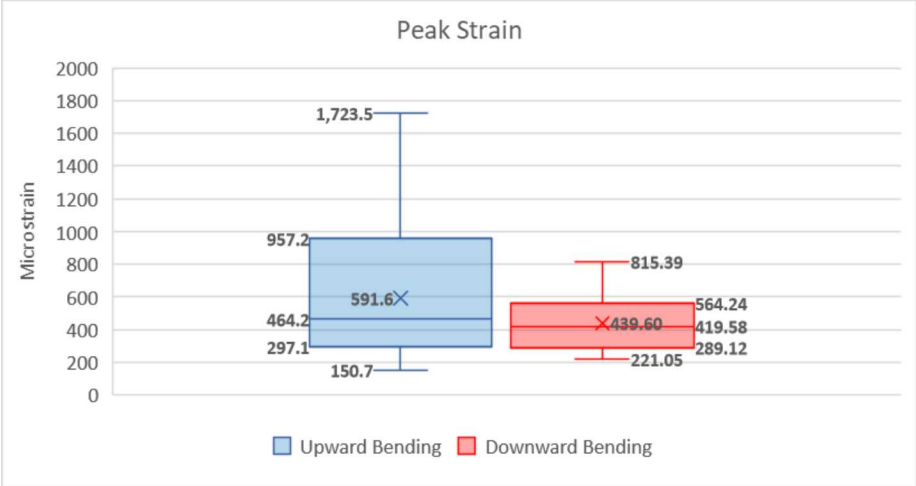

Figure 4-16. Statistics of Negative and Positive Axial Peak Strain (2020 Test).

Figures 4-17 and 4-18 show the peak positive and peak negative value for each of 27 strain gauges respectively in 2020 test. In these figures 0^0 strain gauges are shown in blue, 90^0 gauges are shown in green, and 225^0 gauges are shown in red. The maximum negative peak strain was observed in SG10-0. The next two highest negative values were observed in SG11-0 and SG-12. These three strain gauges were located at the bottom end of the assembly. The higher strains at the bottom end reflect the higher acceleration at this end during the slap down (Figure 4-7). The highest positive peak strain was observed in strain gauge SG3-0, which is closer to the top end of the assembly. The peak strains observed in the strain gauges located on the short spacer grid spans (SG13-0, SG14-0, SG15-0, SG16-0, SG17, and SG18-0) were noticeably lower as expected (Section 3.1.8, Figure 3-20). The lateral (90^0) and combination (225^0) peak strain values were generally lower than the axial ones except a few peak negative strain cases. This is consistent with the vertical upward impact force.

The indication of lateral bending can be seen on the pressure paper. Figure 4-19 displays the scan of the pressure paper that was inserted between the 3rd and 4th rods at the assembly bottom end after the 2020 test. The lateral bending created a widened trace of the rod as shown in this figure.

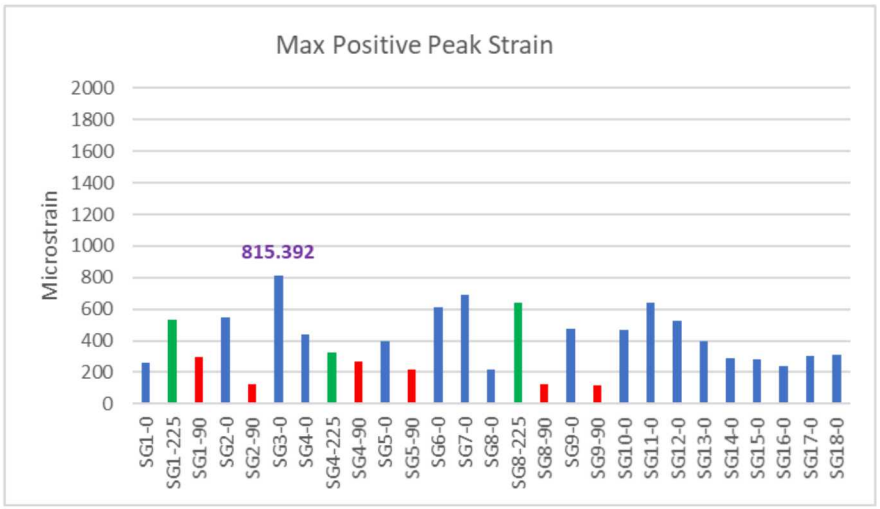

Note: 0^0 strain gauges are shown in blue, 90^0 strain gauges are shown in green, and 225^0 strain gauges are shown in red.

Figure 4-17. Maximum Positive Peak Strains (2020 Test).

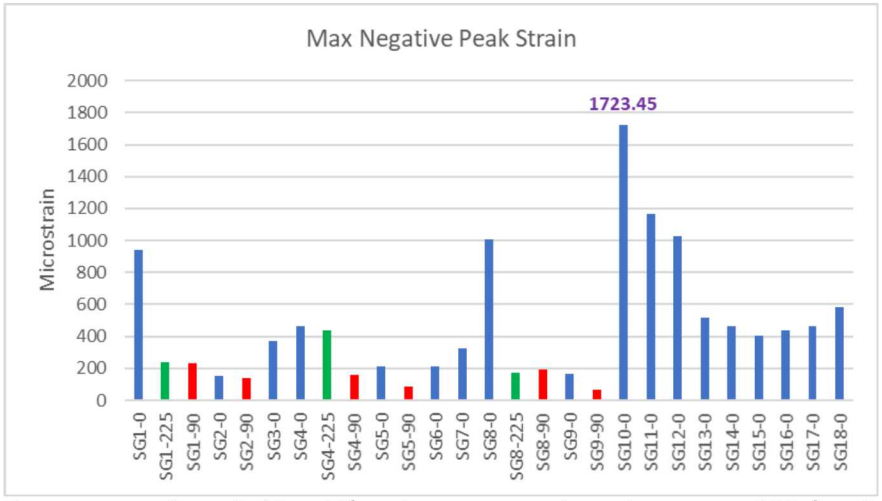

Note: 0^0 strain gauges are shown in blue, 90^0 strain gauges are shown in green, and 225^0 strain gauges are shown in red.

Figure 4-18. Maximum Negative Peak Strains (2020 Test).

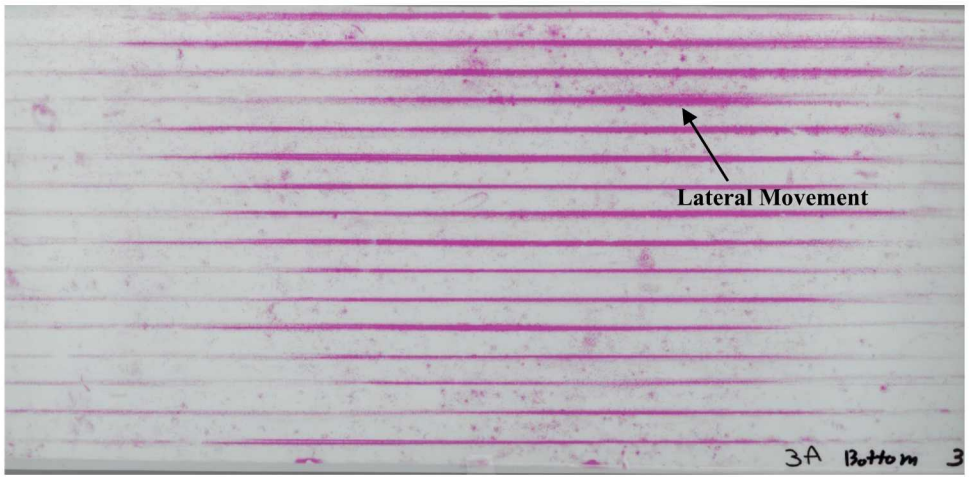

Figure 4-19. Extreme Low Pressure Paper Between the 3rd and 4th Rods at the Bottom End of the Assembly after the 2020 Test.

Figures 4-20 – 4-25 compare the statistics of the strain observed in the 2020 and 2019 tests.

Figures 4-20 and 4-21 compare the peak negative and positive strain values from the 2020 and 2019 tests. The data from all strain gauges (0°, 90°, and 225°) are shown. The peak negative and positive strain values observed in the 2020 test are slightly lower compared to the 2019 test.

Figures 4-22 and 4-23 compare the peak negative and positive axial strain values from the 2020 and 2019 tests. The peak negative and positive axial strain values observed in the 2020 test are somewhat higher compared to the 2019 test.

Figures 4-24 and 4-25 compare the peak negative and positive lateral strain values from the 2020 and 2019 tests. The peak negative and positive lateral strain values observed in the 2020 test are somewhat lower compared to the 2019 test.

Generally, in the 2020 test the strain due to upward and downward bending was somewhat higher and the strain due to the lateral bending was slightly lower compared to the 2019 test. The possible explanation is that the pre-test crushing of the spacer grid in the 2019 test limited the ability of the rods to bend in vertical direction and caused more bending in the lateral direction.

Note that the absolute maximum strain values are very similar in the 2019 test with the old damaged assembly and the 2020 test with the new assembly. Thus, the effects of the pre-test spacer grid crushing are relatively small.

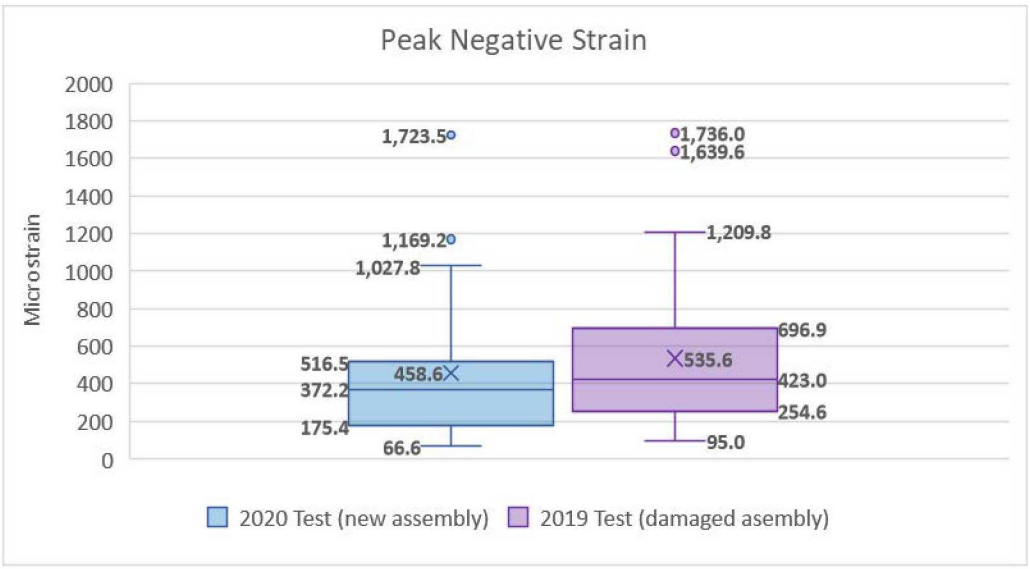

Figure 4-20. Statistics of Peak Negative Strain Values Observed in the 2020 and 2019 Tests.

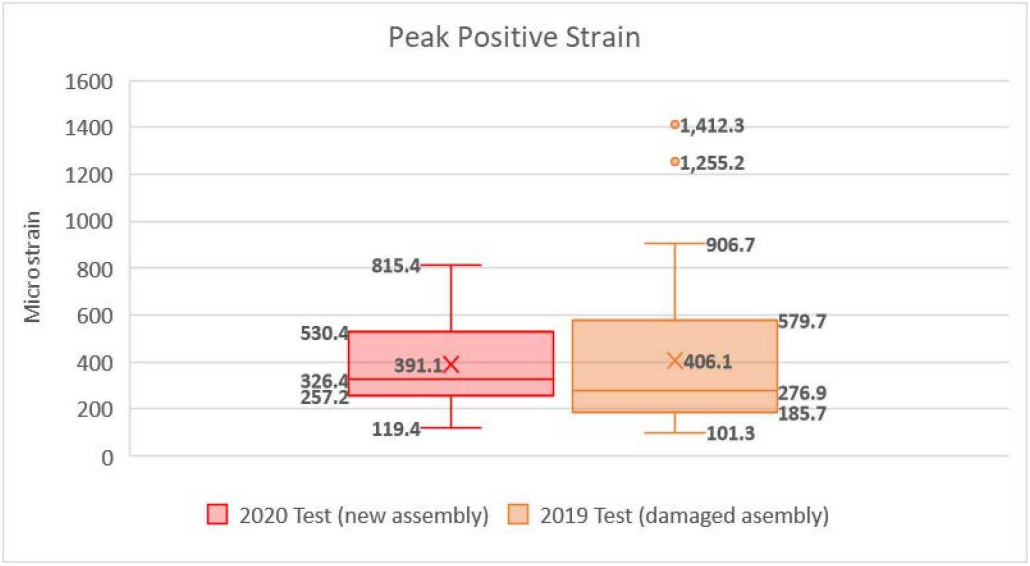

Figure 4-21. Statistics of Peak Positive Strain Values Observed in the 2020 and 2019 Tests.

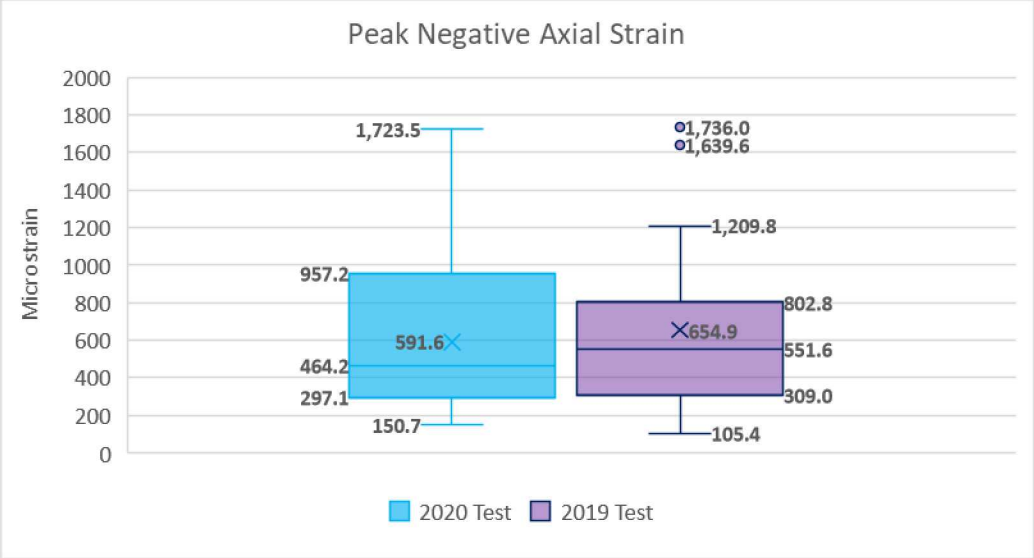

Figure 4-22. Statistics of Peak Negative Axial Strain Values Observed in the 2020 and 2019 Tests.

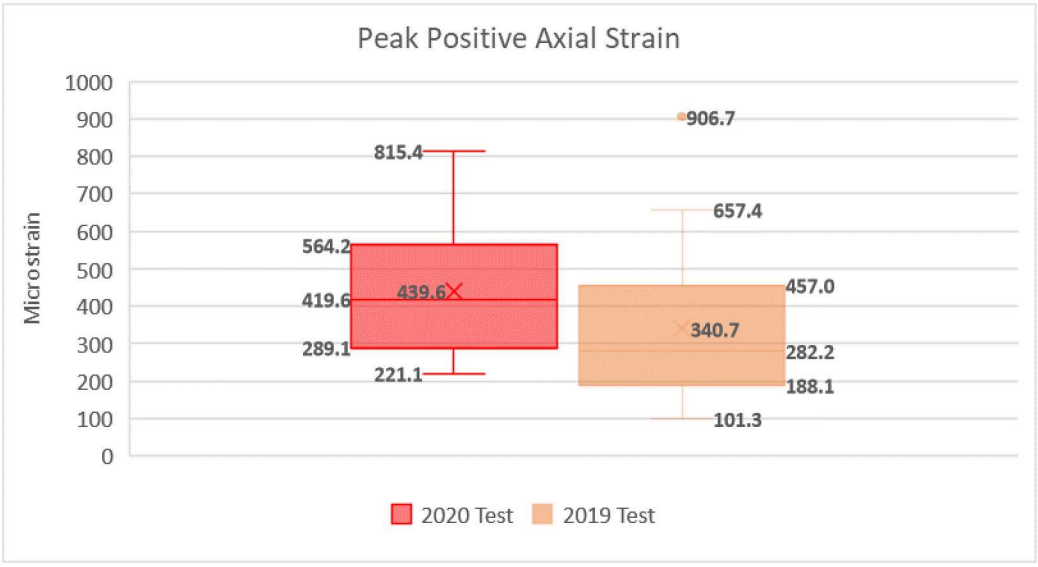

Figure 4-23. Statistics of Peak Positive Axial Strain Values Observed in the 2020 and 2019 Tests.

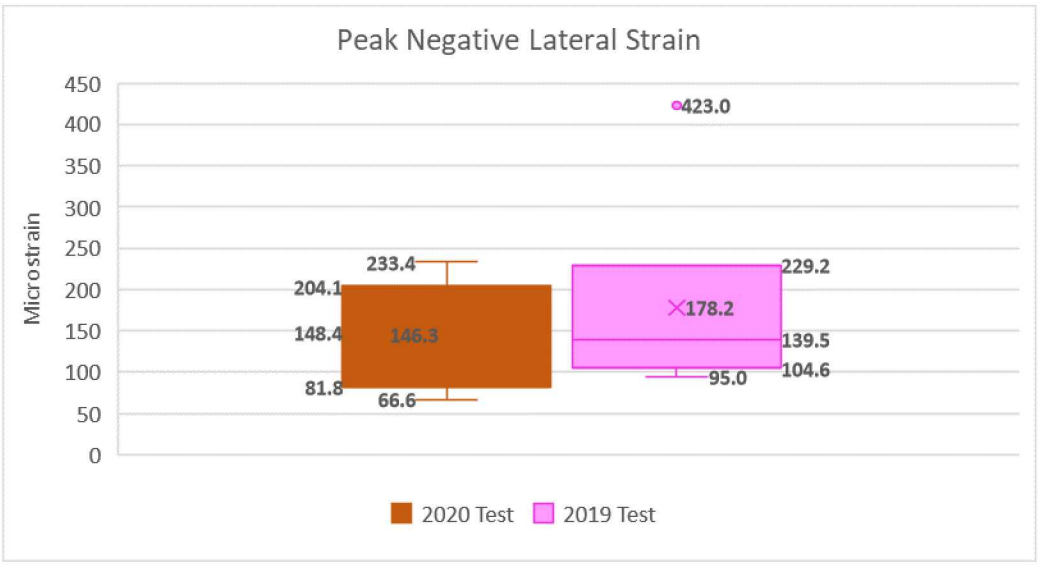

Figure 4-24. Statistics of Peak Negative Axial Strain Values Observed in the 2020 and 2019 Tests.

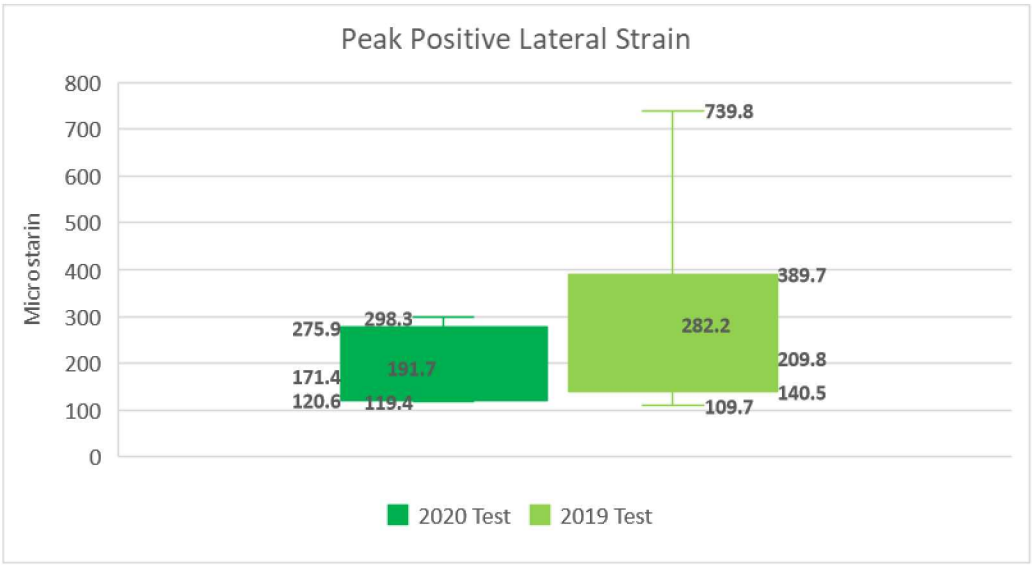

Figure 4-25. Statistics of Peak Positive Lateral Strain Values Observed in the 2020 and 2019 Tests.

Figures 4-26 and 4-27 compare the peak negative and peak positive axial strains measured by the different strain gauges in the 2020 and 2019 tests. Figure 4-28 displays color maps of the peak negative and peak positive strains in the 2020 and 2019 tests. Both, peak negative and peak positive strains are greater on the assembly bottom end in the 2020 test compared to the 2019 test. The peak negative and peak positive strains are lower on the assembly top end in the 2020 test compared to the 2019 test. The strain gauges located in the assembly mid part within the short spacer grid spans measured very similar strains in the 2020 and 2019 tests. This suggests that the slap down of the bottom end of the assembly in the 2019 test did not result in higher accelerations and strains (as it did in the 2020 test). This might be due to the structural changes related to the pre-test damage. The assembly damage was greater at the assembly bottom end.

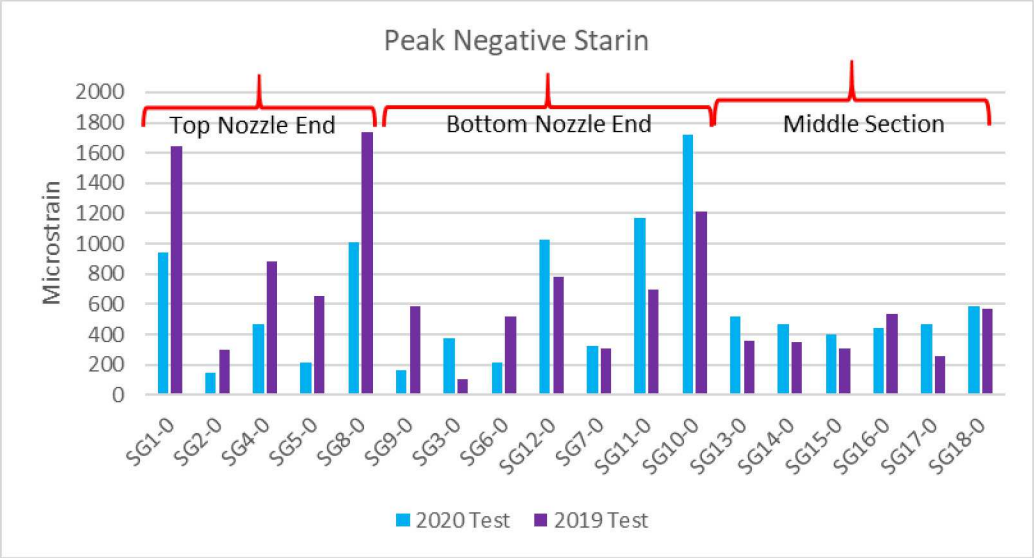

Figure 4-26. Peak Negative Strain Values Observed in the 2020 and 2019 Tests.

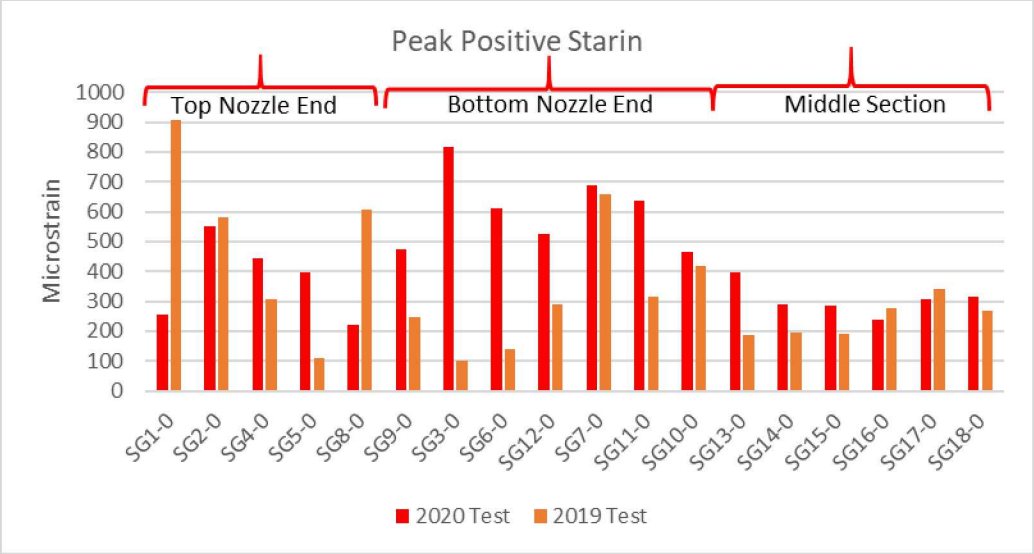

Figure 4-27. Peak Positive Strain Values Observed in the 2020 and 2019 Tests.

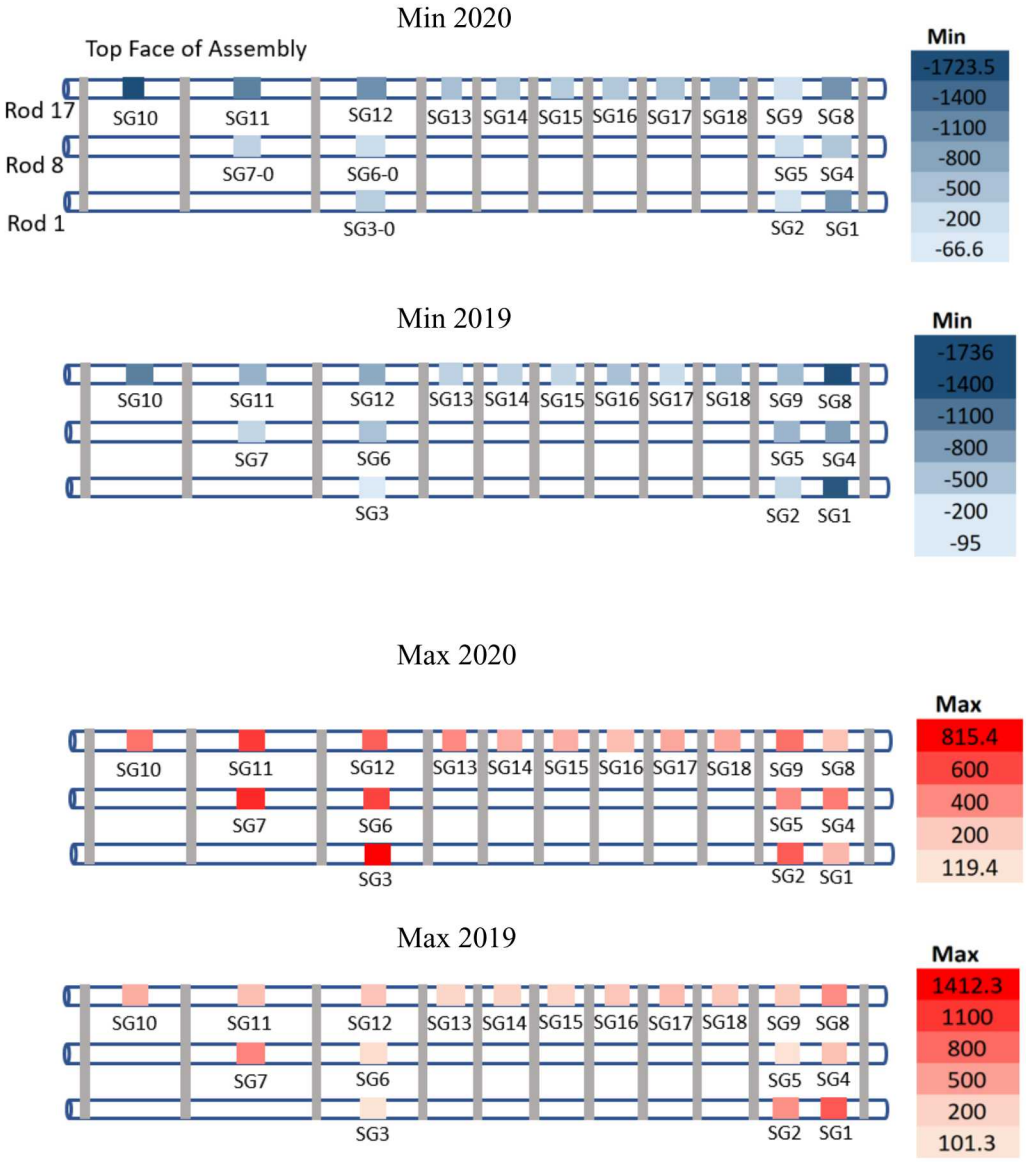

Figure 4-28. Color Maps of the Peak Strain in the 2020 and 2019 Tests.

Figures 4-29 shows the axial strain time histories for the strain gauges located on the top end of the assembly during the first impact in the 2020 test. The time histories of the strain gauges SG1-0 and SG8-0 located on rods 1 and 17 (rod and strain gauge locations are shown in Figure 4-28) are very similar. These are the zircaloy tubes with the lead rope (1) and lead pellets (17). The time history of the strain gauge SG4-0 located on the middle rod (rod 8) shows similar shape, but smaller peak strain value. This is the zircalloy tube with molybdenum pellets. Smaller peak strain values were also observed on zircaloy tube with molybdenum pellets in the MMTT [1]. All of these gauges were located at mid-span between spacer grids 1 and 2 (the long span near the top nozzle). Figure 4-30 shows time histories of the same strain gauges in the 2019 test. The time histories in the 2020 and 2019 tests are very similar, except the peak values were larger in the 2019 test in all three strain gauges.

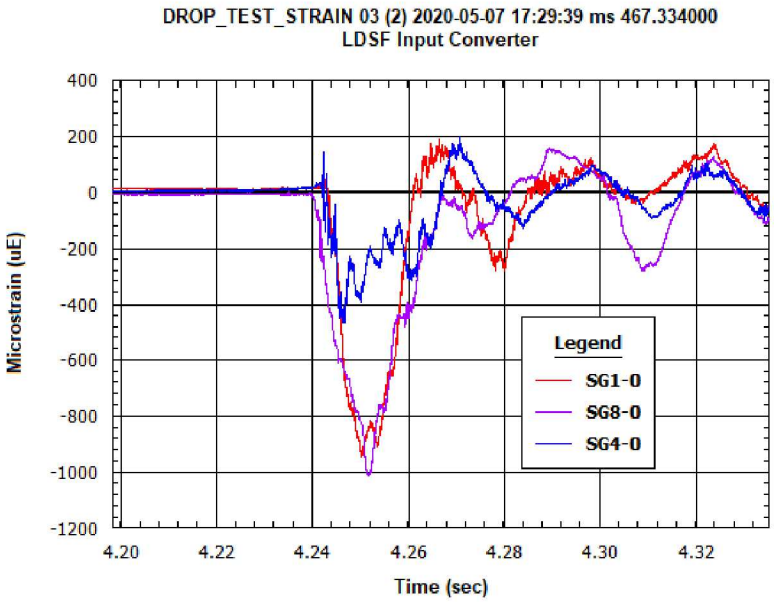

Figure 4-29. Axial Strain Time Histories for the Strain Gauges on the Assembly Top End, 2020 Test.

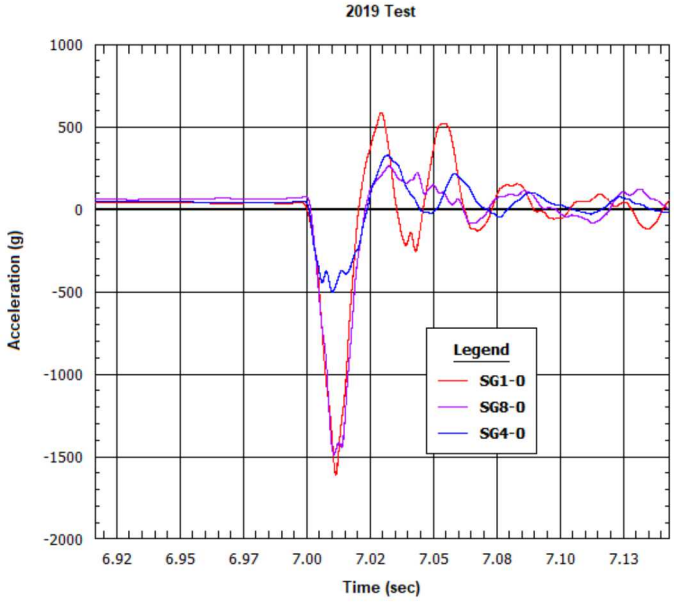

Figure 4-30. Axial Strain Time Histories for the Strain Gauges on the Assembly Top End, 2019 Test.

Figure 4-31 shows the axial strain time histories for the strain gauges located on the bottom end of the assembly during the first impact in the 2020 test. The time histories of the strain gauges SG10-0, SG11-0, and SG12-0 are similar, except the peak strain values are different with the highest peak strain observed in SG10-0. All three locations are in the middle of the three long spans. SG10-0 is in the middle of the long span next to the assembly bottom, where the boundary conditions would lead one to expect the highest mid-span strain values. Figure 4-32 shows time histories of the same strain gauges in the 2019 test. The time histories in the 2020 and 2019 tests are very similar, except the peak values were larger in all three locations in the 2020 test.

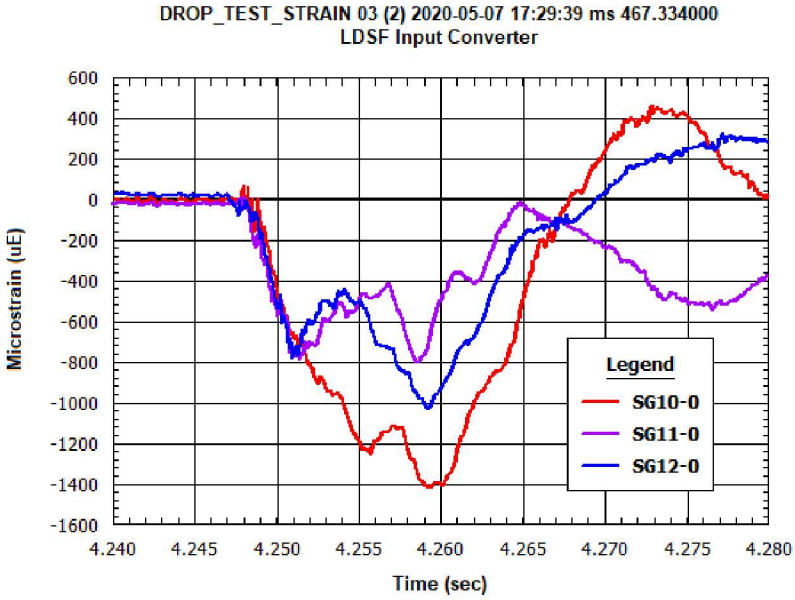

Figure 4-31. Axial Strain Time Histories for the Strain Gauges on the Assembly Bottom End, 2020 Test.

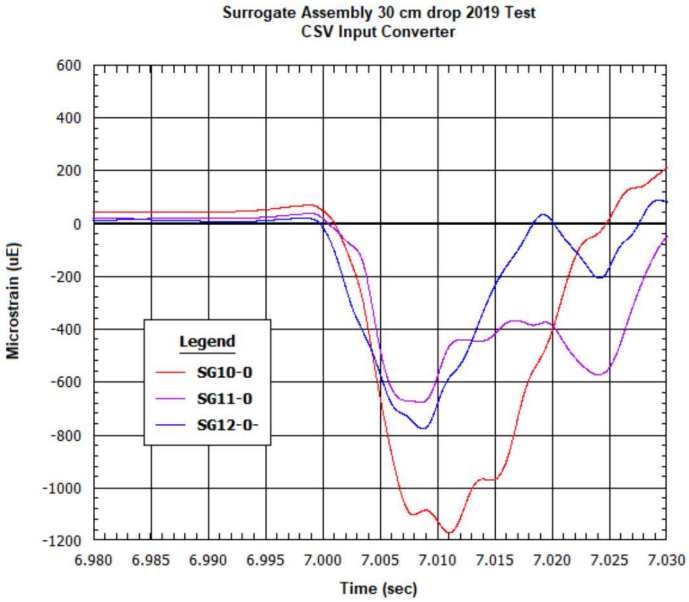

Figure 4-32. Axial Strain Time Histories for the Strain Gauges on the Assembly Bottom End, 2019 Test.

Figure 4-33 shows the axial strain time histories for the strain gauges located on the top end of the assembly during the first impact in the 2020 test. SG8-0 is located in the middle of the long span between spacer grids. SG9-0 is located in the same long span between spacer grids and on the same rod, but it is next to the spacer grid. As a result, an upward curvature occurred at the SG8-0 location and much smaller downward curvature occurred at the SG9-0 location. The response of the other strain gauges located next to the spacer grids (SG2-0, SG3-0, SG5-0, SG6-0, and SG7-0) were similar to SG9-0.

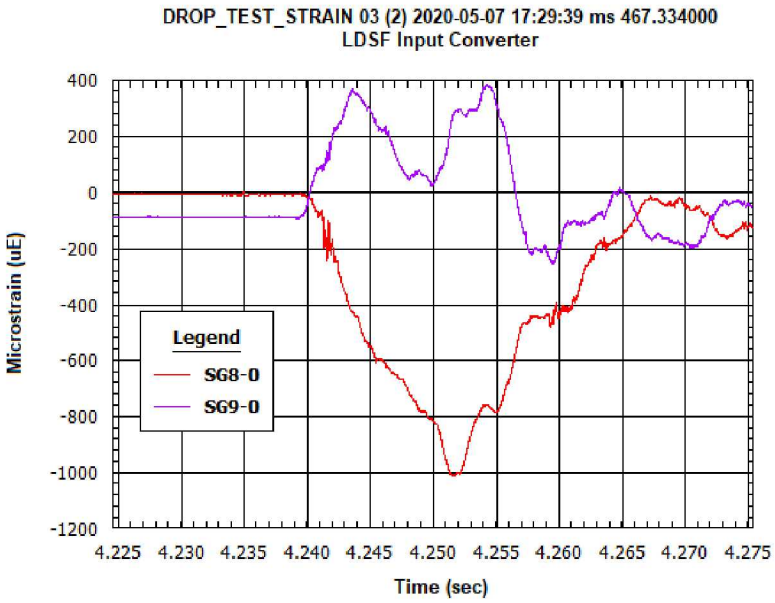

Figure 4-33. Axial Strain Time Histories for the Strain Gauges in the Middle of Spacer Grid Span and Next to the Spacer Grid, 2020 Test.

Figure 4-34 shows the time histories for strain gauges SG1-0, SG1-90 and SG1-225 located at 0^0, 90^0, and 225^0 in the 2020 test. The strain histories indicate upward curvature in SG1-0 and lateral bending in SG1-90. The strain observed in SG1-225 reflects the difference between the strain in SG1-0 and SG1-90. Figure 4-38 shows the time histories for the strain gauges SG1-0, SG1-90 and SG1-225 located at 0^0, 90^0, and 225^0 in the 2019 test. The time histories are very similar to the time histories in 2020 test, except the lateral bending in SG1-90 was smaller.

Figure 4-36 shows the strain SRS for the strain gauges SG1-0, SG2-0, and SG8-0 (assembly top end) and SG10-0, SG11-0, and SG12-0 (assembly bottom end) for the 2020 test. The strain SRS are similar to the acceleration SRS (Figure 4-8). The peak strain is within the frequency domain up to 100 Hz and is associated with the assembly natural frequency.

Figure 4-37 compares the SRS of the strain gauges with the maximum peak strain in the 2020 (SG10-0) and 2019 (SG8-0) tests. The damaged surrogate assembly strain SRS (2019 test) envelops the responses of the new surrogate assembly (2020 test). It has 3 peaks in the lower frequency (up to 10 Hz). These peaks are not present in the new surrogate assembly SRS. They reflect the structural changes in the damaged assembly. In both cases, the main strain response is within the frequency band up to 200 Hz.

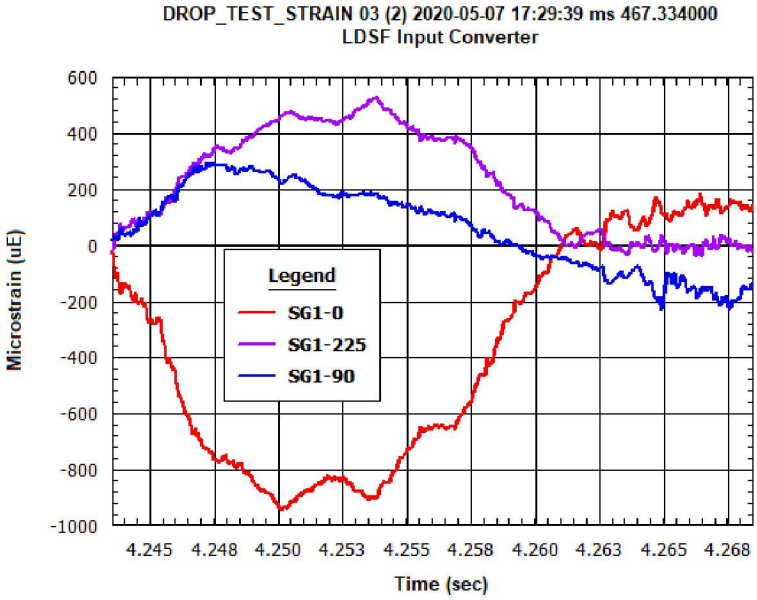

Figure 4-34. Time Histories for the Strain Gauges at 0^0, 90^0, and 225^0, 2020 Test.

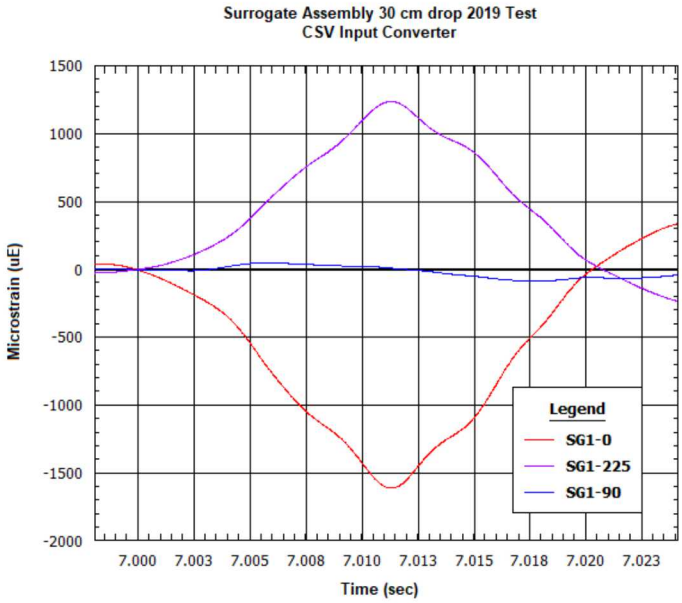

Figure 4-35. Time Histories for the Strain Gauges at 0^0, 90^0, and 225^0, 2019 Test.

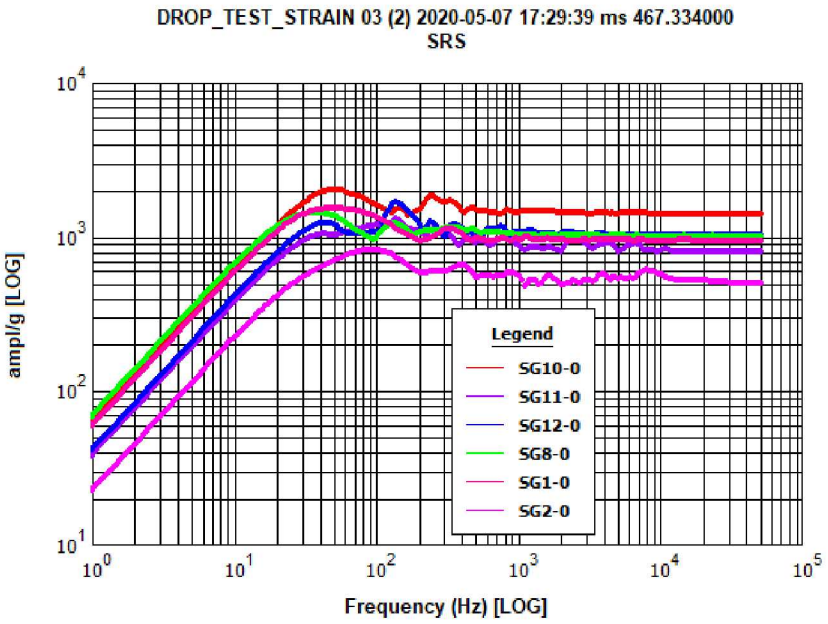

Note: SG1-0, SG2-0, and SG8-0 are on the top end and SG10-0, SG11-0, and SG12-0 are on the bottom end of the new surrogate assembly.

Figure 4-36. Strain SRS on the Surrogate Assembly (2020 Test).

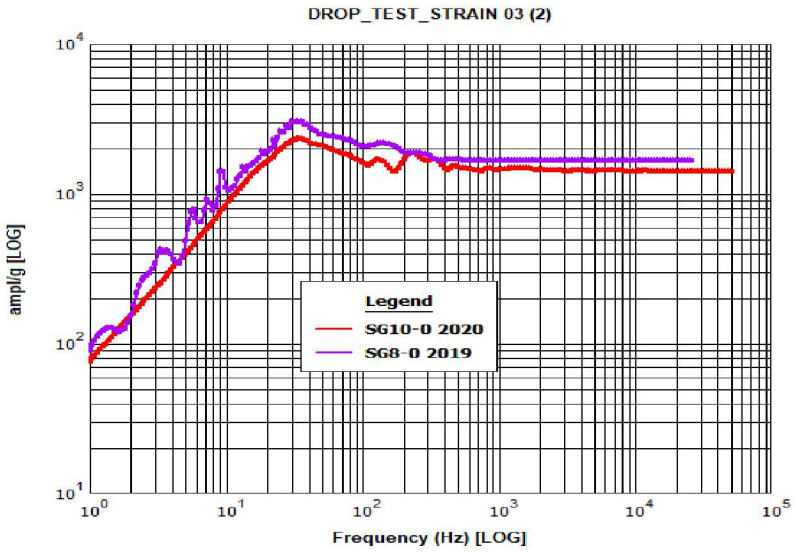

Figure 4-37. Strain SRS of Strain Gauges with Maximum Peak Strain in the 2020 and 2019 Tests.

Figure 4-38 shows the stress-strain curve for low burnup cladding (room temperature) from PNNL-17700 [19]. Also shown in this figure are the minimum and maximum strain values observed in the 2020 test and the corresponding stress range. Figure 4-39 shows the portion of the elastic part of this curve to better illustrate the observed strain and stress ranges. The stress corresponding to the maximum strain value is 22.3 ksi, which is significantly below the yield strength of the cladding. The stress corresponding to the

maximum strain value observed in the 2019 test with the damaged assembly is only slightly higher - 22.9 ksi.

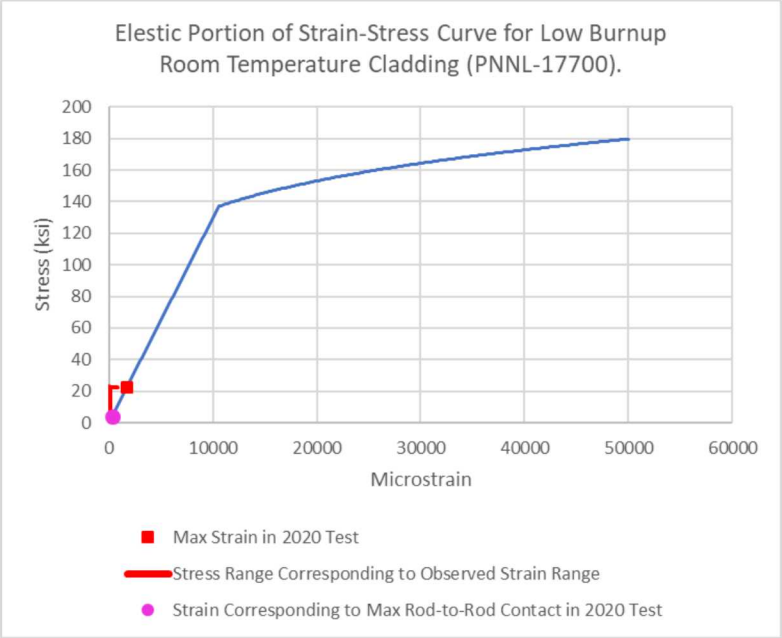

Figure 4-38. Stress Range in the 2020 Test Based on the Strain-Stress Curve for the Low Burnup Cladding [19].

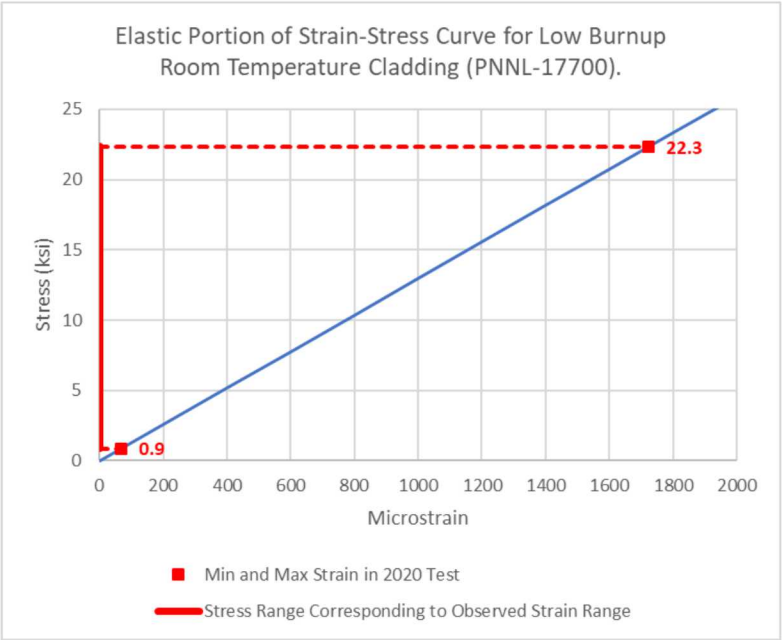

Figure 4-39. Closeup View of the Stress Range in the 2020 Test Based on the Strain-Stress Curve for the Low Burnup Cladding [19].

4.4 Pressure Paper

The pressure paper sheets were inserted between the rods in 2 long and in 2 short spacer grid spans prior to the 2020 test and in 2 long spacer grid spans prior to the 2019 test. The details are provided in Section 3.1.5. After the test, the pressure paper sheets were pulled out, examined, and scanned. The original scans are provided in Appendices B (2020 test) and C (2019 test). The pressure paper sheets with marks (indicating rod-to-rod contact) were analyzed using the method described in Section 4.4.1. Section 4.1.2 presents the results of this analysis.

4.4.1 Data Analysis Method

The marks on the pressure paper indicate rod-to-rod contact. To obtain the contact pressure, the color of a mark has to be compared to the pressure paper color scale. After the best matching color scale ID is determined, it can be converted to the pressure using an appropriate color scale ID versus pressure curve. The appropriate curve is selected based on the temperature and humidity observed during the test.

Visual selection of the best matching shade of the color is not an easy task and the results are subjective based on the person ability to identify the colors. This task is best accomplished using a computer image analysis. A Matlab script was developed to analyze the pressure paper scans. The script takes a reference image (one of the sections of the pressure paper color chart) and extracts all the RGB pixel color data within. It then takes a target image (the pressure paper scan) and makes a blank copy of it with all black pixels. The script goes through all the pixels in the original target image and compares them to the pixel colors of the reference image. If any of those colors match, it puts that pixel in the same spot on the blank copy, essentially building a copy of the target image with all pixels turned black except for the ones that match the color of the reference image. The script also allows for a tolerance, where one can define how close the color values need to be to each other in order to be copied over. The way the "closeness" of colors is calculated is with a standard 3 dimensional 2-point distance formula:

$$Distance_{point\ 1\ to\ point\ 2} = \sqrt{(x_1 - x_2)^2 + (y_1 - y_2)^2 + (z_1 - z_2)^2} \qquad (4\text{-}1)$$

The x, y, and z coordinates are the R, G, and B values of the pixel color. So, the color difference can be referred to as a distance. Examples of how the script works are shown in Figures 4-40 and 4-41. In these figures the image on the right is the reference image, the middle is the target image, and the left is the target image copy with only the matching pixels. In Figure 4-40 the color difference (or tolerance) was set equal to 0. Because the target image was simple, the reference colors were correctly identified in the target image. Figure 4-41 illustrate the color identification in case of a complex color scheme using different tolerance values.

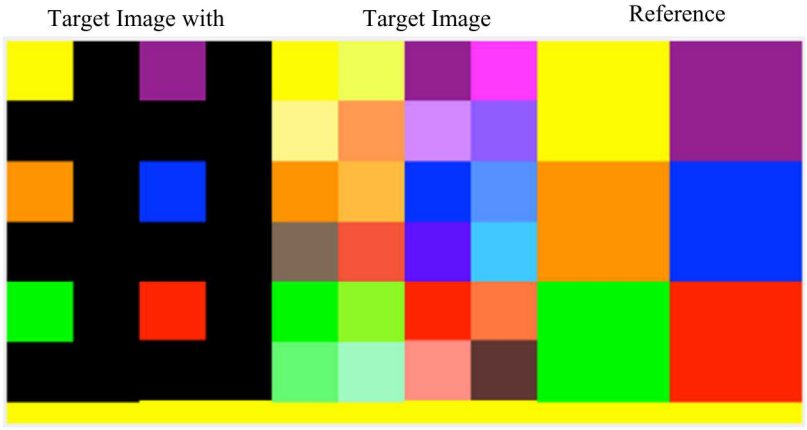

Figure 4-40. Simple Color Scheme Example of Color Identification with Matlab Script.

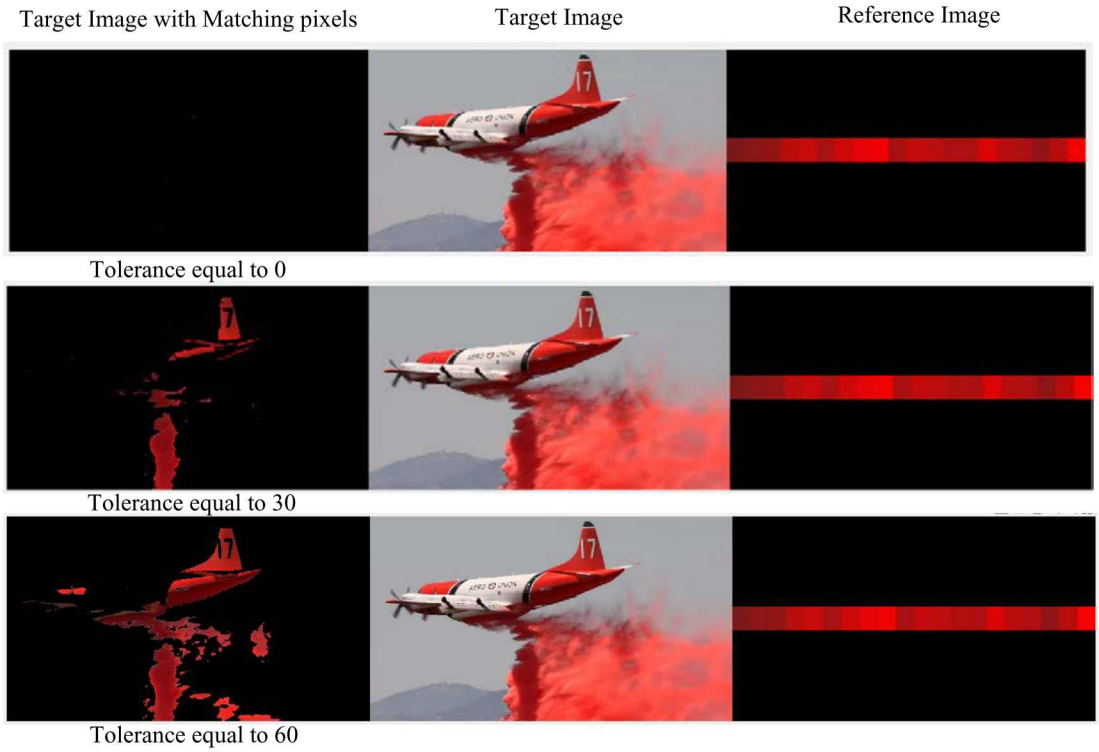

Figure 4-41. Complex Color Scheme Example of Color Identification with Matlab Script.

Because the pressure paper images are complex, introducing tolerance was essential for obtaining reasonable results.

It was also important to mitigate color error or any anomaly pixels that may not be representative of the actual color chart color. The scanned images of the color chart color have some inconsistencies and are not a uniform color. In order to solve this problem, the script counts how many times each pixel color value appears in the reference image, and then selects the top 5 most common pixel colors, rather than all the pixel colors.

A separate Matlab script was developed to determine the applicable color distance criteria. The script takes the top 5 most common pixel colors from each of the color chart colors and finds the distance between all top 5 pixel colors of each image (25 distances in total for two images). The smallest of these distances was selected and then defined as the distance between those two chart colors. Barring the first and last chart color, each chart color has two distances associated with it, the distance to the "previous" color, and the distance to the "next" color. looking at both distances the smallest one was selected. Consequently, when using that color the script would not encompass any of the top 5 colors from a nearby chart color (Note: since the distances are 3-D radii, there will in some cases be overlap between different color "spheres", but none of the radii will encircle any of the other original 5 chart colors.) Figure 4-42 illustrates this visually. The distances determined by this method (Table 4-4) were used in the pressure scan analysis.

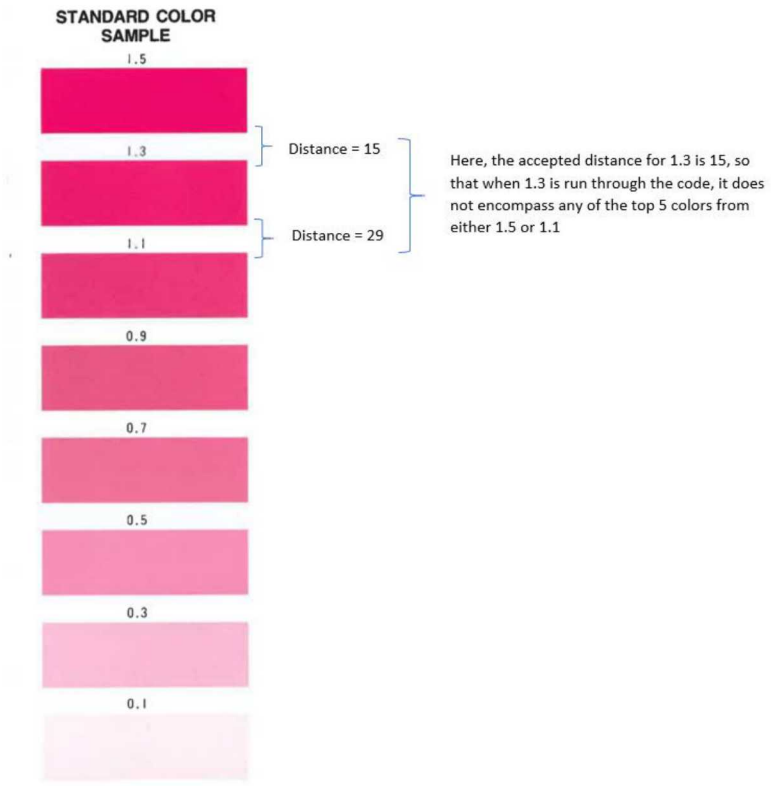

Figure 4-42. Example of Assigning Chart Color Distances.

After the scans were processed, the color chart colors were converted into their corresponding pressure values. The color ID (color density) versus pressure scales were provided with each type of pressure paper. They are shown in Figure 4-43.

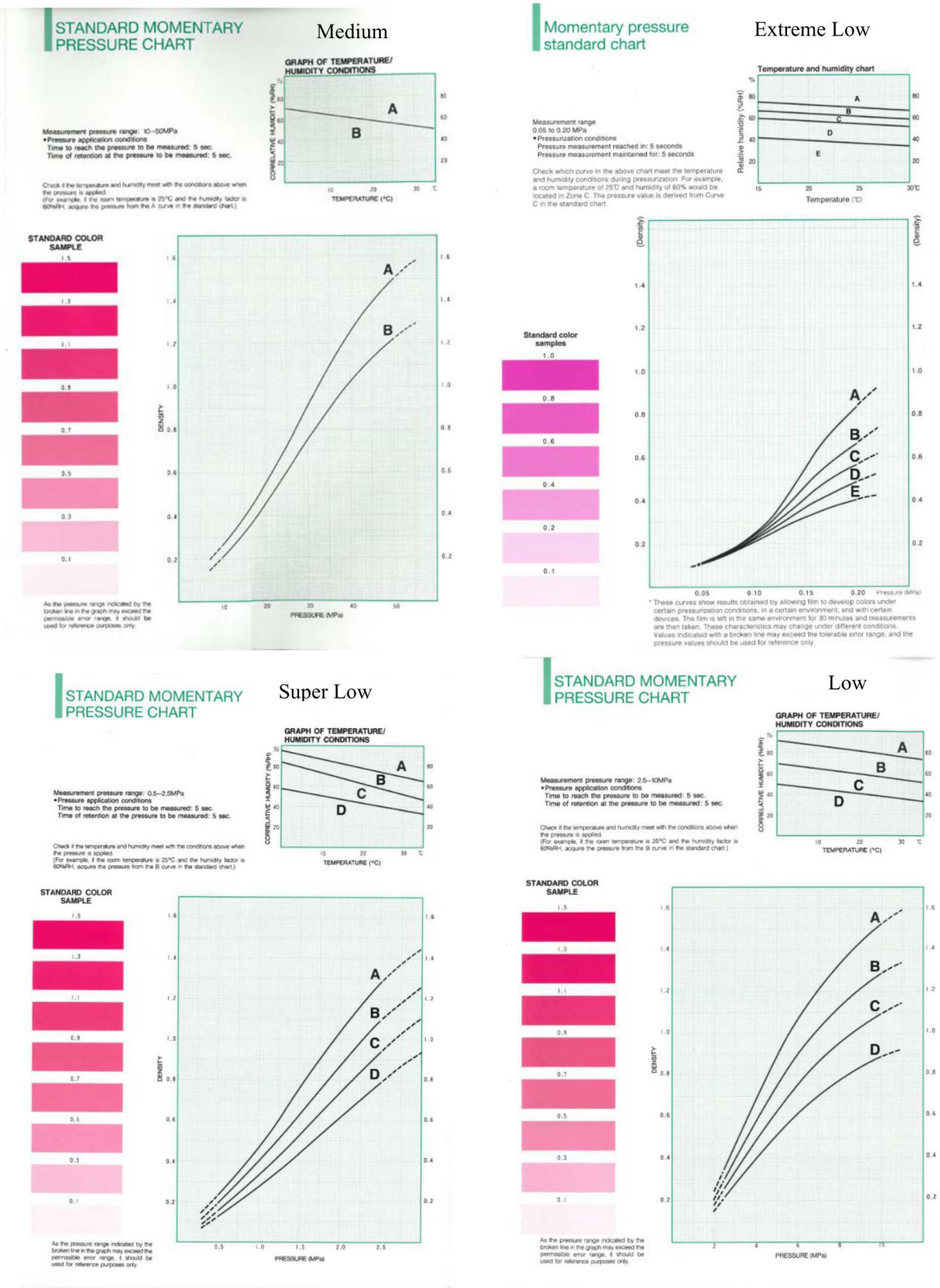

Figure 4-43. Pressure Paper Charts for Different Pressure Paper Types.

The appropriate curve selection was based on the temperature and humidity at the time of testing. The temperature and humidity on June 13, 2019 around 2:12 PM near KAFB was 31^0C and 17% humidity. On May 7, 2020 around 11:30 AM near KAFB the temperature and humidity were 28^0C and 7% humidity. Both of these temperature and humidity combinations fall into the same pressure versus color density curves for each paper type, meaning that the curves used for each paper type were the same for both, May 2020 and June 2019 tests. The type B curve was used for medium, type D for low and super low, and type E for extreme low pressure paper.

The distances (tolerances) and pressures for each color ID and each pressure paper type are summarized in Table 4-4.

Table 4-4. Color Chart Distances and Pressures for the Different Types of Pressure Paper.

	Pressure Paper Parameters							
	Medium Scale							
Color ID	0.1	0.3	0.5	0.7	0.9	1.1	1.3	1.5
Distance	*58*	*51*	*41*	*29*	*29*	*29*	*15*	*15*
Pressure, MPa	<19	19	22	28	35	43	55	>55
Pressure, ksi	<2.76	2.7557	3.1908	4.061	5.0763	6.2366	7.977	
	Low Scale							
Color ID	0.1	0.3	0.5	0.7	0.9	1.1	1.3	1.5
Distance	*58*	*47*	*40*	*25*	*25*	*30*	*15*	*15*
Pressure, MPa	<3.3	3.3	5	7	10.2	>10.2		
Pressure, ksi	<0.4786	0.4786	0.7252	1.0153	1.4794	>1.4794		
	Super Low Scale							
Color ID	0.1	0.3	0.5	0.7	0.9	1.1	1.3	1.5
Distance	*55*	*54*	*39*	*28*	*28*	*24*	*23*	*23*
Pressure, MPa	0.4	1.1	1.7	2.25	2.8	>2.8		
Pressure, ksi	0.058	0.1595	0.2465	0.3263	0.4061	>0.4061		
	Extreme Low Scale							
Color ID	**0.1**	**0.2**	**0.4**	**0.6**	**0.8**	**1**		
Distance	*21*	*21*	*36*	*27*	*27*	*32*		
Pressure, MPa	0.05	0.1	0.2	>0.2				
Pressure, ksi	0.00725	0.0145	0.029	>0.029				

An example of the pressure paper scan processing is shown in Figure 4-44 for the medium pressure paper sheet from the long span between spacer grids of the bottom end of the assembly (between rods 4 and 5). The scan is compared to four colors from the medium type color scale. The comparison to the first color scale color (color ID 0.1) revealed 317,572 color matching pixels. The comparison to the second color scale color (color ID 0.3) revealed 3,694,134 color matching pixels. The comparison to the third color scale color (color ID 0.5) revealed 989 color matching pixels. No color matching pixels were identified when the scan was compared to the fourth color scale color (color ID 0.7). Consequently, the corresponding pressures on this scan range from less than 2.76 ksi to 4.061 ksi (Table 4-4).

The pressure scans were also analyzed to identify the locations with the maximum contact pressure.

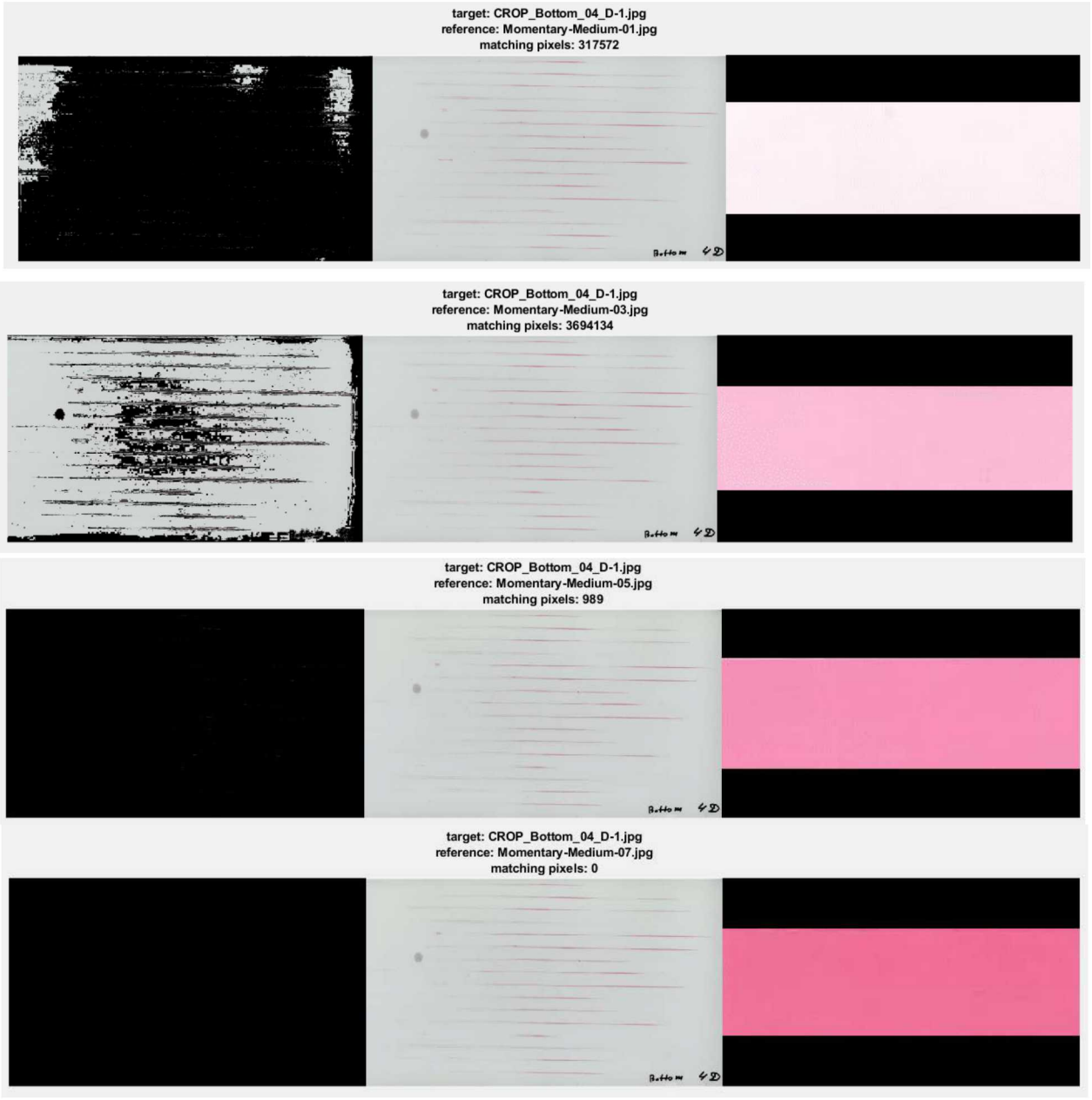

Figure 4-44. An Example of Medium Pressure Paper Scan Processing (Long Span Next to Assembly Bottom End, Pressure Paper Sheet between Rods 4 and 5).

4.4.2 Pressure Paper Analysis Results

After the 2020 test, the pressured paper was pulled out of the four sections where it was placed prior to the test. The 15 pressure paper sheets inserted between the rods in two short spacer grid spans in the middle part of the new surrogate assembly were blank indicating that there was no rod-to-rod contact.

A number of the pressure paper sheets from two long spans between spacer grids (one next to the top and another one next to the bottom end of the assembly) showed the marks indicating rod-to-rod contact. These pressure paper sheets were analyzed using the method described in Section 4.4.1.

4.4.2.1 Pressure Paper Sheets from the Long Span between Spacer Grids at the Bottom End of the Surrogate Assembly

The locations of the medium pressure paper in the long span between spacer grids at the assembly bottom end in 2020 test are shown in Figure 4-45. The medium paper sheet between the rods 8 and 9 had no marks. The medium pressure paper sheet between the rods 4 and 5 had very well-defined marks indicating that rod-to-rod contact occurred between each rod in level 4 and level 5 (Figure 4-46). The medium pressure paper sheet between the rods 12 and 13 had the marks indicating that rods contacted the guide tubes (Figure 4-47).

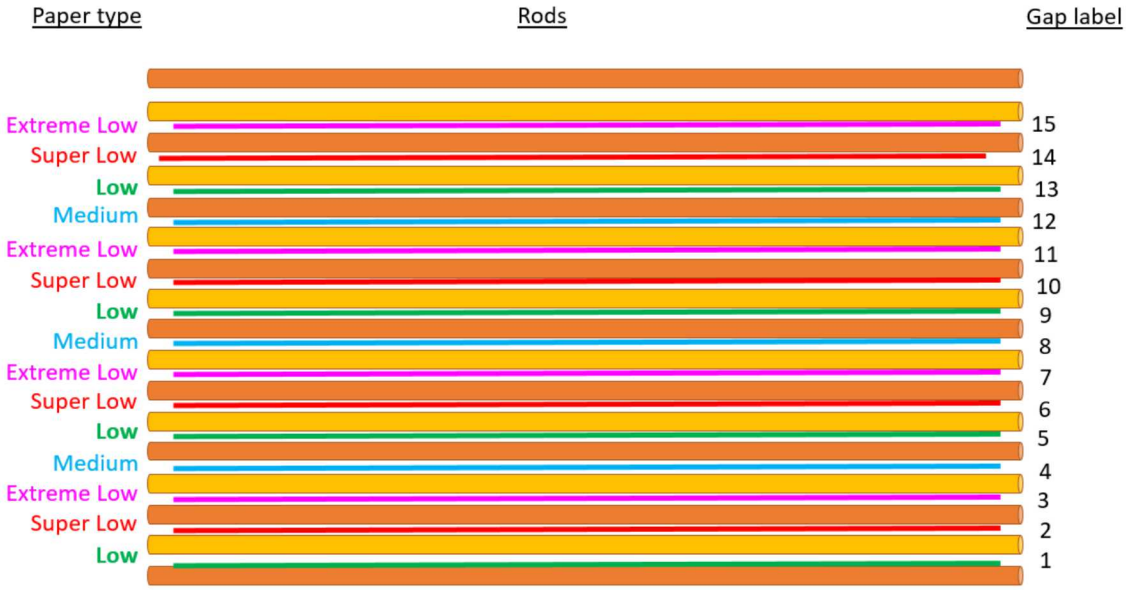

Figure 4-45. Pressure Paper Locations in Long Span between Spacer Grids at the Assembly Bottom End, (2020 Test).

Figure 4-46. Medium Pressure Paper Sheet between the Rods 4 and 5, Assembly Bottom End, Long Span between Spacer Grids (2020 Test).

Figure 4-47. Medium Pressure Paper Sheet between the Rods 12 and 13, Assembly Bottom End, Long Span between Spacer Grids (2020 Test).

During the 2019 test, the super low pressure paper was inserted between the rods 4 and 5 and between the rods 12 and 13 at the assembly bottom end. The scans of these paper sheets are shown in Figures 4-48 and 4-49. The super low pressure paper sheet between the rods 4 and 5 had very well defined marks indicating that rod-to-rod contact occurred between each rod in level 4 and level 5, similar to the 2020 test. The super low pressure paper sheet between the rods 12 and 13 had marks indicating guide tube contact, the same as in the 2020 test. The marks are more pronounced than in the 2020 test because the pressure range of the super low pressure paper was lower.

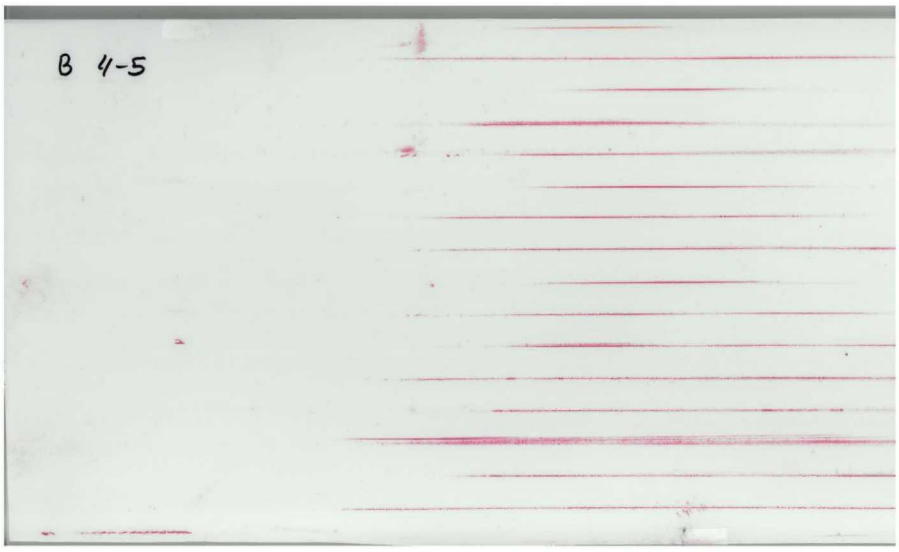

Figure 4-48. Super Low Pressure Paper Sheet between the Rods 4 and 5, Assembly Bottom End, Long Span between Spacer Grids (2019 Test).

Figure 4-49. Super Low Pressure Paper Sheet between the Rods 12 and 13, Assembly Bottom End, Long Span between Spacer Grids (2019 Test).

The results of the medium pressure paper processing are shown in Figure 4-50. The identified pressure range was from less than 2.8 ksi to 3.2 ksi. The pressure paper sheet between the rods 4 and 5 had significantly larger areas with the pressure of 3.2 and 2.8 ksi than the pressure paper sheet between the rods 12 and 13.

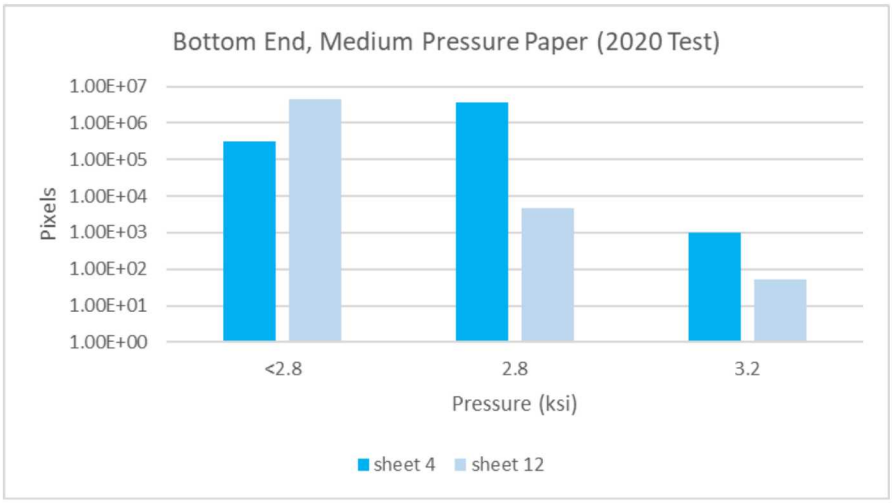

Figure 4-50. Results of the Medium Pressure Paper Processing, Assembly Bottom End, Long Span between Spacer Grids (2020 Test).

The results of the super low pressure paper (2019 test) processing are shown in Figure 4-51. The identified pressure range was from 0.06 ksi to 0.33 ksi. The pressure paper sheet between the rods 4 and 5 had significantly larger areas with the pressure greater than 0.06 ksi than the pressure paper sheet between the rods 12 and 13. It is evident from this example that the super low pressure paper was not capable of capturing the upper end of the rod-to-rod contact pressure (3.2 ksi in 2020 test).

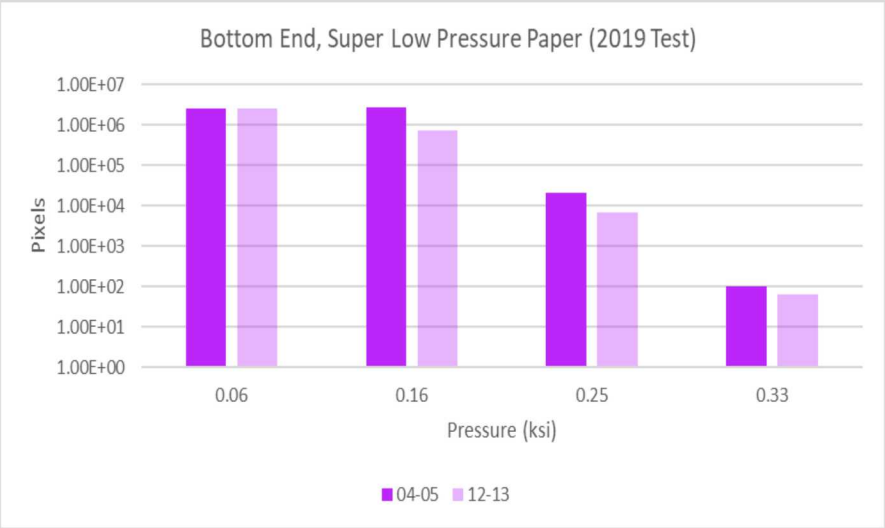

Figure 4-51. Results of the Super Low Pressure Paper Processing, Assembly Bottom End, Long Span between Spacer Grids (2019 Test).

The locations of the low pressure paper in the long span between spacer grids at the assembly bottom end in the 2020 test are shown in Figure 4-47. All sheets showed rod-to-rod contacts. The results of the scan processing are shown in Figure 4-52. The identified pressure range was from less than 0.4786 ksi to 1.4794 ksi. The pressure paper sheet between the rods 1 and 2 had significantly larger areas with the pressure greater than 0.4786 ksi than the pressure paper sheets between the other rods.

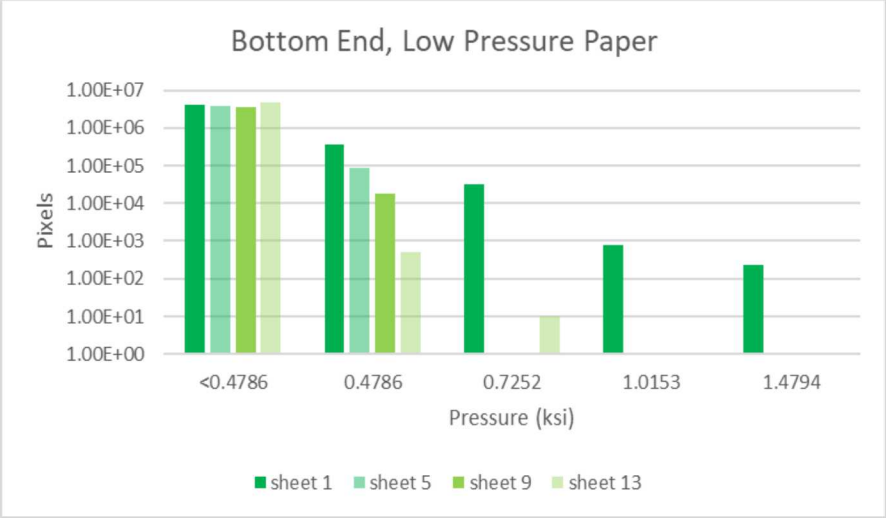

Figure 4-52. Results of the Low Pressure Paper Processing, Assembly Bottom End, Long Span between Spacer Grids (2020 Test).

The locations of the super low pressure paper in the long span between spacer grids at the assembly bottom end in the 2020 test are shown in Figure 4-47. The sheets between the rods 14 and 15 and between the rods 10 and 11 showed very few marks. The results of the scan processing of the sheets between the rods 2 and 3 and between rods 6 and 7 are shown in Figure 4-53. The identified pressure range was from 0.058 ksi to 0.2465 ksi. The pressure paper sheet between the rods 2 and 3 had larger areas with the pressure greater than 0.058 ksi than the pressure paper sheets between the other rods.

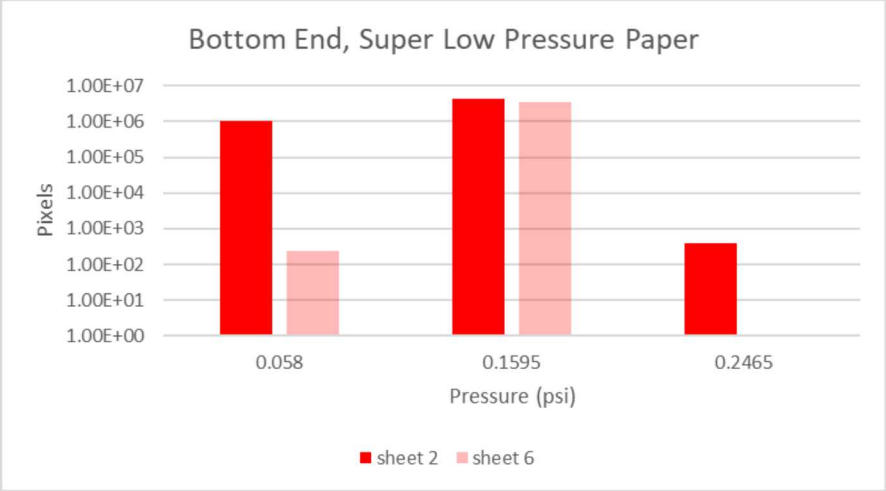

Figure 4-53. Results of the Super Low Pressure Paper Processing, Assembly Bottom End, Long Span between Spacer Grids (2020 Test).

The locations of the extreme low pressure paper in the long span between spacer grids at the assembly bottom end in the 2020 test are shown in Figure 4-47. The sheets between the rods 15 and 16 and between the rods 11 and 12 showed only a few marks. The results of the scan processing of the sheets between the rods 3 and 4 and between rods 7 and 8 are shown in Figure 4-54. The identified pressure range was from 0.00725 ksi to greater than 0.029 ksi. The pressure paper sheet between the rods 3 and 4 had larger areas with the pressure greater than 0.00725 ksi than the pressure paper sheets between the other rods.

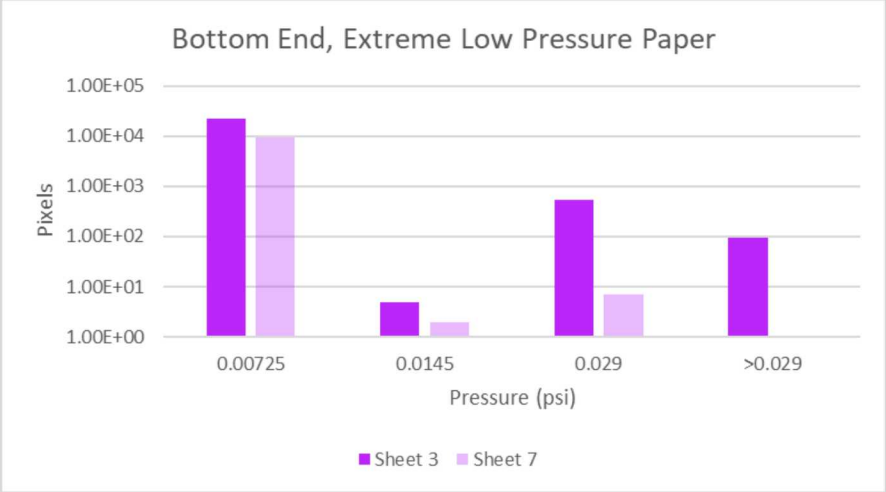

Figure 4-54. Results of the Super Low Pressure Paper Processing, Assembly Bottom End, Long Span between Spacer Grids (2020 Test).

The pressure paper scans were also processed to identify the maximum rod-to-rod contact pressure and the locations at which it was observed. The processed scans are provided in Appendices D (2020 test) and E (2019 test). Figure 4-55 illustrates an example of this processing for the medium pressure sheet between the rods 4 and 5 in the 2020 test. The maximum pressure was 3.190 ksi. The points of the maximum pressure are located at the middle of the span where the bending is maximum. Figure 4-56 illustrate the example of this processing for the super low pressure sheet between the rods 4 and 5 in the 2019 test. The maximum pressure of 0.3 ksi is lower than the actual because the actual contact pressure

was significantly higher than the maximum pressure limit of the super low pressure paper. The points of the maximum pressure are located at the middle of the span, similarly to the 2020 test.

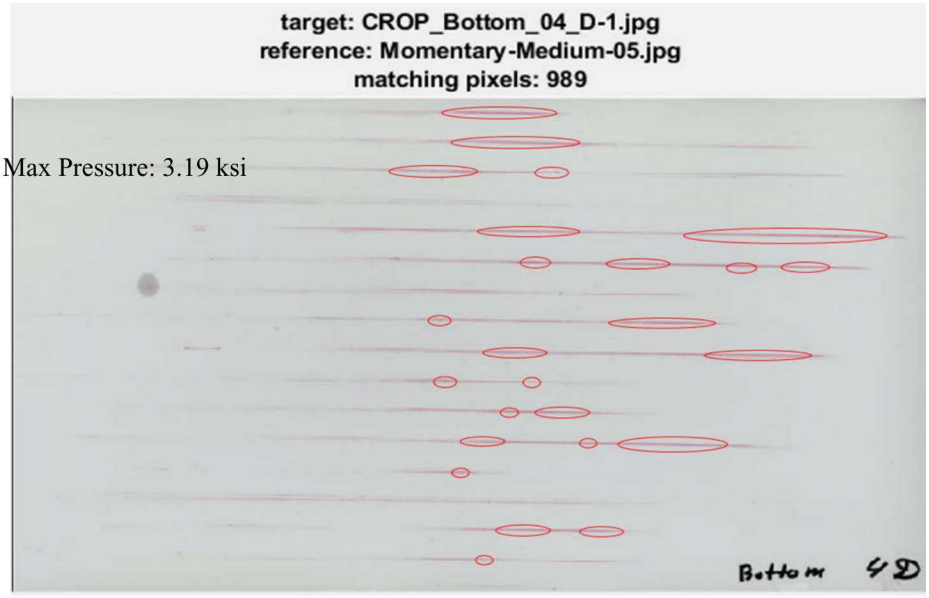

Figure 4-55. Maximum Contact Pressure Locations, Medium Pressure Sheet between the Rods 4 and 5, 2020 Test.

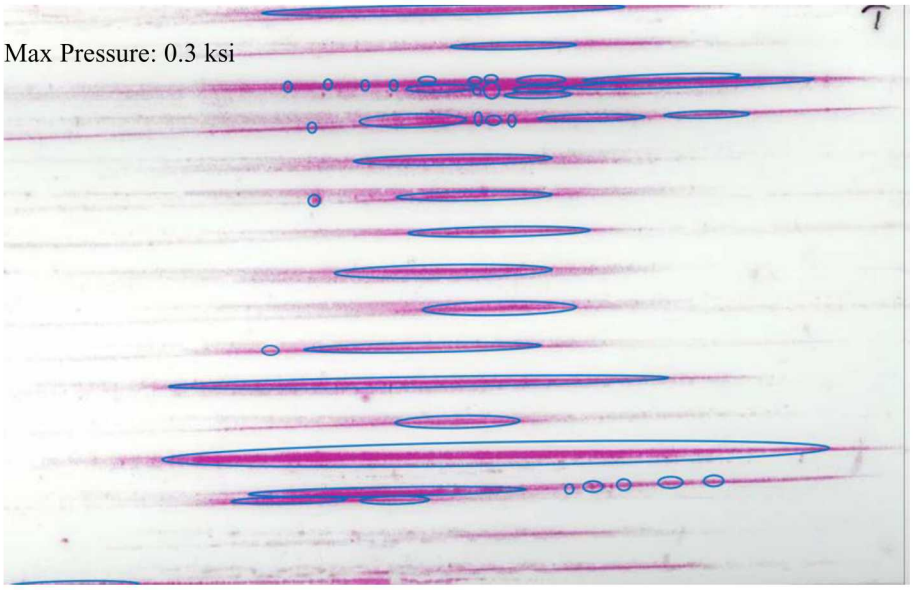

Figure 4-56. Maximum Contact Pressure Locations, Medium Pressure Sheet between the Rods 4 and 5, 2020 Test.

4.4.2.2 Pressure Paper Sheets from the Long Span between Spacer Grids at the Top End of the Surrogate Assembly

The locations of the medium pressure paper in the long span between spacer grids at the assembly top end are shown in Figure 4-57. All four medium paper sheets have very few marks. The medium pressure paper sheet between the rods 3 and 4 had is shown in Figure 4-58. The marks are barely visible in this scan.

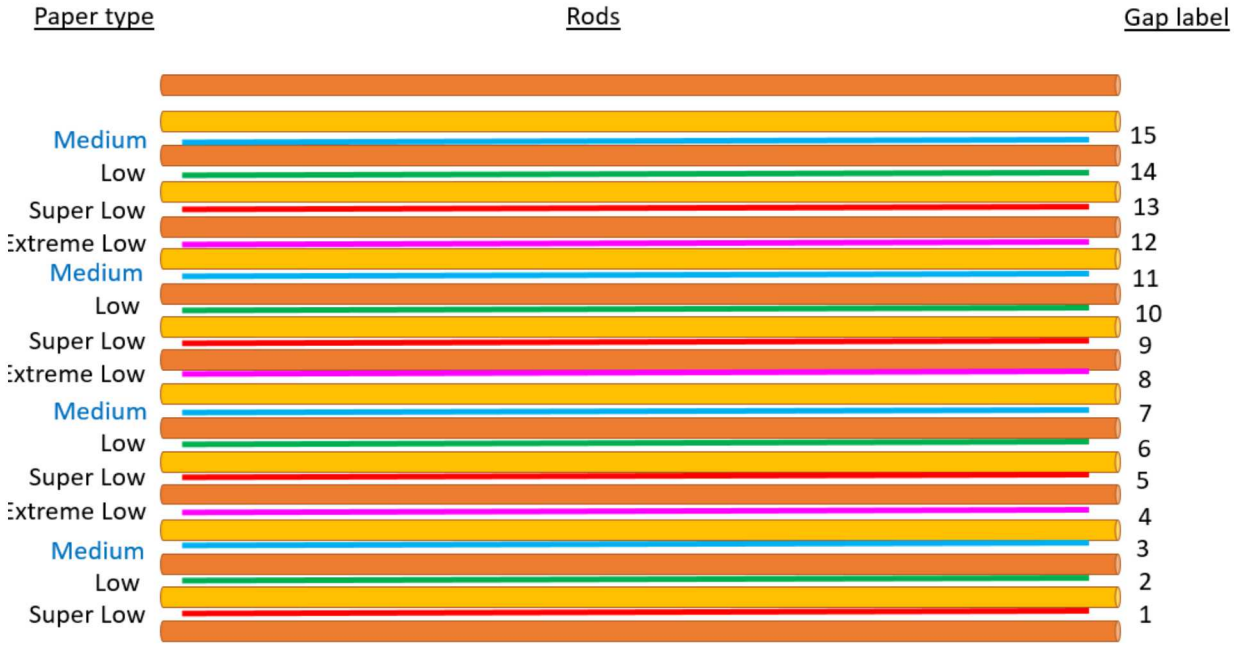

Figure 4-57. Pressure Paper Locations in Long Span between Spacer Grids at the Assembly Top End (2020 Test).

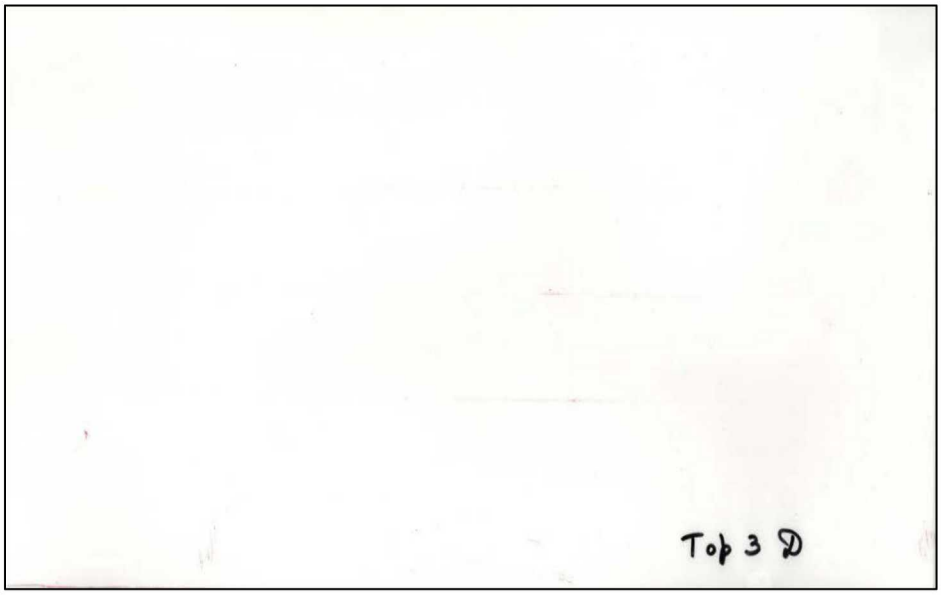

Figure 4-58. Medium Pressure Paper Sheet between the Rods 3 and 4, Assembly Top End, Long Span between Spacer Grids (2020 Test).

During the 2019 test, the super low pressure paper was inserted between the rods 3 and 4 at the assembly top end. The scan of this paper sheet is shown in Figures 4-59. The scan shows very well-defined marks indicating that rod-to-rod contact occurred between each rod in the level 3 and level 4. In the 2020 test, the contact pressure was below the minimum limit of the medium pressure paper. This resulted in practically blank medium paper sheets.

Figure 4-59. Super Low Pressure Paper Sheet between the Rods 3 and 4, Assembly Top End, Long Span between Spacer Grids (2019 Test).

The locations of the low pressure paper in the long span between spacer grids at the assembly top end in the 2020 test are shown in Figure 4-57. The sheets between the rods 10 and 11 and between the rods 14 and 15 were blank. The results of the scan processing for the sheets between the rods 2 and 3 and between the rods 6 and 7 are shown in Figure 4-60. The identified pressure range was from less than 0.4786 ksi to 0.4786 ksi. The pressure paper sheet between the rods 2 and 3 had larger areas with the pressure greater than 0.4786 ksi than the pressure paper sheets between the rods 6 and 7.

The locations of the super low pressure paper in the long span between spacer grids at the assembly top end in the 2020 test are shown in Figure 4-57. The sheets between the rods 13 and 14 and between the rods 9 and 10 showed very few marks. The results of the scan processing of the sheets between the rods 1 and 2 and between rods 5 and 6 are shown in Figure 4-61. The identified pressure range was from 0.058 ksi to 0.4051 ksi. The pressure paper sheet between the rods 1 and 2 had larger areas with the pressure greater than 0.058 ksi than the pressure paper sheet between the rods 5 and 6.

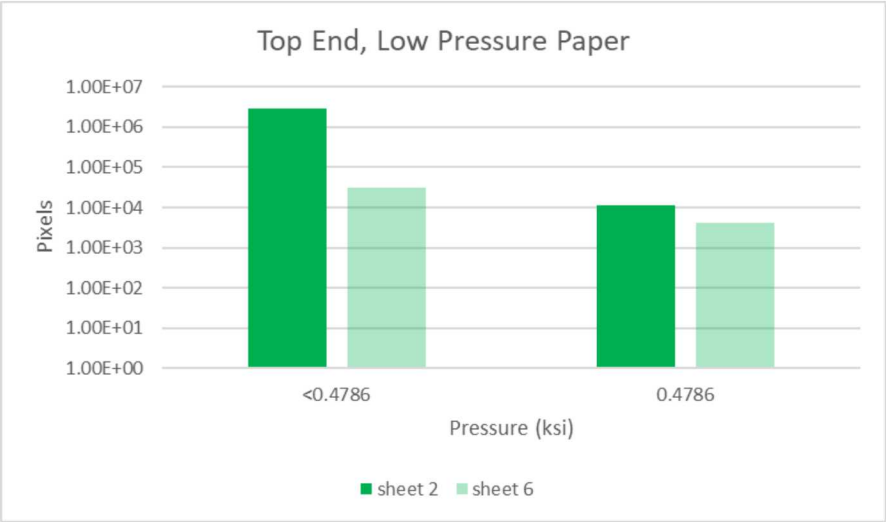

Figure 4-60. Results of the Low Pressure Paper Processing, Assembly Top End, Long Span between Spacer Grids (2020 Test).

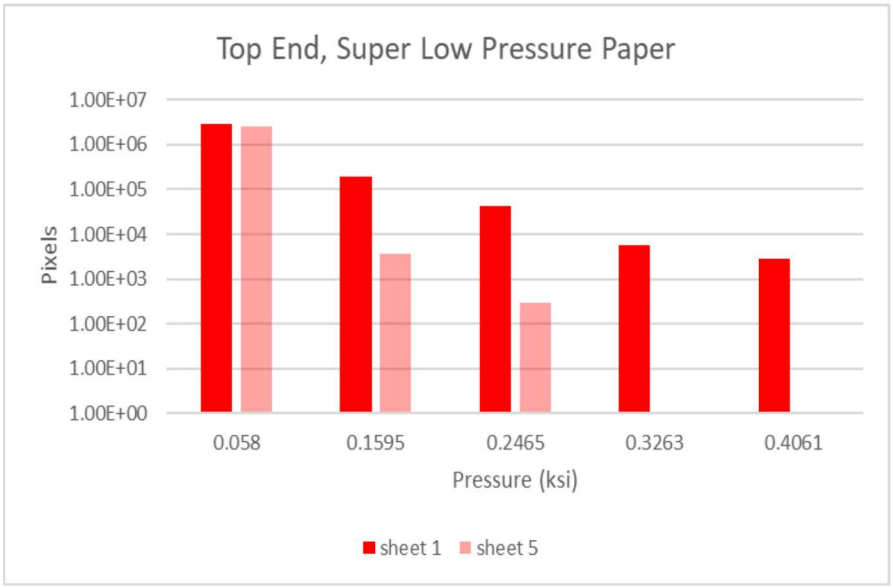

Figure 4-61. Results of the Super Low Pressure Paper Processing, Assembly Top End, Long Span between Spacer Grids (2020 Test).

The locations of the extreme low pressure paper in the long span between spacer grids at the assembly top end in the 2020 test are shown in Figure 4-57. The sheet between the rods 12 and 13 was blank. The results of the scan processing of the sheets between the rods 4 and 5 and between rods 8 and 9 are shown in Figure 4-62. The identified pressure range was from 0.00725 ksi to greater than 0.029 ksi. The pressure paper sheet between the rods 3 and 4 had slightly larger areas with the pressure greater than 0.029 ksi than the pressure paper sheets between the rods 8 and 9.

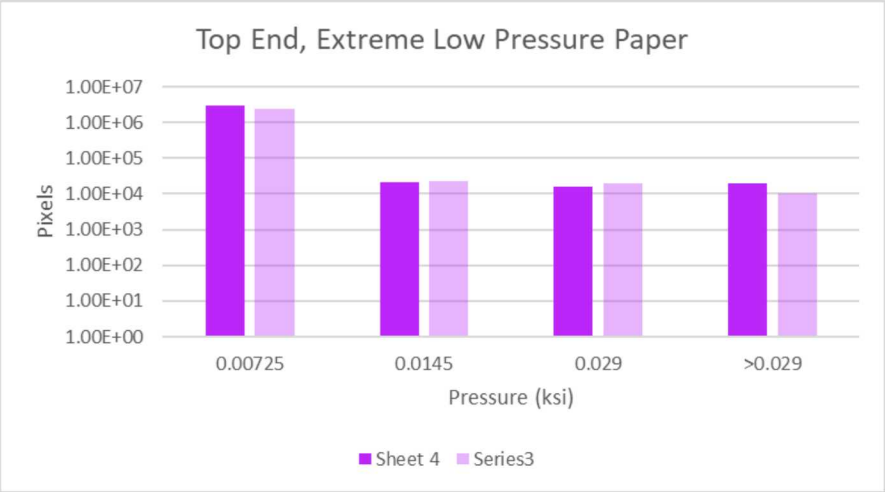

Figure 4-62. Results of the Extreme Low Pressure Paper Processing, Assembly Top End, Long Span between Spacer Grids (2020 Test).

Figure 4-63 illustrates the results of the maximum pressure processing for the super low pressure sheet between the rods 3 and 4 in the 2020 test. The maximum pressure was 0.4061 ksi. The points of the maximum pressure are located at the middle of the span where the bending is maximum. Figure 4-64 illustrate the example of this processing for the super low pressure sheet between the rods 3 and 4 in the 2019 test. The maximum pressure was the same as in the 2020 test. The locations of the maximum pressure points are similar to the 2020 test.

Figure 4-63. Maximum Contact Pressure Locations, Super Low Pressure Sheet between the Rods 3 and 4, 2020 Test.

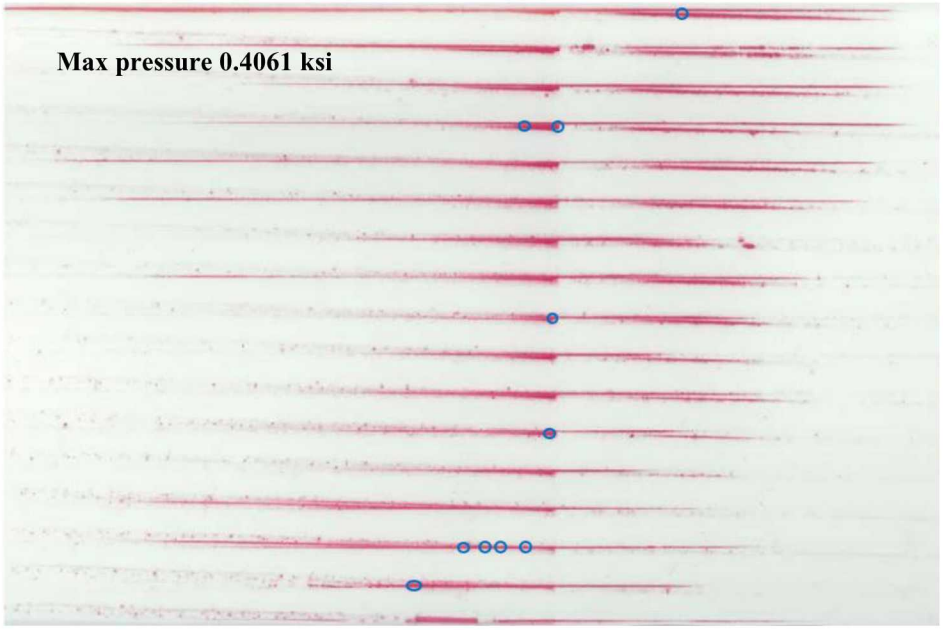

Figure 4-64. Maximum Contact Pressure Locations, Super Low Pressure Sheet between the Rods 3 and 4, 2019 Test.

4.4.2.3 Maximum Rod-to-Rod Contact Pressure

The maximum rod-to-rod contact pressure was estimated for every pressure paper scan, except the blank ones. The results are summarized in Table 4-5.

Each type of the pressure paper has specific pressure range. Figure 4-65 shows the ranges of the four types of the pressure paper used in the 2020 test. Only two types (extreme low and super low) were used in the 2019 test. The pressure range from 1.48 to 2.76 ksi was not covered either by low or medium pressure paper. Note that the gap in the pressure ranges are due to the performance of the pressure paper under high temperature and low pressure conditions. Also shown in Figure 4-67 is the largest maximum pressure observed in the 2020 test.

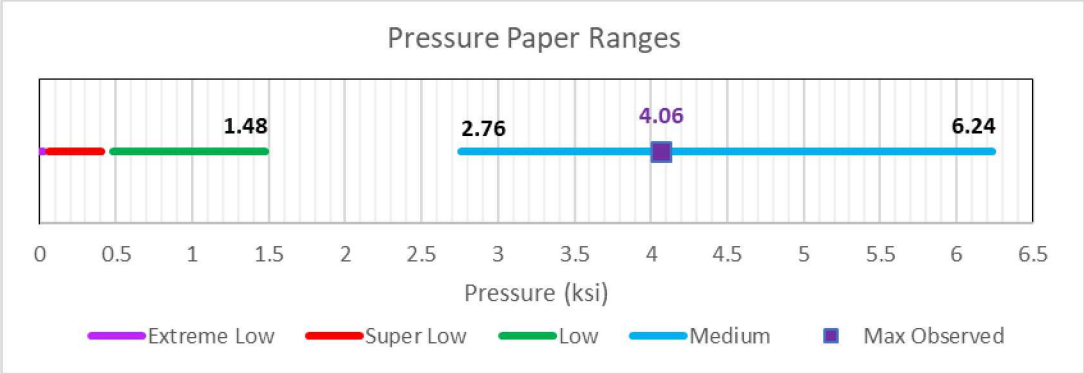

Figure 4-65. Pressure Paper Ranges.

The information on the pressure paper limits was used to identify the data points that do not represent the actual maximum pressure values (the actual value is above the maximum pressure limit). These data points are outlined in Table 4-5. All the maximum pressure values from the extreme low pressure paper in the 2019 test were not representative of the actual maximum pressure. Only the values from the super low

pressure paper scans are provided in Table 4-5 and the data from the bottom and the top end of the assembly are combined. Figure 4-66 shows the maximum rod-to-rod contact pressures at the assembly top and bottom end in the 2020 test. The values that are not representative of the actual maximum values are shown in this figure in red (bottom end) and pink (top end).

Table 4-5. Estimated Maximum Rod-to-Rod Contact Pressure.

	2020 Test				2019 test	
Gap Number	Bottom Labels	Max Pressure (ksi)	Top Labels	Max Pressure (ksi)	Combined Top and Bottom Labels	Max Pressure (ksi)
15	15A	0.029	15D	blank	T 15-16	0.247
14	14B	0.247	14C	0.725	B 14-15	0.247
13	13C	0.725	13B	blank	T 13-14	0.326
12	12D	4.061	12A	0.029	B 2-13	0.326
11	11A	0.029	11D	blank	T 11-12	blank
10	10B	0.247	10C	blank	B 10-11	0.247
9	9C	0.479	9B	0.326	T 9-10	0.406
8	8D	blank	8A	blank	B 8-9	0.247
7	7A	0.029	7D	blank	T 7-8	0.406
6	6B	0.160	6C	0.479	B 6-7	0.406
5	5C	0.479	5B	0.326	T 5-6	0.406
4	4D	3.191	4A	0.029	B 4-5	0.326
3	3A	0.029	3D	2.756	T 3-4	0.406
2	2B	0.247	2C	0.479	B 2-3	0.406
1	1C	1.479	1B	0.406	T 1-2	0.406

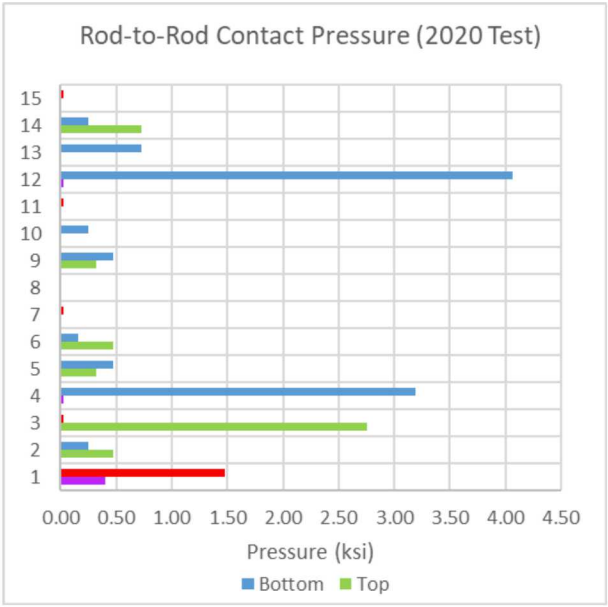

Note: The values that are not representative of the actual maximum values are shown in red (bottom end) and pink (top end).

Figure 4-66. Rod-to-Rod Contact Pressure in the 2020 Test.

Figure 4-67 shows the combined (top and bottom) maximum rod-to-rod contact pressures in the 2019 test. The values that are not representative of the actual maximum values are shown in this figure in orange. The actual maximum pressures were not captured at the bottom rods.

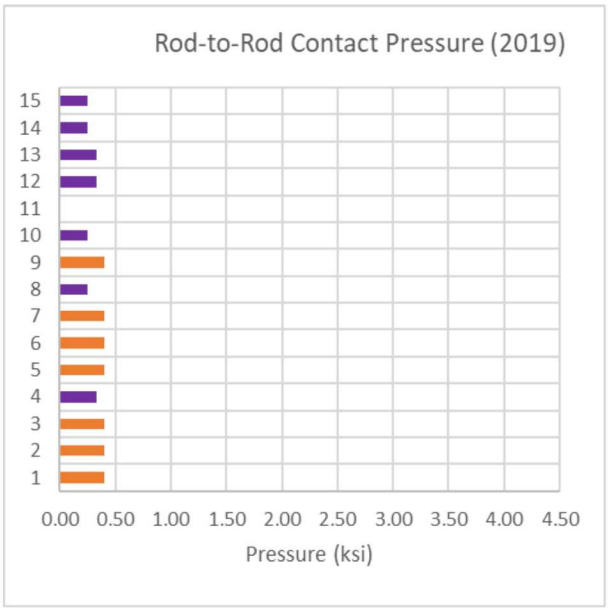

Note: The values that are not representative of the actual maximum values are shown in orange.

Figure 4-67. Rod-to-Rod Contact Pressure in the 2019 Test.

Figure 4-68 shows the maximum rod-to-rod contact pressures in the 2020 and 2019 tests. Only the values that represent the actual maximum pressure values are shown in this figure. The top and bottom rods experienced much higher contact pressures than the rods in the middle. A few rods in the middle did not come into the contact. The contact pressure of 4.1 ksi is a reasonable estimate of the maximum rod-to-rod contact pressure.

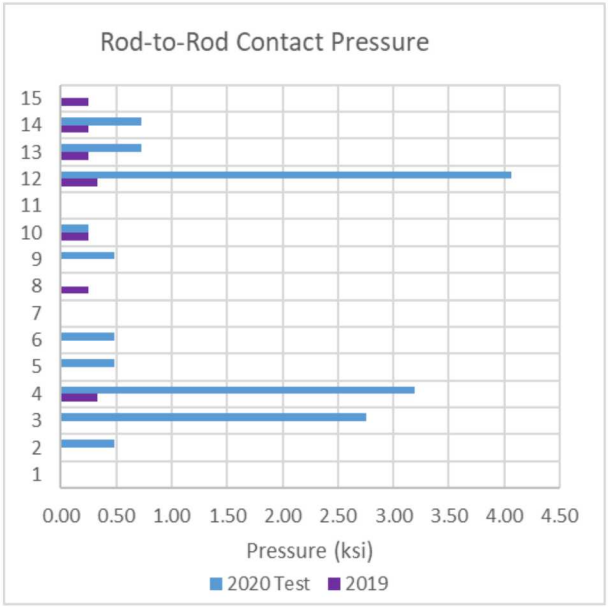

Figure 4-68. Rod-to-Rod Contact Pressure in the 2020 and 2019 Tests.

5. SUMMARY

The 30 cm drop is the remaining NRC NCT regulatory requirement (10 CFR 71.71) for which there are no data on the actual surrogate fuel. While obtaining data on the actual fuel is not a direct requirement, it provides definitive information which aids in quantifying the risk of fuel breakage resulting from a cask drop from a height of 30 cm or less. The 30 cm drop test with the full-scale surrogate assembly conducted in May 2020 was the last step needed for quantifying the strains on the surrogate assembly rods.

The full-scale surrogate assembly used in the 2020 test was built using a new 17x17 PWR Westinghouse skeleton filled with the copper rods and 3 zircaloy rods from the old full-scale surrogate assembly. Felt pads were attached to the bottom of the basket tube containing the surrogate assembly prior to the 30 cm drop to adequately represent the effects of the impact limiters and the cask. Note that felt "programming material" has been used extensively in past drop tests and is known to be a good material for programming a desired shock pulse. The felt pad configuration was determined during the previous series of tests. The acceleration pulses observed on the surrogate assembly during the test were in good agreement with the expected pulses. This confirmed that during the 30 cm drop the surrogate assembly experienced the same conditions as it would if it was dropped in the cask with the impact limiters.

A 30 cm drop test was also conducted in June 2019 with the old full-scale surrogate assembly. The old assembly was damaged when accidently dropped prior to the test from the height of about 7 inches without felt pads attached. Comparison of the 2020 and 2019 test data provided useful information regarding the strain due to the pre-existing damage. This information can also be applied to situations where there are multiple drops.

The post-test examination of the new surrogate assembly showed the maximum grid crushing of 6.1 mm on the left side of the assembly at grid 10 (second spacer grid from the bottom nozzle end) in the 2020 test. The old assembly had slightly larger spacer grid deformation (the maximum grid crushing was 6.3 mm) in the 2019 test, except at a few locations. The spacer grid locations with the largest deformation were the same (bottom slap down end that hit the target a few milliseconds later than the top end) on the damaged (2019 test) and on the new (2020) surrogate assemblies.

During the 30 cm drop the impact occurred first on the top end of the assembly in the 2020 and 2019 tests. The assembly bottom end was a slap down end. The peak accelerations on the assembly top end were higher in the 2019 test compared to the 2020 test. The peak accelerations on the bottom end were lower in the 2019 test compared to the 2020 test. It appears that the pre-test assembly damage (crushed spacer grid) or slight differences in initial impact angle resulted in a smaller slap down effect in the 2019 test.

In the 2020 test the maximum negative peak strain (corrected for bias) was recorded by strain gauge SG10-0 (1,723 microstrain). The next two highest negative values were recorded by SG11-0 (1,169 microstrain) and SG-12 (1,067 microstrain). These three strain gauges were located at the bottom end of the assembly. In the 2019 test the maximum negative peak strain (corrected for bias) was recorded by strain gauge SG8-0 (1,736 microstrain) located on the top end of the assembly. Smaller strains were recorded by the strain gauges located within the short spans between spacer grids in the 2020 and 2019 tests compared to the ones located in the long spans as expected from the pre-test modeling. The data collected in the 2020 and 2019 tests suggest that the effects of the pre-test spacer grid crushing on the rod strain are relatively small.

Generally, in the 2020 test the strain due to upward and downward curvature was somewhat higher and the strain due to lateral bending was slightly lower compared to the 2019 test. The possible explanation is that the pre-test crushing of the spacer grid in the 2019 test limited the ability of the rods to bend in the vertical direction and caused more bending in the lateral direction.

Pressure paper was inserted between the rods within the two long spans between spacer grids (top and bottom end of the assembly) and within two short spans between spacer grids (mid-part of the assembly) prior to the 2020 test. The pressure paper range was from 0.00725 ksi to 6.24 ksi. The pressure paper sheets from the two short spans were blank after the 2020 test. All, except a few, pressure paper sheets from the two long spans between spacer grids showed marks indicating either rod-to-rod or rod-to-guide tube contact in 2020 test. The top and bottom rods experienced much higher contact pressures than the rods in the middle. A contact pressure of 4.1 ksi is a reasonable estimate of the maximum rod-to-rod contact pressure in the 2020 test. The points of the maximum pressure are located at the middle of the span where the bending is maximum.

In the 2019 test the pressure paper range was from 0.00725 ksi to 1.48 ksi. As a result, the actual maximum pressure was captured only in a few locations. At these locations, the maximum contact pressure was higher in the 2020 test than in the 2019 test. A possible explanation is that the pre-test spacer grid crushing in the 2019 test limited the rod bending as well as their capability to come into contact or broadened the length of contact along the rod and thereby reduced the peak contact stress.

The major conclusion that can be drawn from the 30cm drop test is that the fuel rods will maintain their integrity after being dropped 30 cm or less. This is demonstrated in Figures 5-1 – 5-3.

Figure 5-1 shows the stress-strain curve for low burnup cladding (room temperature) from PNNL-17700 [19]. Also shown in this figure are:

- minimum and maximum strain values observed in the 2020 test and the corresponding stress range
- maximum rod-to-rod contact pressure in the 2020 test and the corresponding maximum strain.

Figure 5-2 shows the portion of the elastic part of this curve to better illustrate the observed strain and stress ranges. The stress corresponding to the maximum strain value was 22.3 ksi in 2020 test. The maximum rod-to-rod contact pressure was 4.1 ksi. Both values are significantly below the yield strength of the cladding. The stress corresponding to the maximum strain value observed in the 2019 test with the damaged assembly was only slightly higher - 22.9 ksi.

Figure 5-3 shows the fatigue curve from O'Donnell-Langer [20] and the NRC curve based on CIRFT data [21]. The maximum bending strain and the strain corresponding to the maximum rod-to-rod contact pressure in 2020 test are placed in both fatigue curves. The number of cycles to failure with the maximum observed bending strain magnitude is 855 for the fatigue curve from [20] and 3.00E04 for the fatigue curve from [21]. The number of cycles to failure with the strain corresponding to the maximum rod-to-rod contact pressure is 3.0E07 for the fatigue curve from [20] and 4.2E20 for the fatigue curve from [21]. Consequently, the cladding is expected to maintain its integrity even after multiple 30 cm drops.

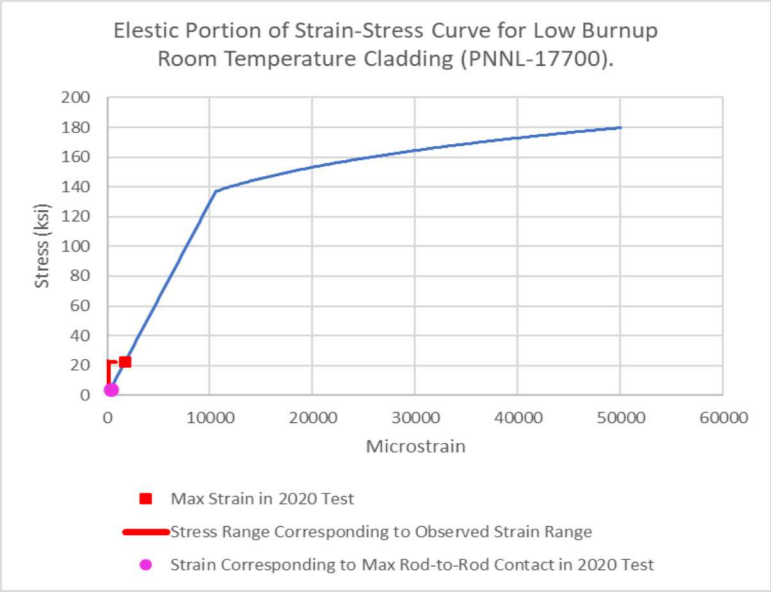

Figure 5-1 Stress and Rod-to-Rod Contact Pressure Range in the 2020 Test Based on the Strain-Stress Curve for the Low Burnup Cladding [19].

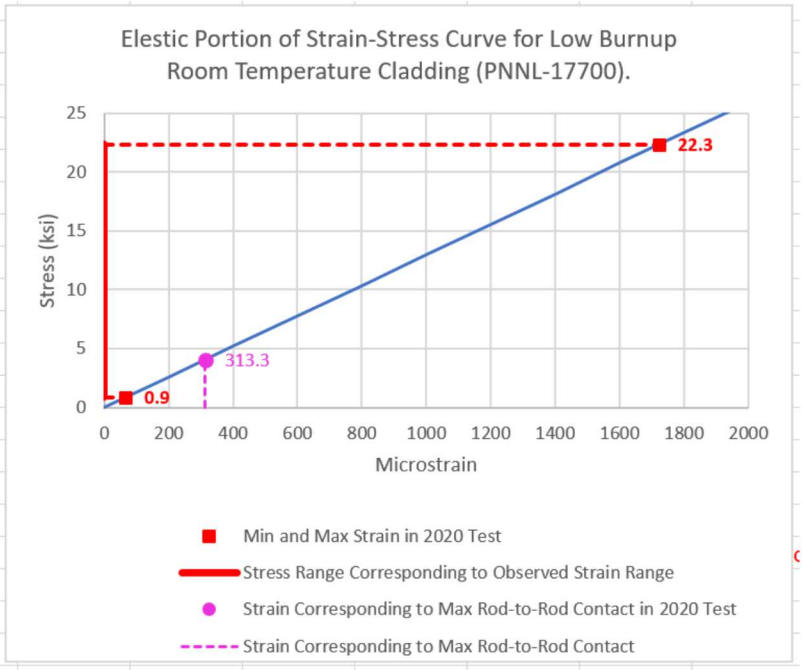

Figure 5-2. Closeup of the Stress and Rod-to-Rod Contact Pressure Range in the 2020 Test Based on the Strain-Stress Curve for the Low Burnup Cladding [19].

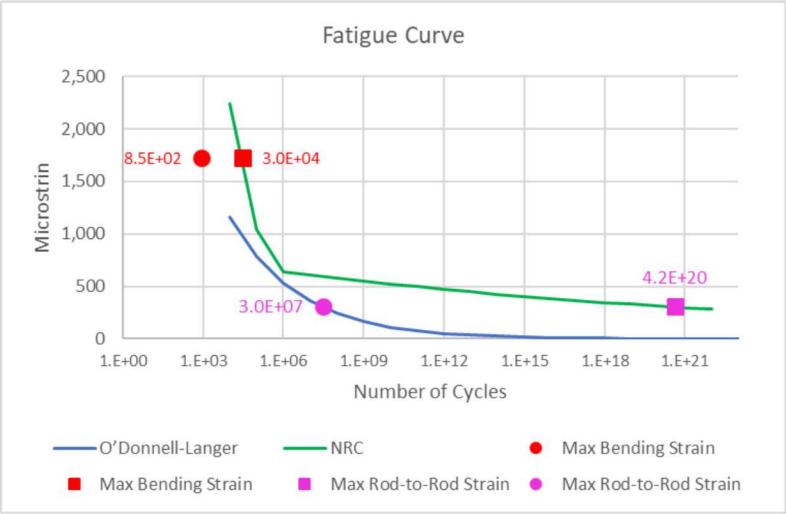

Note: The fatigue curves are from {20} and [21].

Figure 5-3. Number of Fatigue Cycles with the Maximum Bending and Rod-to-Rod Strain Observed in the 2020 Test.

6. REFERENCES

1. Sandia National Laboratories, "*Data Analysis of ENSA-DOE Rail Cask Tests"*, https://www.osti.gov/biblio/1532526-data-analysis-ensa-doe-rail-cask-tests.
2. Kalinina, E., N. Gordon, D. Ammerman, W. Uncapher, S. Saltzstein, and C. Wright, 2018. "*Results and Correlations from Analyses of the ENSA ENUN 32P Cask Transport Tests*", Proceedings of the Pressure Vessels and Piping (PVP) Conference, Prague, Czech Republic, 2018.
3. Kalinina, E., C. Wright, L. Lujan, and S. Saltzstein, 2019. "*Shock Environments for the Nuclear Fuel Transportation System (Transportation Platform, Cask, Basket, and Surrogate Assemblies) during Rail Transport*", Proceedings, PATRAM-2019, New Orleans, LA, August 2019.
4. Kalinina, E., C. Wright, L. Lujan, and S. Saltzstein, 2019. "*Shock Environments for the Nuclear Fuel Transportation System (Transportation Platform, Cask, Basket, and Surrogate Assemblies) during Heavy-Haul Transport and handling*", Proceedings, PATRAM-2019, New Orleans, LA, August 2019.
5. Kalinina, E., L. Lujan, C. Wright, and S. Saltzstein, 2019. "*Shock Environments for the Nuclear Fuel Transportation System (Transportation Platform, Cask, Basket, and Surrogate Assemblies) during Ocean Transport*", Proceedings, PATRAM-2019, New Orleans, LA, August 2019.
6. Kalinina, E., C. Wright, L. Lujan, and S. Saltzstein, 2019. "*Shock Environments for the Nuclear Fuel Transportation System (Transportation Platform, Cask, Basket, and Surrogate Assemblies) during Specialized Rail Tests*", Proceedings, PATRAM-2019, New Orleans, LA, August 2019.
7. Kalinina, E., D. Ammerman, C. Grey, M. Arviso, C. Wright, L. Lijan, S. Saltzstein, S. Ross, N. Klymyshyn, B. Hanson, A. Palacio, I. Fernandez, G. Garmendia, G. Calleja, W. Choi, 2019. "*International Multi-Modal Spent Nuclear Fuel Transportation Test: The Transportation Test Triathlon*", Proceedings of the IAEA International Conference on the Management of Spent Fuel from Nuclear Power Reactors: Learning from the Past, Enabling the Future, Vienna, June 2019.
8. Klymyshyn, N.A., P. Ivanusa, K. Kadooka, C.J. Spitz, P.J. Jensen, S.B. Ross, and B.D. Hanson, 2018. "*Modelling and Analysis of the ENSA/DOE Multimodal Transportation Campaign*", PNNL-28088. Pacific Northwest National Laboratory, Richland, WA, 2018.
9. Sandia National Laboratories, "*Cask Transportation Test".*

   https://www.youtube.com/watch?v=wGKtgrozrGM&feature=youtu.be
10. Kalinina, E., D. Ammerman, C. Grey, M. Arviso, C. Wright, L. Lujan, G. Flores, S. Saltzstein. 2019. *"30 cm Drop Tests".* SAND2019-15256 R, December 17, 2019.
11. Kalinina, E., D. Ammerman, C. Grey, G. Flores, S.J. Saltzstein, N.A. Klymyshyn, 2019. "*Full-Scale Assembly 30 cm Drop Test* ", MRS 43rd Symposium on Scientific Basis for Nuclear Waste Management, Vienna, October 2019.
12. Kalinina, E., D. Ammerman, C. Grey, M. Arviso, S. Saltzstein, F. Wille, T. Quercetti, A. Palacio, I. Fernandez, N. Klymyshyn, and S. Ross, 2019. "*Horizontal 30 cm Drop Test of 1/3 Scale ENSA ENUN 32P Dual Purpose Cask*", Proceedings, PATRAM-2019, New Orleans, LA, August 2019.
13. Flores, G., E. Kalinina, and D. Ammerman, 2020. "*Full-Scale Surrogate Assembly Drop Test Plan"*, March 2020.
14. Flores, G., 2020. "*Quality Assurance Implementation Procedure, Westinghouse 17x17 STD Fuel Assembly Surrogate Drop Test"*, Sandia National Laboratories, March 2020.
15. Ammerman, D.J., 2020. "*Margin of Safety for Lifting Loaded Fuel Assembly Tube*", Sandia National Laboratories internal document, Albuquerque, NM, 2020.

16. Klymyshyn, N.A., 2015. "*ENSA Impact Tests Model*", PNNL 2015.
17. Smallwood, D., 1981. *"An Improved Recursive Formula for Calculating Shock Response Spectra"*, Shock and Vibration Bulletin, Vol 51, No. 2, pp. 211-217.
18. Stearns, S.D. and R.A. David, 1988. "*Signal Processing Algorithms".* Prentice-Hall, Inc., Upper Saddle River, New Jersey.
19. Geelhood, K.J., C.E. Beyer, and W.G. Luscher, 2008. "*PNNL Stress/Strain Correlation for Zircaloy"*, PNNL-17700, July 2008.
20. O'Donnell, W.J. and B.F. Langer, 1964. "*Fatigue Design Basis for Zircaloy Components"*, Nuclear Science and Engineering (20):1–12.
21. NUREG-2224, "*Dry Storage and Transportation of High Burnup Spent Nuclear Fuel"*. Draft for Comment, 2018.

This page is intentionally left blank.

Appendices

Surrogate Assembly 30 cm Drop Test

List of Figures

Appendix A Spacer Grid Photos

This appendix provides the photos from the examination of the surrogate assembly spacer grid after the 2020 30 cm drop test. The height of the spacer grid was measured on the left and on the right sides of the surrogate assembly. Figure A-1 shows the spacer grid measurement nomenclature.

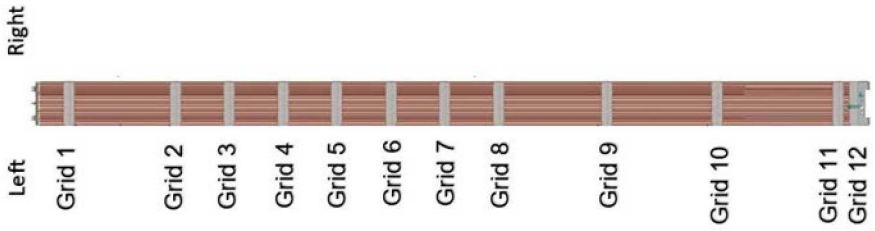

Figure A-1. Spacer Grid Measurement Nomenclature.

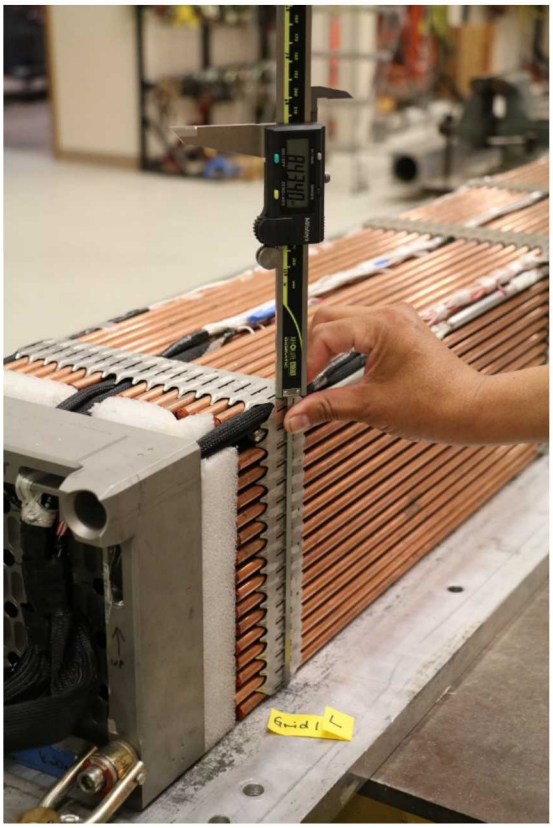

Figure A-1. Spacer Grid 1, Left.

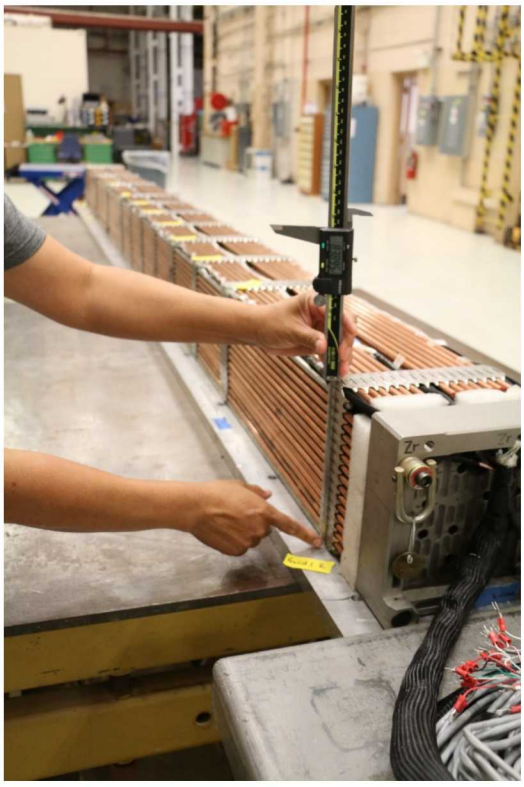

Figure A-2. Spacer Grid 1, Right.

Figure A-3. Spacer Grid 2, Left.

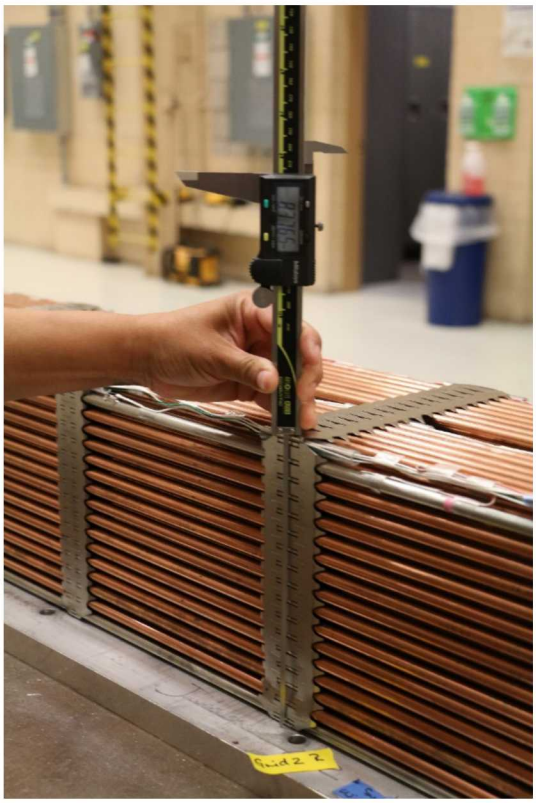

Figure A-4. Spacer Grid 2, Right.

Figure A-5. Spacer Grid 3, Left.

Figure A-6. Spacer Grid 3, Right.

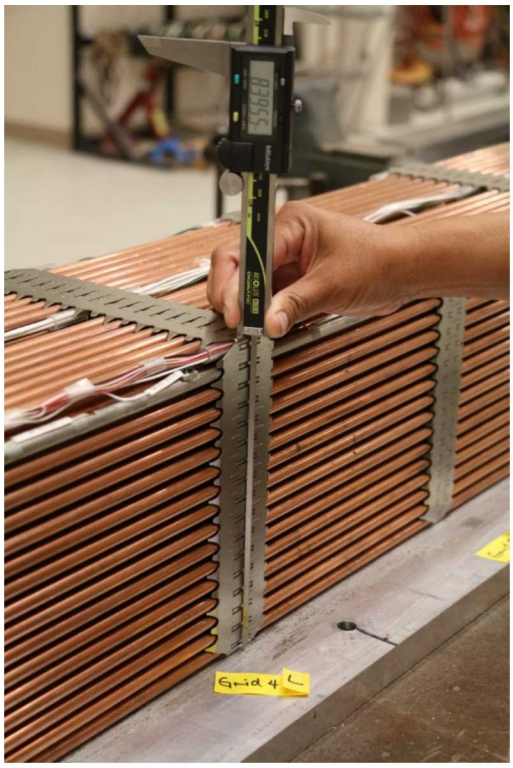

Figure A-7. Spacer Grid 4, Left

Figure A-8. Spacer Grid 4, Right.

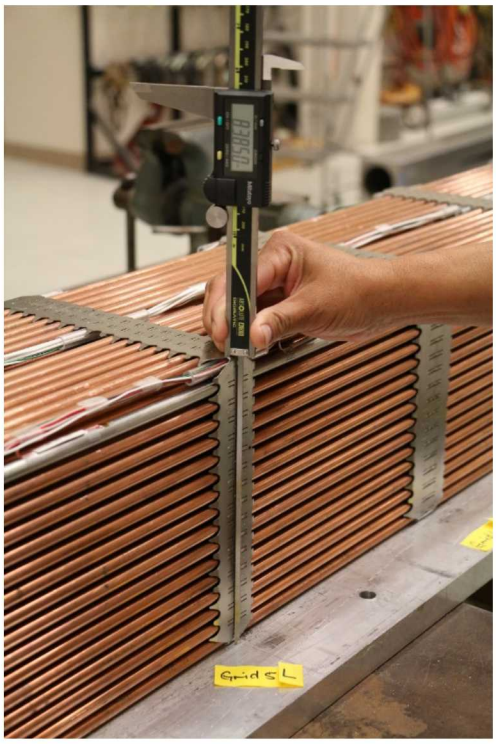

Figure A-9. Spacer Grid 5, Left.

Figure A-10. Spacer Grid 5, Right.

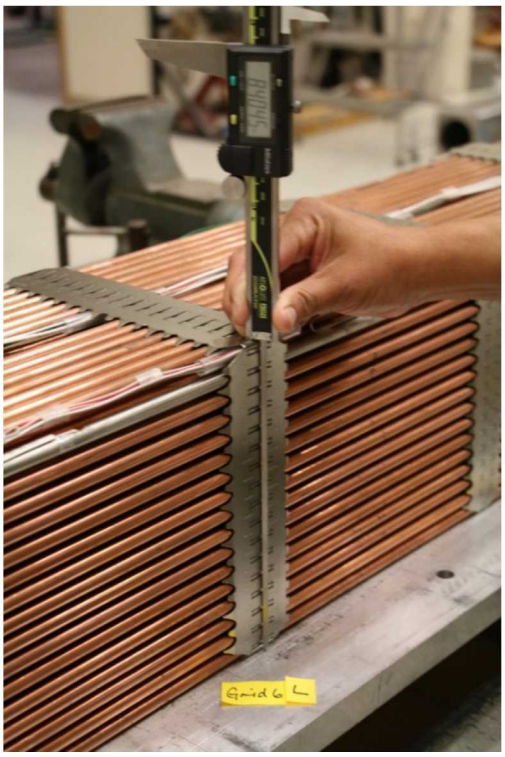

Figure A-11. Spacer Grid 6, Left.

Figure A-12. Spacer Grid 6, Right.

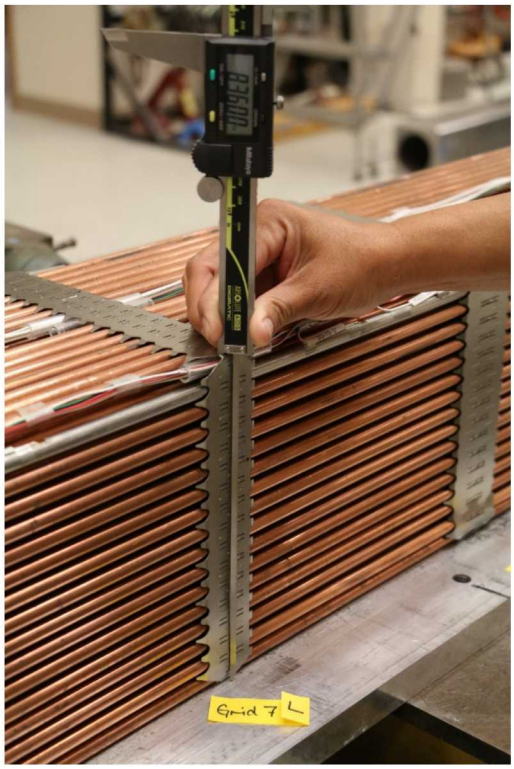

Figure A-13. Spacer Grid 7, Left.

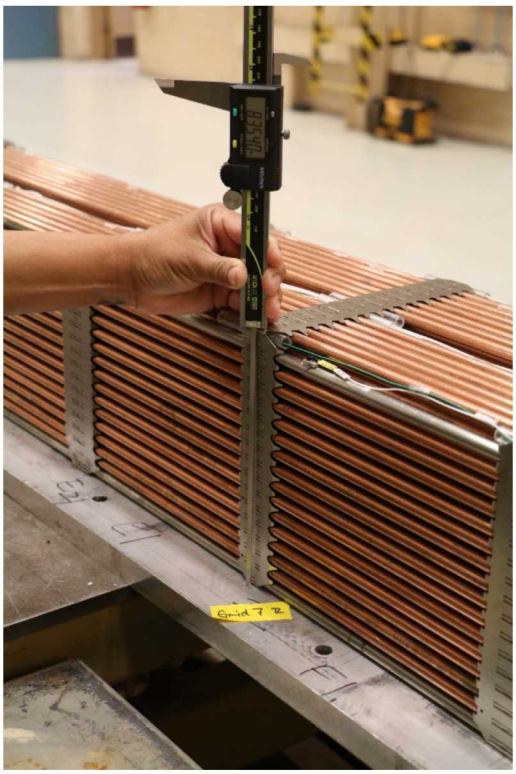

Figure A-14. Spacer Grid 7, Right.

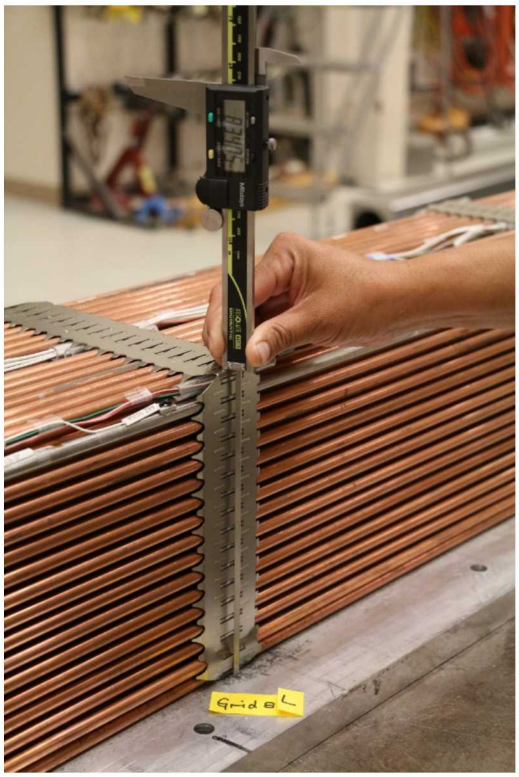

Figure A-15. Spacer Grid 8, Left.

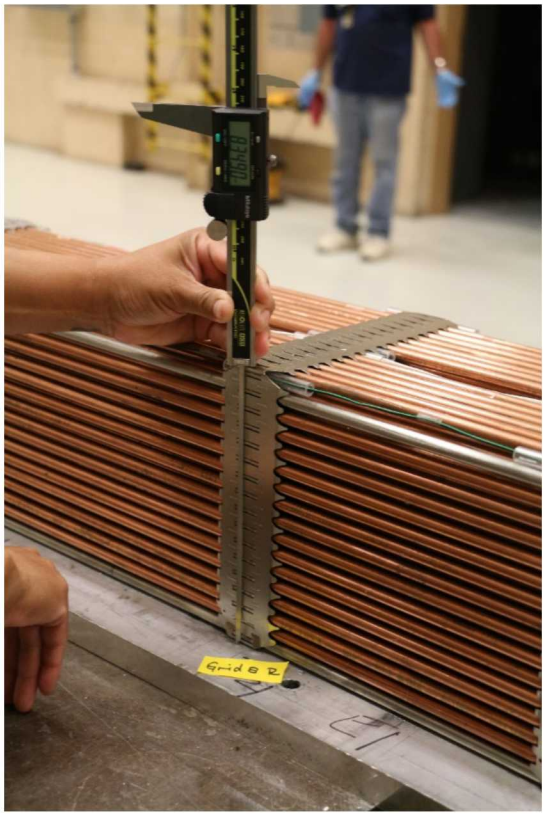

Figure A-16. Spacer Grid 8, Right.

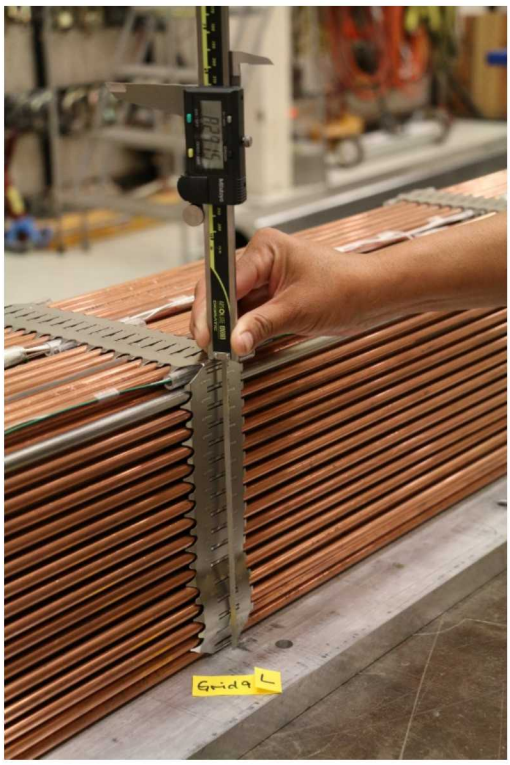

Figure A-17. Spacer Grid 9, Left.

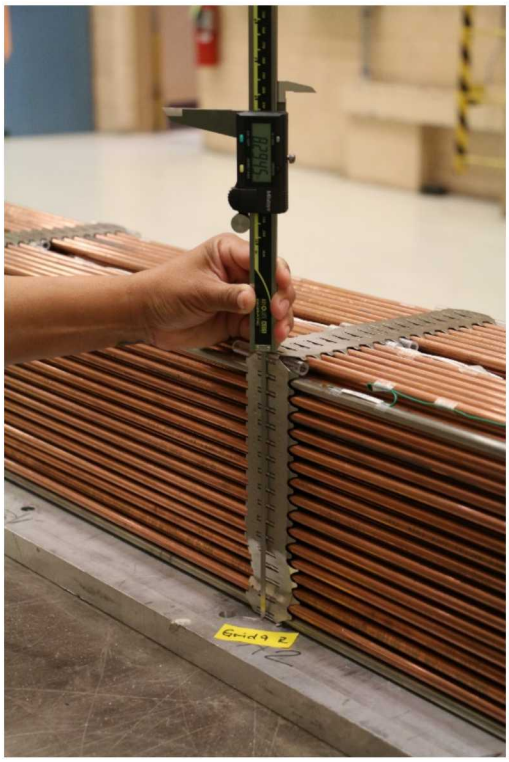

Figure A-18. Spacer Grid 9, Right.

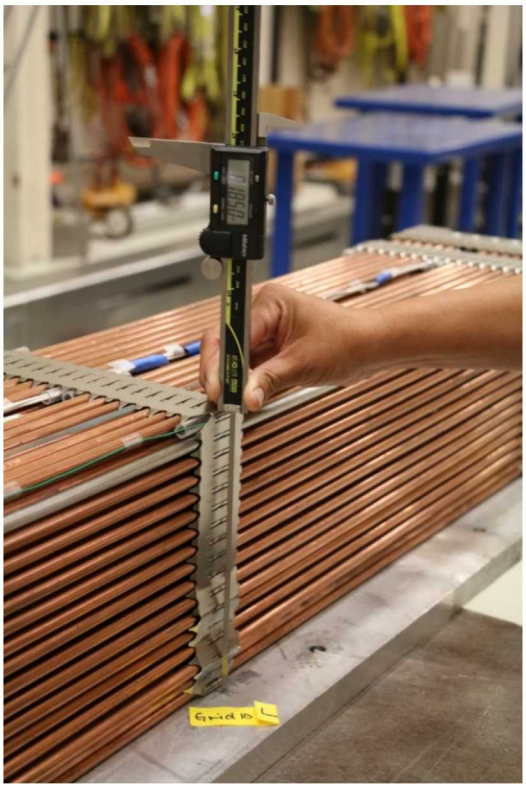

Figure A-19. Spacer Grid 10, Left.

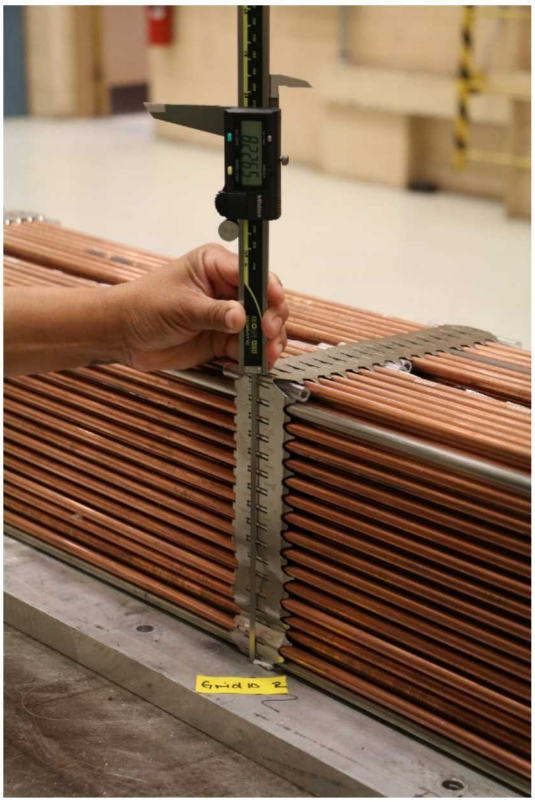

Figure A-20. Spacer Grid 10, Right.

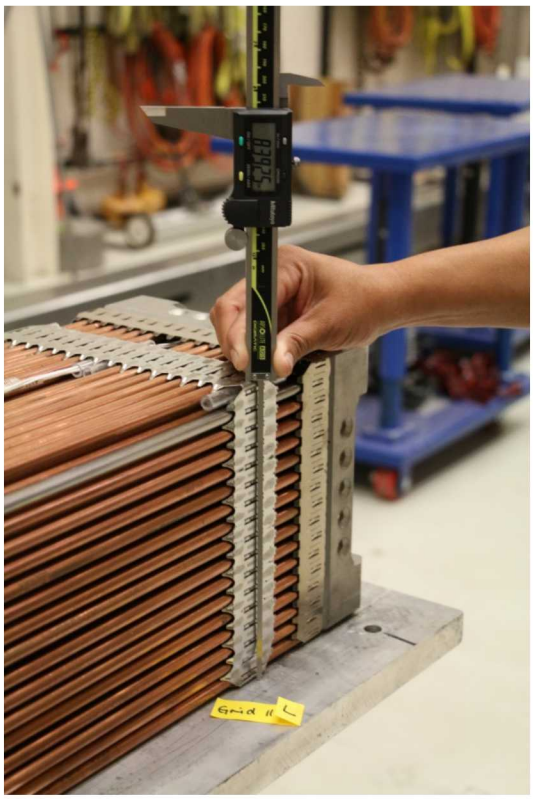

Figure A-21. Spacer Grid 11, Left.

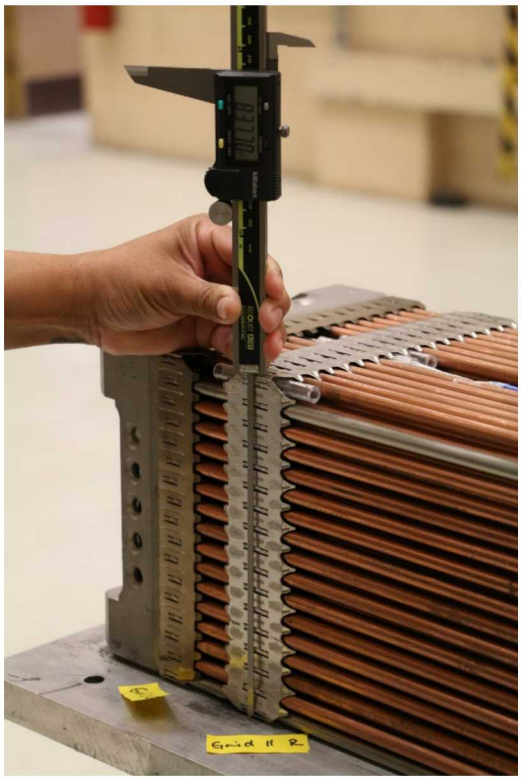

Figure A-22. Spacer Grid 11, Right.

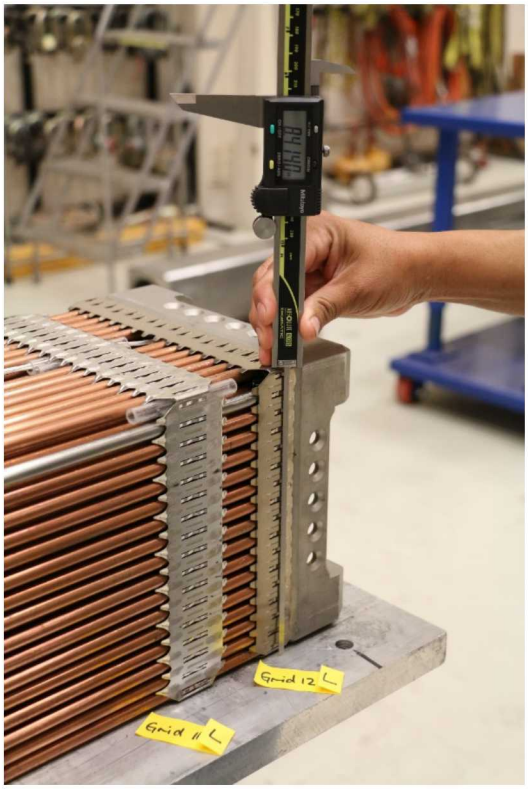

Figure A-23. Spacer Grid 12, Left.

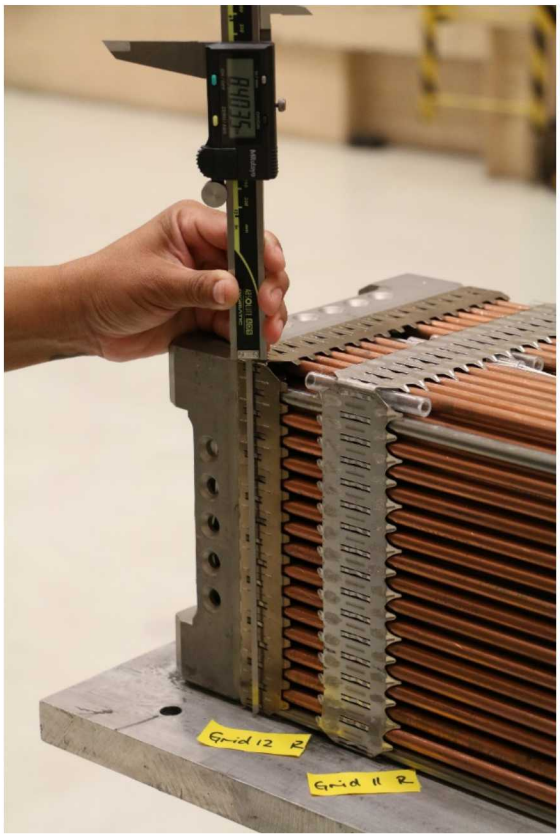

Figure A-24. Spacer Grid 12, Right.

Appendix B Pressure Paper Scans from May 2020 30 cm Drop Test

This appendix provides the original pressure paper scans from May 2020 30 cm drop test. Fifteen scans are from the long span next to the assembly bottom and fifteen scans are from the long span next to the assembly top (Figure B-1). The scans from two short spans were blank and are not included. The notation Bottom_01_C1 means that the pressure paper sheet is from the long span next to the assembly bottom, the paper is type C (Low), and it was placed between the rods 1 and 2 counting from the bottom up.

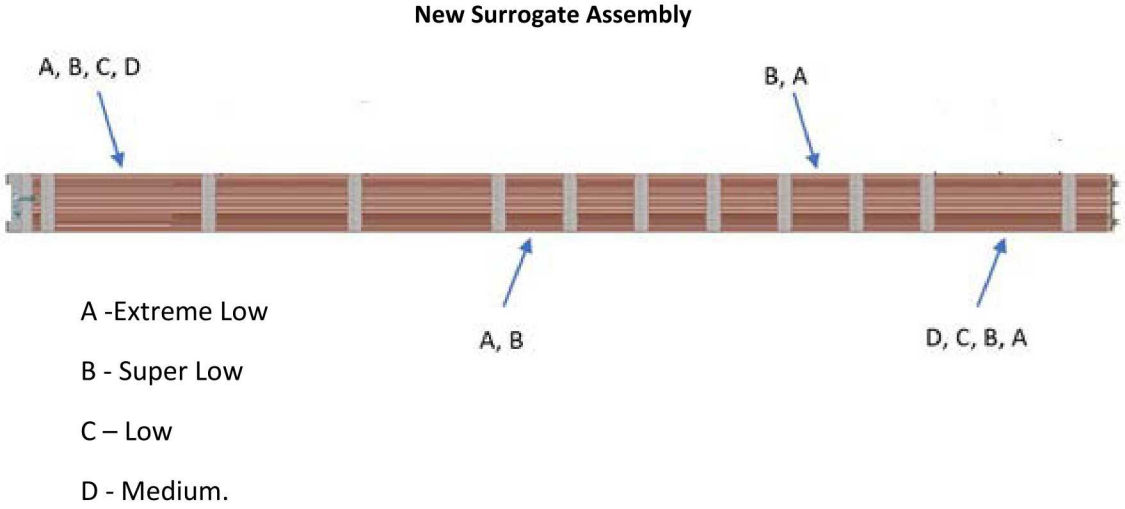

Figure B-1. Pressure Paper Locations and Specifications in May 2020 Test.

Figure B-2. May 2020 Bottom_01_C-1.

Figure B-3.May 2020 Bottom_02_B-1/

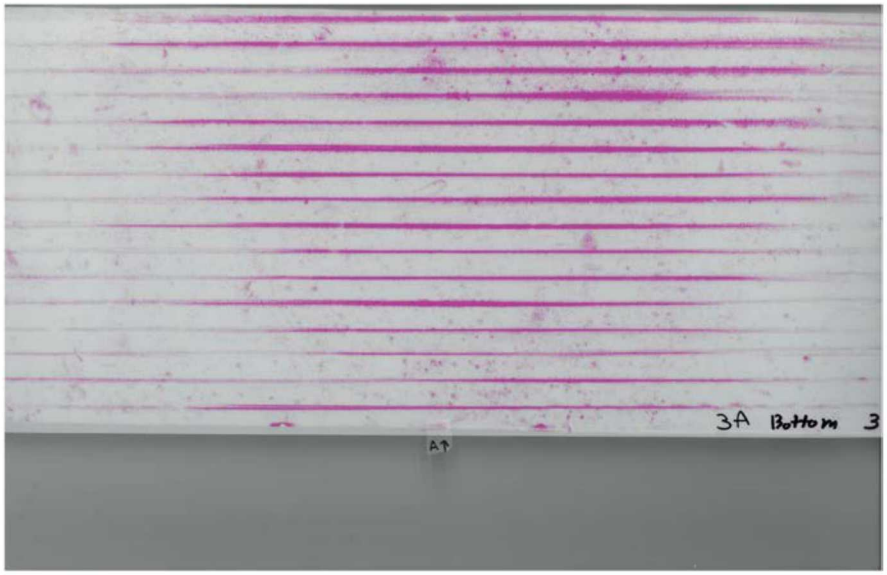

Figure B-4. May 2020 Bottom_03_A-1.

Figure B-5. May 2020 Bottom_04_D-1.

Figure B-6. May 2020 Bottom_05_C-1.

Figure B-7. May 2020 Bottom_06_B-1.

Figure B-8. May2020 Bottom_07_A-1.

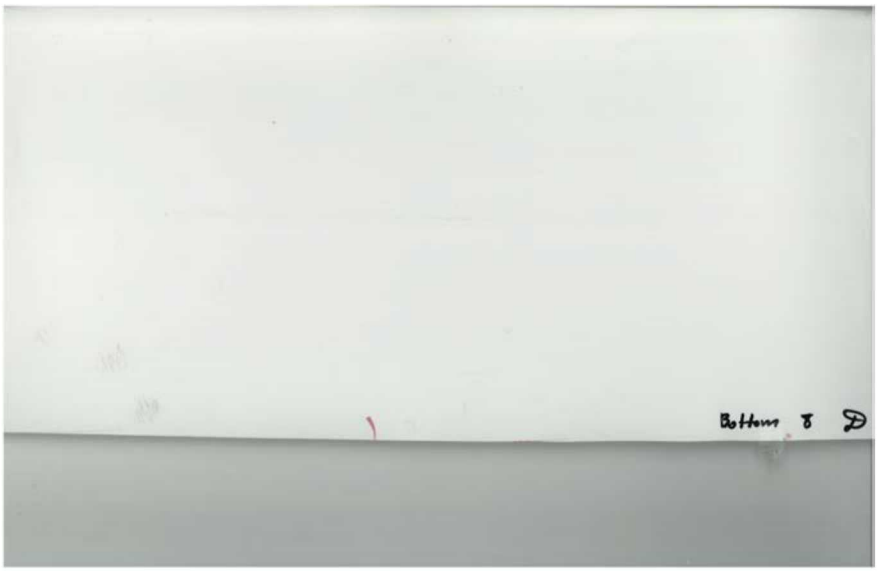

Figure B-9. May 2020 Bottom_08_D-1.

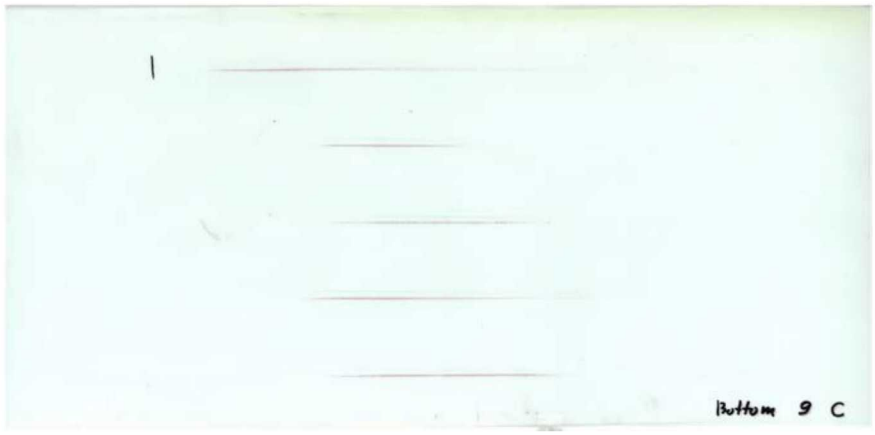

Figure B-10. May 2020 Bottom_09_C-1.

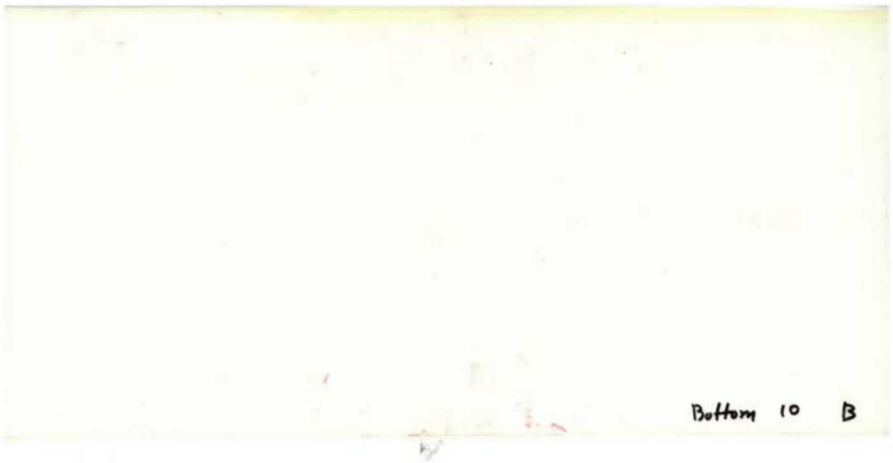

Figure B-11. May 2020 Bottom_10_B-1.

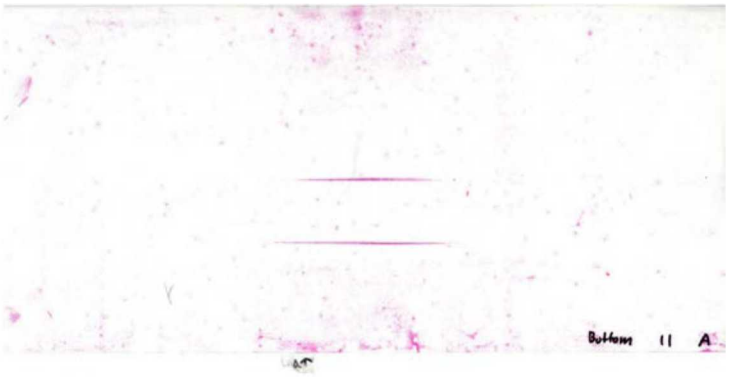

Figure B-12. May 2020 Bottom_11_A-1.

Figure B-13. May 2020 Bottom_12_D-1.

Figure B-14. May 2020 Bottom_13_C-1.

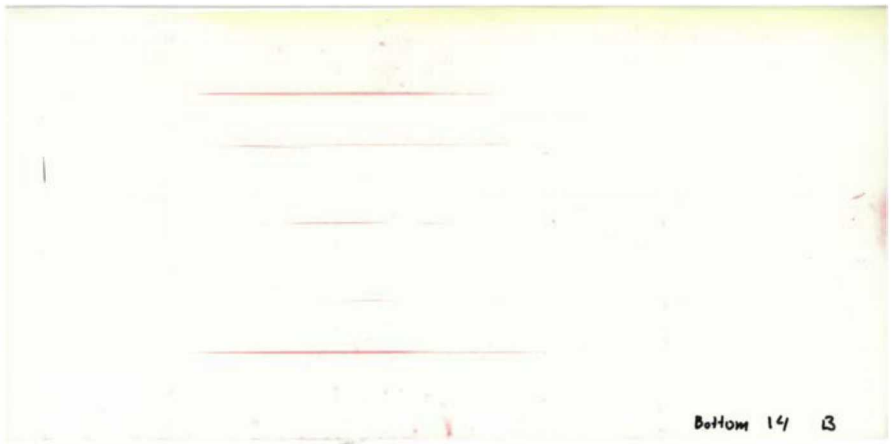

Figure B-15. May 2020 Bottom_14_B-1.

Figure B-16. May 2020 Bottom_15_A-1.

Figure B-17. May 2020 Top_01_B-1.

Figure B-18. May 2020 Top_02_C_Rescan_06292020-1.

Figure B-19. May 2020 Top_03_D-1.

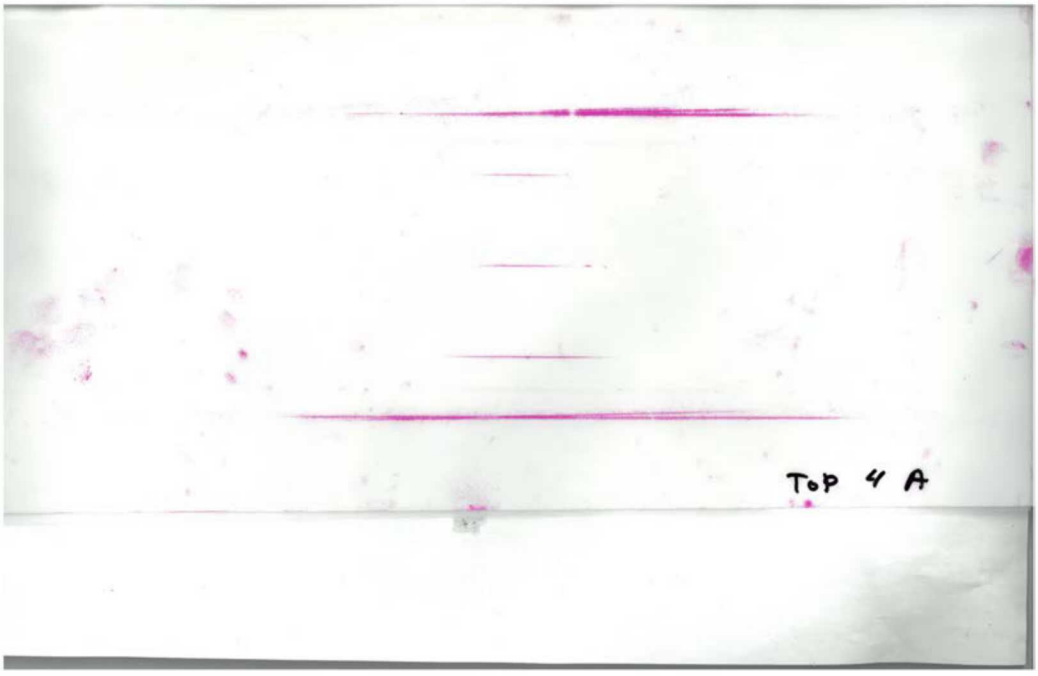

Figure B-20.May 2020 Top_04_A-1.

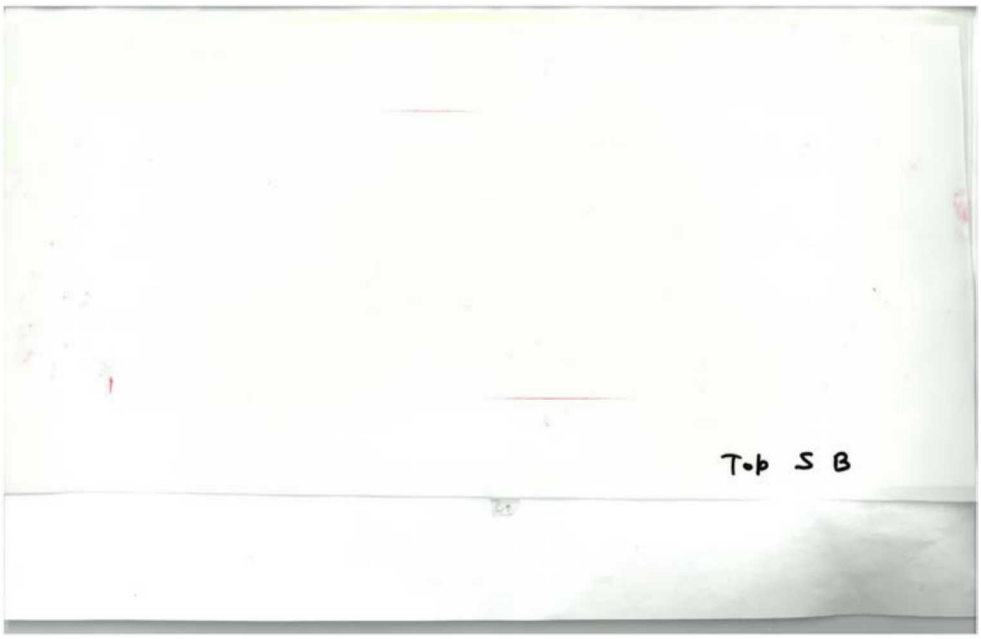

Figure B-21. May 2020 Top_05_B-1.

Figure B-22. May 2020 Top_06_C_Rescan_06232020-1.

Figure B-23. May 2020 Top_07_D_Rescan_06232020-1.

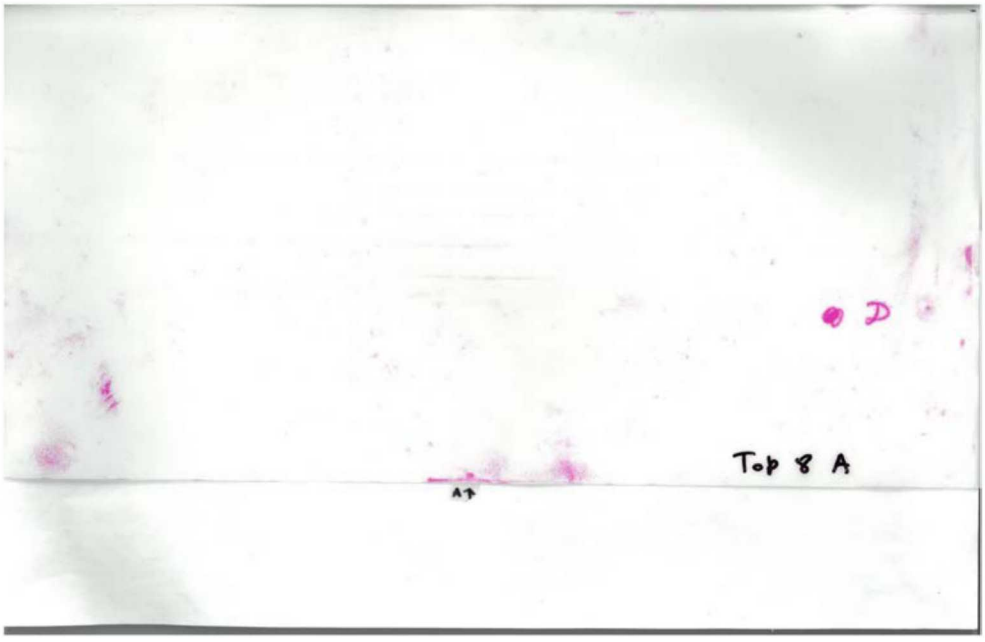

Figure B-24. May 2020 Top_08_A-1.

Figure B-25. May 2020 Top_09_B-1.

Figure B-26. May 2020 Top_10_C-1.

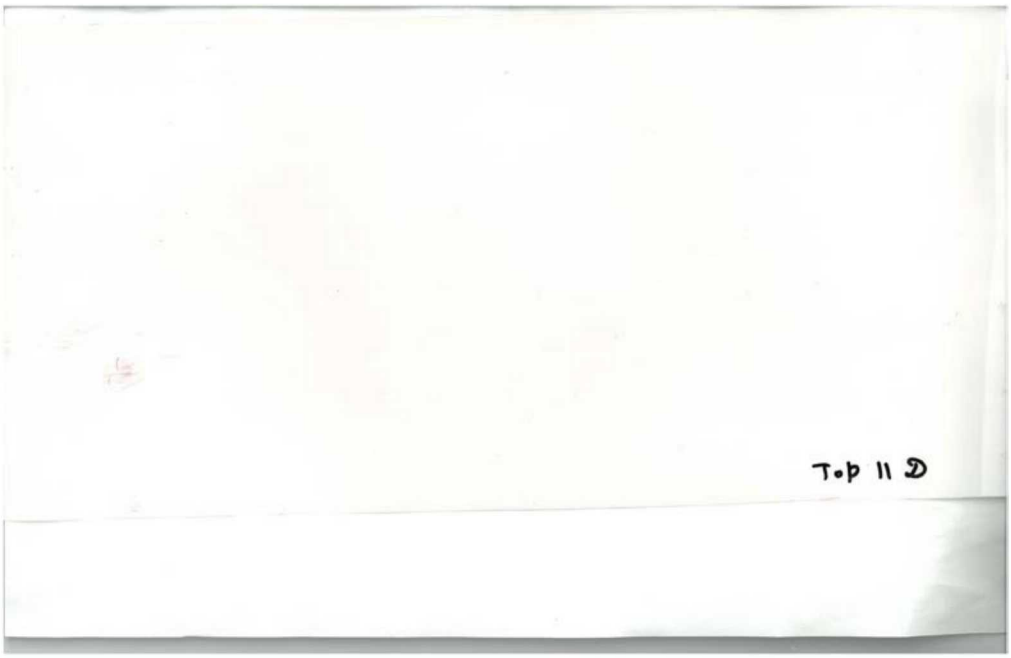

Figure B-27. May 2020 Top_11_D-1.

Figure B-28. May 2020 Top_12_A-1.

Figure B-29. May 2020 Top_13_B-1.

Figure B-30. May 2020 Top_14_C_Rescan_06232020-1.

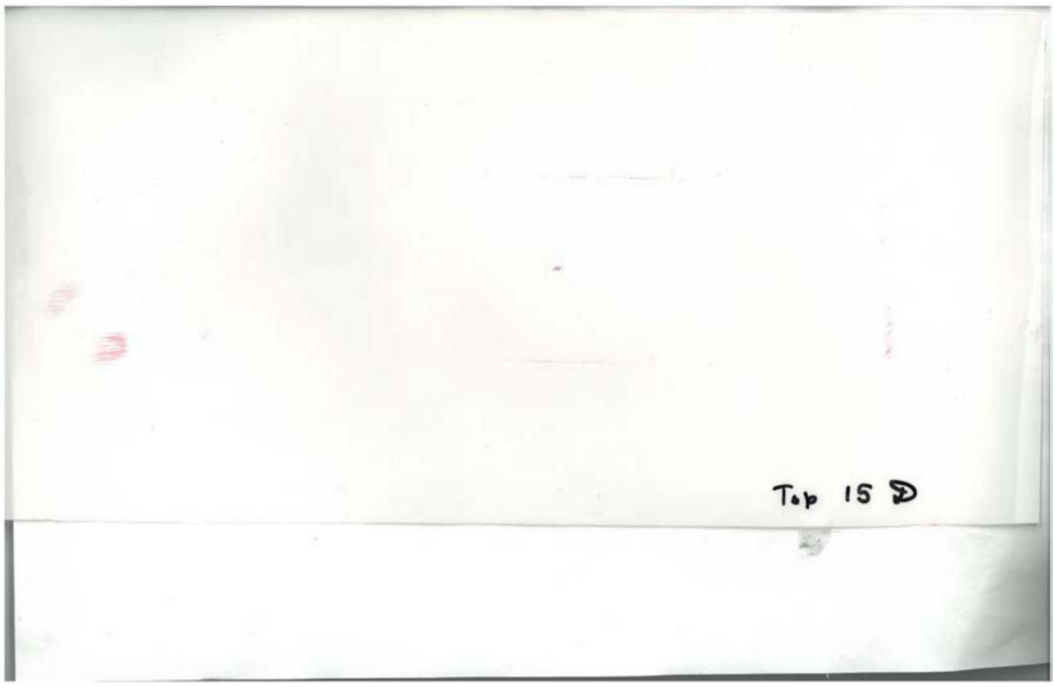

Figure B-31. May 2020 Top_15_D-1.

Appendix C Pressure Paper Scans from June 2019 30 cm Drop Test

This appendix provides the original pressure paper scans from June 2019 30 cm drop test. Fifteen scans are from the long span next to the assembly bottom and fifteen scans are from the long span next to the assembly top (Figure B-31). The notation B_01_02 means that the pressure paper sheet is from the long span next to the assembly bottom and the pressure paper was placed between the rods 1 and 2 counting from the bottom up. Figure B-31 provides the pressure paper types used in this test.

Figure C-1. Pressure Paper Locations and Specifications in June 2019 Test.

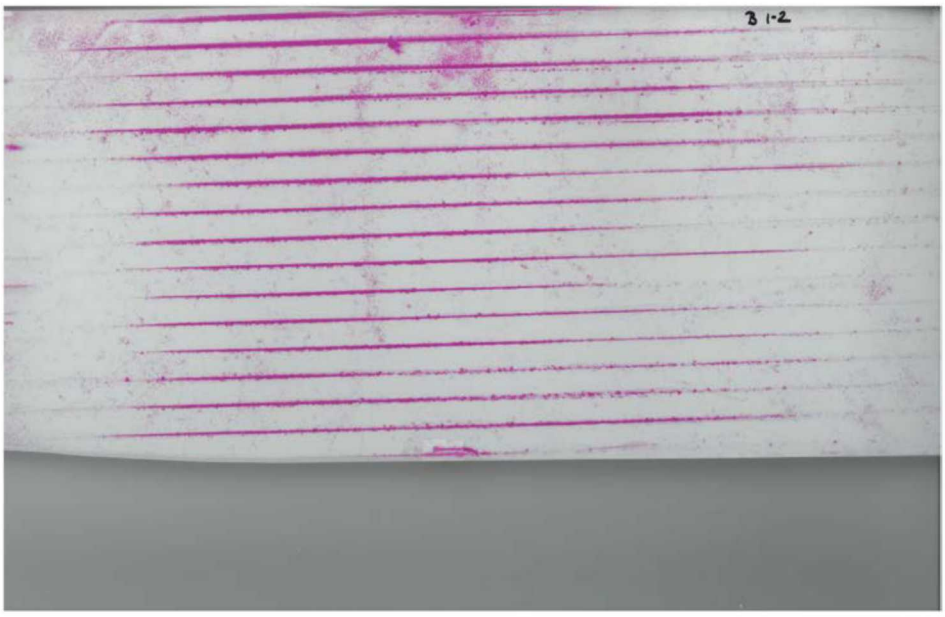

Figure C-2. June 2019 B 01-02 Rescan 08_2020-1.

Figure C-3. June 2019 B 02-03 Rescan 08_2020-1.

Figure C-4. June 2019 B 03-04 Rescan 08_2020-1.

Figure C-5. June 2019 B 04-05-1.

Figure C-6. June 2019 B 05-06 Rescan 08_2020-1.

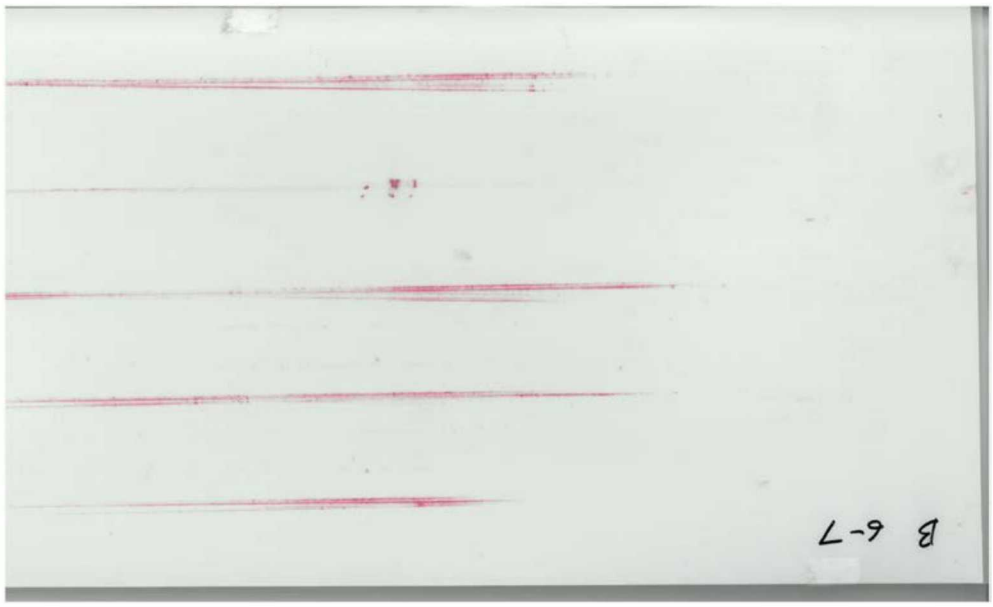

Figure C-7. June 2019 B 06-07-1.

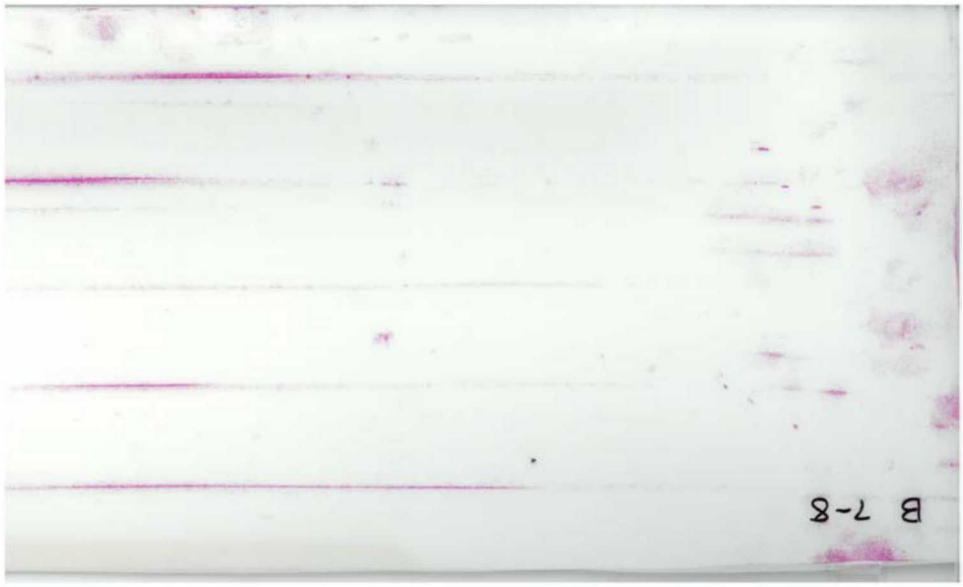

Figure C-8. June 2019 B 07-08-1.

Figure C-9. June 2019 B 08-09-1.

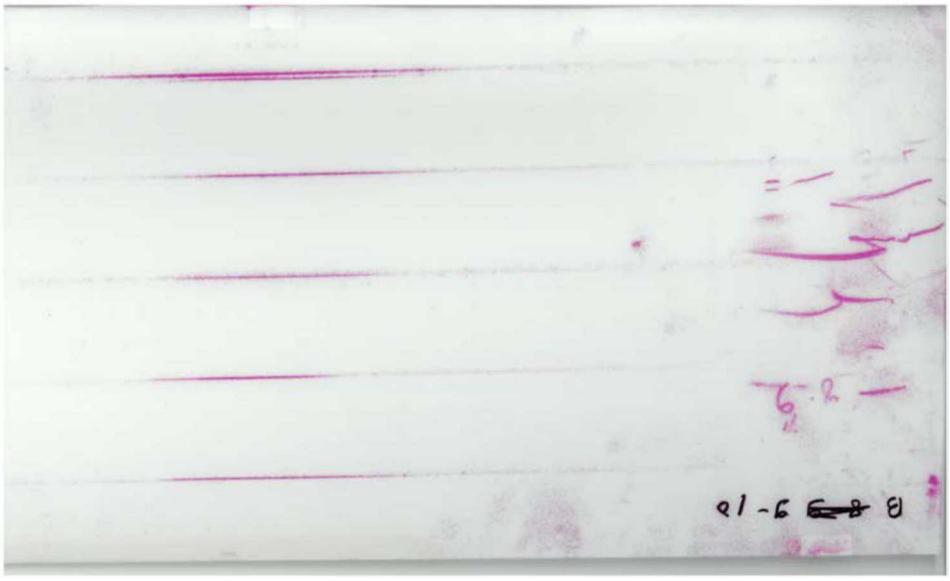

Figure C-10. June 2019 B 09-10-1.

Figure C-11. June 2019 B 10-11-1.

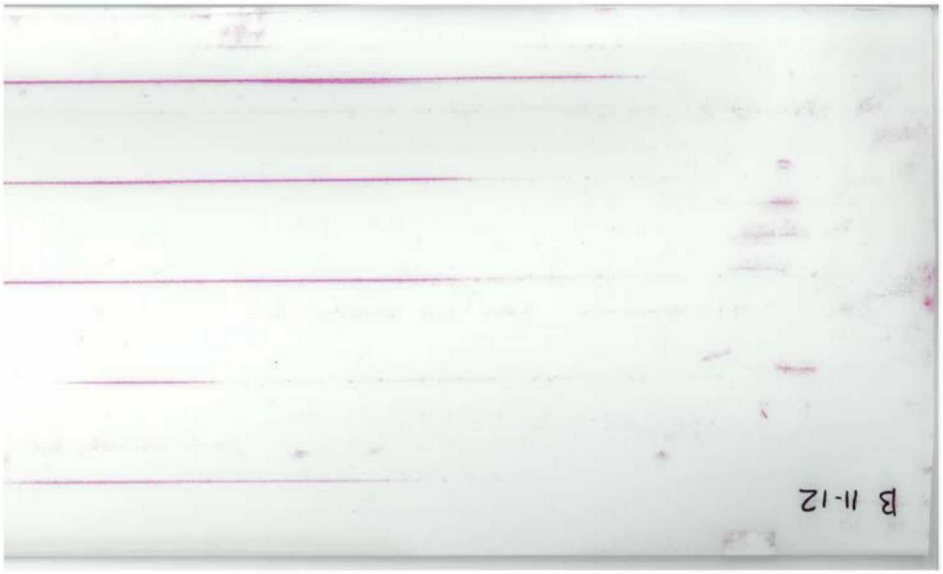

Figure C-12 June 2019 B 11-12-1.

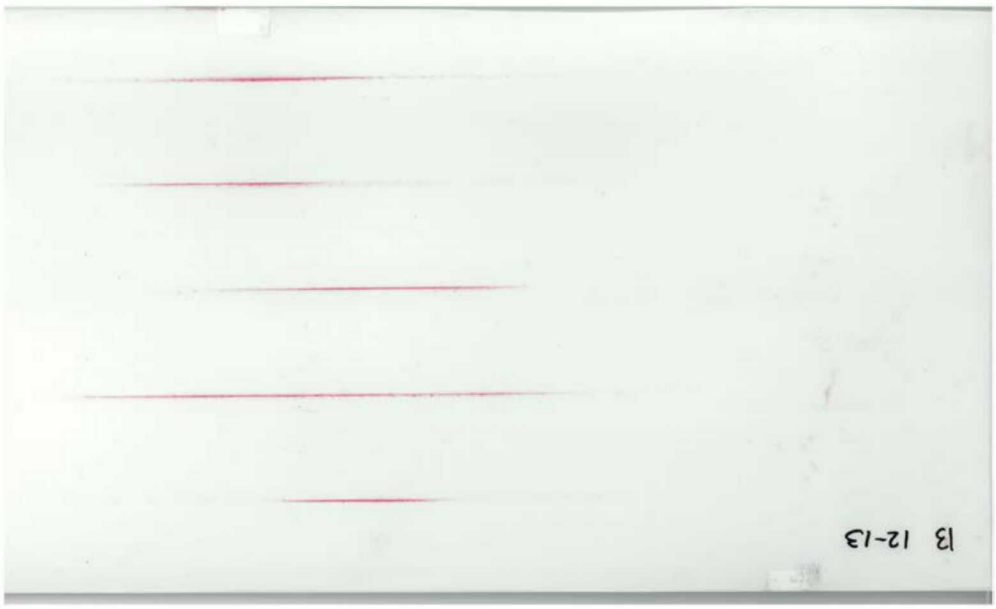

Figure C-13. June 2019 B 12-13-1.

Figure C-14. June 2019 B 13-14-1.

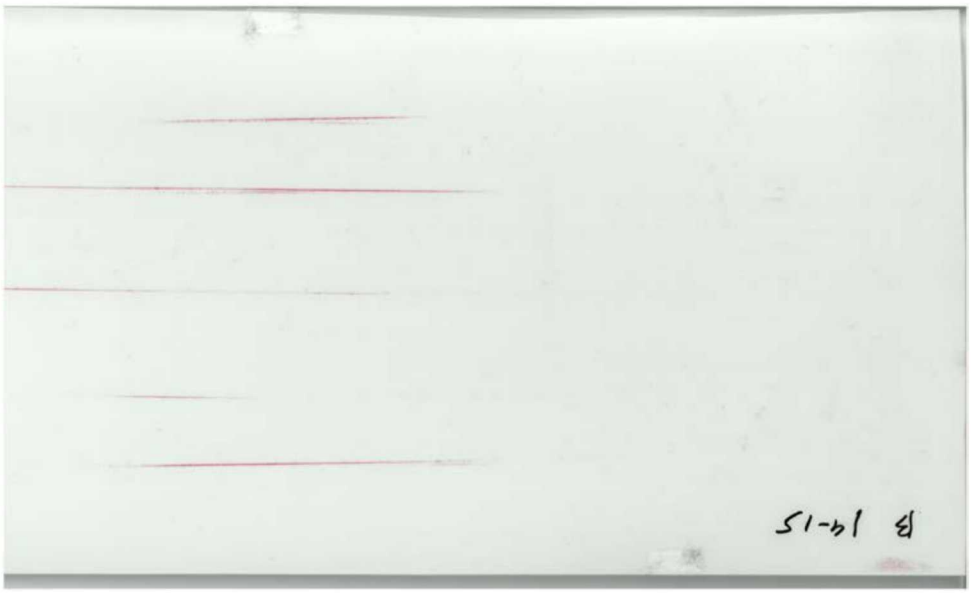

Figure C-15. June 2019 B 14-15-1.

Figure C-16. June 2019 B 15-16-1.

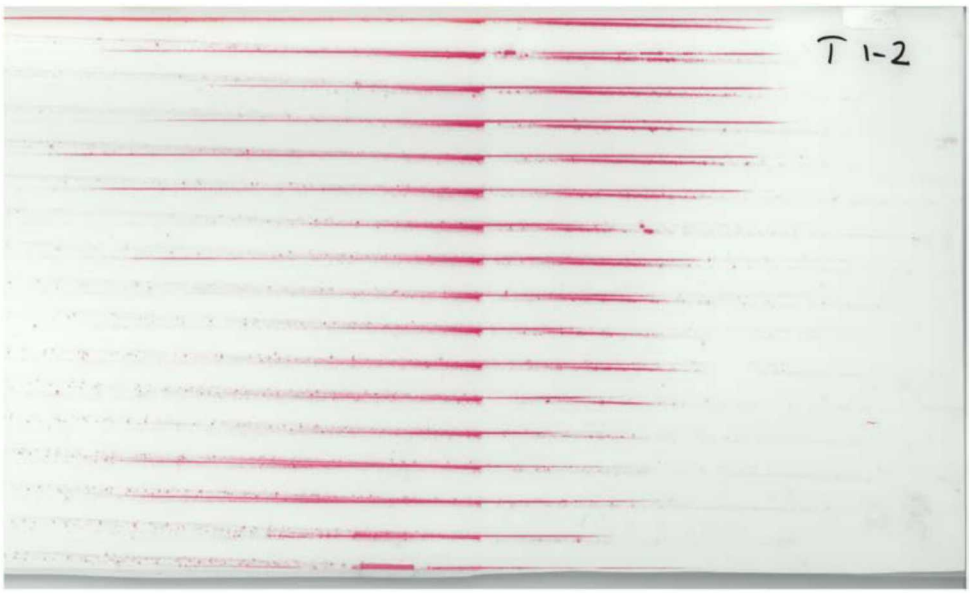

Figure C-17. June 2019 T 01-02-1.

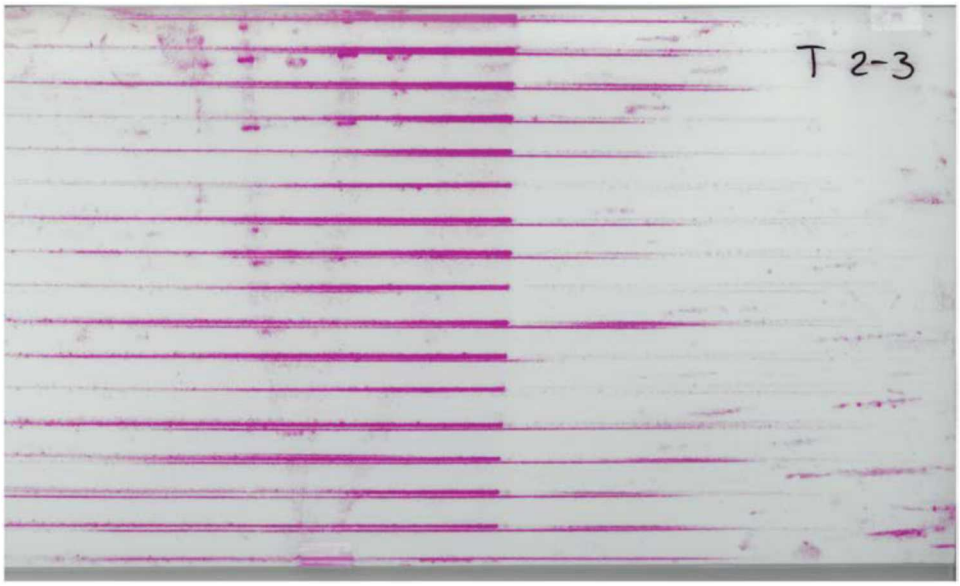

Figure C-18. June 2019 T 02-03-1.

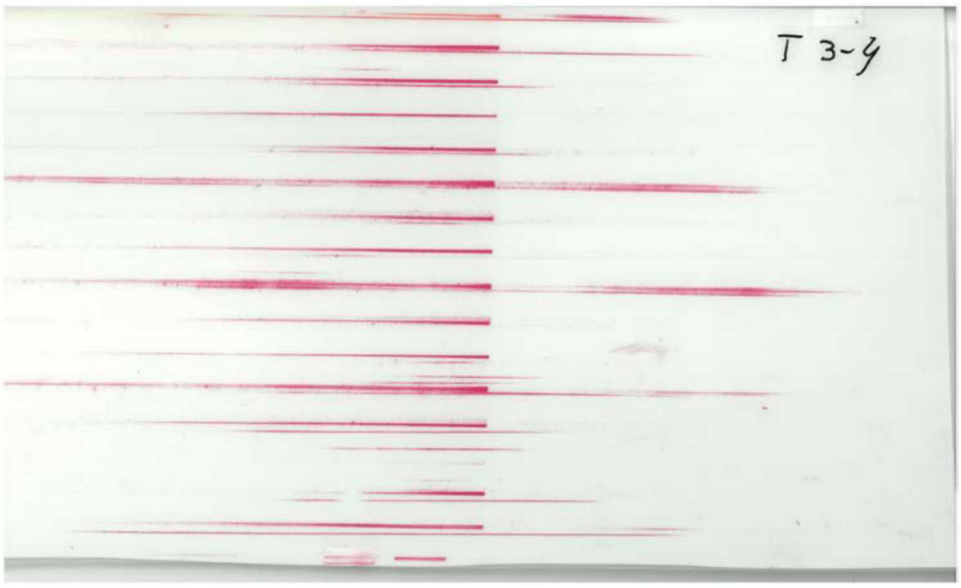

Figure C-19. June 2019 T 03-04-1.

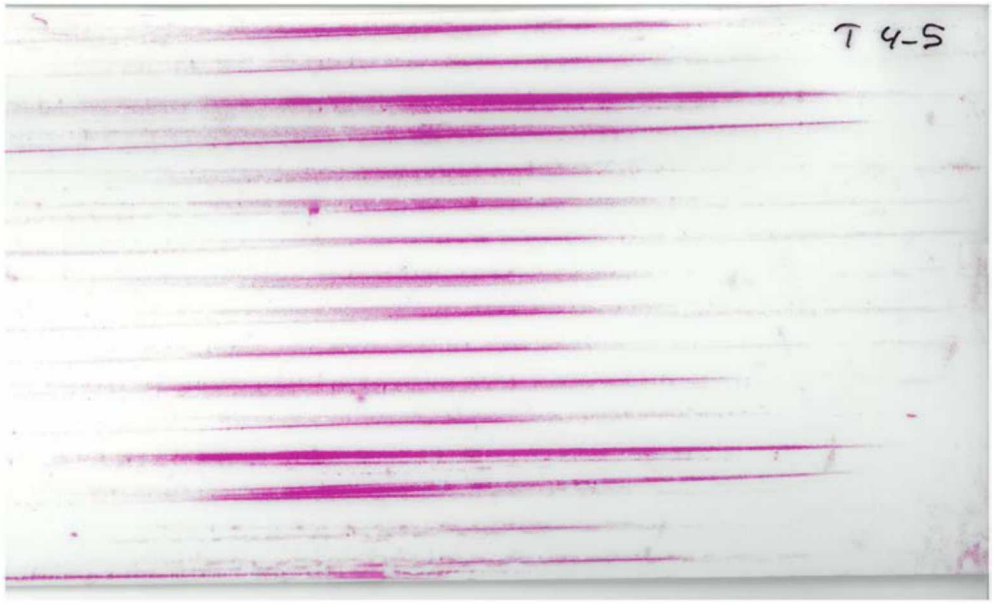

Figure C-20. June 2019 T 04-05-1.

Figure C-21. June 2019 T 05-06-1.

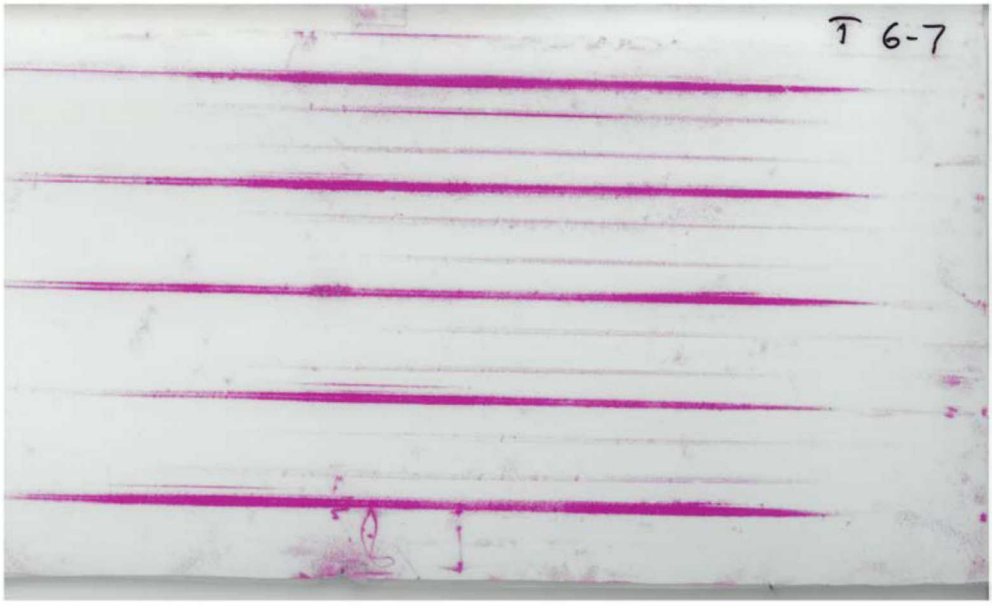

Figure C-22. June 2019 T 06-07-1.

Figure C-23. June 2019 T 07-08-1.

Figure C-24. June 2019 T 08-09-1.

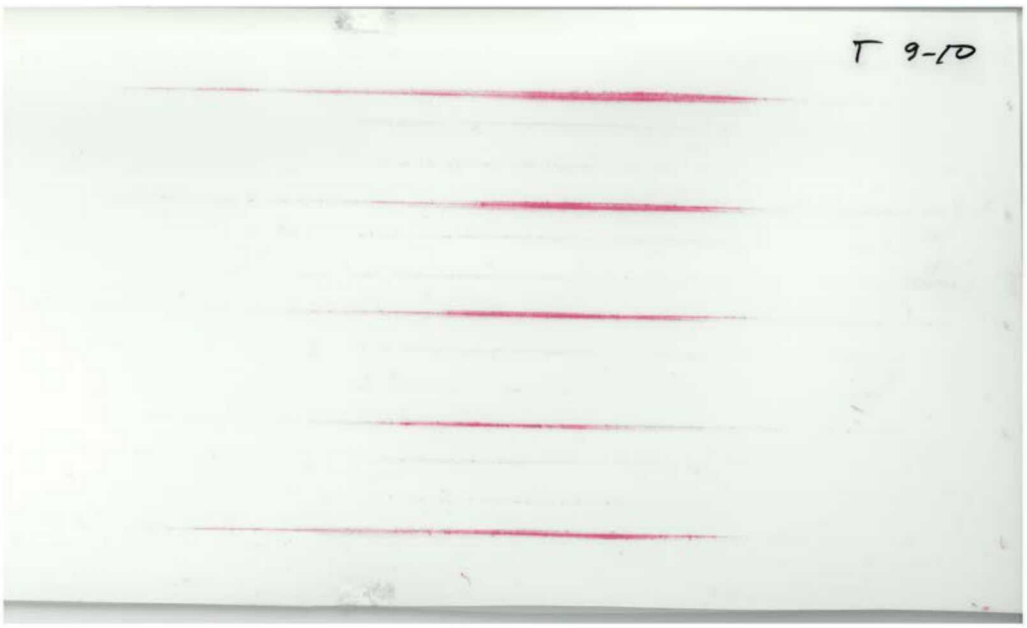

Figure C-25. June 2019 T 09-10-1.

Figure C-26. June 2019 T 10-11-1.

Figure C-27. June 2019 T 11-12-1.

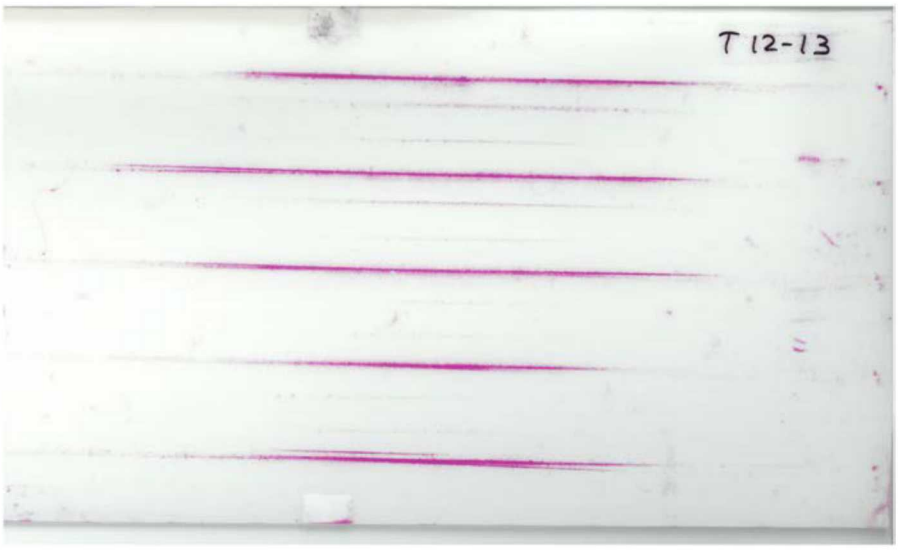

Figure C-28. June 2019 T 12-13-1.

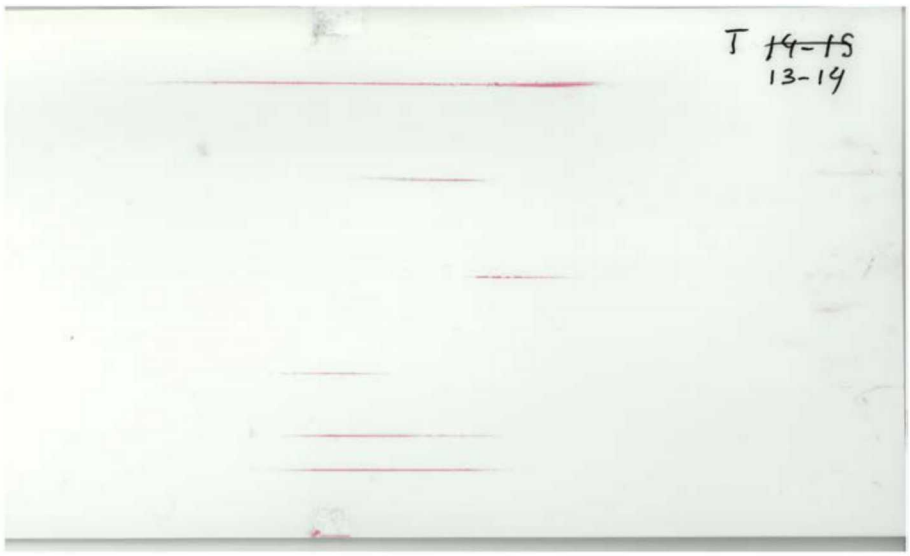

Figure C-29. June 2019 T 13-14-1.

Figure C-30. June 2019 T 14-15-1.

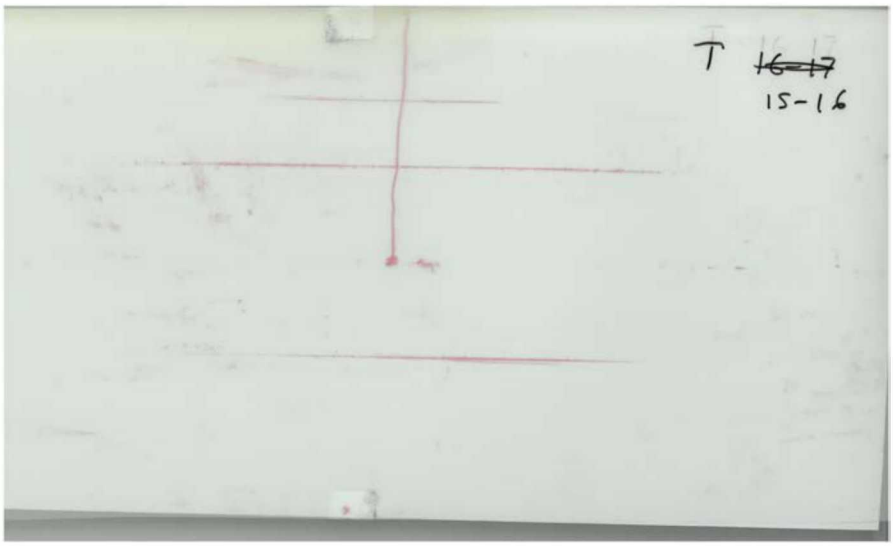

Figure C-31. June 2019 T 15-16-1.

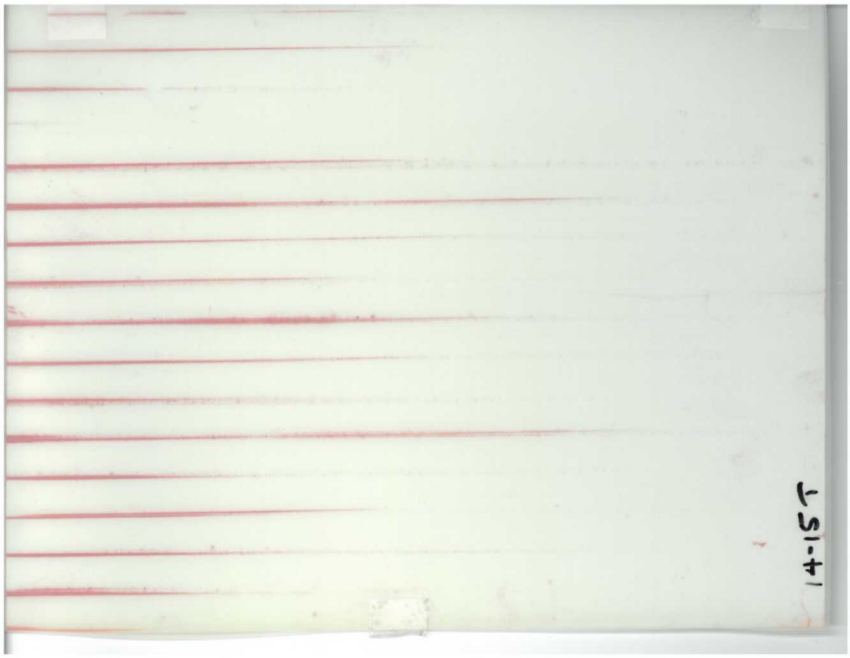

Figure C-32. June 2019 Additional 14-15T.

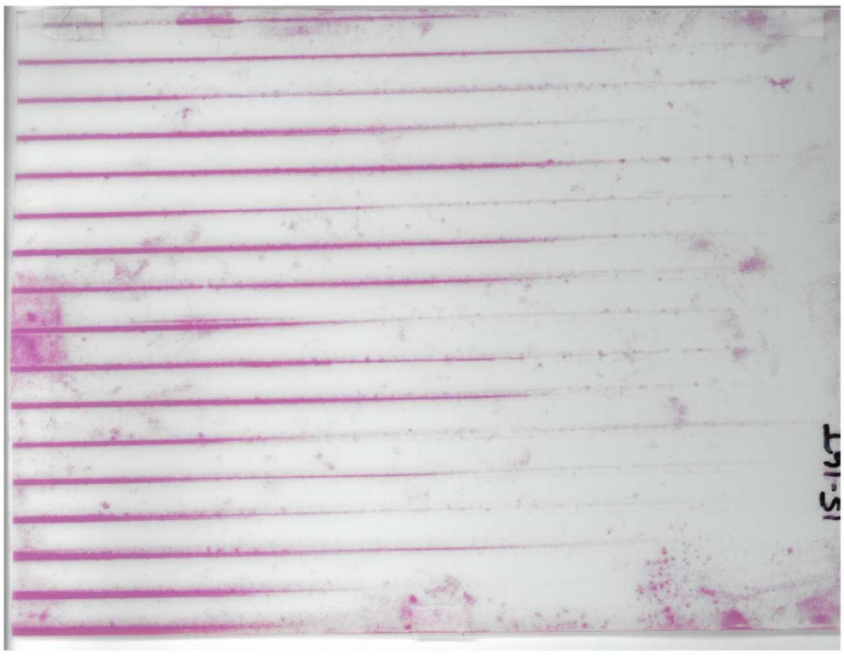

Figure C-33. June 2019 Additional 15-16T.

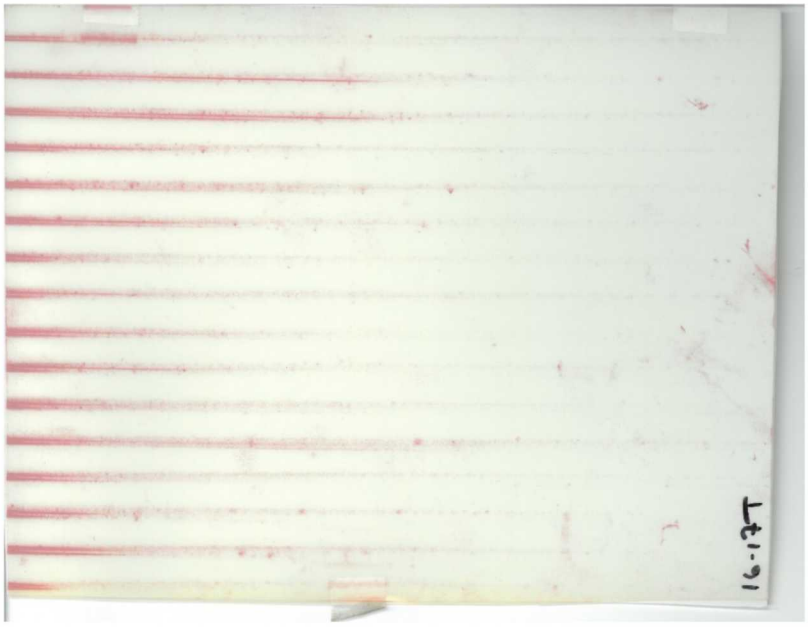

Figure C-34. June 2019 Additional 16-17T.

Appendix D Results from Pressure Paper from May 2020 Test Processing

The maximum rod-to-rod contact pressure was estimated for every pressure paper scan from 2020 test, except the blank ones. The results of the processing are shown in the figures below.

Bottom: Medium

Figure D-1. Momentary-Medium-05.

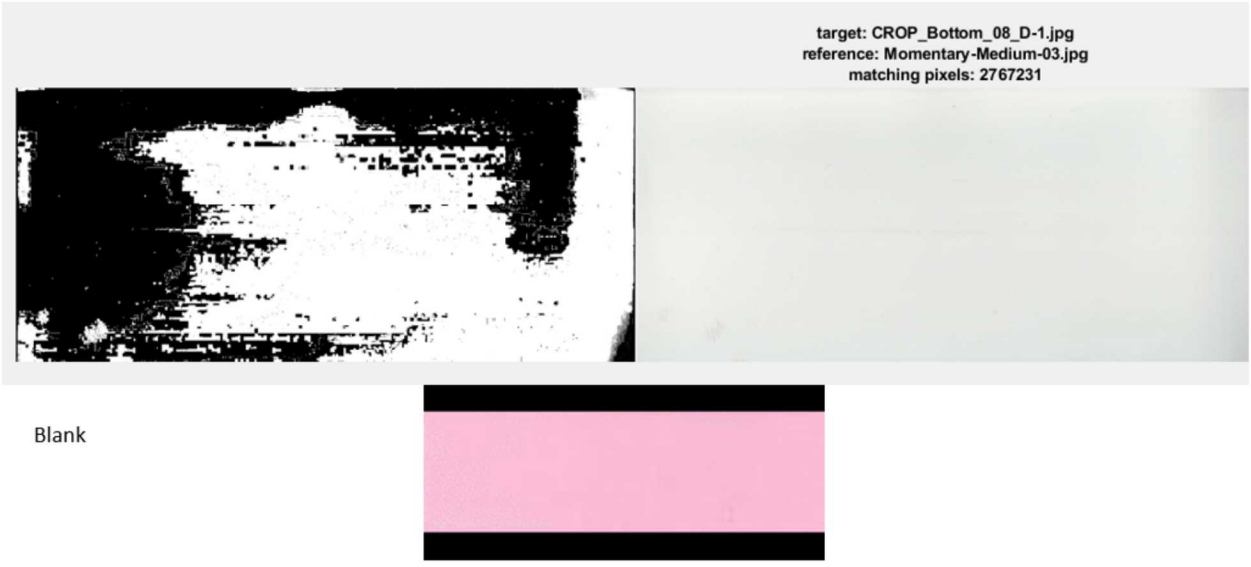

Figure D-2.Bottom 08_D-1.

Figure D-3. Bottom 12_D-1.

Bottom: Low

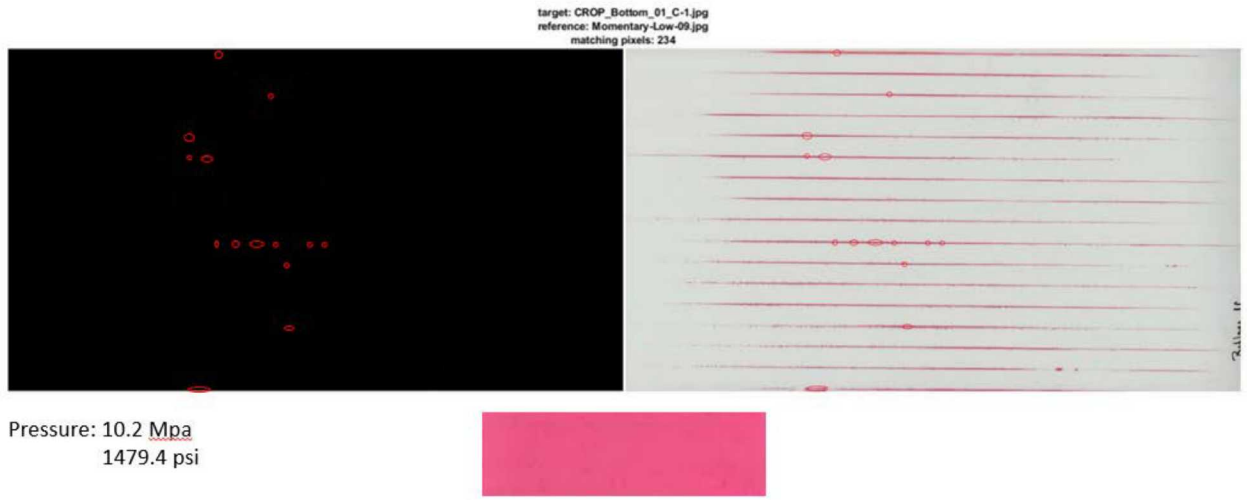

Figure D-4. Bottom 01_C-1.

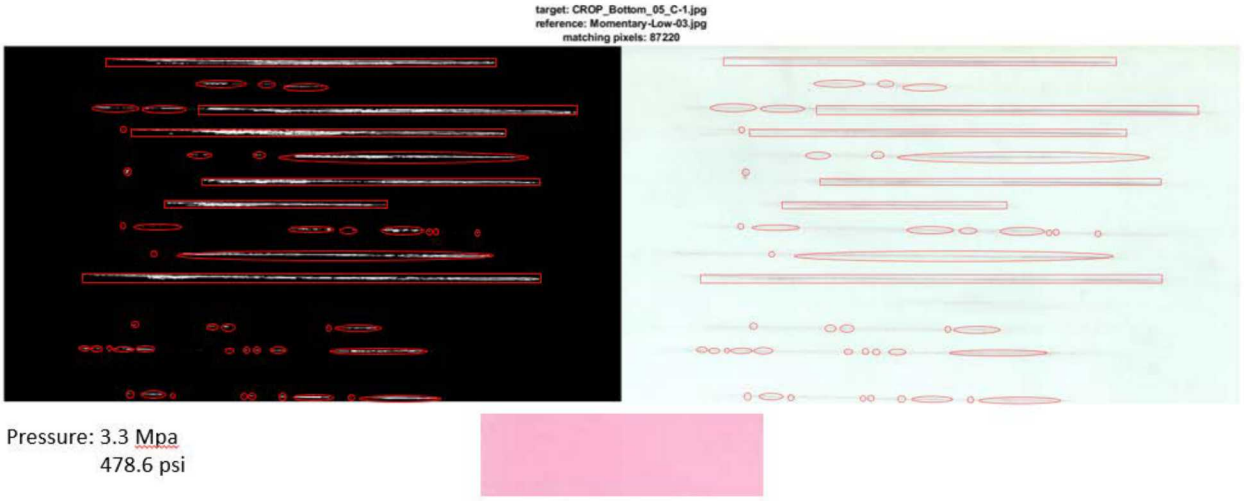

Figure D-5. Bottom 05_C-1.

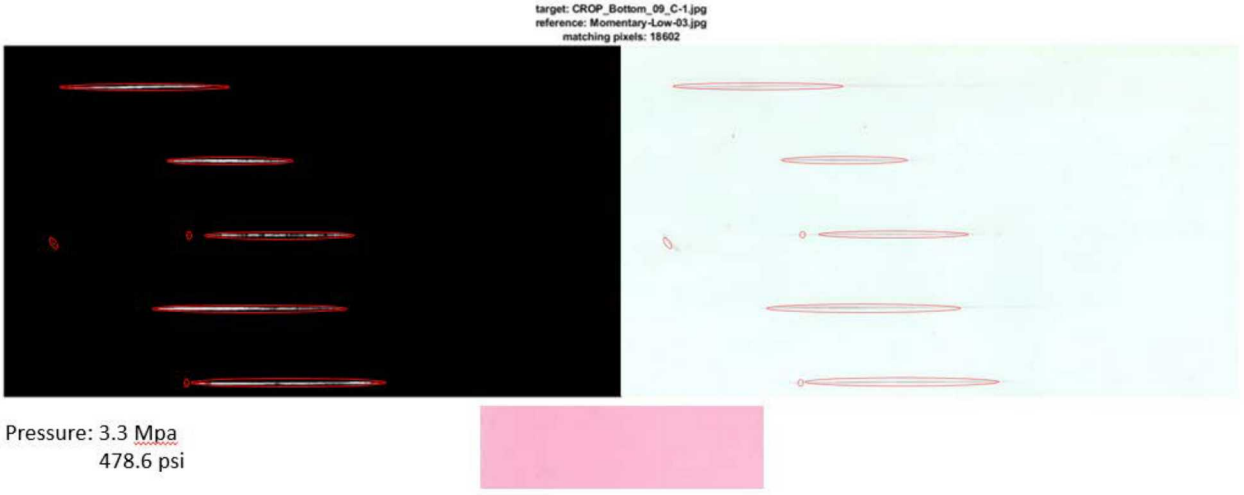

Figure D-6. Bottom 09_C-1.

Figure D-7. Bottom 13_C-1.

Bottom: Super Low

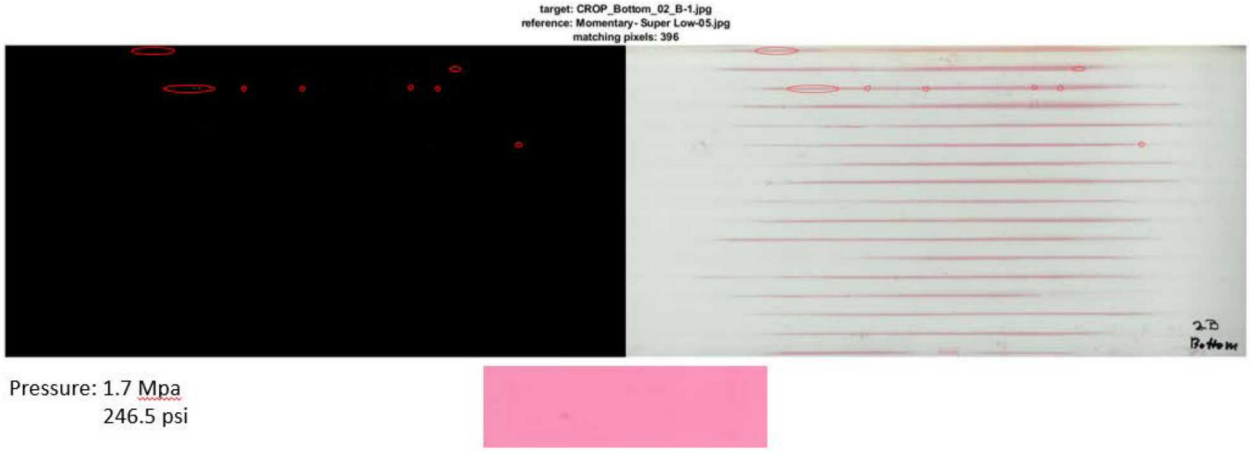

Figure D-8. Bottom 02_B-1.

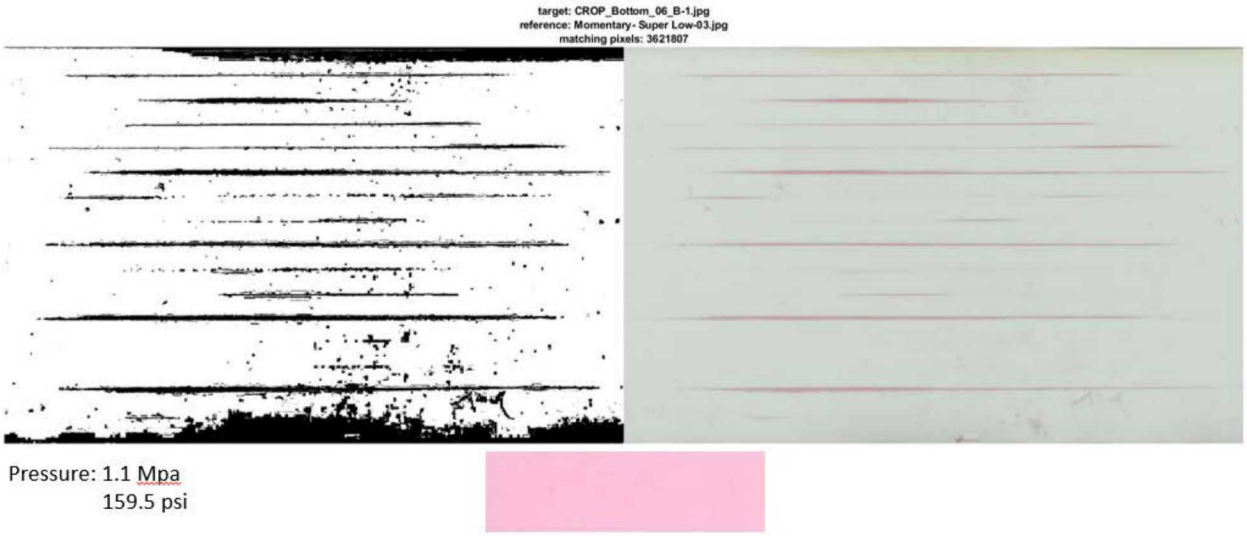

Figure D-9. Bottom 06_B-1.

Figure D-10. Bottom 10_B-1.

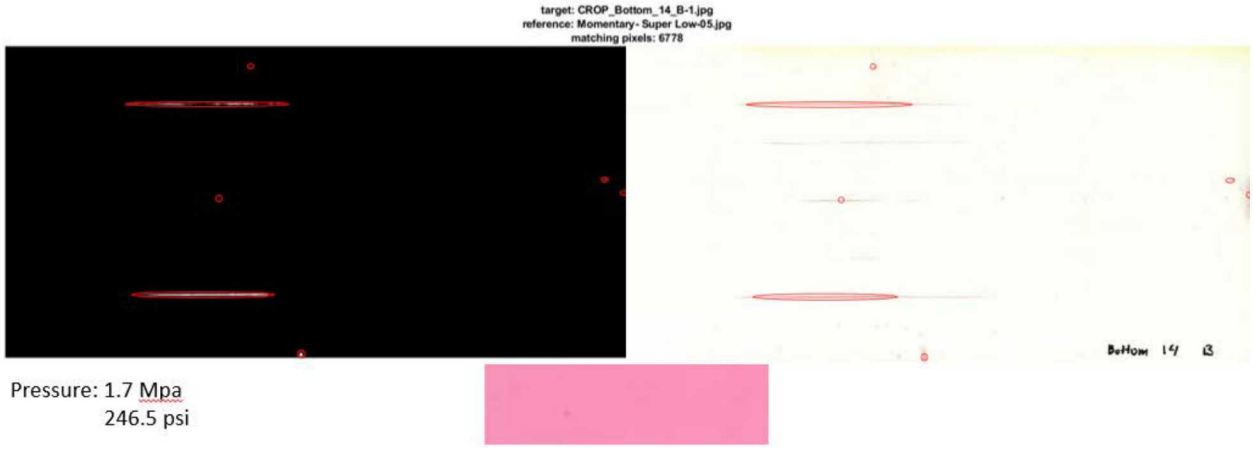

Figure D-11. Bottom 14_B-1.

Bottom: Extreme Low

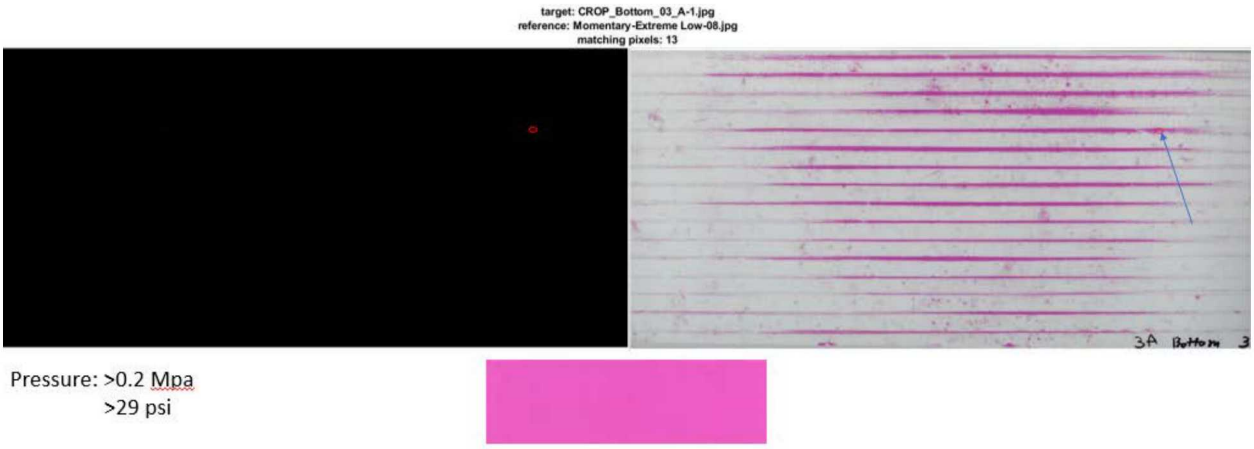

Figure D-12. Bottom 03_A-1.

Figure D-13. Bottom 07_A-1.

Figure D-14. Bottom 11_A-1.

Figure D-15. Bottom 15_A-1.

Top: Medium

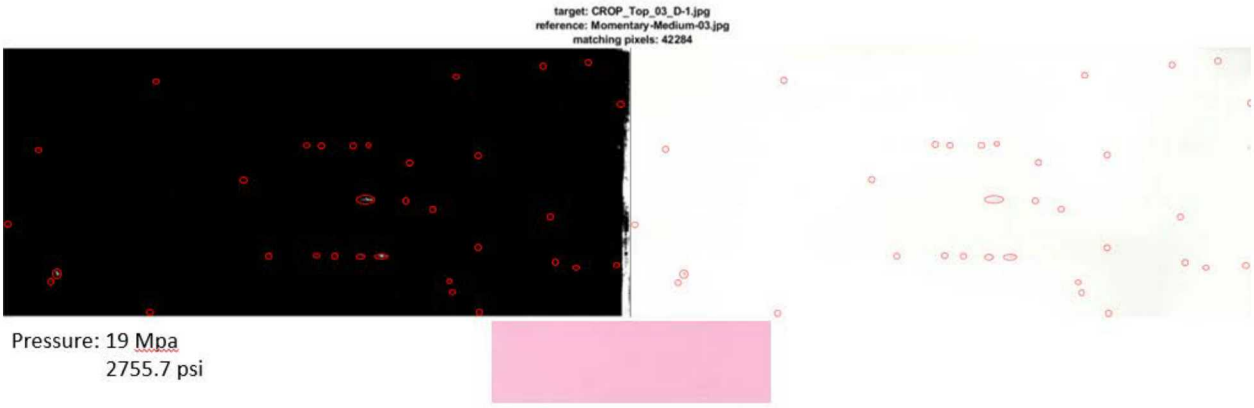

Figure D-16. Top 03_D-1.

Figure D-17. Top 07, 11, 15_D-1 All Blank.

Top: Low

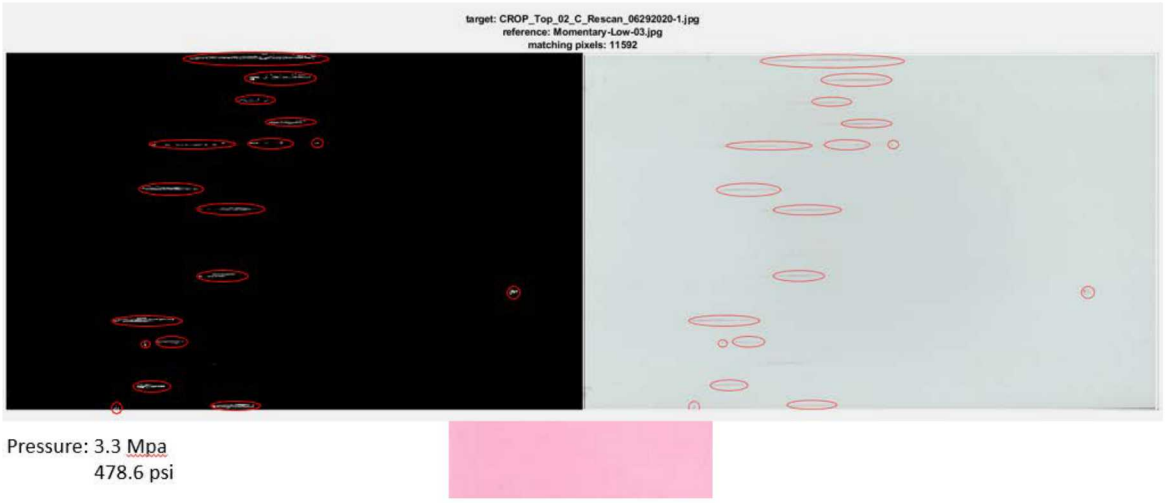

Figure D-18. Top 02_C_Rescan.

Figure D-19. Top 06_C_Rescan.

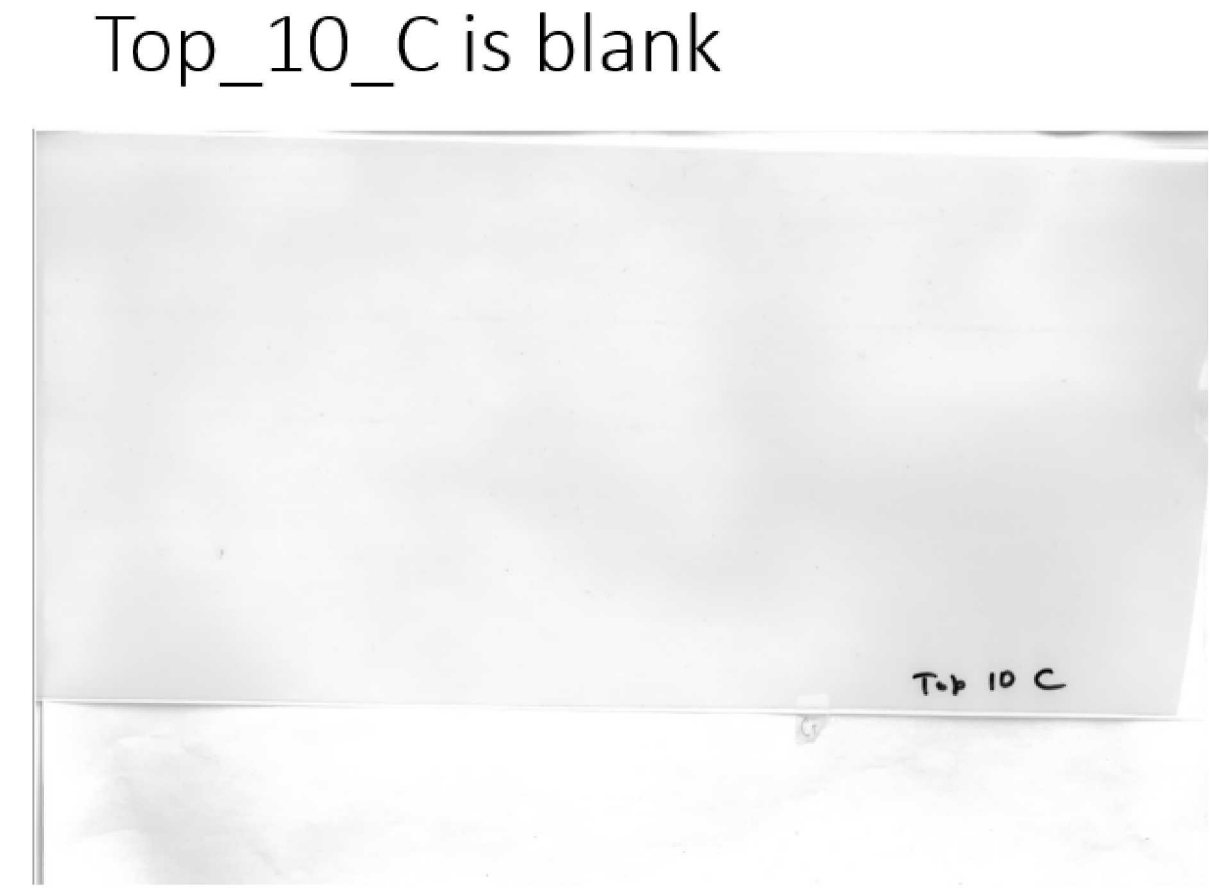

Figure D-20. Top 10_C is Blank.

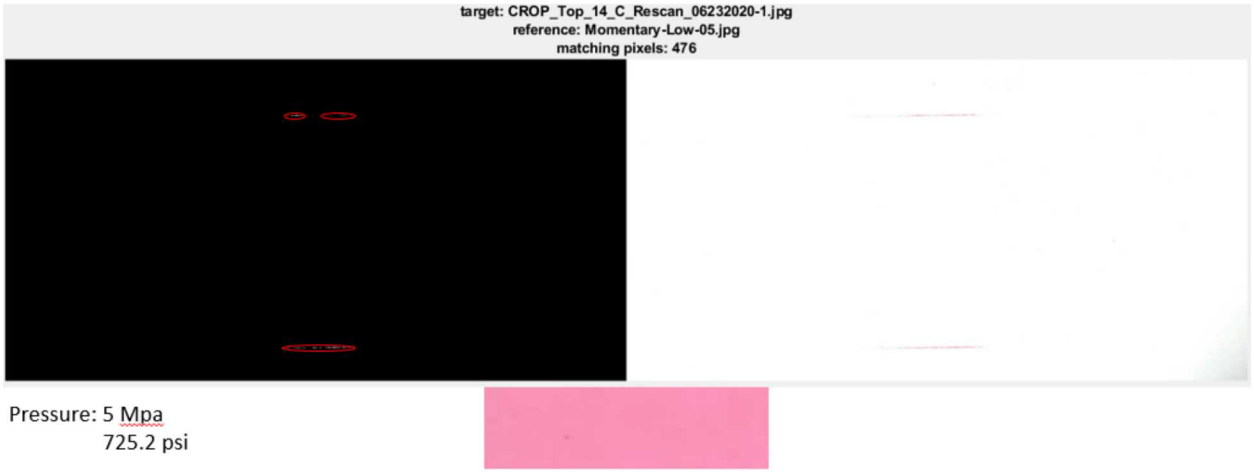

Figure D-21. Top 14_C_Rescan.

Top: Super Low

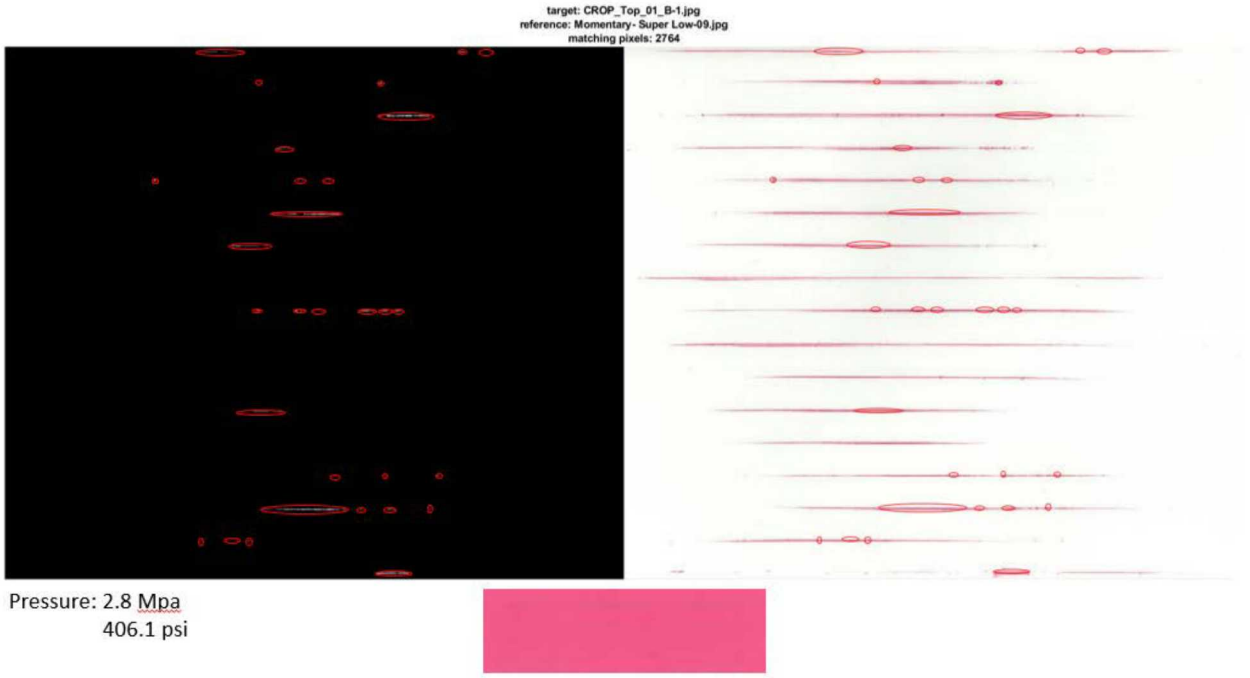

Figure D-22. Top 01_B-1.

Figure D-23. Top 05_B-1.

Figure D-24. Top 09_B-1.

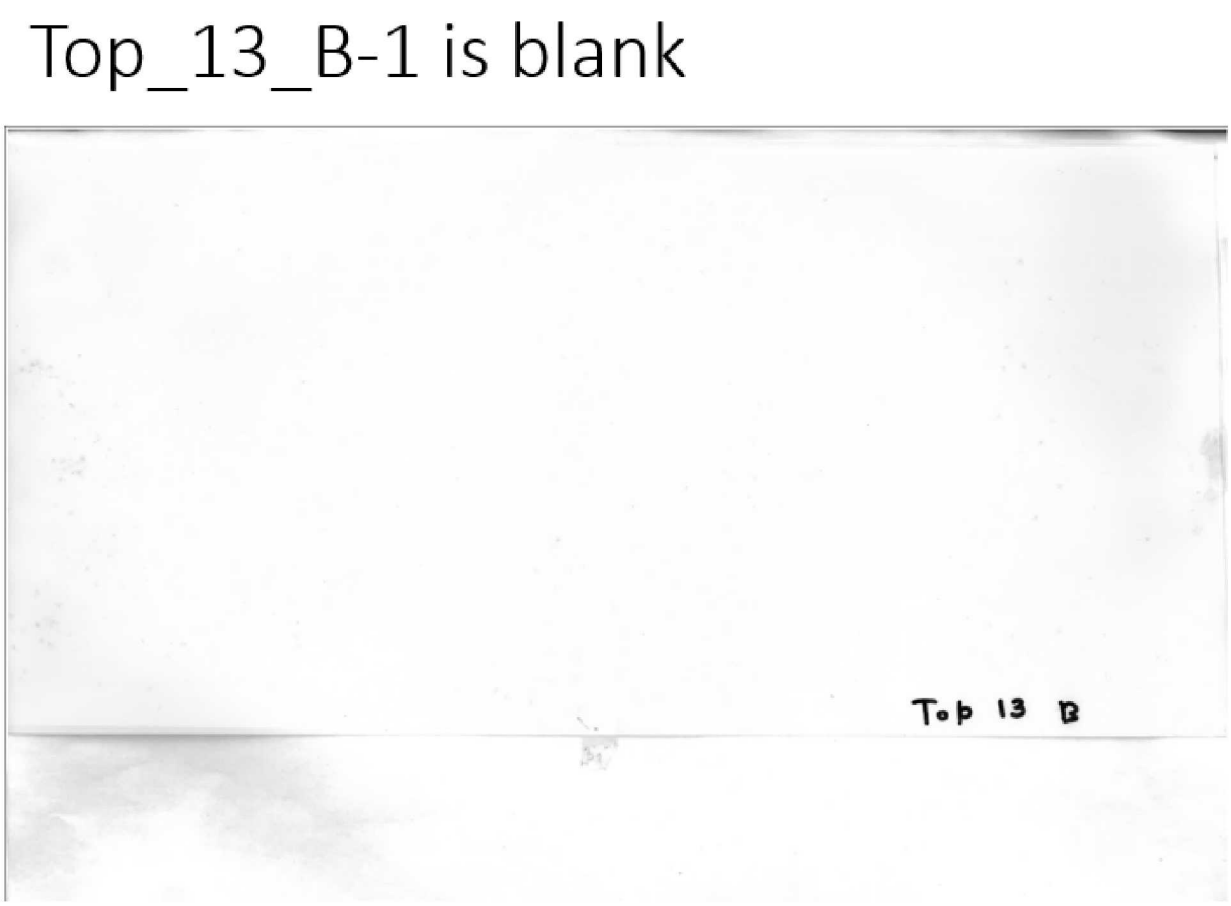

Figure D-25. Top 13_B-1.

Top: Extreme Low

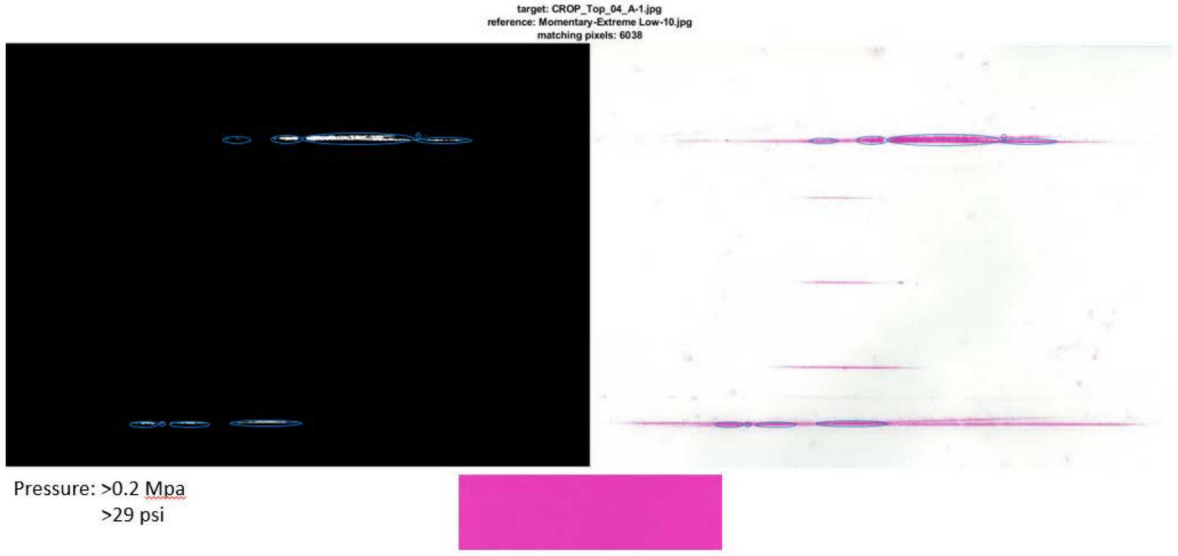

Figure D-26. Top 04_A-1.

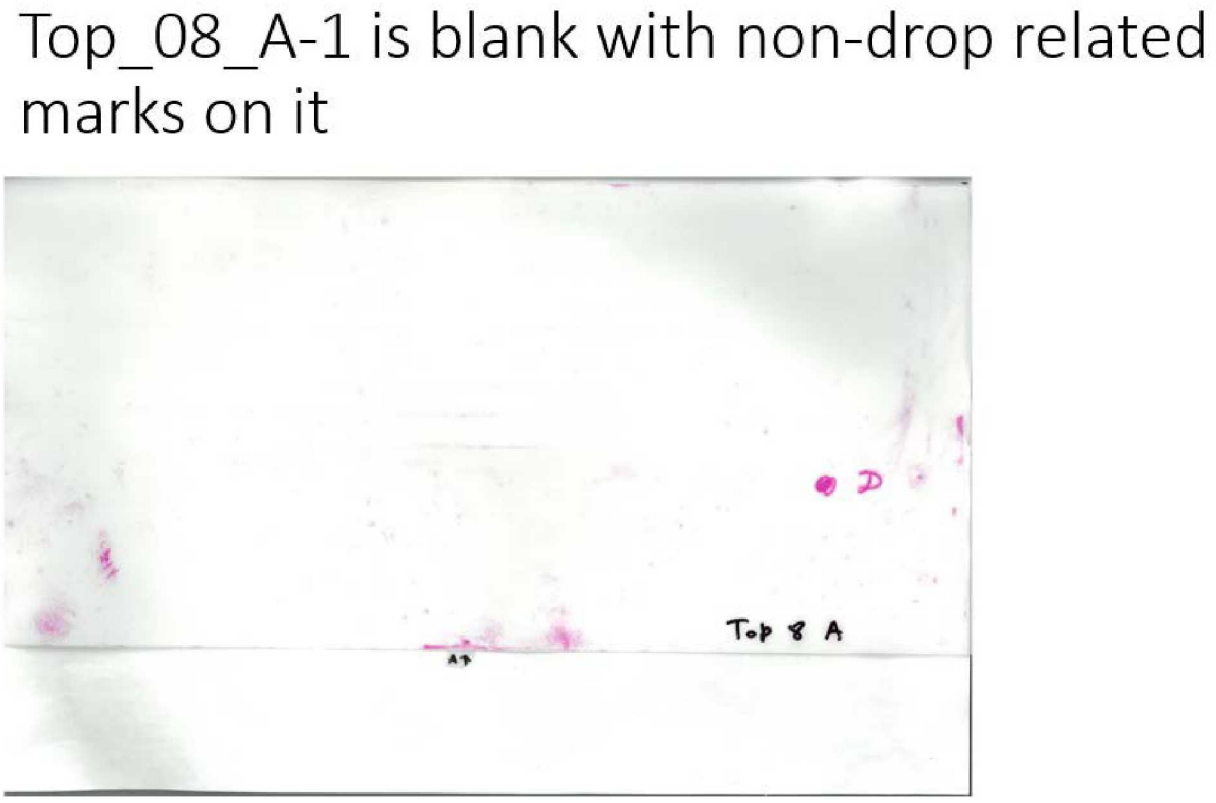

Figure D-27. Top 08_A-1 is blank with non-drop related marks on it.

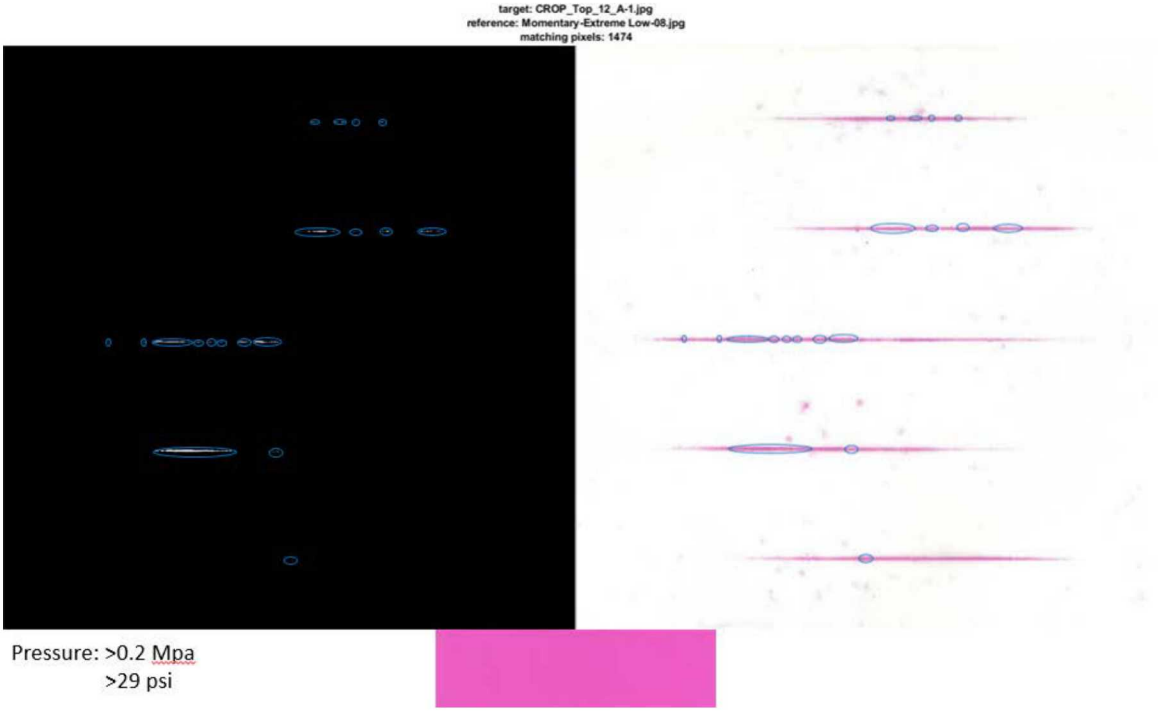

Figure D-28. Top 12_A-1.

Appendix E Results of Pressure Paper from June 2019 Test Processing

The maximum rod-to-rod contact pressure was estimated for every pressure paper scan from 2019 test, except the blank ones. The results of the processing are shown in the figures below.

Bottom: Extreme Low

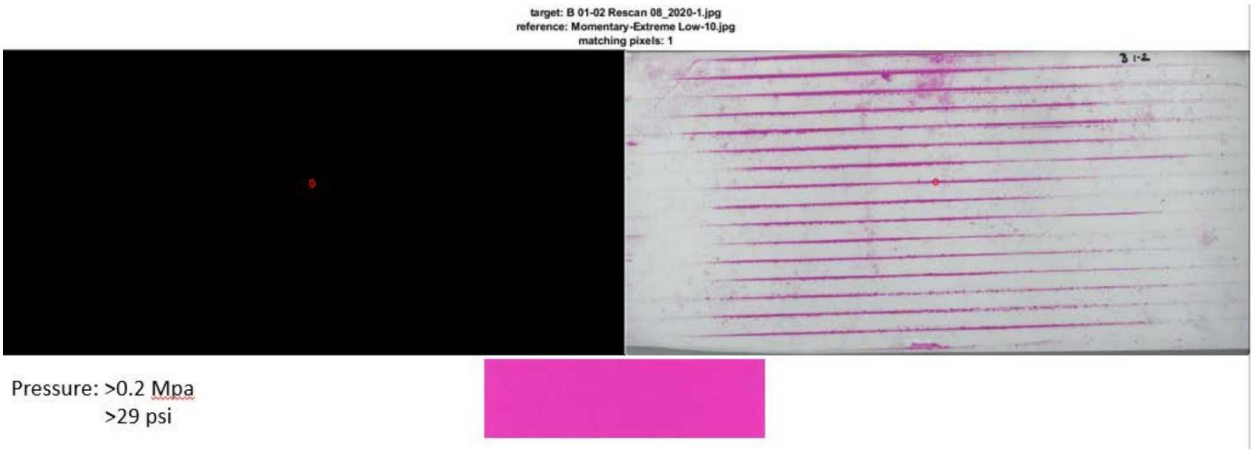

Figure E-1 B 01-02 Rescan.

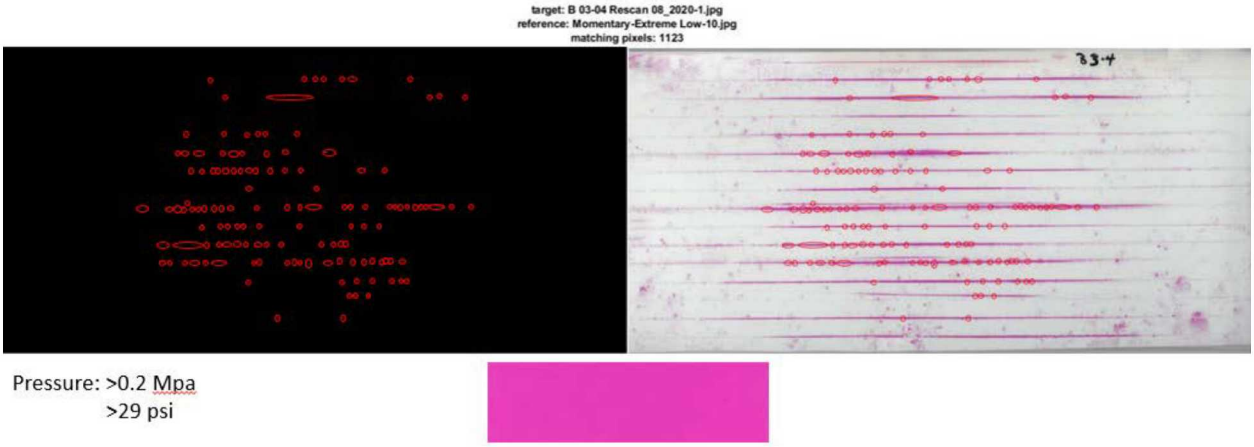

Figure E-2. B 03-04 Rescan.

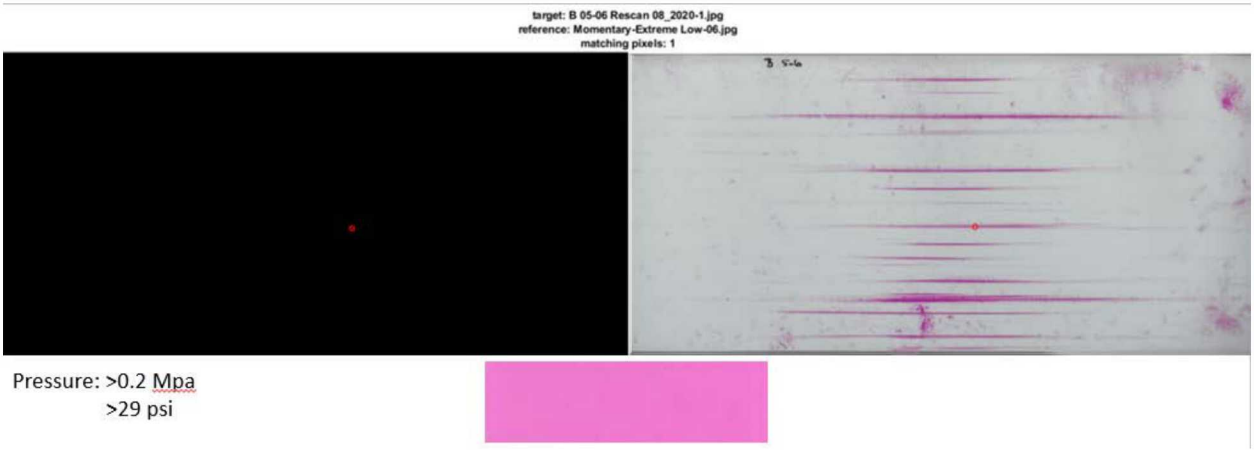

Figure E-3 B 05-06 Rescan.

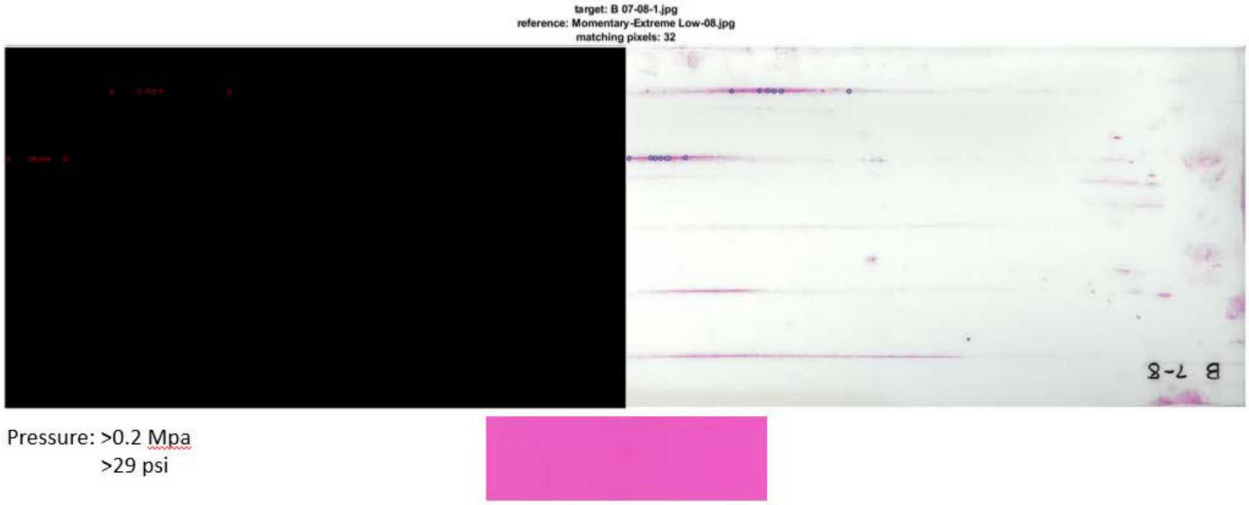

Figure E-4. B 07-08.

Figure E-5. B 09-10.

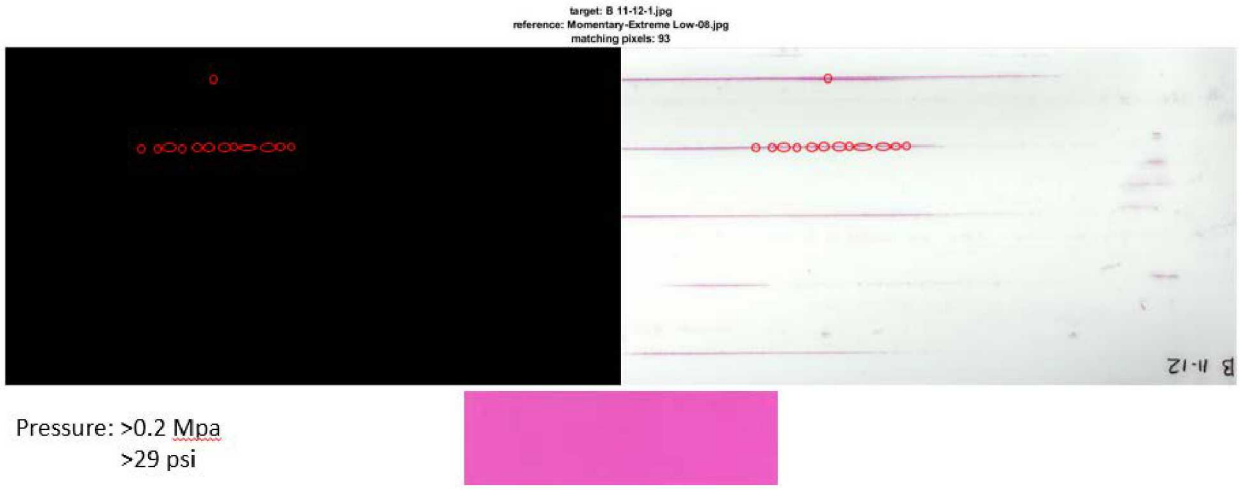

Figure E-6. B 11-12.

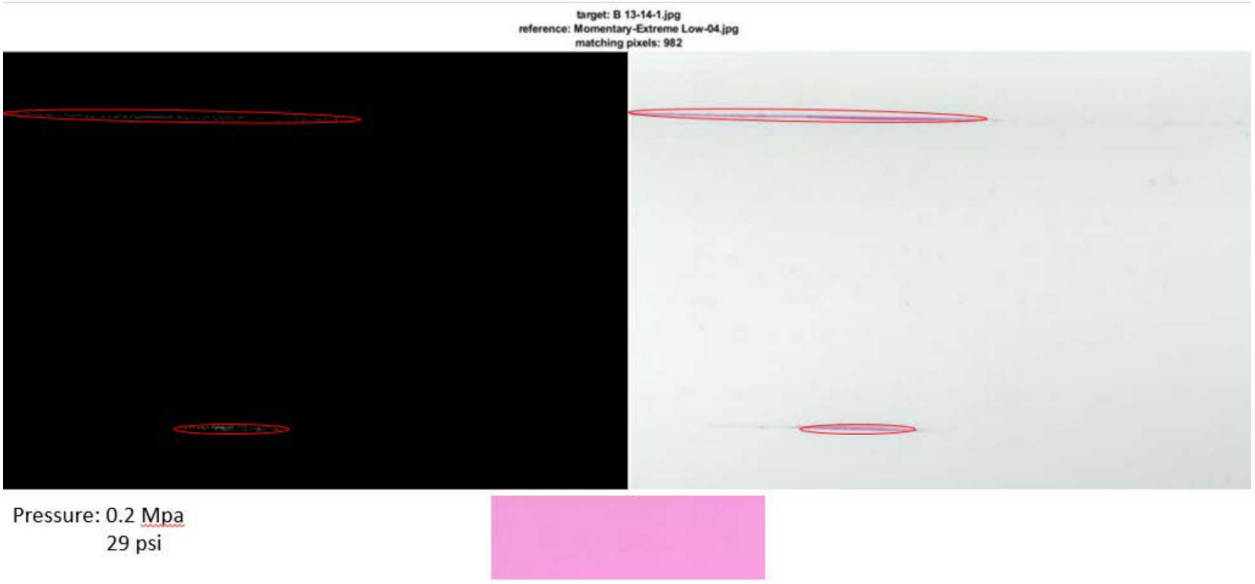

Figure E-7. B 13-14.

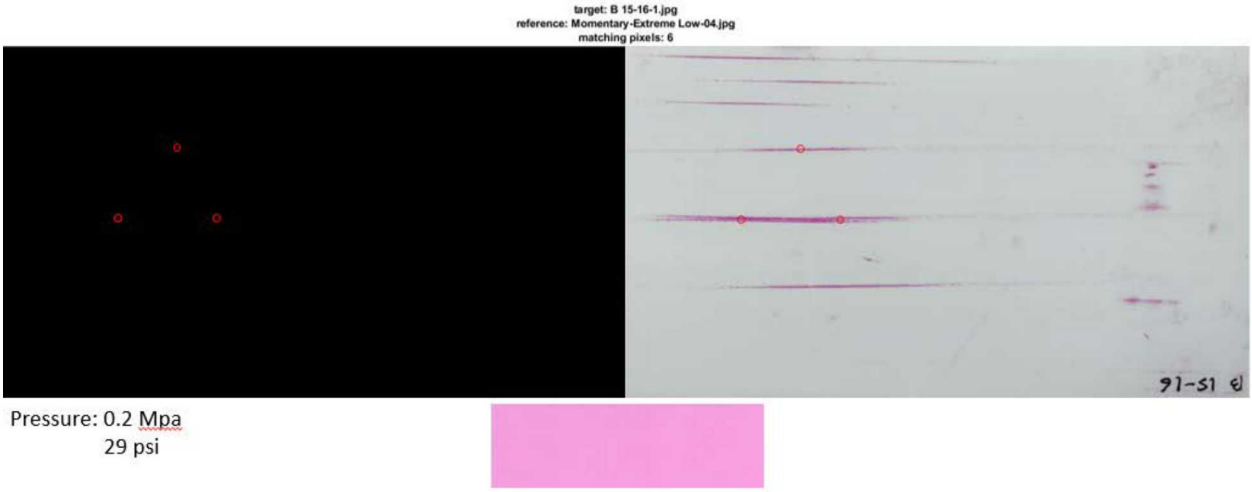

Figure E-8. B 15-16.

Bottom: Super Low

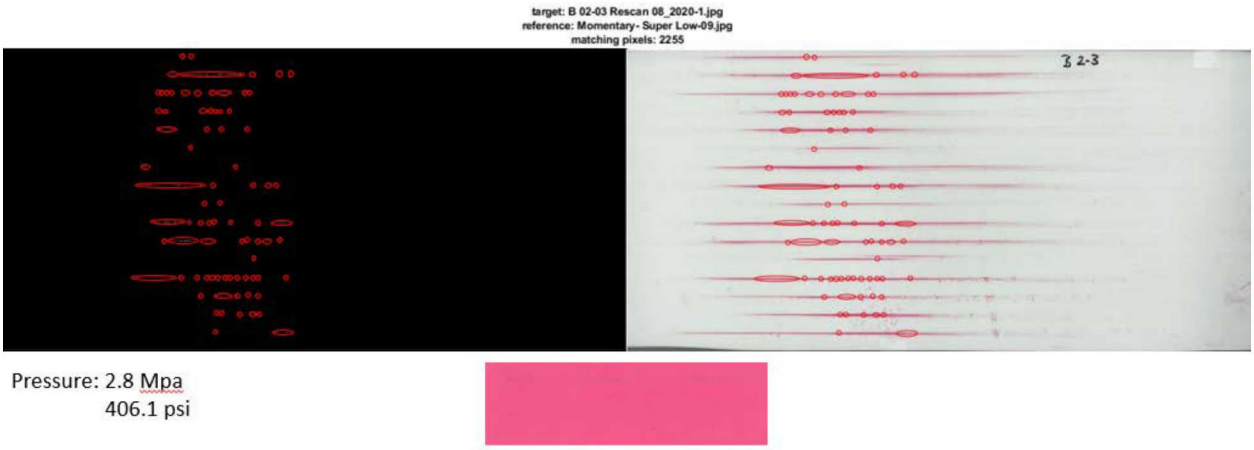

Figure E-9. B 02-03 Rescan.

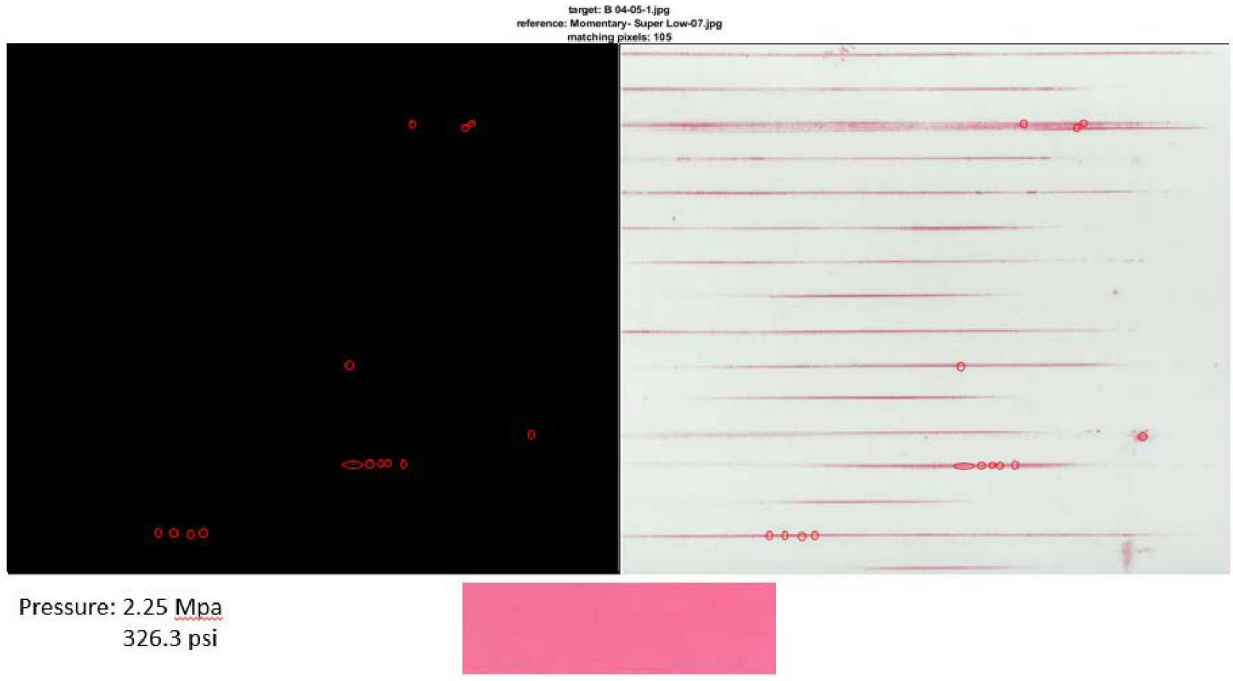

Figure E-10. B 04-05.

Figure E-11. B 06-07.

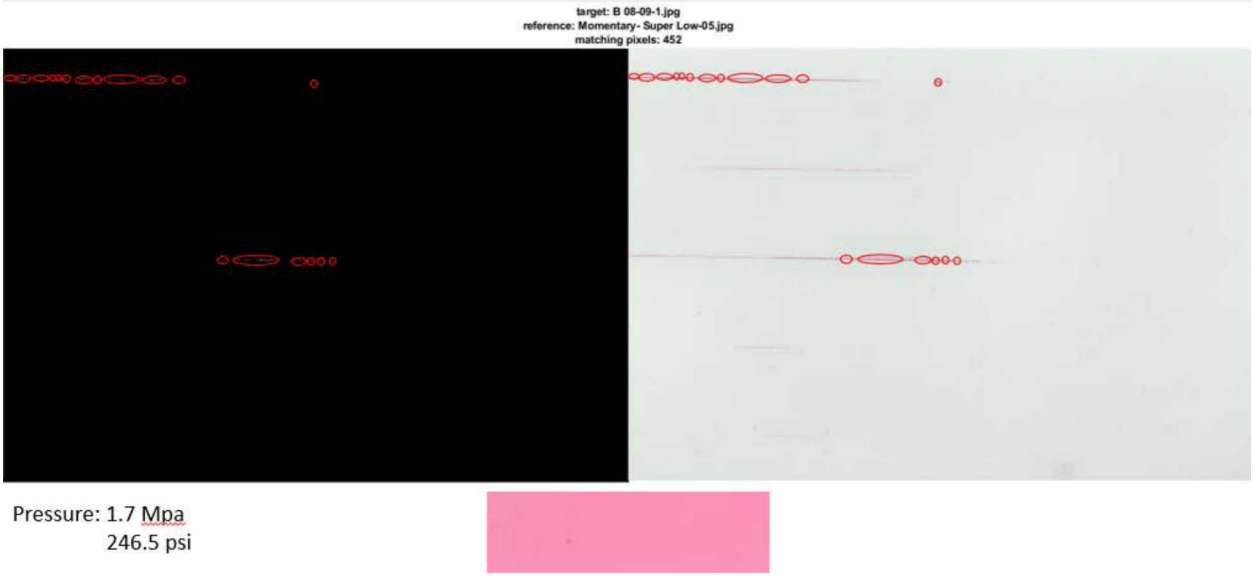

Figure E-12. B 08-09.

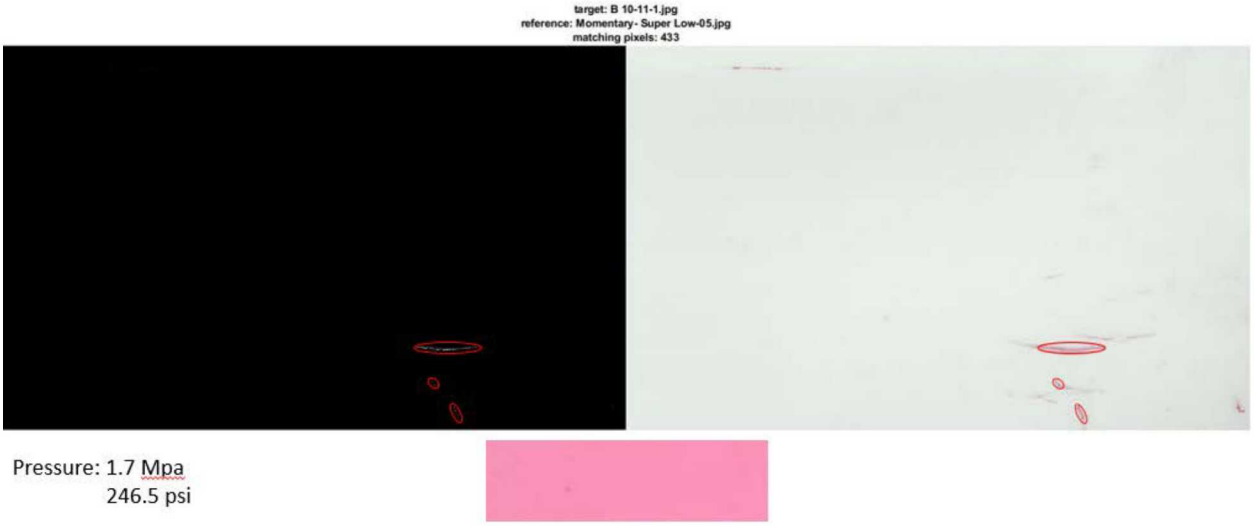

Figure E-13. B 10-11.

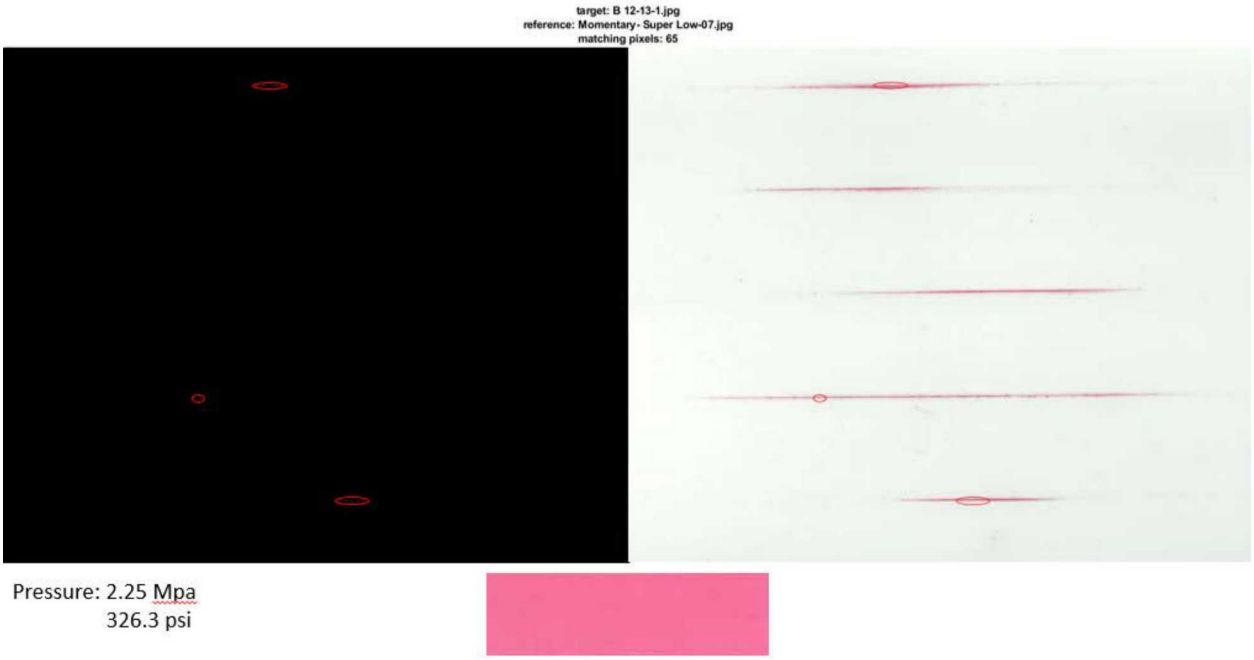

Figure E-14. B 12-13.

Figure E-15. B 14-15.

Top: Extreme Low

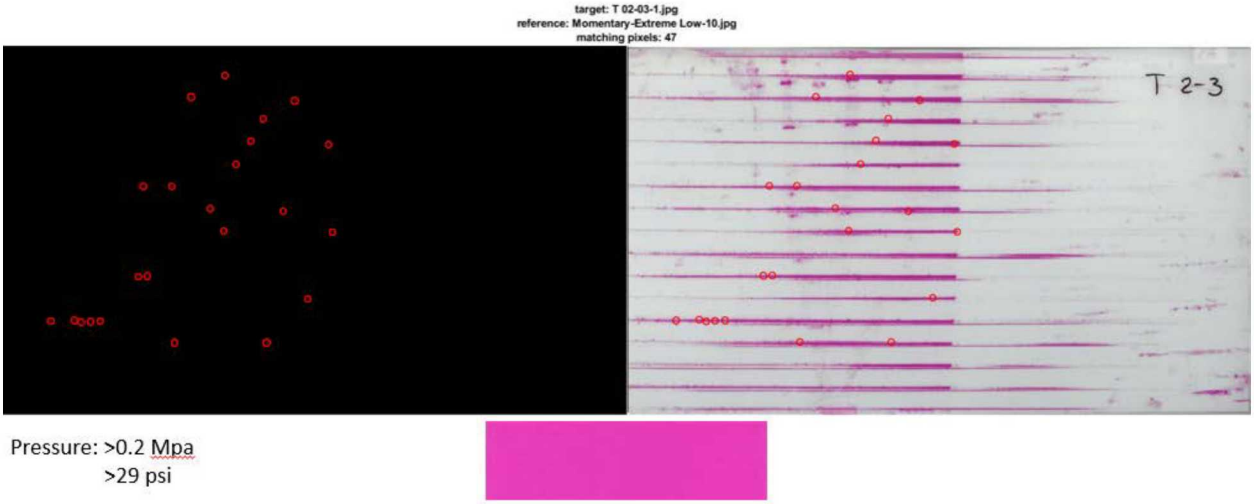

Figure E-16. T 02-03.

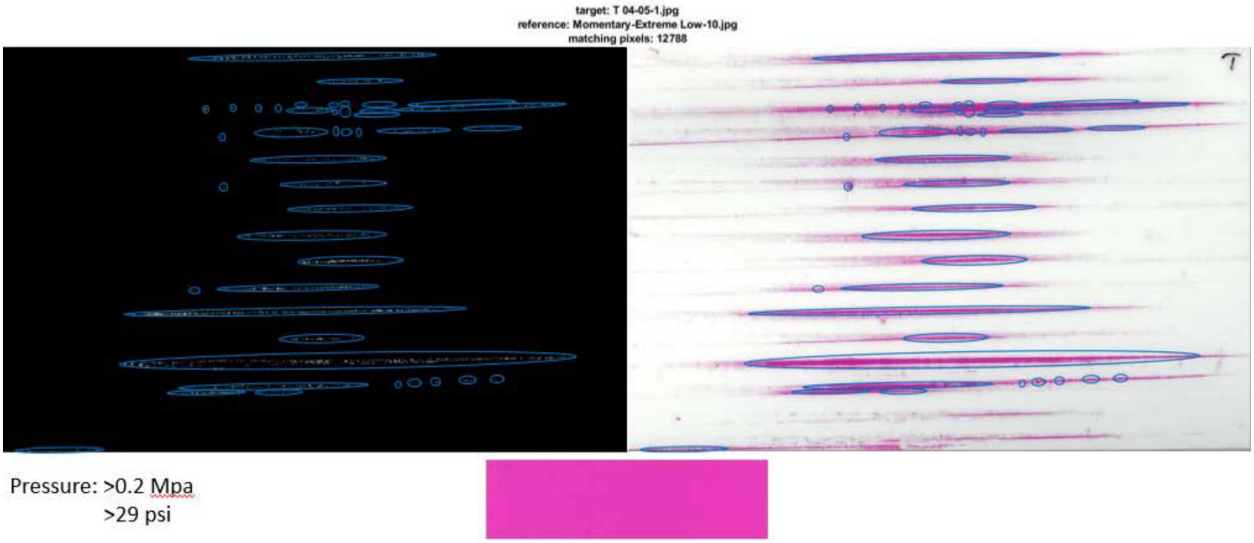

Figure E-17. T 04-05.

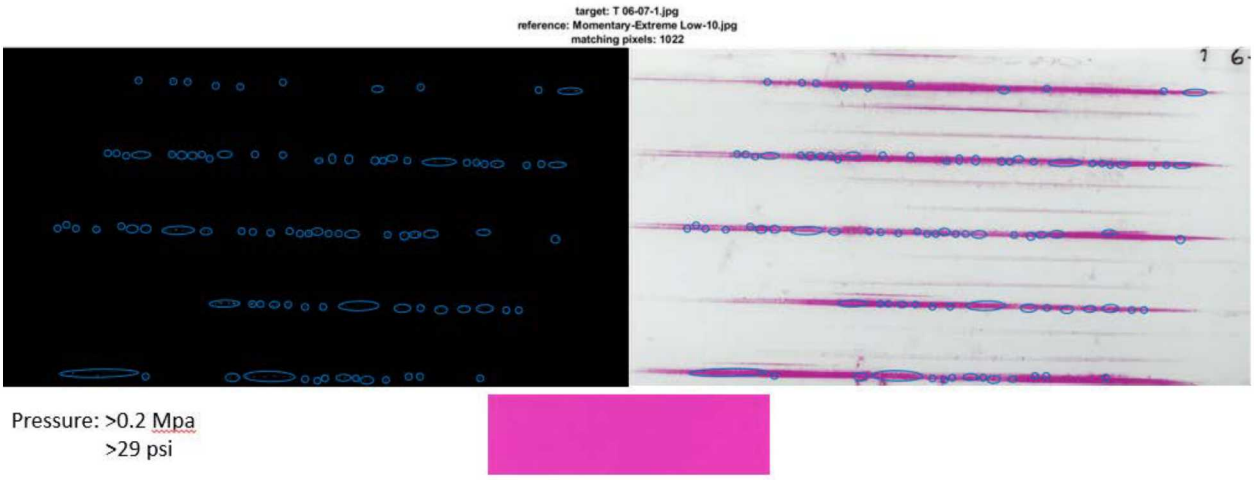

Figure E-18. T 06-07.

Figure E-19. T 08-09.

Figure E-20. T 10-11.

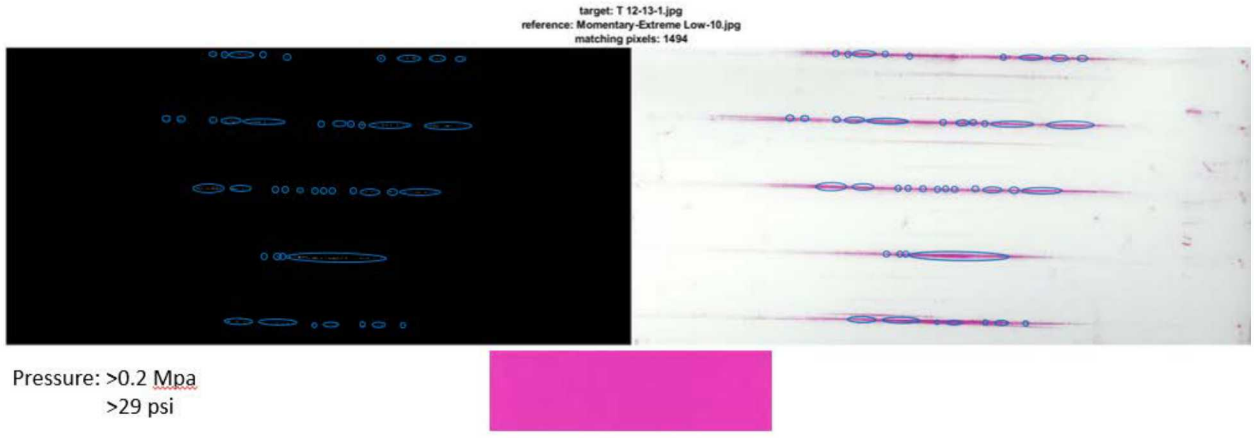

Figure E-21. T 12-13.

Figure E-22. T 14-15.

Top: Super Low

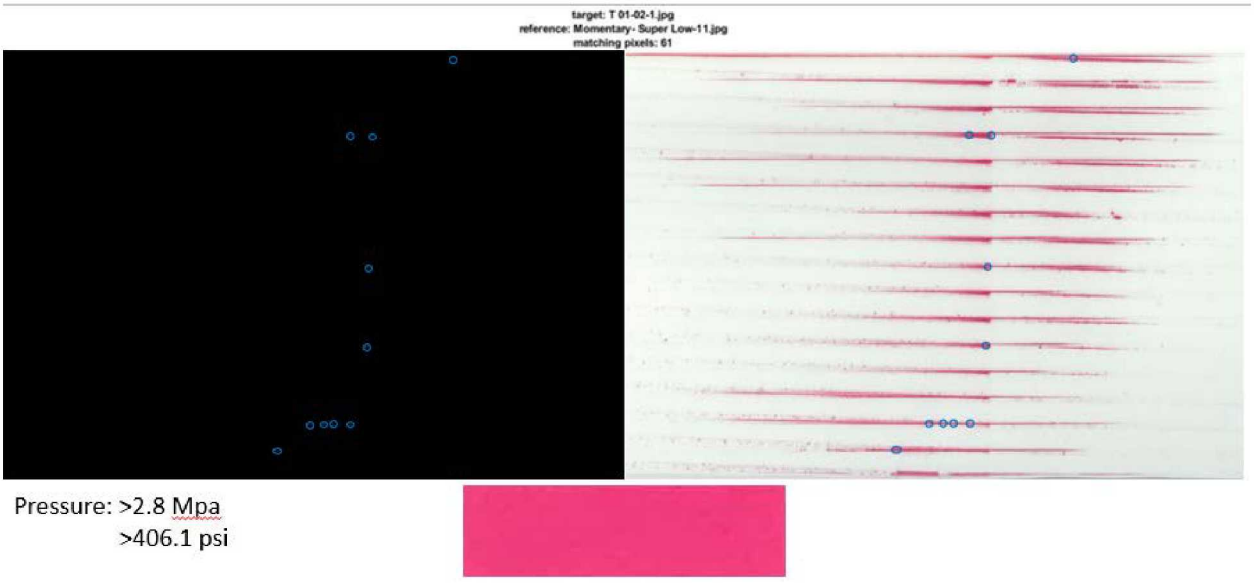

Figure E-23. T 01-02.

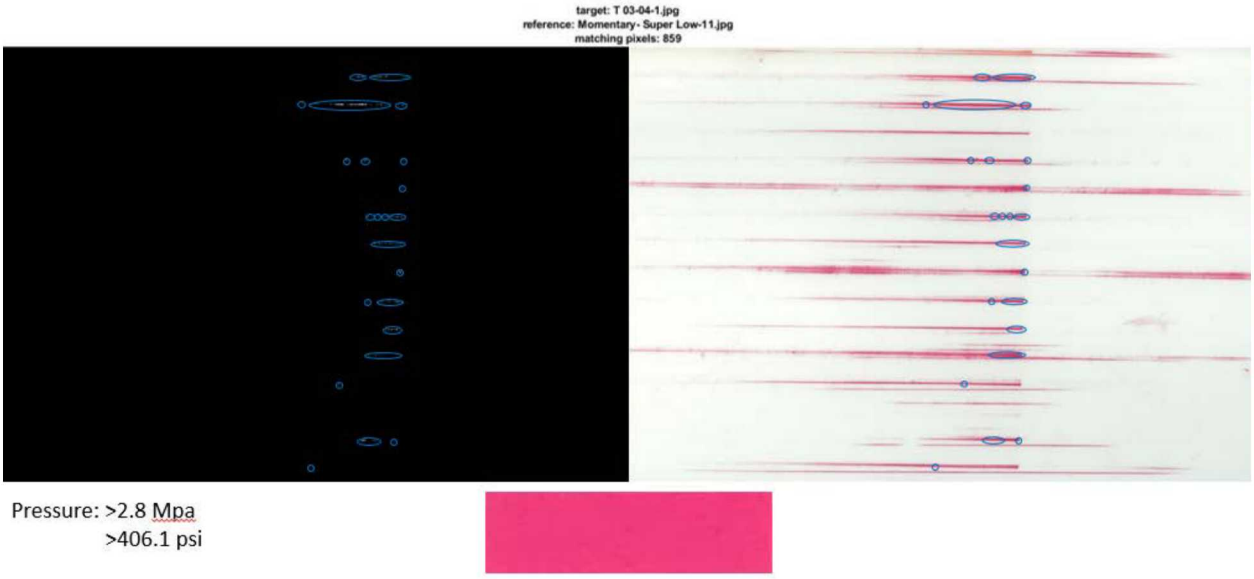

Figure E-24. T 03-04.

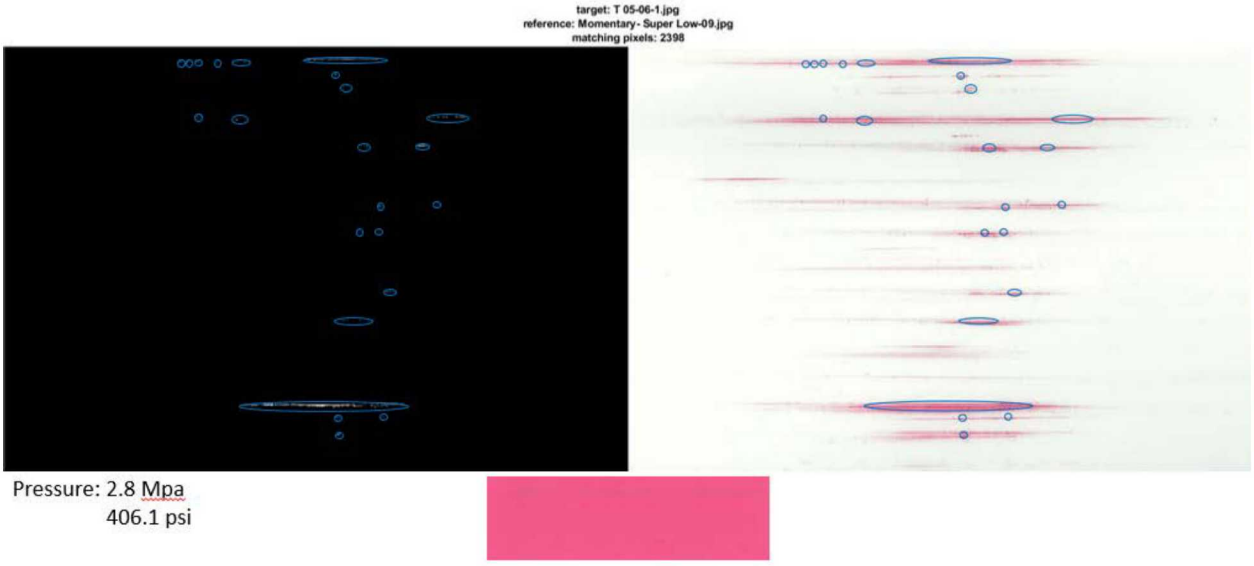

Figure E-25. T 05-06.

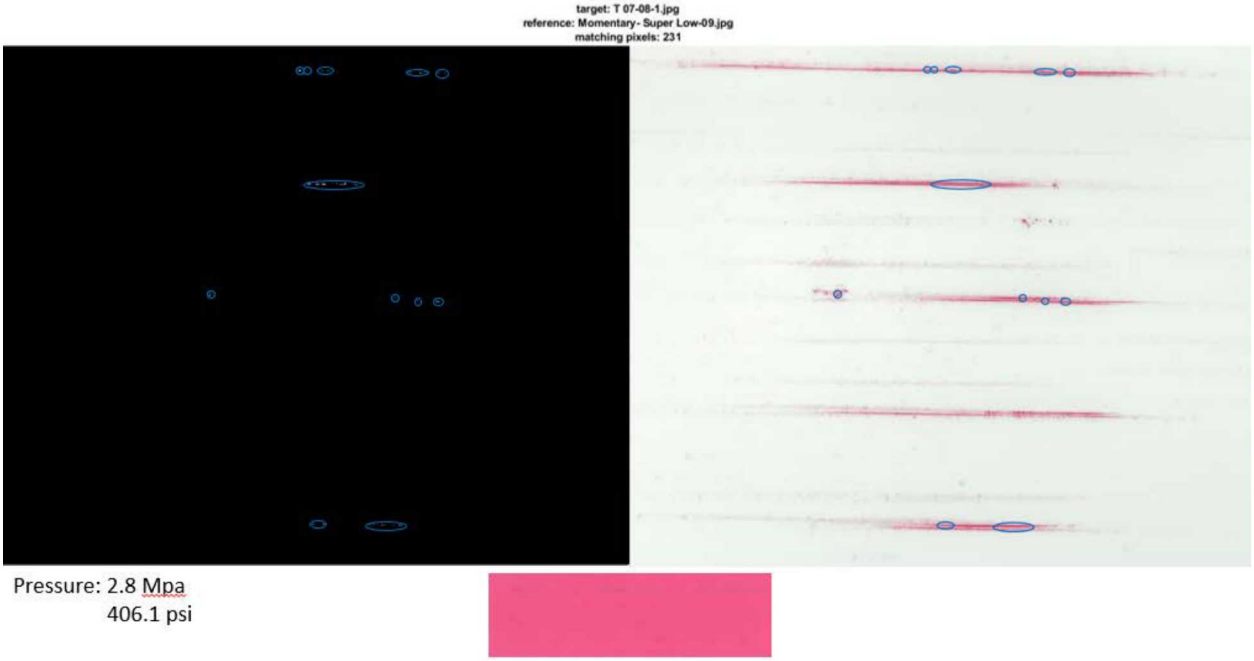

Figure E-26. T 07-08.

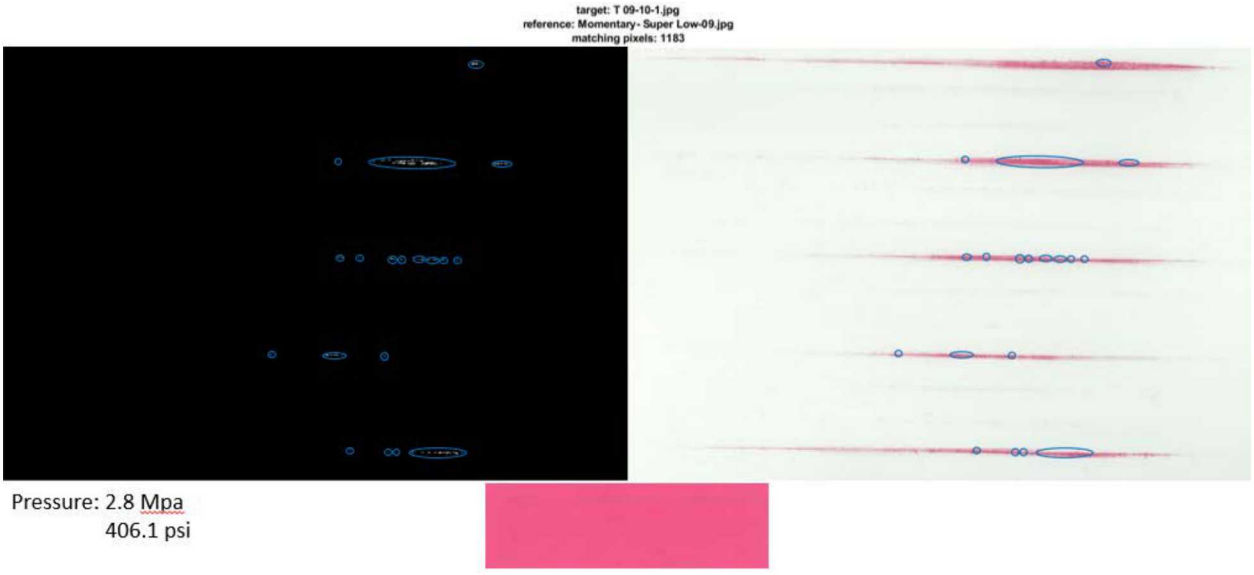

Figure E-27. T 09-10.

Figure E-28. T 10-11 is blank.

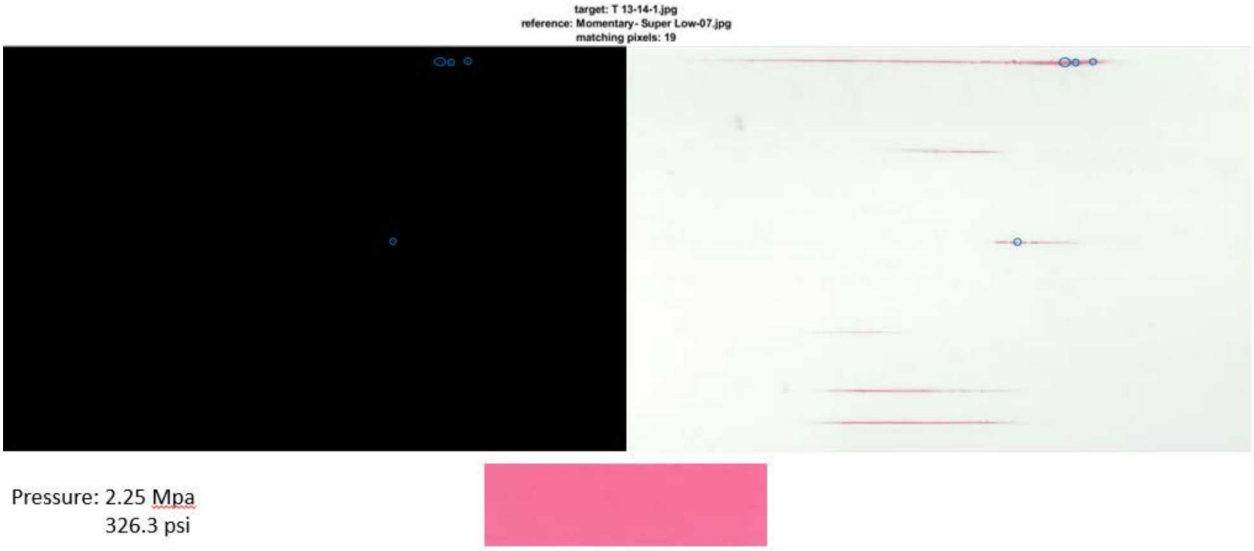

Figure E-29. T 13-14.

Figure E-30. T 15-16.

Additional-Top: Extreme Low

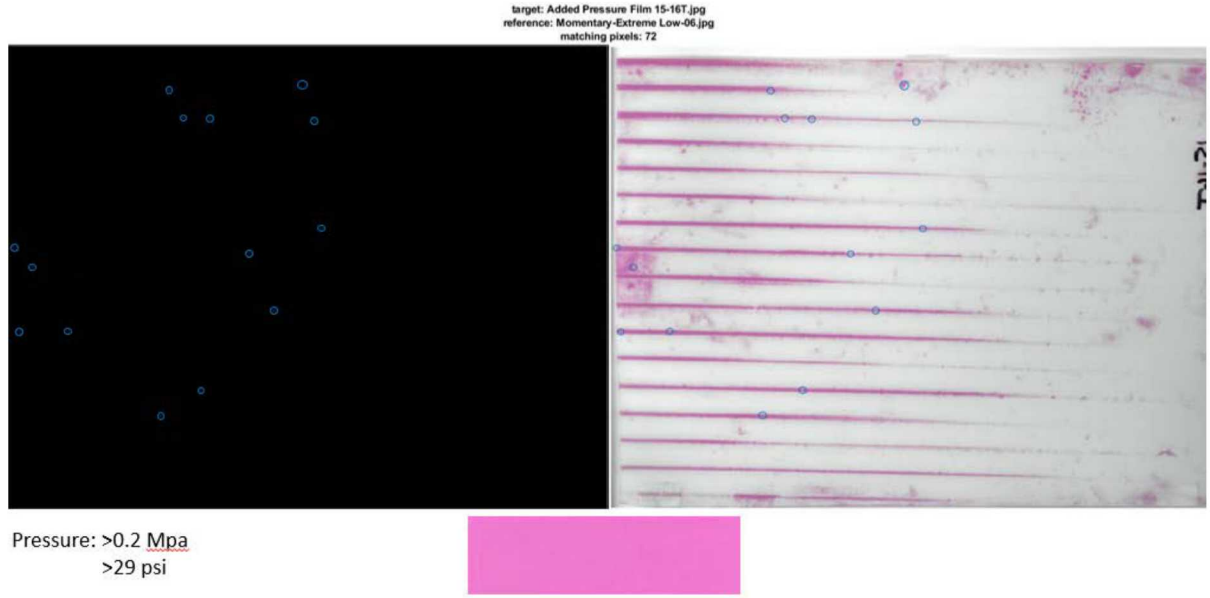

Figure E-31. Added Pressure Film 15-16T.

Additional-Top: Super Low

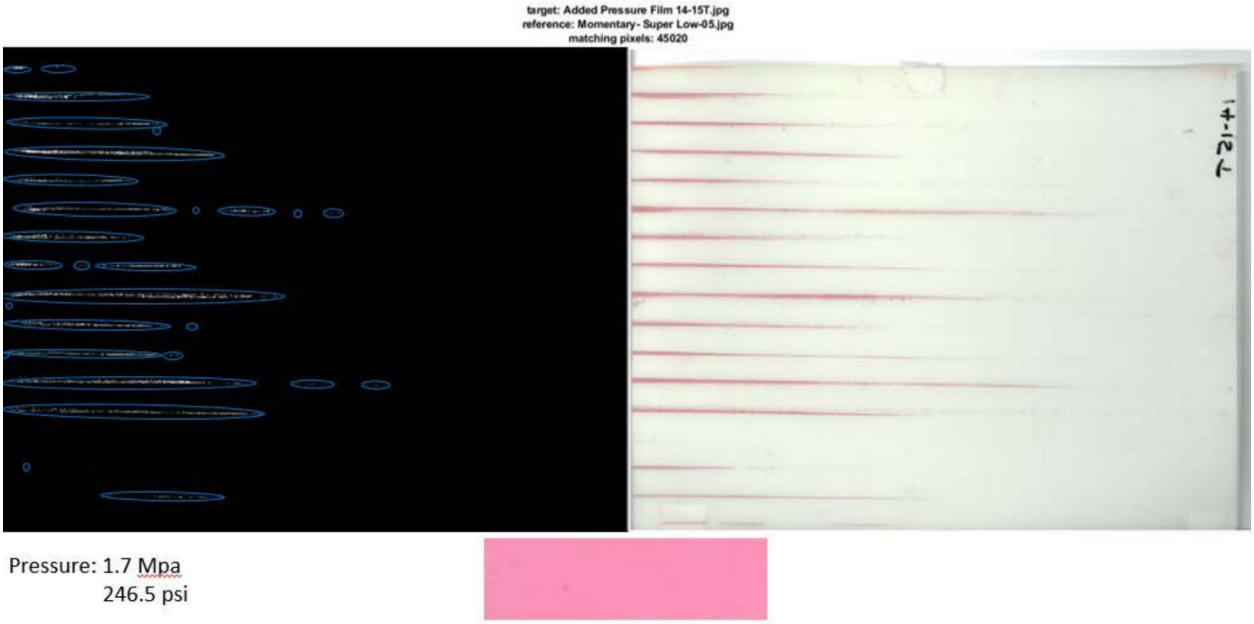

Figure A-25. Added Pressure Film 14-15T.

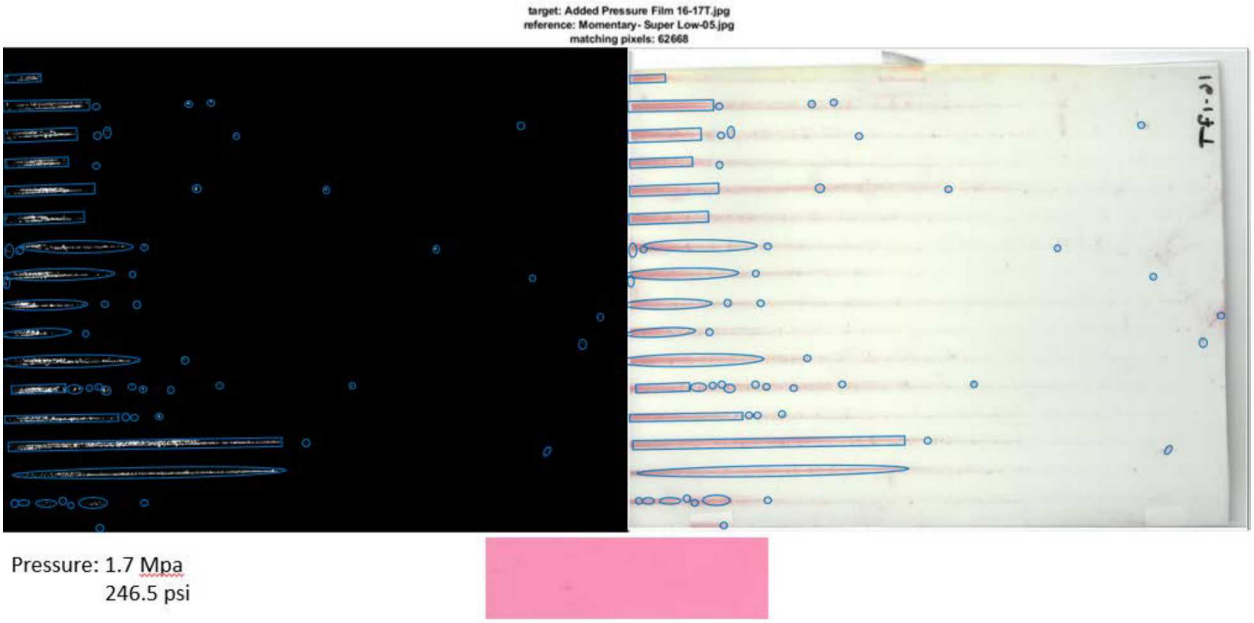

Figure E-32. Added Pressure Film 16-17T.